



universität
wien

DISSERTATION / DOCTORAL THESIS

Titel der Dissertation / Title of the Doctoral Thesis

„Simulating MICADO:
the future of near infrared astronomy“

verfasst von / submitted by

Kieran Leschinski, MSc

angestrebter akademischer Grad / in partial fulfilment of the requirements for the degree of
Doktor der Naturwissenschaften (Dr. rer. nat.)

Wien, 2018 / Vienna, 2018

Studienkennzahl lt. Studienblatt /
degree programme code as it appears on the student
record sheet:

A 796 605 413

Dissertationsgebiet lt. Studienblatt /
field of study as it appears on the student record sheet:

Astronomie / Astronomy

Betreut von / Supervisor:

Univ. Prof. Dr. João Alves

Simulating MICADO

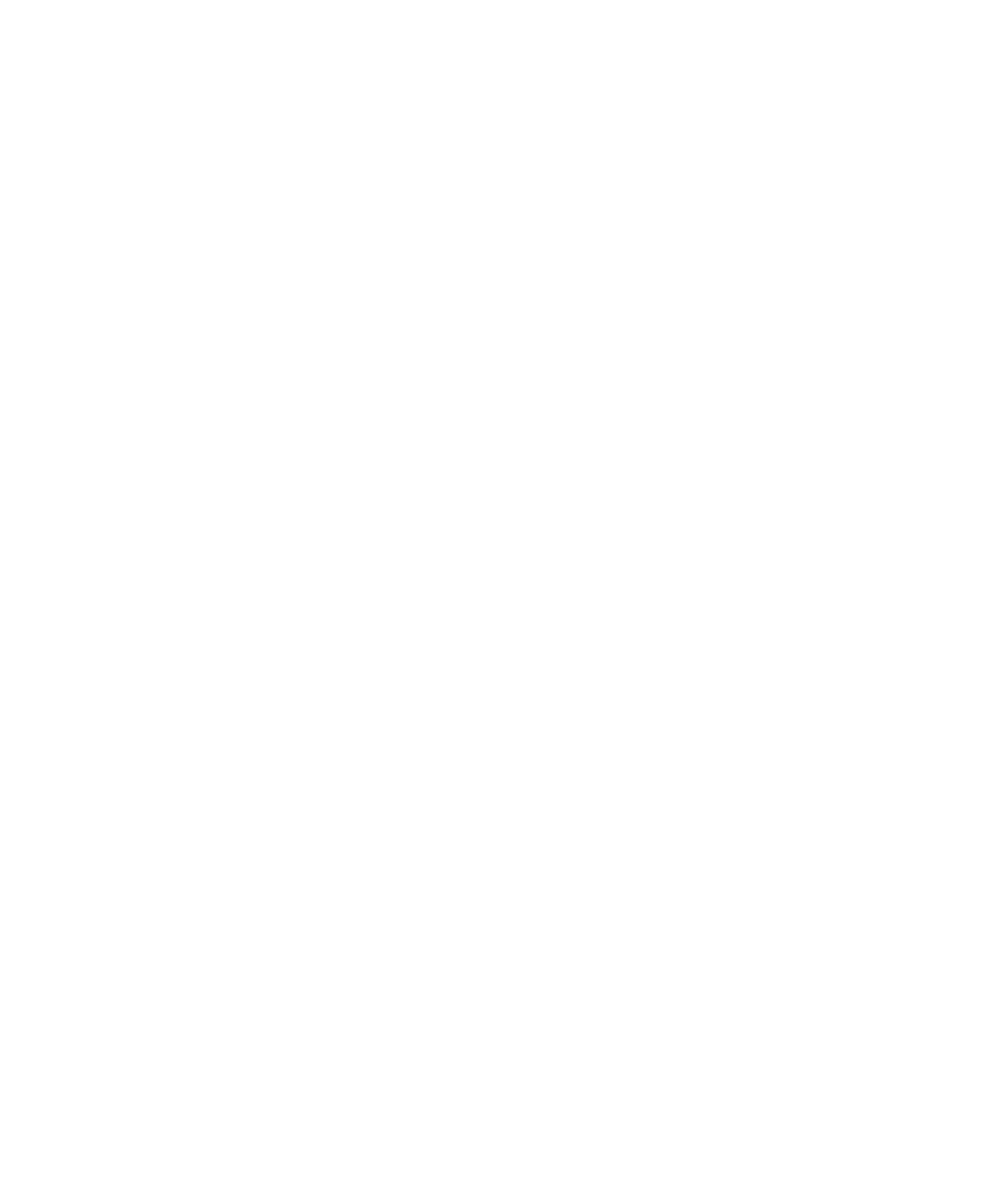
the future of near infrared astronomy

by Kieran Leschinski

In memoriam patris meae

“In theory, this is complicated, and in practice it is even more difficult.”

GMT consortium on polishing aspherical 8 m-class mirrors

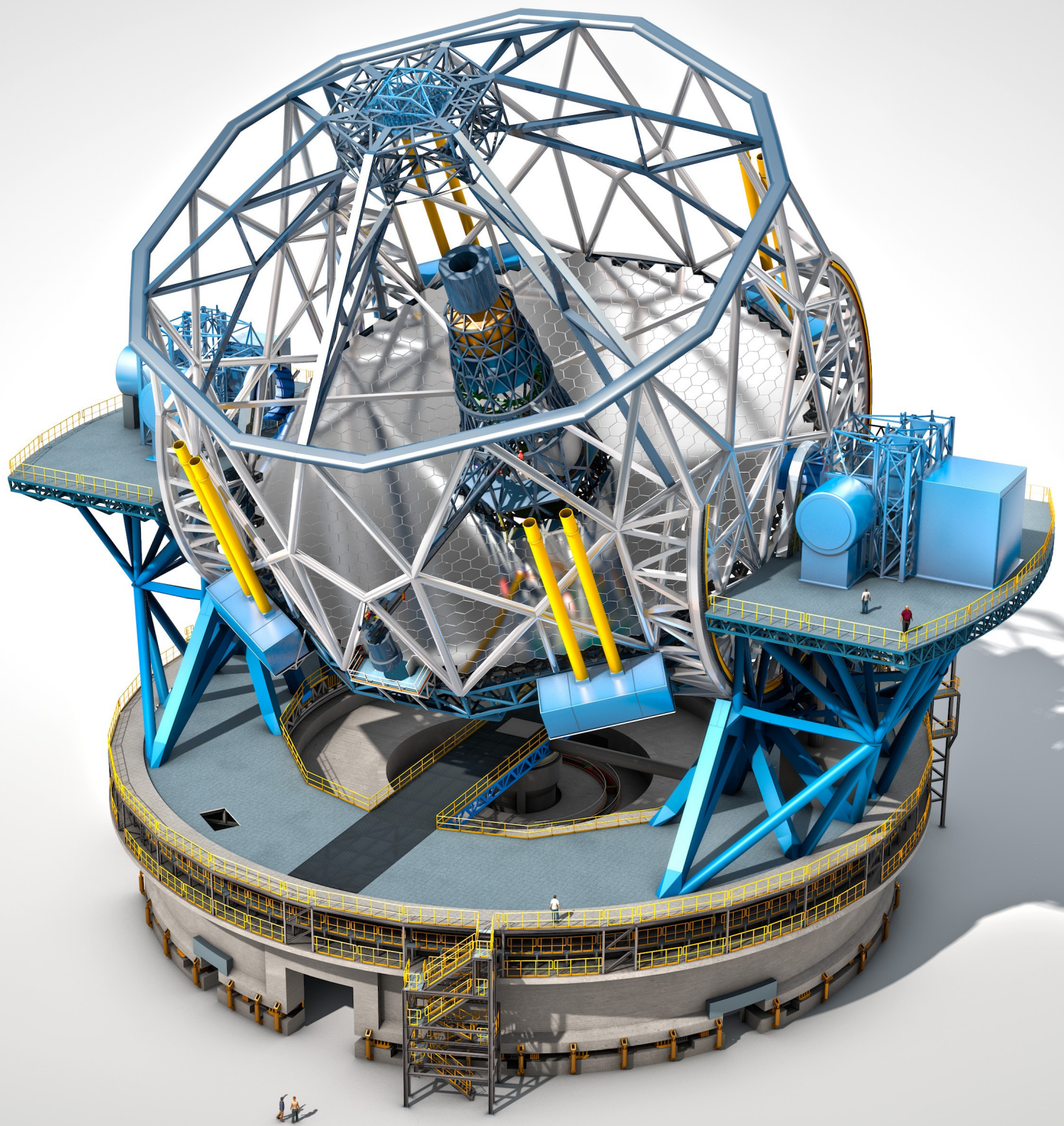


Credit: Image courtesy of ESO. An artists impression of the ELT during operations at night time. The laser guide stars can be seen emanating from the corners of the telescope. The lasers are tuned to reflect off the ionised sodium layer at around 90km altitude. The ELT's adaptive optics systems will use these artificial stars to map the turbulence in the atmosphere and alter the shape of the deformable mirrors on millisecond time scales to correct for this. This will allow the ELT to take full advantage of the resolution provided by a 39 m primary mirror.



An artist's impression of the European Extremely Large Telescope (ELT) structure. The image shows a massive, white, multi-tiered optical telescope mounted on a large, circular concrete foundation. The central support tower is tall and cylindrical, with several smaller platforms extending from its sides. The main mirror, consisting of numerous small segments, is visible at the bottom left. The entire structure is set against a dark, star-filled background.

Credit: Image courtesy of ESO. A artists impression of the structure of the ELT. The 39 m segmented primary mirror is clearly visible as is the support tower in the centre. The support tower houses the tertiary (M3), quartary (M4), and quinary (M5) mirrors. On either side of the telescope are the Nasmyth platforms where the suite of instruments will be installed. MICADO will be situated directly behind the straight-through port and underneath the relay optics bench - about where the square box is on the right platform. Each of the Nasmyth platforms has a footprint as large as any single unit telescope from the VLT. When in operation the entire 5000 tonne main strucutre will rotate to counteract the natural rotation of the night sky.



Abstract

The era of the extremely large telescopes will soon be upon us and with it the ability to observe smaller, fainter and more distant objects than ever before. Such revolutionary facilities will open up whole new parameter spaces to astronomers. With the almost 40 m main mirror of the European extremely large telescope it will be possible to directly detect extra-solar planets, to observe the environments immediately surrounding super-massive black holes, chart the motions of the stars closest to the centre of the Milky Way, and to resolve the structure of the universe's very first galaxies. Indeed many of the discoveries that will be made with this new telescope have not yet been imagined.

MICADO will be the first-light near-infrared wide-field camera for ESO's extremely large telescope, providing diffraction limited imaging over a 50 arcsec field of view. During the development of such an instrument it is imperative that all parties (e.g. the design, calibration, and science teams) have a platform with which to exchange information regarding the current state of the instrument. With this in mind I have developed an instrument data simulator for MICADO: SimCADO. This software package allows users to simulate realistic observations with MICADO and the ELT well in advance of the observatory going on sky. Not only will it be useful for the development of the MICADO data flow systems, the ability to simulate observations will allow astronomers to conduct feasibility studies for proposed future observations. The earlier such studies are carried out, the more preparation work can be done to ensure the scientific output of MICADO and the ELT is maximised.

In this doctoral thesis I present in detail the design and implementation of the SimCADO software package. I show how the software can model the current design of the ELT/MICADO optical system, as well as how I verified the accuracy of the simulations against real data by configuring the software to simulate the VLT/HAWKI optical system. I also describe three applications of the software in the context of both astronomical research and instrument design. These include: 1) how SimCADO can be used to predict the sensitivity limits (both bright and faint) of the ELT/MICADO system, 2) how I used SimCADO to simulate many different dense stellar fields akin to star formation regions in order to determine the limits of future studies into the stellar initial mass function, and 3) how SimCADO can

help determine the most cost effective and efficient way to manufacture the set of MICADO filters in order to meet the requirements for photometric precision.

The SimCADO software is nearing maturity but can already be used to simulate the imaging modes of MICADO. In this thesis I also present a detailed road-map for the continued development of the software. SimCADO will be a very useful tool when it comes to observations with MICADO and the ELT, and it is my hope that it soon finds its way into the standard toolbox of every near infrared astronomer.

Kurzfassung

Die Ära der Riesenteleskope steht vor der Tür. Sie wird uns ermöglichen, Himmelsobjekte zu beobachten, die kleiner, leuchtschwächer und weiter entfernt sind als je zuvor. Mit diesen revolutionären Einrichtungen eröffnen sich komplett neue Parameter Räume für Astronomen. Mit dem circa 40 m Hauptspiegel des European extremely large telescope wird es möglich sein, Exoplaneten direkt zu finden, die unmittelbare Umgebung von supermassiven schwarzen Löchern zu beobachten, die Bewegung von Sternen im Zentrum der Milchstraße aufzuzeichnen und die Struktur der ersten Galaxien des Universums aufzulösen. Mit diesem Teleskop werden wohl viele Entdeckungen gemacht werden, die sich heute noch niemand vorstellen kann.

Bei MICADO handelt es sich um die erste weitwinkel nahinfrarot Kamera des ELT (Extremely Large Telescope) der ESO, welche beugungsbegrenzte Bilder mit einem Blickwinkel von über 50 Bogensekunden liefern sollte. Während der Entwicklungsphase von solchen riesigen Instrumenten ist es nicht nur praktisch, sondern notwendig, eine Plattform zu haben, die allen Projektbeteiligten einen Austausch von Information bezüglich des neuesten Standes des Instruments ermöglicht und diesen fördert. In diesem Rahmen wurde das Instrument Data Simulator Softwarepaket namens SimCADO entwickelt. Dieses Softwarepaket erlaubt es den Benutzern realistische Beobachtungen mit MICADO und dem ELT zu simulieren, lange bevor sie in Betrieb genommen werden. Es wird nicht nur für die Entwicklung von MICADO Datenstromsystemen nützlich sein, sondern die Möglichkeit Beobachtungen zu simulieren wird es Astronomen erlauben Machbarkeitsstudien für geplante zukünftige Beobachtungen zu erstellen. Je früher solche Studien erstellt werden können, desto mehr Vorbereitungsarbeit kann gemacht werden um sicher zu stellen, dass MICADO und ELT effizient genutzt werden.

In dieser Dissertation werden das Design, die Implementierung, und drei Anwendungsbeispiele des Softwarepaketes präsentiert. Es wird gezeigt, wie die aktuellste Version des optischen Systems von ELT/MICADO mit SimCADO modelliert werden kann, und auch wie ein Vergleich zwischen simulierten Daten und echten Daten des VLT/HAWKI Instruments verwendet wurde, um die Genauigkeit der Software zu verifizieren. Die folgenden drei Anwendungen der Software werden beschrieben: 1) wie mit SimCADO die Empfindlichkeitsgrenze in Bezug auf die Leuchtstärke

für das ELT/MICADO system vorhergesagt werden kann, 2) anhand von mit SimCADO simulierten Beobachtungen kann bestimmt werden, wo die Grenzen der nächsten Generation von Beobachtungen der sogenannten ursprünglichen Massenfunktion liegen, und 3) wie die Anwendung von SimCADO die effizienteste und kostengünstigste Anschaffung des MICADO Filtersatzes ermöglicht.

Die SimCADO Software wird immer ausgereifter und kann schon dazu verwendet werden, die Imaging-modi von MICADO zu simulieren. In dieser Doktorarbeit wird außerdem eine detaillierte Roadmap für die weitere Entwicklung dieser Software präsentiert. SimCADO wird ein sehr nützliches Werkzeug für Beobachtungen mit MICADO und ELT und hoffentlich wird es bald zu den Standard Programmen für jeden Nahinfrarot Astronomen gehören.

Contents

Abstract	i
Kurzfassung	iii
1 Introduction	1
1.1 The current state of near infrared astronomy	1
1.2 The era of the extremely large telescopes	4
1.2.1 The European Extremely Large Telescope	5
1.2.2 The ELT mirror design	5
1.2.3 The ELT instrumentation	7
1.3 MICADO - the Multi-AO Imaging Camera for Deep Observations	9
1.3.1 Science drivers for MICADO	10
1.3.2 MICADO design	12
1.3.3 MICADO observing modes	17
1.4 SimCADO - the instrument data simulator for MICADO	18
1.5 Goals of the Thesis	19
1.6 Thesis Overview	21
2 SimCADO - an instrument data simulator package for MICADO at the E-ELT	23
2.1 Overview	23
2.2 Publication Details	24
2.3 Introduction	25
2.4 SimCADO - the data simulation effort for MICADO	26
2.4.1 SimCADO user groups	26
2.4.2 Design requirements for SimCADO	27
2.4.3 Imaging vs Spectroscopy	28
2.5 Data model behind SimCADO	29
2.5.1 A note on SimCADO's internal representation of spectral data	29
2.5.2 The main classes of the SimCADO user interface	29
2.5.3 An short example of using the main SimCADO classes	32
2.5.4 Method behind applying an OpticalTrain	33

2.5.5	Generating input for simulations	34
2.5.6	Modules behind the scene	36
2.6	Modelling the optical path	36
2.6.1	Representing elements in the optical train in SimCADO	36
2.6.2	Aspects of the optical train to be included in later releases	38
2.7	Conclusion	39
2.8	Acknowledgements	39
2.9	References	39
3	Verifying SimCADO and Predicting MICADO limiting magnitudes	43
3.1	Overview	43
3.2	Publication Details	44
3.3	Introduction	45
3.4	SimCADO - the Python package for simulating MICADO imagery	46
3.4.1	Motivation and Scope	46
3.4.2	The SimCADO audience	46
3.4.3	SimCADO as an Instrument Data Simulator	47
3.5	The physical effects modelled by SimCADO	47
3.5.1	Atmosphere	47
3.5.2	The ELT	48
3.5.3	MICADO	50
3.5.4	MICADO Detector Array	51
3.6	Validating SimCADO with raw HAWK-I data	51
3.6.1	Modelling HAWK-I with SimCADO	52
3.6.2	HAWKI-I Sensitivity with SimCADO	52
3.6.3	Comparison of SimCADO images with real observations	52
3.7	Predictions for MICADO’s point source sensitivity	54
3.7.1	Point source sensitivity vs exposure time	54
3.7.2	Point source saturation limits	54
3.7.3	Spectral type with distance	57
3.8	Discussion, open issues and assumptions	58
3.8.1	Discussion on the differences between the simulated and the real HAWK-I images	58
3.8.2	Accuracy of the SimCADO sensitivity predictions	59
3.8.3	Future functionality for SimCADO	60
3.9	Summary	61
3.10	References	61

3.11 Appendix A: Distance estimates for main sequence stars in KS band	63
3.12 Appendix B: Comparison of the HAWK-I and MICADO configuration files	63
4 Science use case: Studying the initial mass function with MICADO	65
4.1 Overview	65
4.2 Publication Details	68
4.3 Introduction	71
4.4 Data sets	72
4.4.1 Parameter Space	72
4.4.2 Artificial clusters	73
4.4.3 Observations	73
4.4.4 Source extraction and matching	74
4.5 Results and Discussion	74
4.5.1 Lower observable masses for given star densities	74
4.5.2 The cores densities of young star clusters	75
4.5.3 Application to observable young clusters	76
4.6 References	77
5 Optimal filter design for MICADO with SimCADO	83
5.1 Overview	83
5.2 Publication Details	84
5.3 Executive Summary	87
5.4 Applicable documents and references	87
5.5 Definitions	88
5.6 Context	88
5.7 Data	89
5.7.1 Spectra	89
5.7.2 Filter Set	89
5.8 Method	90
5.8.1 Total wing flux leakage	90
5.8.2 Splitting the red wing into near-red and thermal-red windows	93
5.9 Results	95
5.9.1 Transmission coefficients excluding a thermal-red blocking filter	96
5.9.2 Transmission coefficients including a thermal-red blocking filter	98
5.10 Summary	99
5.11 Ideas for future experiments	100

6 Future Work	103
6.1 SimCADO Road Map	103
6.1.1 Future functionality for SimCADO	105
6.1.2 Additional observing modes	108
6.1.3 General ELT first-light simulation package	109
6.2 Detailed verification of various atmospheric components with HAWKI109	109
6.3 Science feasibility studies with SimCADO	111
6.3.1 The shape of the IMF	111
6.3.2 Variation in the IMF of the Galactic centre (and elsewhere) .	112
6.3.3 The spatial structure of star formation in the early universe .	113
7 Summary and Conclusion	115
7.1 Summary	115
7.1.1 The design of SimCADO	115
7.1.2 Verifying SimCADO and predicting MICADO sensitivity levels	116
7.1.3 Observational limits of future IMF studies with SimCADO .	118
7.1.4 Determining the optimal filter coating design for MICADO .	119
7.1.5 Future work with SimCADO	120
7.2 Concluding remarks	121
References	123
A HAWK-I observing proposal to verify SimCADO	131
A.1 Overview	131
A.2 Submission Details	131
B ADASS Conference Proceedings	141
B.1 Astronomical Data Analysis Software and Systems 2015	141
B.2 Astronomical Data Analysis Software and Systems 2016	146
B.3 Quotes which did not reach the title page	151

List of Figures

0.1	The ELT at night	7
0.2	The ELT structure	9
1.1	The ELT optical design	6
1.2	The MICADO optical design	13
2.1	SimCADO data model	28
2.2	Simulated star cluster	33
2.3	Simulation work flow	35
3.1	Default transmission and emission curves	48
3.2	ELT pupil and PSF	49
3.3	MICADO detector field of views	51
3.4	HAWK-I sensitivity plot	52
3.5	2MASS vs SimCADO aperture photometry	54
3.6	HAWK-I vs SimCADO aperture photometry	55
3.7	HAWK-I vs SimCADO image comparison	56
3.8	MICADO sensitivity predictions	57
3.9	Spectral types vs distance J band	59
3.10	Dense stellar cluster comparison	60
3.11	Spectral types vs distance Ks band	64
4.1	The shape of the two most popular IMF formalisms	66
4.2	Cluster densities with distance	73
4.3	Lowest observable mass with distance	75
4.4	Core densities of observable clusters	76
4.5	Results for 1 000 stars arcsec ⁻² cluster	80
4.6	Results for 10 000 stars arcsec ⁻² cluster	81
5.1	Spectra and filter transmission curves	89
5.2	Wing transmission vs Fractional flux increase	91
5.3	Example of total leakage for different blocking coefficients	92

5.4	Where the thermal red filter should start	94
5.5	Example of total leakage with thermal red filter	94
5.6	Transmission coefficients excluding a thermal-red blocking filter	96
5.7	Total leaked flux excluding a thermal-red blocking filter	97
5.8	Transmission coefficients including a thermal-red blocking filter	98
5.9	Total leaked flux including a thermal-red blocking filter	99

List of Tables

1.1	Surfaces in the ELT/MICADO optical train	14
2.1	Core and optional python dependencies for SimCADO	27
2.2	Elements of the optical train emulated by SimCADO	31
3.1	SimCADO RMS Wavefront errors	50
3.2	Comparison of HAWK-I detection limits	53
3.3	List of HAWK-I archive images	53
3.4	MICADO sensitivity predictions	58
3.5	MICADO saturation predictions	58
4.1	List of extragalactic IMF studies	72
4.2	Core densities bases on tidal radius	79
5.1	List of applicable documents and references	87
5.2	List of definitions	88
5.3	Filter characteristics	90
5.4	Total leaked flux for example blocking coefficients	92
5.5	Leakage from required vs optimised blocking coefficients	93
5.6	Leakage from required vs optimised blocking coefficients with a thermal red filter	95
5.7	Summary table with leaked flux from optimised blocking coefficients	100
6.1	SimCADO roadmap	104

Introduction

1.1 The current state of near infrared astronomy

Near infrared astronomy is currently enjoying a heyday: a period of great vigour, strength, and success¹. Over the last 20 years major advances in infrared detector technology have led to the realisation within the astronomical community that, in many cases, infrared observations deliver superior science compared to optical observations. This has led to great interest and investment in infrared observing infrastructure. Many of the major breakthroughs in Galactic centre astronomy, high redshift galaxies, star formation, the interstellar medium, brown dwarfs, and exoplanets owe their success to infrared observations, and the techniques behind these observations.

The Galactic centre for example is hidden behind an almost 30 magnitudes thick wall of dust and gas at optical wavelengths. Even if a telescope large enough to peer through these clouds existed, the central parsec is so densely populated that seeing limited telescopes would never be able to resolve the individual stars in this region. Tracing the orbits of the stars closest to the supermassive black hole at the Galactic centre and hence determining its position (see e.g. [Ghez et al. 2000](#); [Eckart and Genzel 1996](#)) was only possible because: 1) the dust and gas are an order of magnitude more transparent in the near infrared ([Rieke and Lebofsky 1985](#)), and 2) near infrared adaptive optics systems are capable of providing diffraction limited imaging for the current generation of 8 m and 10 m-class telescopes.

Near infrared astronomy has also enabled the detection of galaxies from the first billion years of the universe's history, corresponding to redshifts greater than $z > 6$. At these redshifts the Lyman- α emission line is shifted into the NIR wavelength range ($\lambda > 850\text{nm}$). This means that the Lyman- α line of early universe galaxies vigorously forming stars (so-called Lyman- α emitters, or LAEs) is only detectable

¹<http://www.dictionary.com/browse/heyday>

with NIR spectrographs. So-called Lyman break galaxies (LBG) show a stark drop-off in flux around the Lyman- α line. There are several reasons for the natural flux barrier (see the review by [Dunlop 2013](#)), however this barrier also moves out of the visible and into the infrared range for redshifts greater than $z > 6$. Without infrared observations these galaxies would be much more difficult to detect and the $z > 6$ universe would in general be much more difficult to explore.

The advantage of infrared observations in the field of exoplanets is most obvious when the intrinsic temperature difference between stars and planets is considered. The blackbody emission of solar and super-solar mass stars ($T > 4000$ K) peak in the visual (and ultraviolet) wavelength ranges. The low surface temperatures of exoplanets (relative to their host stars) mean that their blackbody peaks generally fall in the mid-infrared wavelength range ($3 < \lambda < 20\mu\text{m}$). Direct observations of exoplanets are therefore easiest in the mid-infrared where the contrast between stars and planets is lowest. Additionally the small on-sky angular distances between exoplanets and their host stars mean that observations benefit greatly from the AO-assisted diffraction limited images that are (currently) only available at infrared wavelengths.

Although the existence of infrared radiation has been known since [Herschel \(1800\)](#) experimented with a prism and a “Dr. Wilson’s sensible thermometer”², the development of modern detector technology has largely been driven by military research. Fortunately for astronomy, this has led to a rapid increase in the size and quality of infrared detector arrays over the last half a century. HgCdTe detector arrays can nowadays be reliably produced in arrays of 2048×2048 pixels, with the next generation of 4k arrays already under development ([Hall 2011](#)). Such large arrays have made it possible for large portions of the infrared sky to be mapped. For example OmegaCAM on the VISTA survey telescope at Paranal uses an array of sixteen 2k chips to cover an area of 1.6 degrees in a single image (e.g. [Meingast et al. 2016](#)).

As mentioned above the invention of adaptive optics (AO) systems has vastly improved the performance of ground-based infrared observations. Turbulence in the atmosphere deforms the incoming wavefront of light. By using a series of

²This is not a typo. In Herschel’s paper from 1800 he distinctly refers to his control thermometer by the full product name: A “Dr Wilson’s sensible thermometer”, named after a physician in Glasgow who manufactured thermometers at the time.

wavefront sensors combined with actuators placed behind one (or more) of the mirrors in the optical train, these wavefront deformations can, to a large extent, be corrected. Several natural and mechanical factors mean that AO systems function better at longer wavelengths. For example (see [Max 2009](#)): the atmospheric refractive index decreases with wavelength; the atmospheric coherence length increases with wavelength, and hence the relative wavefront distortions decrease with wavelength; the speed and magnitude of wavefront variations reduces with wavelength, and the larger PSF FWHM requires less high frequency modes on the deformable mirror; this results in slower response times needed by the control electronics, and more relaxed step size requirements of the deformable mirror actuators. All of these effects conspire against better performance of adaptive optics systems at shorter wavelengths. By incorporating deformable mirrors with AO control systems into the current 10 m-class telescopes, observations can be routinely conducted at the diffraction limit (~ 50 mas) of these telescopes (see e.g. VLT/NACO [Rousset et al. 2003](#), Keck [Wizinowich et al. 2000](#), Gemini [Rigaut et al. 2012](#)).

The current generation of 10 m-class telescopes have been in operation for almost 20 years. Over much of the last decade large consortia and organisations have been designing the next generation of “extremely large” telescopes with primary mirror diameters ranging from 25 m at the giant Magellan telescope (GMT, [McCarthy et al. 2016](#)) to 38 m at the European extremely large telescope (ELT, [Gilmozzi and Spyromilio 2007](#)). The largest of these, the ELT, will enable a factor of five increase in resolution thanks to the various adaptive optics systems that will be available. All three first light instruments are being designed to work in the infrared, with only one (HARMONI) being at all sensitive to visual wavelengths. The James Webb space telescope (JWST), the successor to Hubble, has also been designed to work almost exclusively in the near and mid infrared regimes³. It is therefore easy to see why infrared observations will play a major, if not premier, role in the future of astronomy. With this in mind the next few sections are devoted to introducing the telescope and the instrument which will undoubtedly be two of the greatest assets to astronomers for decades to come: the Extremely Large Telescope and its near infrared imaging camera MICADO.

³The JWST instruments can technically be used at visual wavelengths, however this is limited to wavelengths longer than 600 nm

1.2 The era of the extremely large telescopes

The field of optical and infrared astronomy is currently split between large 10 m class ground based telescopes (e.g. The VLT unit telescopes, Keck, Subaru, etc.) and smaller space based telescopes (e.g. Hubble, Spitzer). These facilities provide amazing images of the universe, however they each have their limits. The space based facilities are limited by the diffraction limit of the primary mirror. The Hubble Space Telescope (HST) has a mirror diameter of 2.4 m and therefore a diffraction limit around 100 mas in the near infrared ($\sim 1.2 \mu\text{m}$) and around 50 mas in the visible ($\sim 550 \text{ nm}$) wavelength range. However the lack of atmosphere means that Hubble can observe sources as faint as $I \sim 28^{\text{m}}$, given a long enough exposure time. Because the 10^m class ground based telescope have primary mirrors $\sim 3\text{-}4\times$ larger than Hubble, their theoretical diffraction limit is also $\sim 3\text{-}4\times$ smaller. Unfortunately the dynamic nature of the atmosphere prevents most 10 m class telescopes from ever reaching their full diffraction limited imaging potential. The angular resolution of ground-based telescopes is therefore dependent on the atmospheric Seeing, rather than the physical diffraction limit of the atmosphere. Over the last 20 years adaptive optic systems (e.g. NAOS, GeMS, MAD, etc.) have been developed to counteract the effect of the atmosphere. This has allowed many of the largest telescopes to achieve various levels of diffraction limited imaging in the near infrared wavelength ranges. However due to the presence of a warm atmosphere, the level of background flux limits the sensitivity of these telescopes. For example, NACO has a limiting magnitude of $J \sim 24^{\text{m}}$ for a 1 hour observation ([Rousset et al. 2003](#)).

When they first came online, this generation of telescopes revolutionised the field of astronomy. Astronomers could see fainter objects much clearer than ever before. However twenty years have passed since the 8-10 m class telescopes took the stage and much of the discovery space opened up by these telescopes has been filled. It could be argued that we now understand the near infrared universe pretty well on scales of $\sim 100 \text{ mas}$, and in order to make major progress we need another order of magnitude increase in resolving power.

Enter the era of the extremely large telescopes. Shortly after the completion of the VLT facility at Paranal, the European astronomical community began planning

the next generation of telescopes. A series of grand designs were put forward by the community which eventually lead to the decision by ESO in 2006 to study the feasibility of a 40 m class telescope. The European Extremely Large Telescope was born.

1.2.1 The European Extremely Large Telescope

Known as the E-ELT until June 2017, and now just simply the ELT, its 39 m primary mirror will allow astronomers to resolve the optical and near infrared universe at scales $15\times$ smaller than achievable with Hubble and $5\times$ smaller than with the current 8-10 m class telescopes. Additionally the collecting power of the 978 m^2 mirror will finally allow ground-based observations to exceed the sensitivity of Hubble. Such observing capabilities will open up whole new parameter spaces. With the ELT it will be possible to directly detect extra-solar planets, to observe the environments immediately surrounding super-massive black holes, and to resolve the structure of the universe's very first galaxies. Indeed many of the discoveries that will be made with this new telescope have not yet been imagined.

The ELT will follow a 5-mirror anastigmatic design in order to assure the best optical quality over a large ($\sim 10'$) field of view. The two adaptive mirrors (M4 and M5) will be directly connected to the adaptive optics relay. They will be responsible for flattening the wavefront and removing the atmospheric seeing component of the point spread function (PSF). The fifth mirror will also be capable of directing light to instruments located either side of the telescope at the two Nasmyth foci. Three instruments sensitive to the visible ($0.4\text{ }\mu\text{m} < \lambda < 0.8\text{ }\mu\text{m}$), near infrared ($0.8\text{ }\mu\text{m} < \lambda < 3\text{ }\mu\text{m}$) and mid infrared ($3\text{ }\mu\text{m} < \lambda < 20\text{ }\mu\text{m}$) will be available from first light, alongside a multi-conjugate adaptive optics system.

1.2.2 The ELT mirror design

The segmented mirror design used by several of the largest 10 m class telescopes (e.g. Keck, GranTeCan) has paved the way for manufacturing primary mirrors of almost any size. The ELT's primary mirror (M1) will consist of 798 hexagonal segments (see Figure 1.1 for a graphical representation of the mirror design⁴).

⁴<https://www.eso.org/public/images/eso1704a/>

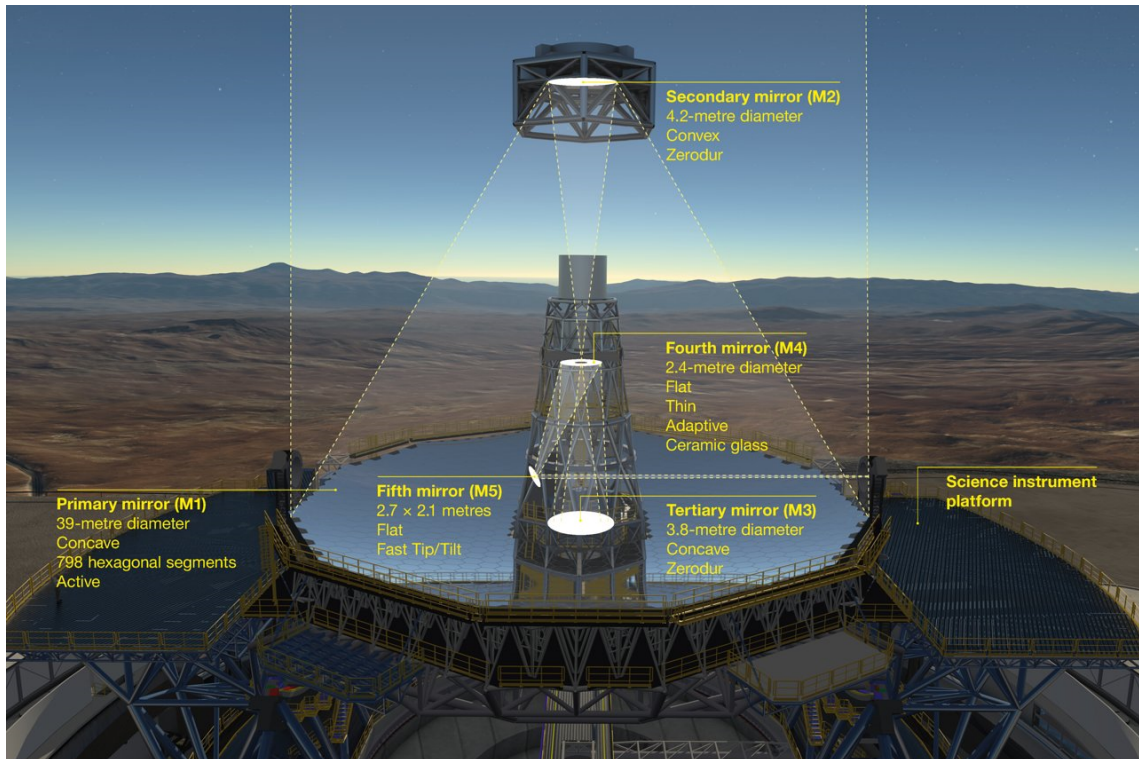


Figure 1.1. Credit: Courtesy of ESO. The ELT optical design. The first three mirrors direct incoming light towards the quaternary mirror (M4). Here approximately 8000 actuators will remove the distortions in the wavefront caused by upper atmospheric turbulence by deforming the mirror's surface on millisecond time scales. The quinary mirror (M5) removes the ground-layer component of the wavefront through its function as a tip-tilt mirror and directs the incoming light to one of the two pre-focal stations on the Nasmyth platforms.

These segments will be grouped into 6 sections, with each section corresponding to a 60° area falling between the spider arms of the secondary mirror support structure. Each of the 798 segments will be individually steerable in order to allow for fine tuning of the mirror alignment. The secondary (M2) and tertiary (M3) mirrors will be 4 m class mirrors, with the secondary suspended ~ 20 m above the primary mirror. The quaternary (M4) will be the primary deformable mirror and will be conjugated to the main upper atmospheric turbulence layer. It will contain ~ 8000 actuators and will be continually deformed every few milliseconds in order to counteract the dynamic nature of the wavefront due to the effects of the upper atmosphere. In order to avoid over extending the actuators and introducing high levels of stress into the glass, M4 will also be segmented. Similar to the primary mirror, M4 will be split into 6 arc-like petals, each matching a 60° section of the primary mirror. The quinary (M5) will be a flat mirror with tip-tilt functionality. It will be responsible for removing the disturbances caused by the ground layer of the atmosphere and for directing the incoming light to either of the Nasmyth platforms.

As it will be impossible to re-coat all 798 segments at once, several segments will be removed on a daily basis for re-coating. The original plan for the ELT called for a 7th section worth of mirror segments to be manufactured. This would allow each segment being sent for re-coating to be immediately replaced, thus avoiding any gaps in the primary mirror. Due to cost concerns at the time of writing the procurement of this 7th section has been delayed. While not critical to the operation of the telescope, the missing segments will surely introduce artefacts to the point spread function. Exactly how detrimental this will be for certain science cases still needs to be investigated though.

1.2.3 The ELT instrumentation

At the time of writing the construction of the ELT has begun. The mountain top at Cerro Armazones has been cleared and the observatory's foundations are being laid. Work has commenced on the design and construction of the dome and the main structure. ESO has also signed contracts for the production of the first six sections worth of primary mirror segments, as well as for the sensor systems for the mirror support structures. The contract for the polishing of the secondary mirror has also been awarded.

The first light instruments have been chosen and the memoranda of understanding have been signed with the responsible consortia. These instruments will be:

MICADO - Multi-AO Imaging Camera for Deep Observations

The first light diffraction limited imaging camera for the ELT ([Davies et al. 2010](#)). MICADO will be sensitive to the near infrared wavelength range ($0.8\mu\text{m} < \lambda < 2.35\mu\text{m}$) and will cover the standard suit of wide and narrow band filters (e.g. J, H, K_S, Pa β , Br γ). MICADO will offer two imaging modes: wide-field mode with a 4 mas plate scale and a $\sim 50''$ field of view, and zoom mode with a 1.5 mas plate scale and a $\sim 20''$ field of view, suitable for astrometric imaging. There will also be a long slit spectroscopic mode with a spectral resolution of up to $R \sim 8000$. MICADO will be discussed in much greater detail in Section [1.3](#).

HARMONI - The High Angular Resolution Monolithic Optical and Near-infrared Integral field spectrograph

The work-horse spectrograph for observations in the visible and near-infrared range ($0.47\mu\text{m} < \lambda < 2.45\mu\text{m}$) - see [Thatte et al. \(2010\)](#). It will be an integral field spectrograph providing an array of 152x206 with spatial resolutions ranging from 4 mas to 60 mas depending on the required field of view. Each spaxel will have a spectral resolution of up to $R \sim 18000$ in the infrared and $R \sim 3500$ in the visible range.

METIS - The Mid-infrared ELT Imager and Spectrograph

The mid-infrared instrument for the ELT, described in [Brandl et al. \(2016\)](#). METIS will be a jack-of-all-trades, providing imaging and spectroscopic capabilities in the wavelength range $3\mu\text{m} < \lambda < 19\mu\text{m}$. Diffraction limited imaging and long slit spectroscopy will be possible over the whole wavelength range. The imaging mode will have a field of view of $\sim 11''$ while the long slit will provide a spectral resolution on the order of $R \sim 10^3$. Additionally a high resolution integral field spectrograph will be included to provide $R \sim 10^5$ spectra for specific $\Delta\lambda \sim 50\text{ nm}$

bandpasses in the wavelength range $3\mu\text{m} < \lambda < 5\mu\text{m}$. METIS has been nicknamed the “Planet Hunter” because it offers the best chance for astronomers to directly detect and study planets, and their atmospheres, orbiting around other stars.

The relatively small fields of view of HARMONI and METIS ($\sim 10''$) mean that these instruments will work well with relatively simple adaptive optics solutions. Consequently the respective consortia are developing their own solutions in house. MICADO, and indeed any future instrument that wishes to observe over a wider field of view (e.g. more than $30''$), will suffer from excessive degradation of the PSF with increasing distance from the guide star(s). In order to provide a relatively homogeneous Strehl ratio over the full field of view, the ELT will also include a dedicated multi-conjugate adaptive optics system by the name of MAORY (Multi-conjugate Adaptive Optics RelaY for the ELT). The MAORY module ([Diolaiti 2010](#)) will include a second deformable mirror and will therefore be able to correct for wavefront deviations not accounted for by the ELT’s own deformable mirror (M4). MAROY will use up to 3 natural guide stars (NGS) and the 6 laser guide stars (LGS) of the ELT to track and further correct the wavefront allowing diffraction limited imaging over the full two arcminute field of view.

With all the development work currently under way it is not improbable that the ELT will be on sky by the end of 2024 and providing the first science observations during 2025.

1.3 MICADO - the Multi-AO Imaging Camera for Deep Observations

As the name suggests MICADO will be “the” standard imaging camera for the ELT. It’s not difficult to see why: It has the largest field of view of all three first light instruments, it will provide diffraction limited imaging capabilities, astrometric and coronagraphic imaging modes, possibly fast ($\sim 10\text{s of ms}$) windowed imaging mode, as well as long slit spectrographic modes. MICADO will also be able to take advantage of the MAORY ([Diolaiti et al. 2016](#)) multi-conjugate adaptive optics (MCAO) module once it is installed at the telescope. By using the stand-alone single conjugate adaptive optics (SCAO) module, MICADO should provide Strehl ratios as high as $\sim 70\%$ in the Ks ($\lambda \sim 2.2\mu\text{m}$) band, albeit only over very small ($\sim 5\text{-}10''$)

distances from the guide star. With the MCAO module the peak performance will decrease, however, a more or less constant Strehl ratio ($>30\%$) is to be expected over the full $\sim 50''$ field of view. The detector array will consist of 9 HAWAII-4RG chips, each with 4096×4096 pixels. The 978 m^2 area of the ELT's primary mirror will allow MICADO to reach a detection limit of $>29^{\text{m}}$ in AB magnitudes for the J, H and K_S filters. All of these characteristics combined will open up a completely new observation space in which major discoveries can be made.

1.3.1 Science drivers for MICADO

The key science drivers for MICADO cover a broad range of important astrophysical topics. The fact that MICADO is such an all-purpose instrument and can be used for almost any science case, played a large role in MICADO being chosen as one of the first light instruments for the ELT. Several of the main areas in astronomy for which MICADO will provide answers are listed below⁵:

The Galactic Centre is our primary laboratory for studying general relativity. By studying the orbits of the stars closest to the supermassive black hole at the centre of our own galaxy we are able to better understand many of the more subtle aspects of Einstein's theories of relativity. Additionally, MICADO's sensitivity to faint sources will allow us to finally investigate the low mass population of the galactic centre and to start answering questions like: did these stars form in situ? And if so, how does the high gravitational potential so close to the supermassive black hole affect star formation processes?

The formation and evolution of galactic nuclei and black holes appear to be intrinsically linked to the evolution of the galaxy as a whole. Thus in order to understand the past, present and future of galaxies, it is fundamental to understand the engines at their centres. MICADO should allow us to put constraints on the parameters which describe galactic nuclei such as the morphology, colour gradient, stellar population, and luminosity function for these regions.

Galaxy Evolution over cosmic time is essential to our understanding of how the current universe formed. Yet there are still many open questions like: At what point

⁵The material from this section is presented in much more detail in the MICADO primary science case document.

do the different aspects of a galaxy, like thin and thick disks, bulges and globular clusters, form? What role do mergers play in the growth and early evolution of galaxies? How were the first galaxies formed? Early universe galaxies were much smaller than today's galaxies, with diameters on the order a kiloparsec. At a redshift of $z \sim 2$ this equates to about 0.1", or the diffraction limit of Hubble. MICADO will offer us the same or greater sensitivity than Hubble, yet it will be able to resolve structures $15\times$ smaller. This will allow astronomers to study in detail the structure and spatial extent of the processes involved in the early evolution of the first galaxies.

Astrometry of Globular Clusters and Dwarf Spheroidal Galaxies gives us the possibility to search for the long fabled intermediate mass black hole (IMBH). Owing to MICADO's ability to resolve objects on the 10 mas scale, it will be possible to map the kinematics of a large portion of stars in the cores of both globular clusters and dwarf spheroidal galaxies with an optimistic precision of down to $50\mu\text{as yr}^{-1}$. This will allow astronomers to determine the mass profiles and gravitational potentials of not only these central regions, but of the clusters and galaxies as a whole, and allow us to map the stellar and dark matter content as well as narrow down possible locations of IMBHs.

Resolved stellar populations tell us more about the history of a galaxy than any other indicator. The composition of stars in different populations tells us about the metallicity of the galaxy at the time they formed and their relative numbers can tell us how vigorously the galaxy has formed stars during different epochs in the past. Additionally the youngest population of a galaxy is not only an excellent indicator of the rate and spatial extend of current star formation, but also offers us the opportunity to probe the physics behind the star formation process. With MICADO's impressive resolution and sensitivity we will be able to resolve stars in the densest parts of star forming regions in other galaxies, as well as detect the oldest stars still on the main sequence in the local universe. This will give us unparalleled access to the most recent, as well as the ancient history of the galaxies in our neighbourhood. Finally variable stars like Cepheids are a cornerstone of the universal distance ladder, with many of the higher level distance indicators firmly rooted in Cepheid-derived distances. Being able to resolve individual Cepheids in all the local Group galaxies will provide the opportunity to further beat down the errors on the local Hubble constant and to bring it in line (or not) with the value derived from other methods (e.g. CMB, SN-1a, BAO, etc)

Planets and Planet Formation are a theme much closer to home, which allows us to start asking the question: are we alone? Current observations allow us to characterise the inner regions of exoplanet systems very well. They do not provide much information on the outer regions of these systems and how these regions might have an effect on the structure of the inner planets. Only direct imaging on the <100 mas scale will be able to offer insights into how critical the interactions and formation processes of outer region planets have been for a planetary system as a whole.

Solar System Science aims to understand the environment out of which the planets in our solar system, and indeed the Earth, were formed. However current telescopes only allow direct imaging of the largest bodies ($D>100\text{ km}$). The resolution of MICADO will allow for the smaller, and much more plentiful objects, to be studied and properties like shape, spin, albedo, surface composition, and number of possible companions to be determined. This in turn will provide density and composition estimates and limits for the bodies generally understood to be the remnants of our Sun's nascent gas cloud. MICADO's resolving power will also allow time-domain studies of the surface features of gas giants to be conducted on much smaller scales than currently accessible⁶, allowing us to further refine models of the gas dynamics and compositions of the solar system's most massive planets.

As can be seen from the list above there are high hopes for MICADO. The leap that can be made with a factor 5-10 improvement in resolution has been compared to Galileo pointing a telescope towards Jupiter and revealing its four major moons. It is the author's opinion that this comparison is somewhat hyperbolic as it is very unlikely that any modern-day astronomers will be convicted to life long house arrest by a religious entity for their discoveries. However at least among the astronomical community, it is expected that the discoveries made by MICADO and the other ELT first light instruments will transform the scientific landscape for decades to come.

1.3.2 MICADO design

MICADO was conceived with the aim of delivering Nyquist sampled diffraction limited images of the near infrared over as large a field of view as possible. The current design goes to great lengths to respect this purpose. The limited amount

⁶From Earth based observatories on the ground and in space.

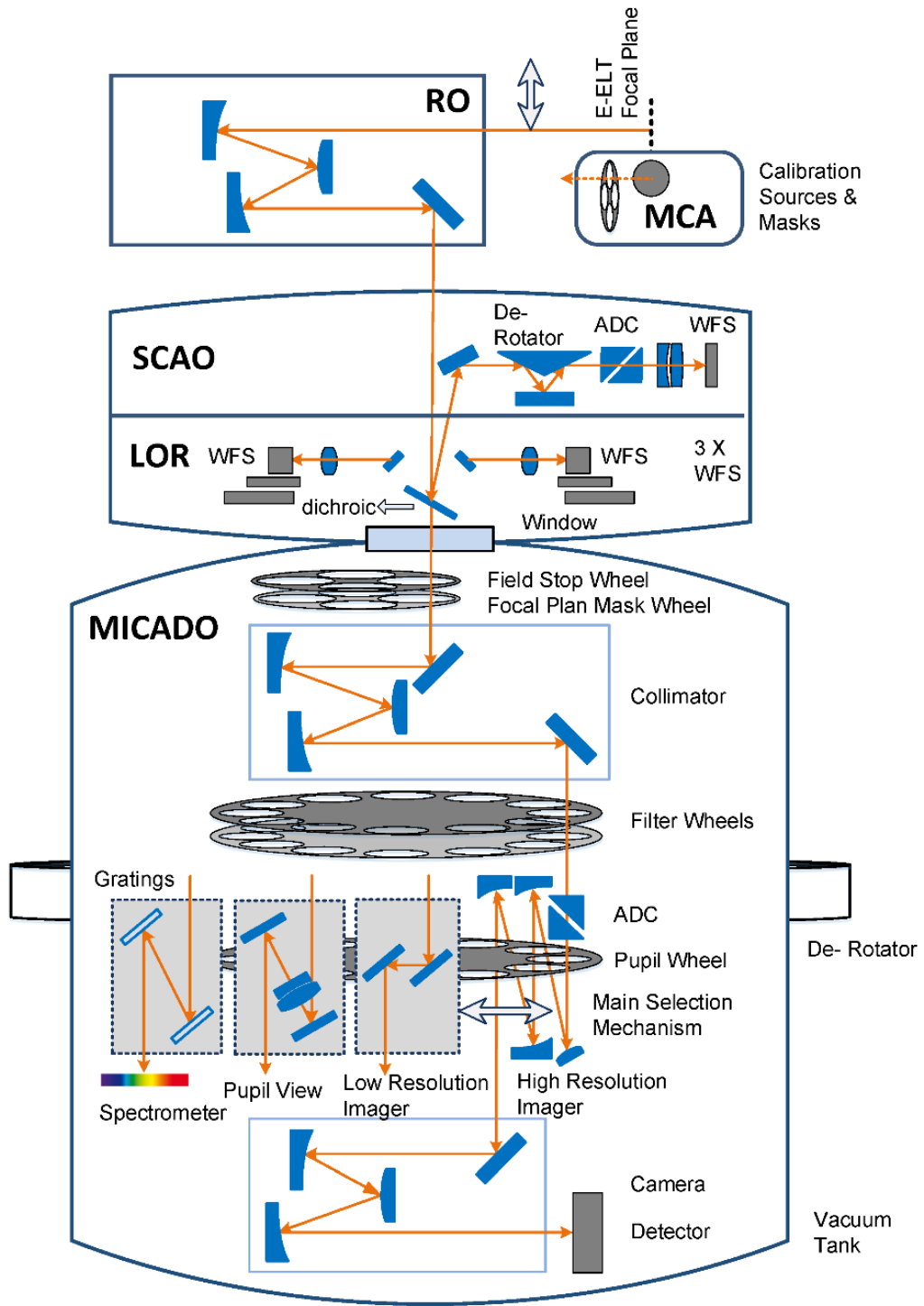


Figure 1.2. Credit: Courtesy of the MICADO consortium. The MICADO optical train is split into three main sections: the relay optics (RO) which, depending on the status of the MAORY module, contain either 4 or 7 optical surfaces; the warm fore-optics containing the wavefront sensors and the SCAO module; and the MICADO cryostat, containing the bulk of the MICADO optics.

Table 1.1. A list of the surfaces for each of the components in the combined optical path for the base configuration of the ELT, the relay optics, and MICADO. Here the simple relay optics and the wide-field mode are used. An additional 5 surfaces would need to be added for the zoom mode with MAORY acting as the optical relay.

Component	Surfaces
Warm Optics	
ELT	5
Relay optics	4
SCAO dichroic	2
Cold Optics	
Entrance window	2
Collimator	5
Filter	2
ADC	8
Pupil optics	2
Re-imager	4
Detector	1
Total	35

of optical components and the large detector array pave the way for MICADO to provide exactly what it set out to do. That said, given that it will be the workhorse NIR imager for a great many years, secondary functionality was added to the design under the assumption that it does not detract from the performance of the imaging modes. Figure 1.2 shows a schematic of the MICADO optical train. This section describes the optical train in detail.

Between the ELT and MICADO there will be a set of relay optics (RO). There are currently two possibilities for this. In case MAORY is not ready by first light, a basic relay will be installed. This will consist of a series of 4 mirrors to direct the light directly from the pre-focal station towards the MICADO entrance window. During daytime operations and calibration runs the relay optics will also direct light coming from the calibration unit (MCA) towards MICADO.

When MAORY is ready it will replace the simple relay optics. MAORY will be the multi-conjugate adaptive optics system that will allow diffraction limited imaging with a relatively constant⁷ PSF structure over the full MICADO field of view and

⁷Relatively constant being a subjective term, and meaning with respect to the SCAO mode which is only really useful in the vicinity of the guide star.

beyond. The current design of MAORY adds two additional mirrors and a wavefront sensor pick-off dichroic to the relay, bringing the total number of surfaces in the relay optics up to seven. Of the six mirrors one will be a deformable mirror capable of removing the wavefront distortions from the second most turbulent layer – generally the layer at 12.7 km altitude. By utilising all three adaptive mirrors in the optical train, MAORY aims to provide Strehl ratios of at least 30%, and with a goal of 45%, in the Ks band over the full MICADO field of view. A small side note is that neither the simple relay nor MAORY will be cooled and as such all mirrors will add photons to the background emission. That said, the additional photons from the $\sim 3 \text{ m}^2$ combined area of the MAORY mirrors will pale in comparison to the background emission from the 978 m^2 .

The first point of contact for the incoming light in MICADO is the pick-off dichroic for MICADO’s own single-conjugate adaptive optics (SCAO) module. Here visible light is reflected and passed through a derotator and an atmospheric dispersion corrector (ADC) to the wavefront sensor. This module is used to control the ELT’s adaptive mirrors (M4 and M5) if MAORY is not available. Infrared light passes through the dichroic and enters the cryostat. The first focal plane is just behind the cryostat window and it is here that the field stop wheel and the mask wheel are located. These wheels are used to limit the size of the field of view for the various imaging modes. The long slits for the spectroscopy mode is also situated here alongside the coronagraphic masks, which need to be in the focal plane in order to remove the core of the PSF.

Following the field stop and mask wheels are five mirrors, three of which collimate the incoming beam for the filter and pupil wheels, and the ADC. MICADO will have two filter wheels with slots for over 30 filters. The current selection of filters contains the regular gamut of broad (e.g. I, Y, J, H, and Ks) and narrow (e.g. Pa β , FeII, Br γ , etc.) band filters, as well as a series of medium band filters covering the red and blue halves of each broad band filter. The primary motivation for including these medium band filters is to better study the photometric properties of, and to better determine the redshifts to, Lyman break galaxies using the photometric drop-out technique.

Next in the optical train comes the atmospheric dispersion corrector (ADC). As the light passes through the atmosphere differential refraction causes a shift in images along the zenith angle. The ADC consist of four co-rotating prisms which

counteract this effect and realign the images at different wavelengths. Although this effect is generally considered small, without the ADC the J band ($\lambda \sim 1.2 \mu\text{m}$) PSF core would extend over 40 mas, or 10 pixels, in the MICADO wide-field mode for observations conducted at a zenith distance of 30° . The four prisms of the ADC introduce a further eight surfaces into the optical train. By assuming a transmission of 98% per surface, the ADC has a total transmission of only 85%. This is however still better than the alternative without the ADC.

MICADO was conceived as a diffraction limited wide-field imager. However in order to enable precision astrometry on the order of $\sim 50 \mu\text{as}$, a zoom imaging mode with a plate scale of 1.5 mas was incorporated. A optics wheel, similar to the filter wheel, was added to switch the optics needed for a 4 mas or a 1.5 mas plate scale. As astrometric imaging needs the most stable optical setup, the four mirrors for the zoom optics will be fixed to the MICADO main structure as the default optical path. To switch to wide-field mode, two bypass mirrors will be rotated into the optical path to circumnavigate the zoom optics. Additional optics, namely the grating for the spectrographic mode, and a lens to enable the pupil plane to be imaged, were added to the pupil wheel. These additional optical components also bypass the zoom mode mirrors.

The final part of the optical train consists of another four mirrors, three of which play the role of the re-imager. The collimated beam is focused onto the focal plane detector array (FPA) consisting of nine HAWAII-4RG infrared detector chips. The detectors are the next generation in the HAWAII-RG family which have become the standard detector chips for near infrared instruments. The 4RG chips will contain 4096×4096 pixels and have a pixel size of $15 \mu\text{m}$. If the characteristics of the previous generation are anything to go by, they will have an average quantum efficiency of $\sim 90\%$ over the $0.8 \mu\text{m}$ to $2.4 \mu\text{m}$ wavelength range. The minimum exposure time for this mode is dictated by the read-out frequency of 200kHz for each of the 64 channels per detector. This results in a minimum read-out time of 2.6 seconds⁸. For more details on the chips and detector layout, see chapter 3.

⁸A single channel read operation actually only takes 1.3 s, however to generate a single read-out frame requires a minimum of two read and one reset operations. As the reset operation is fast relative to the reads, the minimum exposure time is limited by the two read operations.

In the basic configuration, i.e. without MAORY, and in wide-field imaging mode, the full optical train will consist of 35 optical components. The surfaces in the optical train are summarised in Table 1.1.

1.3.3 MICADO observing modes

MICADO's primary mode of operation will be the wide-field imaging mode, however, it will offer a series of other observing options. The current list of imaging modes include:

- Wide-field imaging: Long exposure imaging over a $\sim 50''$ field of view with a plate scale of 4 mas and a minimum read-out time of 2.6 s.
- Zoom-mode imaging: Long exposure imaging over a $\sim 20''$ field of view with a plate scale of 1.5 mas and a minimum read-out time of 2.6 s. This mode will be useful for astrometry science cases as the over-sampled PSF will make astrometric precisions of down to ~ 50 mas possible.
- Fast imaging: Available only for small predefined windows on each detector. The HAWAII-4RG chips can be over-clocked to read out pixels at a rate of 2 MHz, enabling 100x100 pixel windows to be continuously read out every 5 ms.
- Narrow slit spectroscopy: Using slit dimensions of $\sim 3'' \times 16$ mas and providing a spectral resolution of $R < 20\,000$. Its primary targets will be point sources. The slow frame rate imaging mode will be used to read-out images of the spectral traces caused by the use of two gratings in the pupil plane. Spectral traces will be available for either the I-J spectral range ($\lambda < 1.45 \mu\text{m}$) or the H-K spectral range ($\lambda > 1.45 \mu\text{m}$). This is to avoid overlap of the spectral orders at different wavelengths.
- Wide slit spectroscopy: The same instrumental setup as for narrow slit spectroscopy, but with a slit width of 48 mas and with a spectral resolution of $R < 10\,000$. Primary targets are extended sources.

- High contrast imaging: This mode is foreseen to “Achieve meaningful contrast at small inner working angles”, however, details on the design are somewhat difficult to come by.

As MICADO marches inevitably towards its final design review in 2020 there will no doubt be changes to both the optical design and the range of observing modes on offer. At the time of writing though, the optical design seems to have a very solid footing and the author would be surprised if any drastic changes were made between now and the construction phase.

1.4 SimCADO - the instrument data simulator for MICADO

Similar to Physics, Astronomy is entering the era where it is becoming ever more common that observations are used to confirm discoveries made in simulations, rather than the other way around. Software that can simulate how observations will look before they are made, will be immensely helpful for testing out new ideas and planning observations with the ELT. Observing time on the ELT and on the 30 m class telescopes will be extremely expensive and rare. There are also a myriad of complex effects (segmented mirror PSF, Airy rings, ADC residuals and jitter, NCPAs, etc) which are irrelevant in the Seeing limited domain, but which play a large role in the diffraction limited regime. Therefore it will be very useful to visualise possible observations before they are made.

The MICADO project is a multi-million Euro project spread over five countries. When finished, the camera will also be one of the most important instruments for near infrared astronomy for at least the next decade. Astronomers will use MICADO to answer many of today’s outstanding questions, such as: do intermediate mass black holes exist? What are the processes behind star formation in the earliest galaxies? Is the initial mass function truly universal? Are other earth like planetary systems protected by gas giants? In order to best answer these questions, and do it most efficiently with the limited time available at the ELT, the MICADO consortium as well as the astronomy community need to know what MICADO’s true capabilities are well before the instrument goes on sky.

With these two goals in mind, the data flow work package was tasked with creating a piece of simulation software that will mimic not only the capabilities of MICADO, but also be able to simulate the effects of the atmosphere, the ELT, and any other optics between the telescope and the instrument. Thus the design brief for SimCADO was born.

SimCADO is a python package that takes descriptions of individual components of the optical train and combines them into a digital model of the atmosphere, telescope and instrument. When given a description of an astronomical source, it simulates the effect that the whole optical train has on the incoming light rays and projects these rays on to the detector array. The detector model can be “read out” and produces a multi-extension FITS file with the images from the detector, much in the same way the real instrument electronics would. The FITS files are compatible with all the standard astronomical tools and can be treated just like real observations.

A large part of this thesis is devoted to describing the SimCADO software, how it was designed, how it works, who it is for, as well as presenting a series of applications of the software. Hence I will not go into much more detail in this section. All that is left to say is that SimCADO is a tool that should prove to be very useful in the years leading up to the ELT coming online and hopefully beyond. I have spent the better part of the last three years building⁹ and improving the software, advertising it, and educating others on how to use it. I therefore sincerely hope that it finds its way into the standard toolbox of every near infrared astronomer.

SimCADO can be found on my Github repository at <https://github.com/astromyk/SimCADO/> and the python package and documentation is hosted at <http://www.univie.ac.at/simcado/>.

1.5 Goals of the Thesis

Over the course of the last three years, as a member of the data flow work systems team (a so-called “data-flower”), I have run the full software life cycle for SimCADO. I designed, programmed, tested, documented and released SimCADO to both the

⁹According to Github statistics, I contributed 80% of the code base and 100% of the documentation.

MICADO consortium and the astronomy community. I have also played the role of advertiser, teacher and tech-support at conferences and workshops to help build awareness of the tool and its usefulness to the community. I have used the software myself to look into my personal fields of interest, star formation and the initial mass function. Additionally I have used it to investigate topics of interest for others, both scientific and instrumental. With the contents of this thesis I hope to communicate these activities.

The main goals of my work with SimCADO were as follows:

- **Design and build a piece of software which simulates the raw images that MICADO at the ELT will produce.** This software should include descriptions of all aspects of the optical train from above the atmosphere to the FITS file produced by the detector read-out electronics, including, but not limited to: the atmosphere, the mirrors of the ELT, the relay optics, the MICADO optics and the detector electronics. The software should function such that it can be substituted for the real optical system in the data flow pipeline.
- **Verify that the software works.** In order to act as a substitute for MICADO and the ELT, the software should produce images of common scientific targets, such as star clusters or galaxies. The software should work in such a manner that the output can be directly compared to existing observations, and through such comparison show that the output is scientifically accurate.
- **Demonstrate how the software can be used to aid in the design of MICADO.** The software will be available to the MICADO consortium as a tool to help with different aspects of the instrument's design. As such it should be shown in this thesis that the software can deliver useful results for a defined instrument design use case.
- **Demonstrate how the software can be used to demonstrate the science that will be conducted with MICADO.** As with the previous point, this thesis should show that the software can indeed be used to simulate scientifically realistic images for the ELT/MICADO optical system. The goal here is to demonstrate that feasibility studies for various astronomical topics can be

conducted with the software, and that it is not too early to start laying the ground work for future observations with MICADO.

I also have several, somewhat more grandiose, goals regarding SimCADO for both the medium and long term. Most of these are described in detail in chapter 6, however for the most part, they are beyond the scope of this thesis. In the thesis I mainly want to showcase the SimCADO software and how the simulated data, which it is capable of generating, will benefit not only the MICADO consortium, but also the astronomy community at large.

1.6 Thesis Overview

The thesis is organised in the following way: In chapter 2 I present a paper written for SPIE, where I describe the need for the SimCADO package, the intended audience, and the software design for SimCADO. The paper describing the data used in SimCADO, as well as how we verified SimCADO's output against archive data from HAWK-I at the VLT, is included in chapter 3. This paper also presents the first sensitivity predictions for MICADO at the ELT. Chapter 4 describes one of the science cases that I have investigated with SimCADO. The science case is summarised in a short paper on the limits of source detection in crowded regions with the goal of determining the lowest observable mass for star forming regions outside the Milky Way. This sets limits on how deeply the IMF can be resolved with MICADO. SimCADO was also used in an investigation of filter wing blocking coefficients. This is described in a technical note to the MICADO consortium in chapter 5. The future of SimCADO and my research with this tool is given in chapter 6. This is followed by a brief discussion of my results and a summary of the thesis in 7.

SimCADO - an instrument data simulator package for MICADO at the E-ELT

2.1 Overview

As mentioned in the previous chapter, SimCADO was initially conceived as a means to replace the atmosphere, telescope, and instrument during the development of the data processing framework. However during the design phase of SimCADO we identified many other potential actors who could benefit from the software. Therefore we designed SimCADO to be as flexible as possible. Rather than simply simulating a set of predefined observations that would test the reduction software, we included the functionality to describe any celestial object using a combination of spectral and spatial data. Indeed for most science cases, setting up the description of the source is the most time-consuming part of the simulations. For the user, simulating the images with SimCADO is a relatively straight forward process.

At the time of writing the MICADO preliminary design review is set for October/November 2018. Hence the design for the optical train for MICADO is liable to change. Grand changes, although not expected, are also not improbable. Thus I was forced by necessity to keep the optical train module flexible. This means that intrinsically SimCADO contains no data relating specifically to MICADO or the ELT. Every aspect of the optical path from the source object, through the optics and detector, and into the resulting FITS files is controllable by keyword-value pairs, à la sextractor. Any instrument specific information must be provided in external files, either in ASCII or FITS format. This allows old data files to be exchanged for new ones as they became available within the MICADO consortium. Although all the default values and files reflect those needed to model the MICADO optical train, all of these can be exchanged by the user to model any telescope and imaging instrument set-up. Indeed in chapter 3 I describe using SimCADO to model the VLT/HAWK-I optical train for verification purposes. In this chapter however I

concentrate on describing the code model and implementation of SimCADO with a view to modelling the ELT/MICADO optical train.

One point that is not made in this chapter, but should still be mentioned, is that SimCADO was always meant to be an instrument data simulator (IDS), not an end-to-end (E2E) simulator. The difference between these two types is described extensively in the A&A manuscript in chapter 3. The crux of the distinction is that SimCADO is made to run quickly and use data that has been pre-computed (e.g. PSF, transmission cuves, etc). SimCADO was never designed for ray-tracing or photon following simulation approach (see section 3.4.3). In contrast, an end-to-end simulator is designed to do these things, and in doing so wastes a lot of time and computing power by recomputing aspects of a simulation which do not vary from run to run.

This chapter is made up of a paper published in the proceedings of SPIE. SPIE is, in my experience, by far the most common journal for publications relating to instrument simulators. All other instrument simulators use their proceedings paper in SPIE as the standard reference work. At the time of publication I was still implementing the code base for SimCADO. As such, the following paper concentrates solely on the code design and implementation, as well as the algorithms and data flow involved in modelling the optical train.

2.2 Publication Details

Title: SimCADO - an instrument data simulator package for MICADO at the E-ELT

Authors: Kieran Leschinski, Oliver Czoske, Rainer Köhler, Michael Mach, Werner Zeilinger, Gijs Verdoes Kleijn, João Alves, Wolfgang Kausch, Norbert Przybilla, the A* consortium, and the MICADO consortium

Status: Published in the Proceedings of SPIE 9911, Modelling, Systems Engineering, and Project Management for Astronomy VI.

DOI: 10.11117/12.2232483

Own contributions: Everything related to SimCADO, including but not exclusively: design, implementation, presentation, documentation, and promotion. According to Github statistic, I have committed over 80% of the code base.

SimCADO - an instrument data simulator package for MICADO at the E-ELT

K. Leschinski^a, O. Czoske^a, R. Köhler^{b,a}, M. Mach^a, W. Zeilinger^a, G. Verdoes Kleijn^c
J. Alves^a, W. Kausch^{a,b}, N. Przybilla^b,
the A* consortium*, and the MICADO consortium†

^a Institute for Astrophysics, University of Vienna, Türkenschanzstraße 17, 1180 Vienna,
Austria;

^b Institut für Astro- und Teilchenphysik, Universität Innsbruck, Technikerstraße 25/8, 6020
Innsbruck, Austria;

^c Kapteyn Astronomical Institute, University of Groningen, Postbus 800, 9700 AV Groningen,
The Netherlands

ABSTRACT

MICADO will be the first-light wide-field imager for the European Extremely Large Telescope (E-ELT) and will provide diffraction limited imaging (7mas at 1.2μm) over a ~53 arcsecond field of view. In order to support various consortium activities we have developed a first version of SimCADO: an instrument simulator for MICADO. SimCADO uses the results of the detailed simulation efforts conducted for each of the separate consortium-internal work packages in order to generate a model of the optical path from source to detector readout. SimCADO is thus a tool to provide scientific context to both the science and instrument development teams who are ultimately responsible for the final design and future capabilities of the MICADO instrument. Here we present an overview of the inner workings of SimCADO and outline our plan for its further development.

Keywords: E-ELT, MICADO, SimCADO, instrument simulator, image simulation

1. INTRODUCTION

The global astronomical community is currently embarking on an ambitious journey to construct the largest optical and near-infrared telescopes the world has ever seen. The European Southern Observatory (ESO) has recently put into motion plans to build the largest of these next generation telescopes. The European Extremely Large Telescope (E-ELT),¹ with its 39m primary mirror and intrinsic adaptive optic systems, aims to observe the faintest and most distant objects in the universe at the diffraction limit. MICADO² - the Multi-AO Imaging CAmera for Deep Observations - will be the near-infrared (NIR) wide-field camera available at the E-ELT at first-light.

MICADO will be the work-horse instrument for imaging observations. It will provide diffraction limited images in the near infrared (NIR) wavelength range over a field of view (FoV) of $\sim 53 \times 53$ arcsec² in wide-field mode by using an array of nine 4096 x 4096 pixel detectors with a plate-scale of 4 mas. A zoom mode, with a plate-scale of 1.5 mas, will also be provided for a FoV of $\sim 16 \times 16$ arcsec². Additional observation modes also include a long slit spectrograph with R~4000, windowed high time resolution imaging and high contrast imaging. Observing at the diffraction limit will be facilitated by either a Single Conjugate Adaptive Optics (SCAO) system or MAORY's Multi-Conjugate Adaptive Optics (MCAO) system.

* The A* consortium comprises the Astronomy and Astrophysics departments at: - the University of Vienna - Universität Innsbruck - Johannes Kepler University Linz - the University of Graz - in collaboration with the Johann Radon Institute for Computational and Applied Mathematics (RICAM)

† The MICADO consortium has partners in Germany (the Max Planck Institute for extraterrestrial Physics (PI institute), the Max Planck Institute for Astronomy, the Observatory of the University of Munich, and the Institute for Astrophysics of the Georg-August University), France (CNRS/INSU, represented by LESIA), the Netherlands (NOVA, with specific contributions to MICADO from the University of Groningen, the University of Leiden, and the NOVA optical/infrared instrumentation group), Austria (the A* consortium), and Italy (INAF, represented by the Observatory of Padova).

For further information please contact Kieran Leschinski: kieran.leschinski@univie.ac.at

As the complexity of observatories and instruments increases, so too has the need to predict exactly how instruments will perform. In order to achieve this goal, the current generation of instrumentation projects are investing time and effort in developing instrument data simulators during their design phases (e.g. PhoSim for the LSST,³ TOAD for 4MOST,⁴ HSIM for HARMONI,⁵ the METIS simulator⁶). The MICADO consortium is no different. We are currently in the process of completing SimCADO, an instrument data simulator for MICADO. SimCADO is a python package that collects and combines the efforts of the various consortium-internal work packages and provides a framework for simulating raw output images based on the most recent design of the instrument. SimCADO does not aim to simulate each and every photon along its path from the source to the read out electronics, instead SimCADO transforms the incoming photon flux by using array and matrix operations which best represent the spectral and spatial effects generated by each optical element along the optical train.

This paper is organised in the following manner: Section 2 provides background to the SimCADO project and outlines the intended user groups. Section 3 gives an overview of how SimCADO models and applies the effects that each of the optical components has on the incoming photon flux. The data model behind SimCADO, and how the user interacts with the package is described in Section 4. This section also discuss the limitations of SimCADO as well as outline the plans for future updates to the package.

2. SIMCADO, THE DATA SIMULATION EFFORT FOR MICADO

SimCADO is a data simulation package written for Python 3 with the goal of generating realistic mock detector plane array read out files for MICADO and the E-ELT. It allows the user to see the effect that the optical train has on the incoming photons by providing the user with raw data sets that will be similar to what MICADO will produce during a typical observing run. SimCADO is also highly configurable. The user is able to simulate various observational scenarios, e.g. the use of different adaptive optics (AO) systems, or set the effectiveness of different subsystems along the optical train, e.g. the performance of the derotator or atmospheric dispersion corrector (ADC). These aspects of SimCADO are covered in greater detail in Sec. 4.

2.1 SimCADO user groups

Besides simulation related deliveries towards ESO, the idea for such an instrument data simulator was born out of the needs of various work-package teams within the MICADO consortium, namely the:

Science team

The task of the science team is to define and develop the primary science drivers for the MICADO instrument. In order to better determine the feasibility of these science cases, the team requires a tool with which to consistently simulate calibrated images for each case.

Data reduction pipeline team

In order to begin the development of the data reduction pipeline before the instrument enters the construction phase, the data reduction pipeline team (also known as the data flow system (DFS) team) will need sets of simulated raw images from the detector array. These test data sets can be provided by an instrument data simulator. With such data the team will test the performance of algorithms to correct for the instrumental fingerprint and determine physical calibration for the instrument.

Instrument design team

To create MICADO many work packages are required, which in turn means a large number of sub-systems need to be modelled in detail. However modelling the entire optical train at the level of detail used for each sub system would require a prohibitive effort. A tool which takes the results of each sub-system modelling effort and uses these to quickly model the whole optical train - from source to read out - will be useful for deciding between hardware solutions and software solutions for correcting instrumental effects.

Instrument control software team

Knowing quantitatively how various parameters affect the image quality is crucial for designing the software needed to drive the instrument and for determining how much observing time to allocate for various types of targets.

Table 1. Core and optional python dependencies for SimCADO

Core dependencies		Optional dependencies	
Name	Version	Name	Version
numpy	>1.10	matplotlib	>1.5
scipy	>0.17	poppy	>0.4
astropy	>1.1	photutils	>0.2

SimCADO aims to meet all these needs. In the immediate future, SimCADO will be the tool that the Science and Instrument design teams use as they iterate on the design of the optical train. By allowing both teams to visualise the effect of different designs on the detector array image, a design for MICADO can be chosen which best balances the desires of the science goals with the feasibility of hardware solutions.

It should also be noted that the MICADO consortium is required to provide data for an Exposure Time Calculator (ETC) to ESO, which will be made available to the astronomical community. The ETC provides the community with basic quantitative information regarding the capabilities of MICADO and is the first stop when testing out the feasibility of new ideas for observations. SimCADO will provide the quantitative information on the capabilities of MICADO needed to power the ETC.

Looking further into the future, we intend for the astronomical community to also benefit from SimCADO. As time on the E-ELT will be in high demand and difficult to obtain, it is important that the astronomical community be able to plan the best possible observing strategies. Being able to predict the outcomes of different schemes and techniques will assist in achieving the highest scientific return once the E-ELT is on line. The ability to simulate what will be possible in 10 years will also allow the astronomical community to lay down road-maps for the next decade as well as conduct the ground work needed to best understand these future observations.

2.2 Design requirements for SimCADO

Balancing the needs of the various user groups is not an easy task. For example, while each user would like simulations which take into account as many physical effects as possible, most users would prefer not to need access to a computing cluster and/or support staff in order to run the simulations. For many use cases the interaction of photons with the various media in the instrument are of little importance and quick results take preference. However other user groups will indeed be interested in the difference in the signal to noise (S/N) ratio for different detector read-out schemes.

In order to provide a tool which meets the largest number of needs of the above mentioned user groups, we set ourselves the following requirements for SimCADO.

SimCADO should:

1. run in a language common among the astronomical community,
2. be quick to install and run on an average personal computer,
3. not require that the user be familiar with the inner workings of MICADO,
4. give the user control over the simulation parameters including those relating to the optical train,
5. maintain a modular design that can be easily adapted to the many upcoming design changes,
6. use standard file types at the interface between the user and SimCADO.

There are two main reasons behind the decision to restrict SimCADO to the architecture of a personal computer. Firstly, if the simulation effort is centrally managed and run, there is the possibility for a large bottle neck to occur in the work flow. If instead, the user can run SimCADO on her or his own laptop, she or he would be able to produce results in a much more timely manner. Furthermore, by decentralising the simulation effort, the amount of science cases that can be tested is no longer limited by the man-power or hardware available to the simulation team.

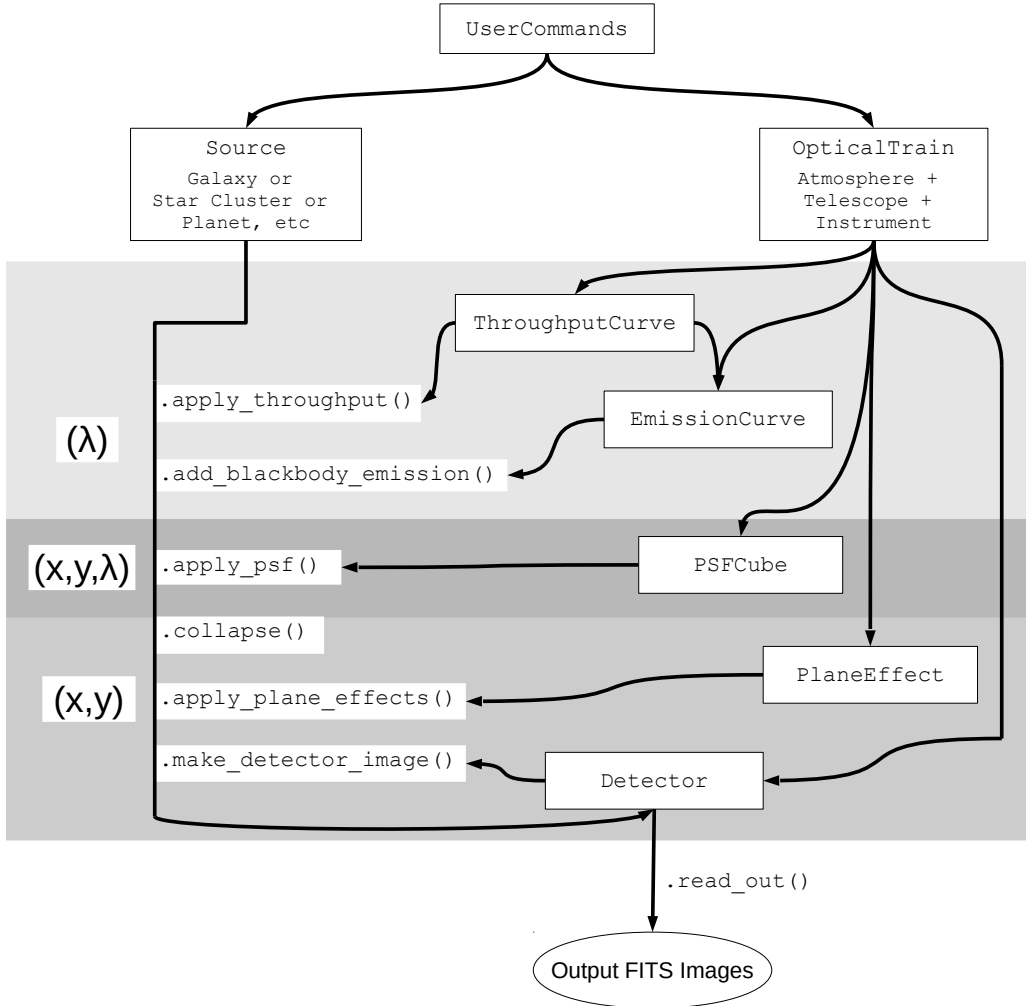


Figure 1. The simple version of the data model for SimCADO. Each of the boxed CamelCase words represents a class in SimCADO. The arrows show how each class interacts with the others. Words beginning with a dot are pseudo code functions to describe what is happening at that point during a SimCADO simulation run. An instance of the **UserCommands** class controls how each element in an instance of the **OpticalTrain** class is applied to a **Source** class object. The resulting image is held in a instance of the **Detector** class. How this process happens is described in section 3.4

2.3 Imaging vs Spectroscopy

MICADO is the first-light wide-field imaging camera for the E-ELT, and as such its main purpose is to provide imagery of the sky. While MICADO does offer a long-slit spectrographic mode, the priority for the MICADO design is to provide diffraction-limited imaging over the field of view. We have also adopted this approach. The current version of SimCADO only provides functionality for imaging in the wide-field and zoom modes.

3. DATA MODEL BEHIND SIMCADO

While designing SimCADO, we identified four main aspects involved in simulating MICADO detector array images. These were:

- A representation of the source of photons
- A model of the optical path
- A description of the detector
- A list of parameters needed to control the simulation

The primary user interface (UI) of SimCADO involves class objects representing each one of these aspects. Running a simulation involves combining the data held within each of the four data structures in a manner representative of the whole optical system - See Figure 1. This can either be executed automatically or manually, depending on whether the user wishes to view the intermediate data[‡] or is simply interested in the final output.

3.1 A note on SimCADO's internal representation of spectral data

Before the main SimCADO classes are introduced, it is important to mention that the SimCADO data model does not use a data-cube (x,y,λ) to represent the photons travelling through the optical train. Instead the objects to be “observed” are converted into a list of point sources which are described by four values: two-dimensional coordinates on the plane of the sky, a reference to a unique spectrum and a weighting (i.e. a scaling of the intensity) for that instance of the spectrum. The decision to move away from the traditional data-cube model was motivated by both the need to reduce the amount of RAM required as well as reduce the amount of operations executed during a simulation. For example, a single MICADO detector array image contains nine 4k chips, each with ~ 16 million pixels. If each pixel is $4\times$ oversampled in each direction and 4 byte integers are used, the size of the resulting image in memory will be:

$$9 \times (4096 \times 4096) \times 4^2 \times 4 \text{ Bytes} \approx 10 \text{ GB} \quad (1)$$

Note that this is a single oversampled monochrome detector array image. If the data-cube were to also include more than one wavelength, its size in memory would increase proportionally to the number of spectral channels. In the case of a K-band image of a field of stars with spectra taken from the Pickles (1998)⁷ library ($\delta\lambda=0.5\text{nm}$) the data-cube would need to contain over 800 layers. The resulting memory requirements would be ~ 8 TB, far exceeding the capacity of the current generation of high-end laptops. By realising that for the most part, space is rather empty, and that therefore the majority of a data cube is also empty, SimCADO is able to circumvent this memory problem. The internal representation of photon sources by a pair of coordinates and a reference to a spectrum allows all the empty space, which would otherwise be represented in memory by zeros, to be ignored. Furthermore, in many science case simulations there is a large redundancy with regards to the number of unique spectra used. By only using references to the unique spectra, SimCADO further saves on memory and computational operations. The result of this vector-like representation is a vast reduction in computation time. Section 3.4 describes how SimCADO manipulates data in this form.

3.2 The main classes of the SimCADO user interface

The four class objects which represent the above-mentioned aspects are described in the following sections in greater detail. They are available in the upper level of the SimCADO package, i.e. `simcado.OpticalTrain` or can be called from their respective modules, i.e. `simcado.optics.OpticalTrain`.

[‡]Intermediate data in SimCADO does not refer to intermediate positions along the optical train, rather to how the distribution of photons on the focal plane changes at intermediate stages during a simulation after certain optical effects have been applied. E.g. after the transmission curves have been applied, but before the PSF has been taken into account.

3.2.1 Source

The `Source` class is used to represent photon sources with a position and a spectrum. Examples include light from a star, galaxy or a planet. The class contains a list of unique spectra, a list of coordinates for each photon source, and a list of references which match each photon source to a spectrum in the list of spectra. The advantage of using this approach is that objects with highly similar spectra can both reference the same list position, thereby reducing the number of spectra that need to be manipulated during a simulation.

An example of the benefit of this approach is the simulation of observations to map the star formation regions in galaxies. In SimCADO a galaxy is represented by an oversampled grid (typically $4 \times$ the detector pixel scale) of “point sources”. Much like in real observations, the spectrum for each grid element is the summation of the spectra for each source of photons (e.g. stars, nebula, etc) contained within the area of that grid element. For a basic example of a use case scenario, one can say that a typical galaxy contains a population of old stars (>1 Gyr) with an almost homogeneous spatial distribution, and a population of young stars (<1 Gyr) which exist in clusters scattered throughout the galaxy. Each grid element has its own unique position, yet elements that only contain an older stellar population all reference the spectrum for a “generic” older population. The same can be true for the younger population. The advantage in terms of computation time by exploiting such redundancy in the spectral domain is obvious.

In keeping in line with an object oriented methodology, the `Source` class contains a variety of methods to manipulate the internal data, and/or generate and return images of the source object. For a full list of the class methods, the reader is directed to the SimCADO documentation, however here is a brief list of the most useful methods in the `Source` class:

- `photons_in_range(λ_1, λ_2)` extracts the number of photons in a given wavelength range, $[\lambda_1, \lambda_2]$, from each spectrum.
- `image_in_range(λ_1, λ_2 , psf)` generates a two dimensional image for a specific wavelength range, $[\lambda_1, \lambda_2]$, based on a supplied `psf` kernel.
- `apply_optical_train(OpticalTrain)` models the effects that the supplied `OpticalTrain` object will have on photons being emitted by the sources (e.g. PSF, transmission, jitter, etc). An image is generated for how the photons would be distributed on each chip in the focal plane array before they are converted to photo-electrons in the detector chips. These images are then passed onto the `Chips` contained in a `Detector` object (see below).

It should be noted that a `Source` object will not hold any images. Rather its internal methods generate images and pass these to the `Detector` objects. Internal images are generated on an oversampled detector pixel grid. The oversampling factor is an attribute of the optical train and can be set by the user.

3.2.2 OpticalTrain

As the name suggests, the `OpticalTrain` contains all the information needed to model the effects of the entire optical path on the incoming photons from sources held within a `Source` object. The optical train in this sense covers everything between where the photons were “emitted” and when they are converted into photo-electrons in the chips on the detector array. For the preset MICADO optical train, this includes: the atmosphere, the E-ELT, the MAORY⁸ instrument (optional, depending on AO mode), all aspects of the MICADO optical configuration and the MICADO detector array. For the elements being developed outside the MICADO consortium, i.e. the E-ELT and MAORY, SimCADO currently uses the information made public during the respective phase A studies. For the elements being developed by the MICADO consortium, SimCADO combines information garnered from the latest consortium-internal documents. Table 2 lists which elements of the atmosphere+E-ELT+MICADO optical train are currently simulated by SimCADO.

When initialised, an `OpticalTrain` object reads in all the information necessary to model the optical path. This can either be read in from a pre-prepared optical train file, or from files which relate to individual aspects of the optical train (e.g. transmission curves in ASCII format, or FITS images with PSF kernels, etc.).

Table 2. Elements of the optical train emulated by SimCADO. * These items currently use very basic models. The models are expected to improve as the detectors are tested. Section 4 describes how these elements are represented in SimCADO in detail.

Element	Dimension	Effects
Atmosphere	λ	Transmission, Emission
E-ELT	(x, y, λ)	Mirror transmission and emission, vibration, tracking errors
AO-corrected PSF	(x, y, λ)	MCAO, SCAO, No AO
Entrance Window	λ	Transmission
Filter Set	λ	Transmission
Optical Design	(x, y, λ)	Distortion, Transmission
ADC	(x, y, λ)	Wavelength dependent shifts
Derotator	(x, y)	Field rotation
Detector	(x, y, λ)	Quantum efficiency, detector noise, persistence*, cross-talk*

As the effect of the transmission curves of each element is cumulative, `OpticalTrain` combines all transmission curves internally into a “master” transmission curve [§]. It is this “master” transmission curve which is then applied to the spectra in a `Source` object.

`OpticalTrain` currently assumes that the two major sources of background photons - the atmosphere and the primary mirror - can be taken as approximately spatially constant [¶] with an associated spectrum. In the case of the atmosphere, this emission spectrum is taken from `SkyCalc`.^{11,12} Because of the assumed spatial constancy, only transmission effects apply to the background photons. As such, `OpticalTrain` immediately calculates and stores the average number of background photons through the specified filter bandpass.

The PSF kernels used for the two major AO modes (MCAO and SCAO) are kept in FITS files delivered with the package so that they can be easily updated. They currently do not change over the field of view. Field-varying PSF kernels will be implemented once updated kernels are available from the MCAO and SCAO teams. The user may also use their own PSF kernel in the form of a FITS image file, providing the correct FITS keywords are in the header, or generate analytical PSFs with SimCADO’s built-in functions (See Section 3.6).

Other wavelength-independent effects, such as field rotation or telescope jitter, are applied directly through built-in functions. The required parameters are parsed through the `UserCommands` object required to initialise an `OpticalTrain` object.

3.2.3 Detector

Although only a single element in the whole optical train, the detector is the final interface between the incoming photons and the observer. The detector chips are the primary source of systematic effects in raw images, therefore it is very important to both understand, and be able to model the detector chip characteristics accurately.

The `Detector` class contains a list of `Chip` objects and the layout of the chips in the focal plane. It also holds information about how the chips are to be read. Each `Chip` object contains the information about its own noise properties. When the focal plane image of a `Source` is created, the image is re-binned and passed straight onto the relavent chips. For quick simulations, the `.readout()` method samples the signal on the chips only once (at the end of an exposure) and applies a Poisson noise distribution to the expected signal. If simulation time is not an issue, a full up-the-ramp read-out sequence is used. As the time between non-destructive read-outs (typically

[§]OpticalTrain actually creates three “master” transmission curves - one for each of the major sources of photons:

- 1) `tc_source` - equivalent to the throughput for the astronomical source. It contains all transmission curves, i.e. the atmosphere, E-ELT mirrors, and transmission through MICADO
- 2) `tc_atmo` - equivalent to the throughput for the atmospheric photons. It contains all transmission curves minus the atmospheric transmission , i.e. E-ELT mirrors and transmission through MICADO
- 3) `tc_mirror` - equivalent to the throughput for grey-body photons from the primary mirror - It contains only the total throughput of the MICADO instrument

[¶]For the case of a single detector readout, the assumption of a constant sky background is valid, however, over the course of a night variations in the NIR background have been found - Pedani (2014)⁹ and Moreels (2008).¹⁰ In future releases of SimCADO we will aim to address this issue.

~ 3 sec) is generally small compared with the length of a single exposure, the user should not be surprised by extended simulation times.

Similar to the `OpticalTrain`, a `Detector` object can be created from a series of individual FITS image files representing the noise properties of the chips, and an ASCII table describing the layout of the chips on the detector plane, or it can be read from a pre-prepared detector file.

3.2.4 UserCommands

By default SimCADO uses parameter values that correspond to the MICADO instrument. For ease of use (i.e. so that the user need not pass 20 parameters to every function), all parameters needed to run a simulation are defined and held in a python dictionary in the `UserCommands` class. Also included in the `UserCommands` class are frequently used quantities and vectors, e.g. vectors with the wavelengths of the edges and centres of each wavelength bin used when integrating over the number of photons in a filter bandpass.

Following tools like SExtractor,¹³ a `UserCommands` object can also be initialised from an ASCII file containing keyword-value pairs. The user only needs to list the keyword-value pairs that they want to change - the rest are set to the default values. A `UserCommands` object is used to set up instances of the two main hardware classes: `OpticalTrain` and `Detector`. Attribute values can be updated on-the-fly, although any `OpticalTrain` or `Detector` objects that were created before the change will need to be re-initialised.

3.3 An short example of using the main SimCADO classes

A simple simulation with SimCADO requires very little coding. For example, if we would like to simulate the detector output for a single exposure of a $10^4 M_\odot$ open cluster in the Large Magellanic Cloud ($d \sim 50$ kpc), we first create a `UserCommands` object with all the default values, and use it to generate an `OpticalTrain` object and a `Detector` object.

```
>>> import simcado
>>> cmd = simcado.UserCommands()
>>> opt_train = simcado.OpticalTrain(cmd)
>>> fpa = simcado.Detector(cmd)
```

Next we create a `Source` object for the open cluster using a convenience function from the `optics_utils` module. We call the method `.apply_optical_train()` and pass both the `OpticalTrain` and `Detector` objects. This method is the heart of the simulation, as it converts the lists of point sources held in `Source` into a two dimensional distribution of expected photon flux. Depending on the parameters, i.e. the FoV or spectral resolution required, this step can take anywhere from 10 seconds to 10 minutes. During this process, the “imagery” generated inside the `Source` object is transferred to the `Detector` object.

```
>>> src = sim.optics_utils.source_1E4_Msun_cluster()
>>> src.apply_optical_train(opt_train, fpa)
```

The raw detector array images can then be read out by calling the `Detector`'s `read_out` method. If no filename is specified, the method returns an astropy `HDUList` with a FITS image extension for each chip in the detector array.

```
>>> fpa.read_out(filename="my_raw_image.fits")
```

Figure 2 shows the results of a simple simulation similar to that described in this section.

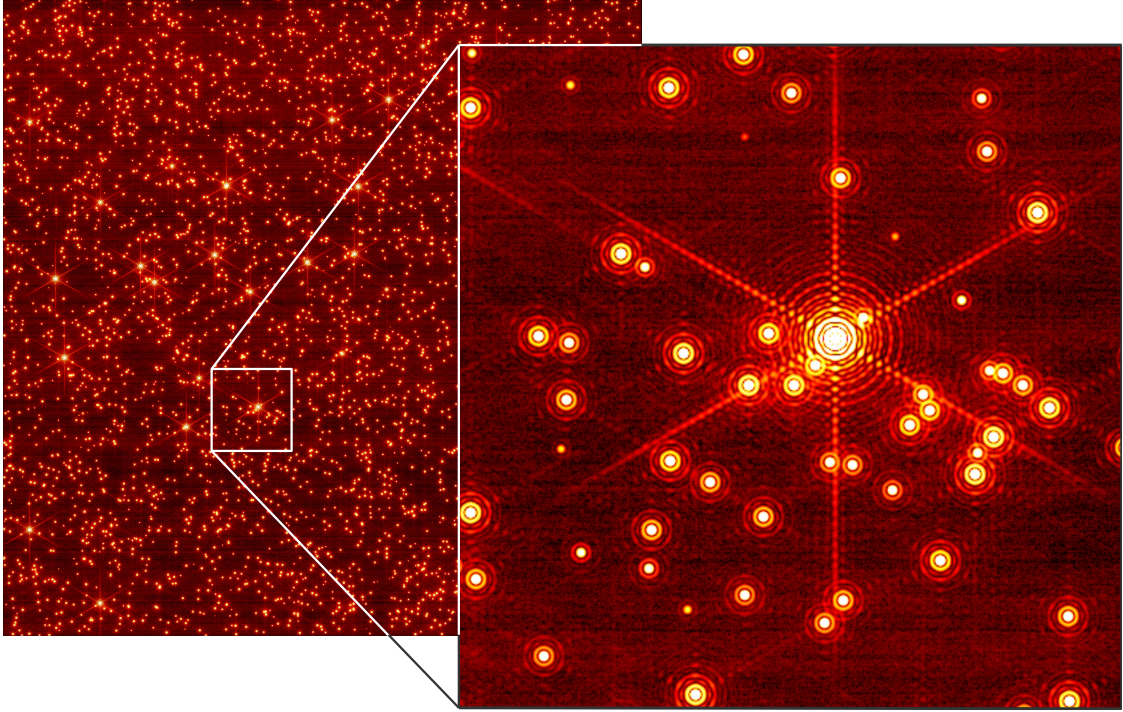


Figure 2. A heart of a compact star cluster in the LMC as might be seen by MICADO. The left image shows the central chip in the 3x3 detector array, corresponding to a FoV of ~ 16 arcsec, or a linear distance of 0.25 pc. The right image shows a 512×512 pixel section of the image. For this simulation the atmospheric effects were removed, so that the diffraction pattern of the E-ELT's primary mirror could be seen, as well as the detector noise from the H4RG chips (courtesy of Bernhard Rauscher's HxRG Noise Generator¹⁴).

3.4 Method behind applying an OpticalTrain

In an ideal world, SimCADO would apply all spectral and spatial changes at the resolution of the input data. However, as previously mentioned, the memory requirements to do this are well outside the limits of a personal computer. The solution to this problem is to split the effects based on dimensionality. For certain elements in the optical train, the spectral and spatial effects can be decoupled (e.g. purely transmissive elements like the filters versus purely spatial effects like telescope vibration). For other elements, most notably the PSF and ADC, all three dimensions must be considered simultaneously. When applying an `OpticalTrain`, SimCADO follows the procedure described graphically in Figure 3. The example used in Figure 3 is for a simplified stellar cluster with only two different stellar types - A0V and K5V type stars.

- (A) The original `Source` object includes an array of spectra for each `unique` photon source (in the case of Figure 3, there are only two unique spectra) and four vectors: `x`, `y`, `ref`, `weight`. `x` and `y` hold the spatial information for each photon source, `ref` connects each source to a spectrum in the array of spectra and `weight` allows the spectrum to be scaled.
 - λ -effects. The first step in `apply_optical_train()` is to combine all optical elements which only act in the wavelength domain (e.g. filters, mirrors, etc.) into a single effect, then apply that effect to the array of spectra in the `Source` object.
- (B) The spectra in the `Source` object are now representative of the photo-electron count at the detector, assuming a perfect optical train and at the internal spatial resolution of the simulation, i.e. *not at the pixel scale of the detector*. The position vectors are converted into a two-dimensional “image” of the `Source`.

- (x,y,λ)-effects. The second step includes creating “slices” through the data. The spectra are binned according to several criteria (ADC shift, PSF FWHM difference, etc) with a spectral resolution anywhere from R=1 to R>100, and the number of photons per source in each wavelength bin is calculated. The sources in each “slice” are scaled according to the number of photons in each bin. The relevant spatial effects (atmospheric dispersion, convolution with PSF kernel, etc.) are then applied to each slice in turn.
- (C) At this stage, the `Source` object contains many spectral slices. Each is essentially the equivalent of a (*very*) narrow-band filter image.
- (D) All spectral effects have been taken into account, and so the binning in the spectral domain is no longer needed. The third step in `apply_optical_train()` is to add all the slices together to create a single monochrome image.
- (x,y)-effects. Fourth in the series of operations is to apply the purely spatial effects (e.g. telescope jitter, field rotation, etc) to the monochrome image.
- (E) The resulting image represents how the incoming photons from the source would be distributed on the focal plane after travelling through the entire optical train. At this point the background photons are also added to the image. Because SimCADO doesn’t take into account the changing sky background, the sky emission is approximated as a constant background photon count determined from an atmospheric emission curve (either provided by the user or generated by `SkyCalc`^{11,12}). The mirror blackbody emission is also approximated as spatially constant. For all filters, with the exception of K, the amount of additional photons due to the mirror is close to negligible.
- detector-effects. The image is resampled down from the internally oversampled grid down to the pixel scale of the detector chips - in the case of MICADO either 4 mas or 1.5 mas, depending on mode. The final step is to add noise in all its forms to the image. Various aspects of the detector noise (correlated and uncorrelated white and pink noise read-out (see Rauscher 2015¹⁴), dead pixels, etc.), as well as photon shot noise for both the atmospheric and object photons are taken into account. Further effects (e.g. detector persistence, cross-talk, etc) are also added to the image at this point.
- (F) The final image represents the spatial distribution of all photo-electrons (from the source object + atmosphere + primary mirror) plus the electronic noise generated by reading out the detector chips. The images from all the chips considered in a simulation are packed into a FITS extension and the FITS file is either written out to disk, or returned to the user if generated during an interactive Python session.

3.5 Generating input for simulations

As the data format used by the `Source` class is not standard, SimCADO contains a module to convert more standard data types into `Source` objects. Currently the SimCADO module `source_utils` offers the following ways to create a `Source` object:

- from a FITS cube,
- from a FITS image plus an ASCII spectrum,
- from an ASCII list of coordinates with references and an ASCII table of spectra,
- from a combination of several `Source` objects,
- by using the in-built functions in `simcado.source_utils` to generate `Source` objects
- by passing a series of arrays already in an iPython Notebook when initialising a `Source` object

`Source` objects can also be saved to disk for later use.

The other input required for SimCADO is the data on the optical train. This can either be supplied in the form of ASCII and/or FITS files which detail all the aspects the user wishes to include in the simulation, or in the form of pre-prepared `OpticalTrain` and `Detector` files.

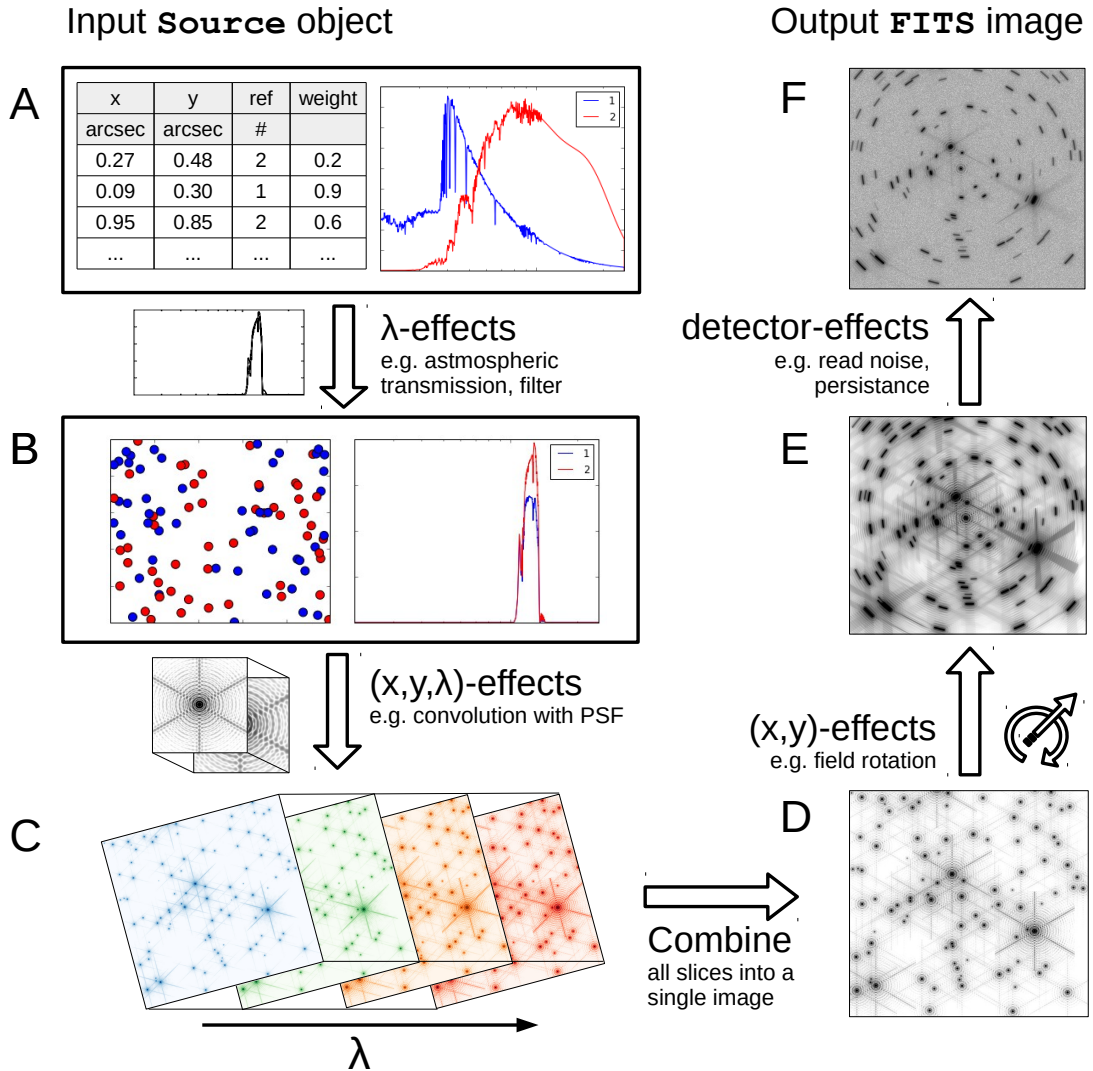


Figure 3. A simplified graphical representation of what happens to a Source object when the method `<Source>.apply_optical_train()` is called. The diagramme is explained in detail in Section 3.4. The flow of events can be summarized so: (A) a Source object for a mock open cluster is created. All effects of the optical train which only act in the wavelength-domain (λ -effects) are applied to the spectra in the array. (B) Several images of the spatial extent of the Source are created and weighted by the number of photons in each low resolution spectral bin. Any elements that affect the incoming photons in all three dimensions (x, y, λ) are taken into account here (C) before (D) the images are added together. Purely spatial effects (e.g. telescope vibrations) are then applied to the (E) monochrome image and detector noise is added. (F) The resulting image represents the spatial distribution of all photo-electrons (from source object + atmosphere + primary mirror) plus the electronic noise generated by reading out the detector chips. A FITS file is either written to disk or returned to the user with an image extension for each chip in the detector array.

3.6 Modules behind the scene

In order for SimCADO to function, several other modules and classes need to be mentioned.

`simcado.psf`

This module contains the classes `PSF` and `PSFCube`. `PSFCube` holds a list of `PSF` objects and provides the functionality to manipulate the `PSF` kernels. The most commonly used class is `UserPSFCube`, which reads in a FITS file containing one or more `PSF` kernels. The module also provides functions to generate a variety of ideal case analytical `PSFs`, including Gaussian, Airy and Moffat `PSF` kernels.

`simcado.spectral`

`spectral` contains the classes used to represent transmission and emission curves. The base class is `TransmissionCurve` and holds, among others, two arrays: `.lam` and `.val` which hold the information about the wavelength and corresponding degree of transmission. By providing units and removing the normalisation, `TransmissionCurve` can be extended to accommodate an `EmissionCurve` with units of [ph/s/bin].

`simcado.spatial`

The `spatial` module contains no class data structures, but rather a series of functions that mimic the purely spatial effects of elements in the optical train. Examples include field rotation, tracking errors and shifts. These effects can either be implemented in a purely linear fashion, for example simulating if the telescope tracking was turned off completely, or in a Gaussian manner, which is instead used to simulate uncertainty in the centre of the tracked position.

4. MODELLING THE OPTICAL PATH

As mentioned in the Section 3.4, SimCADO makes use of the fact that not all elements affect the incoming photons in all dimensions. Filters, for example, strongly alter the incoming spectrum of light, but have a negligible effect on the spatial distribution of the photons. A faulty Derotator on the other hand, has a noticeable effect on how sharp point sources are, however the effect is equal across all wavelengths. As such the effects of each of these two elements can be applied independently of the other to the incoming photons. In the following section, these effects are referred to as spectral (also λ - or 1D-) and spatial (also (x,y)-, or 2D-) effects. The latter include, but are not limited to; shifts, rotations, convolutions and distortions. There are also elements which affect both the spatial and spectral nature of the incoming photons, e.g. the point spread function (PSF) of the telescope. These elements are referred to as spectrospatial (also (x,y, λ)-, or 3D-) elements.

4.1 Representing elements in the optical train in SimCADO

The following section describes how each element in the optical train is represented in SimCADO:

- Atmosphere - (λ)

The atmosphere is the element in the optical train that has the largest effect on the incoming photons, in all three dimensions. However, because of the E-ELT's adaptive optics facilities, the spatial effect of the atmosphere (namely the seeing-limited PSF) will mostly be removed, with the residual being combined with the PSF of the E-ELT. Both the MAORY MCAO¹⁵ and MICADO SCAO¹⁶ teams are in the process of simulating post-AO PSFs, therefore for the purpose of SimCADO only the spectral aspects of the atmosphere need be addressed. Detailed simulations of the transmission and emission curves for the atmosphere have been generated by the `SkyCalc` tool^{11,12} and are used as the default in SimCADO.

- Telescope - (x,y, λ)

There are many aspects on the E-ELT that need to be addressed by SimCADO, each of which is active in a different subset of the three dimensions. These include, but are not limited to:

1. the reflectance of the mirrors - (λ) ,

SimCADO assumes that the same coating will be used for all 5 mirrors. Currently SimCADO uses the reflectance curve provided by ESO for a layered silver-aluminium (AgAl) coating with a magnesium fluoride (MgF_2) protective layer¹⁷||.

2. the thermal emission of the mirrors - (λ) ,

A simple grey-body curve is used to estimate the background photon flux due to the 5 mirrors in the system.

3. the AO corrected PSF - (x,y,λ) ,

Currently SimCADO provides the option to use several obscured types of PSF kernels: analytical PSFs generated on-the-fly which follow the form of a Gaussian, Airy or Moffat function (see Section 3.6; simulated diffraction limited PSFs for a 39m mirror with hexagonal segments using the POPPY package;¹⁸ or external PSFs from the SCAO or MCAO simulation efforts. If the PSF kernels are generated internally, the spectral resolution of the PSFs is adjusted to that of the simulation. If an external FITS file containing PSF kernels is provided, the PSF nearest to the needed wavelength is chosen (although the user is warned if the difference in wavelength is >10 nm.)

4. the residual vibration of the telescope structure - (x,y) ,

Although the AO systems will be able to adapt to the low frequency vibrations, vibrations with frequencies higher than the wavefront sensor (WFS) read-out time will continue to affect the image quality. As vibrations are an artifact of the telescope structure, and not the optics, they are wavelength independent. The vibrations also act on timescales much shorter than a single detector readout, therefore the sum effect of the telescope vibrations can be approximated as an additional convolution with a Gaussian PSF. Currently, SimCADO uses a circular Gaussian kernel, however we will update this model once more information on the vibrational modes of the main E-ELT structure becomes available.

5. the tracking uncertainties - (x,y)

With a pixel-scale of 4mas, tracking an object across the sky becomes rather challenging. During a single detector read-out (~ 3 sec) the sky will have moved almost a full MICADO field of view. This means the tracking system will have updated the position of the image more than 25,000 times during this time. It is improbable that the image position will stay exactly in the centre of the frame during each movement**. Therefore SimCADO also has the functionality to blur the image along a specific vector, either using a Gaussian or linear distribution, in order to simulate errors in the tracking process. Again, once more information becomes available regarding the tracking systems, this aspect will be updated accordingly.

- Instrument - (x,y,λ)

The various elements of the MICADO instrument are represented as a collection of different effects on the incoming photons. As MICADO is still in the preliminary design phase, many of the elemental descriptions are expected to be updated as the instrument design is refined over the next 4 years. The elements modelled by SimCADO are:

1. the cryostat window - (λ)

Currently set to 95% to reflect the current choice of material for the cryostat window. The material exhibits a flat transmission curve through out the NIR wavelength range.

2. the collimator and camera optics $(x,y), (\lambda)$

The current design of MICADO contains nine reflective surfaces which affect both the spectral and spatial characteristics of the incoming photons. However, the spatial effect can be decoupled from the spectral effect due to the purely reflective nature of the optics. Thus the collimator+camera optics

||https://www.eso.org/sci/facilities/eelt/science/drm/tech_data/telescope/

**The AO WFS units will only have read-out ~ 750 frames in the same time period. Although the AO systems may be able to correct for tracking errors, there will still be a residual shift due to these different time scales.

can be split into a spectral component based on the reflectance of the mirror surfaces and a spatial component based on the distortion map of the system.

3. Atmospheric Dispersion Corrector (ADC) - (x,y,λ)

The job of the ADC is to remove the atmospheric dispersion which leads to an elongation of point sources within a filter bandpass. If the ADC is performing as per specifications, there should be no noticeable elongation in the detector images, and hence this element need not be considered in the simulations. However, if the ADC performance is sub-par, then SimCADO adds in a shift along the zenith direction relative to the degree to which the ADC is misbehaving. If the ADC is taken out of the optical train completely, the shift that SimCADO adds to each spectral layer is equal to the full extent of the atmospheric dispersion for the wavelength of the layer at the zenith distance of the observation.

4. Derotator - (x,y)

In order to counteract the rotation of the sky, the entire MICADO cryostat is rotated as an observation takes place. As with the tracking of the E-ELT main structure, there will always be a certain amount of error induced because of the mechanical nature of the derotator. For photon sources near the centre of the FoV, these errors are negligible, however at the edge of the field, the shift become non-trivial. Similar to the ADC in SimCADO, if the derotator is performing perfectly, this effect need not be considered. However if it is turned off, SimCADO adds a rotational blur (see E in Figure 3) to the focal plane image. This can be done linearly, i.e. no derotation, or with a Gaussian distribution, to simulate errors induced by uncertainty in the rate of rotation.

• Detector - (x,y)

The MICADO detector array will consist of nine Teledyne Hawaii-4RG detector chips,¹⁹ similar to the ones used in the JWST NIRSpec Instrument.²⁰ Although the chips are sensitive to a large range of wavelengths, they do not differentiate between photons of different energies. Hence they have a purely spatial effect on the output image. The majority of the work in modelling the noise characteristics of the Hawaii chips has already been done by Rauscher et al. (2012)²¹ and Moseley et al. (2010),²² which led to the development of the HxRG Noise Generator code.¹⁴ SimCADO uses this code to apply detector noise frames to the final chip read-out images.

4.2 Aspects of the optical train to be included in later releases

As time is of the essence during the design phase, we have decided to release the SimCADO core package to certain members of the MICADO consortium. This serves the dual purpose of allowing these members to become familiar with SimCADO, as well as helping us to improve the usability of the code. The core package allows basic simulations of the full MICADO detector array, which will be suitable for the majority of use cases. In future releases for the imaging module of SimCADO we aim to include the following features:

- Observational coordinates - The ability to specify the R.A. and Dec. coordinates, as well as the date and time of any observation will allow various science cases to be tested for specific objects, e.g. solar system bodies, star clusters in nearby galaxies (e.g. NGC300).
- Extra-terrestrial optical path elements - Zodiacal light, galactic extinction, atmospheric extinction and scattered moonlight (bluewards of $1\text{ }\mu\text{m}$) also contribute a non-negligible amount to the background photon flux and should therefore also be included in science case studies
- Variable sky background - As the sky background in the NIR is dominated by OH lines, and the OH density varies over time along the line of sight, the varying sky background emission can also play a large role in determining the sensitivity of long exposure observations.
- Missing segments - According to the plan B construction scenario for the E-ELT, several segments will be missing from the primary mirror each night due to the need to re-coat the mirror surface. This will no doubt affect the PSF.

- PSF variability over the FoV - Currently SimCADO convolves the source image with a single wavelength-dependent PSF. However the PSF at any point in the FoV will depend on the distance to the guide stars being used for the AO correction.
- Updated instrumental distortion map - As the optical design of MICADO progresses, so too will the estimation of the instrumental distortion. For the majority of science cases this effect is negligible, however for astrometric science cases, as well as the data reduction process, the distortion of the pixels over the FoV is very important.

5. CONCLUSION

SimCADO currently contains all the functionality needed to generate realistic mock detector array readout images for the MICADO instrument on the E-ELT. By being written in Python 3 and only requiring `numpy`, `scipy` and `astropy` as the core dependencies, we have met the first and second of our development goals. The third and fourth goals are met by SimCADO’s API. The user does not need to have any prior knowledge of the MICADO instrument to use SimCADO, yet through the `UserCommands` class the user still has full access to all the parameters used to control simulations, if she or he so desires. The `Source`, `OpticalTrain` and `Detector` classes allow for simulations to be run with as little as five lines of code, yet also give access to all the internal mechanisms governing the flow of the simulation. Finally SimCADO fulfils our fifth development goal by accepting input in either the commonly used FITS or ASCII formats, and outputting all data as FITS files. By staying within the standard FITS framework, images generated by SimCADO can therefore be used by the veritable zoo of other programs already in use within the astronomical community.

Just as the primary function of MICADO is wide-field imaging, the current state of the SimCADO package allows the user to simulate mock imagery for the MICADO detector array. In a future release the ability to simulate the spectroscopic capabilities of MICADO will become available. The modularity of the SimCADO design will allow us to add this functionality with minimal effort. However simulations with SimCADO will only ever reflect the current status of the MICADO design. As MICADO matures, so too will SimCADO. Similarly, we will endeavour to incorporate more detailed information on the MAORY and E-ELT designs as it becomes available.

ACKNOWLEDGMENTS

This research made use of Astropy, a community-developed core Python package for Astronomy.²³ This research made use of POPPY, an open-source optical propagation Python package originally developed for the James Webb Space Telescope project.¹⁸ SimCADO incorporates Bernhard Rauscher’s HxRG Noise Generator package for python.¹⁴ SimCADO makes use of atmospheric transmission and emission curves generated by ESO’s SkyCalc service, which was developed at the University of Innsbruck as part of an Austrian in-kind contribution to ESO. This research is partially funded by the project IS538003 of the Hochschulraumstrukturmittel (HRSM) provided by the Austrian Government and administered by the University of Vienna. The authors would also like to thank all the members of the consortium for their effort in the MICADO project, and their contributions to the development of this tool.

REFERENCES

- [1] Gilmozzi, R. and Spyromilio, J., “The European Extremely Large Telescope (E-ELT),” *The Messenger* **127** (Mar. 2007).
- [2] Davies, R., Ageorges, N., Barl, L., Bedin, L. R., Bender, R., Bernardi, P., Chapron, F., Clenet, Y., Deep, A., Deul, E., Drost, M., Eisenhauer, F., Falomo, R., Fiorentino, G., Förster Schreiber, N. M., Gendron, E., Genzel, R., Gratadour, D., Greggio, L., Grupp, F., Held, E., Herbst, T., Hess, H.-J., Hubert, Z., Jahnke, K., Kuijken, K., Lutz, D., Magrin, D., Muschielok, B., Navarro, R., Noyola, E., Paumard, T., Piotto, G., Ragazzoni, R., Renzini, A., Rousset, G., Rix, H.-W., Saglia, R., Tacconi, L., Thiel, M., Tolstoy, E., Trippe, S., Tromp, N., Valentijn, E. A., Verdoes Kleijn, G., and Wegner, M., “MICADO: the E-ELT adaptive optics imaging camera,” in [Ground-based and Airborne Instrumentation for Astronomy III], *Proceedings of the International Society for Optical Engineering* **7735**, 77352A (July 2010).

- [3] Peterson, J. R., Jernigan, J. G., Kahn, S. M., Rasmussen, A. P., Peng, E., Ahmad, Z., Bankert, J., Chang, C., Claver, C., Gilmore, D. K., Grace, E., Hannel, M., Hodge, M., Lorenz, S., Lupu, A., Meert, A., Nagarajan, S., Todd, N., Winans, A., and Young, M., "Simulation of Astronomical Images from Optical Survey Telescopes Using a Comprehensive Photon Monte Carlo Approach," *The Astrophysical Journal, Supplement* **218**, 14 (May 2015).
- [4] Winkler, R., Haynes, D. M., Bellido-Tirado, O., Xu, W., and Haynes, R., "TOAD: a numerical model for the 4MOST instrument," in [Modeling, Systems Engineering, and Project Management for Astronomy VI], *Proceedings of the International Society for Optical Engineering* **9150**, 91500T (Aug. 2014).
- [5] Zieleniewski, S., Thatte, N., Kendrew, S., Houghton, R. C. W., Swinbank, A. M., Tecza, M., Clarke, F., and Fusco, T., "HSIM: a simulation pipeline for the HARMONI integral field spectrograph on the European ELT," *Monthly Notices of the Royal Astronomical Society* **453**, 3754–3765 (Nov. 2015).
- [6] Schmalzl, E., Meisner, J., Venema, L., Kendrew, S., Brandl, B., Blommaert, J., Glaske, A., Lenzen, R., Meyer, M., Molster, F., and Pantin, E., "An end-to-end instrument model for the proposed E-ELT instrument METIS," in [Modeling, Systems Engineering, and Project Management for Astronomy V], *Proceedings of the International Society for Optical Engineering* **8449**, 84491P (Sept. 2012).
- [7] Pickles, A. J., "A Stellar Spectral Flux Library: 1150-25000 Å," *Publications of the Astronomical Society of the Pacific* **110**, 863–878 (July 1998).
- [8] Diolaiti, E., "MAORY: A Multi-conjugate Adaptive Optics RelaY for the E-ELT," *The Messenger* **140**, 28–29 (June 2010).
- [9] Pedani, M., "Sky surface brightness at Mount Graham II. First JHKs science observations with the Large Binocular Telescope," *New Astronomy* **28**, 63–69 (Apr. 2014).
- [10] Moreels, G., Clairemidi, J., Faivre, M., Pautet, D., Rubio da Costa, F., Rousselot, P., Meriwether, J. W., Lehmacher, G. A., Vidal, E., Chau, J. L., and Monnet, G., "Near-infrared sky background fluctuations at mid- and low latitudes," *Experimental Astronomy* **22**, 87–107 (Oct. 2008).
- [11] Noll, S., Kausch, W., Barden, M., Jones, A. M., Szyszka, C., Kimeswenger, S., and Vinther, J., "An atmospheric radiation model for Cerro Paranal. I. The optical spectral range," *Astronomy & Astrophysics* **543**, A92 (July 2012).
- [12] Jones, A., Noll, S., Kausch, W., Szyszka, C., and Kimeswenger, S., "An advanced scattered moonlight model for Cerro Paranal," *Astronomy & Astrophysics* **560**, A91 (Dec. 2013).
- [13] Bertin, E. and Arnouts, S., "SExtractor: Software for source extraction.," *Astronomy & Astrophysics, Supplement* **117**, 393–404 (June 1996).
- [14] Rauscher, B. J., "Teledyne H1RG, H2RG, and H4RG Noise Generator," *Publications of the Astronomical Society of the Pacific* **127**, 1144–1151 (Nov. 2015).
- [15] Arcidiacono, C., Schreiber, L., Bregoli, G., Diolaiti, E., Foppiani, I., Cosentino, G., Lombini, M., Butler, R. C., and Ciliegi, P., "End to end numerical simulations of the MAORY multiconjugate adaptive optics system," in [Adaptive Optics Systems IV], *Proceedings of the International Society for Optical Engineering* **9148**, 91486F (Aug. 2014).
- [16] Clenet, Y., Gratadour, D., Gendron, E., Rousset, G., and Sevin, A., "First GPU-based end-to-end AO simulations to dimension the E-ELT MICADO SCAO mode," in [Proceedings of the Third AO4ELT Conference], Esposito, S. and Fini, L., eds., 29 (Dec. 2013).
- [17] Bocca, M., Vucina, T., Araya, C., Vera, E., and Ahhee, C., "Protected-silver coatings for the 8-m Gemini telescope mirrors," *Thin Solid Films* **502**, 275–280 (Apr. 2006).
- [18] Perrin, M. D., Long, J., Sivaramakrishnan, A., Lajoie, C.-P., Elliot, E., Pueyo, L., and Albert, L., "WebbPSF: James Webb Space Telescope PSF Simulation Tool." Astrophysics Source Code Library (Apr. 2015).
- [19] Hall, D. N. B., "The Development And Use Of The HAWAII 2RG Array And SIDECAr ASIC For 1 - 5 Micron IR Observations With A Preview Of The Coming HAWAII 4RG-15.," in [American Astronomical Society Meeting Abstracts #217], *Bulletin of the American Astronomical Society* **43**, 425.07 (Jan. 2011).

- [20] Rauscher, B. J., Fox, O., Ferruit, P., Hill, R. J., Waczynski, A., Wen, Y., Xia-Serafino, W., Mott, B., Alexander, D., Brambora, C. K., Derro, R., Engler, C., Garrison, M. B., Johnson, T., Manthripragada, S. S., Marsh, J. M., Marshall, C., Martineau, R. J., Shakoorzadeh, K. B., Wilson, D., Roher, W. D., Smith, M., Cabelli, C., Garnett, J., Loose, M., Wong-Anglin, S., Zandian, M., Cheng, E., Ellis, T., Howe, B., Jurado, M., Lee, G., Nieznanski, J., Wallis, P., York, J., Regan, M. W., Hall, D. N. B., Hodapp, K. W., Böker, T., De Marchi, G., Jakobsen, P., and Strada, P., “Detectors for the James Webb Space Telescope Near-Infrared Spectrograph. I. Readout Mode, Noise Model, and Calibration Considerations,” *Publications of the Astronomical Society of the Pacific* **119**, 768–786 (July 2007).
- [21] Rauscher, B. J., Arendt, R. G., Fixsen, D. J., Lander, M., Lindler, D., Loose, M., Moseley, S. H., Wilson, D. V., and Xenophontos, C., “Reducing the read noise of HAWAII-2RG detector systems with improved reference sampling and subtraction (IRS²),” in [*High Energy, Optical, and Infrared Detectors for Astronomy V*], *Proceedings of the International Society for Optical Engineering* **8453**, 84531F (July 2012).
- [22] Moseley, S. H., Arendt, R. G., Fixsen, D. J., Lindler, D., Loose, M., and Rauscher, B. J., “Reducing the read noise of H2RG detector arrays: eliminating correlated noise with efficient use of reference signals,” in [*High Energy, Optical, and Infrared Detectors for Astronomy IV*], *Proceedings of the International Society for Optical Engineering* **7742**, 77421B (July 2010).
- [23] Astropy Collaboration, Robitaille, T. P., Tollerud, E. J., Greenfield, P., Droettboom, M., Bray, E., Aldcroft, T., Davis, M., Ginsburg, A., Price-Whelan, A. M., Kerzendorf, W. E., Conley, A., Crighton, N., Barbary, K., Muna, D., Ferguson, H., Grollier, F., Parikh, M. M., Nair, P. H., Unther, H. M., Deil, C., Woillez, J., Conseil, S., Kramer, R., Turner, J. E. H., Singer, L., Fox, R., Weaver, B. A., Zabalza, V., Edwards, Z. I., Azalee Bostroem, K., Burke, D. J., Casey, A. R., Crawford, S. M., Dencheva, N., Ely, J., Jenness, T., Labrie, K., Lim, P. L., Pierfederici, F., Pontzen, A., Ptak, A., Refsdal, B., Servillat, M., and Streicher, O., “Astropy: A community Python package for astronomy,” *Astronomy & Astrophysics* **558**, A33 (Oct. 2013).

3

Verifying SimCADO and Predicting MICADO limiting magnitudes

3.1 Overview

While the previous chapter was dedicated to the design and implementation of SimCADO, this chapter presents SimCADO as a usable piece of software. Like any piece of software, there will always be bells and whistles that can still be added. There are plenty of aspects that I would like to build into the software, however the current version is more than capable of simulating both of the MICADO imaging modes: the wide-field mode with a plate scale of 4 mas and the zoom mode with a plate scale of 1.5 mas.

The chapter is presented in the form of a manuscript which will soon be submitted to *Astronomy and Astrophysics*. The status of the paper is currently “under internal review” as I’m waiting on the final comments from the co-authors. The paper contains three main sections: Section 3.5 describes the main aspects of the simulated ELT/MICADO optical train and the data used to describe each optical element. This section aims to show the level of complexity already included in the current version of SimCADO.

In order to prove that SimCADO produces meaningful results I set up SimCADO to model the VLT/HAWK-I optical train. I used this “HAWK-ADO” to simulate images of two globular clusters and compared the output images from SimCADO with raw images taken from the ESO archive. Section 3.6 describes the validation study. I had tested the accuracy of output from the numerous individual functions in SimCADO during the code writing phase, however this was the first “real” test of SimCADO’s abilities. Thankfully it passed the test, with the photometric measurement of stars in the simulated images matching those from the real HAWK-I images.

The third topic which I address in the manuscript is the predictive power of SimCADO. Given the success of the validation run against HAWK-I, I am confident simulated observations produced by SimCADO will be close to what a hypothetical MICADO could achieve if it were to perform according to the data we have on-hand. In Section 3.7 I show the results of some simple simulations to find both the faint and bright sensitivity limits of MICADO. To put this into a scientific context I transformed the detection limits into horizons of observability for a set of main sequence stars. Given the increase in angular resolution and corresponding reduction in pixel size compared to current instruments, the greatest gains from MICADO will come from observing point sources. Hence I felt the most useful predictions would therefore be those relating to stellar populations. Chapter 4 elaborates on this point.

3.2 Publication Details

Title: SimCADO I: The imaging modes of the instrument data simulator for MICADO at the ELT

Authors: Kieran Leschinski, Oliver Czoske, Gijs Verdoes Kleijn, Werner Zeilinger, João Alves, Rainer Kohler, Michael Mach, and Stefan Meingast

Status: Under internal review. To be submitted in April 2018.

Own contributions: Everything related to the development of SimCADO and the writing of this paper.

SimCADO I: The imaging modes of the instrument data simulator for MICADO at the ELT

K. Leschinski¹, O. Czoske^{2,1}, G. Verdoes Kleijn³, W. Zeilinger¹, J. Alves¹, R. Köhler^{2,1}, M. Mach¹, and S. Meingast¹

¹ Department of Astrophysics, University of Vienna, Türkenschanzstr. 17, A-1180 Vienna, Austria
e-mail: kieran.leschinski@univie.ac.at

² Institut für Astro- und Teilchenphysik, Universität Innsbruck, Technikerstr. 25/8, A-6020 Innsbruck, Austria

³ Kapteyn Astronomical Institute, University of Groningen, PO Box 800, 9700 AV Groningen, The Netherlands

Received 01.03.2018; accepted TBD

ABSTRACT

Context. When the Extremely Large Telescope comes online at the end of 2024, MICADO will be the near infrared imaging camera available at first light. As part of the design activities for MICADO we have developed SimCADO: an instrument data simulator in the form of a Python package. SimCADO produces simulated data frames for MICADO's nine detector chips by applying the effects of each element along the optical train to a three dimensional (x, y, λ) description of the flux arriving from an astronomical object. Simulated images can be written to disk as FITS files and can be analysed by the standard suite of astronomical software.

Aims. The main aims of this paper are two fold: to introduce the SimCADO software, and to provide preliminary detection limits for MICADO based on SimCADO simulations. By presenting these limits we also aim to raise awareness in the community of the future capabilities of MICADO and the current capabilities of SimCADO.

Methods. To verify the accuracy of SimCADO we compared the characteristics of simulated images of globular clusters with images of the same clusters from the ESO archive. We then used a model of the current optical train design for MICADO to determine the sensitivity limits for MICADO at the ELT.

Results. SimCADO is able to accurately reproduce the image characteristics of raw archival HAWK-I data to within the limits of the model of the UT4/HAWK-I optical train. Using the current design of MICADO, SimCADO finds detection limits in the J, H and Ks filters to be 28.7^m , 27.9^m and 27.3^m (Vega) respectively for a 5σ detection in a 5 hour observation. This leads to the ability to observe for the first time with a ground based observatory individual A0 V stars at a distance of 4 Mpc (i.e. in Centaurus A), and M9 V stars in the Large Magellanic Cloud.

1. Introduction

Over the next decade the era of the extremely large telescopes will begin. The European Extremely Large Telescope (ELT, Gilmozzi & Spyromilio 2007) will provide astronomers with the increase in resolution and sensitivity needed to solve many of the outstanding questions of modern day astronomy.

With a 39 m primary mirror consisting of 798 individually steerable 1.45 m hexagonal mirror segments and a fully deformable quaternary mirror, the ELT will be capable of providing diffraction-limited imaging with the help of the adaptive optics (AO) modules. This corresponds to a core full-width half maximum (FWHM) for the point spread function (PSF) in the J-band ($1.2 \mu\text{m}$) of 8 mas and 14 mas in the Ks-band ($2.16 \mu\text{m}$). Both single- and multi-conjugate modes for the adaptive optics will be possible. Laser guide stars (LGS) will be available to ensure that the ELT will always be able to provide AO-assisted observations.

As the first-light wide-field imaging camera for the ELT, MICADO – the Multi-AO Imaging CAmera for Deep Observations (Davies et al. 2010) – will take advantage of the ELT's near-infrared optimised design to provide images at the diffraction limit. MICADO will provide a wide-field imaging mode and a zoom (narrow-field) mode with 4 mas/pixel and 1.5 mas/pixel plate-scales respectively. The detector plane will consist of nine 4096×4096 detector chips, allowing MICADO to cover a Field of View (FOV) of $55''$ by $50''$ in the wide-field mode and $21''$ by $19''$ in the zoom mode.

MICADO will also contain a series of additional modes, including: a long-slit spectrographic mode with a spectral resolution of up to $R \approx 20\,000$ for point sources and $R \approx 8000$ for extended sources, windowed high-time-resolution (HTR) imaging mode with a read-out speed of up to 250 Hz and a high-contrast imaging mode.

As the scale and complexity of telescopes and instruments increases, so too does the importance of accurately being able to predict the performance of these systems. More and more emphasis is being placed on developing simulation software to model all aspects of new instruments before they enter the construction phase. As part of the development of the MICADO instrument, the Data Flow System (DFS) work package within the MICADO consortium has been tasked with creating a tool to simulate raw detector read-out images based on the current designs of the ELT and MICADO. Here we present SimCADO, the instrument data simulator for MICADO. SimCADO combines the most recent data from the other work packages in the consortium to allow the user to simulate the above mentioned raw data frames that will be produced by the ELT/MICADO optical system. Originally conceived as a tool to aid the development of the data reduction pipeline, SimCADO has also found use among the science team as a way of conducting feasibility studies for various future observations.

In this paper we introduce the SimCADO package and show that it is a useful tool for producing not only accurate simulated images for the MICADO/ELT optical system, but also for any other optical train, such as for HAWK-I on UT4 at the VLT. It

should be noted that the design of SimCADO is described in detailed in Leschinski et al. (2016). Aspects which have been updated in the mean time are detailed in this paper. For all other design aspects the reader should still consult Leschinski et al. (2016). This paper is organised in the following way: Sect. 2 delves briefly into the motivation behind creating SimCADO as well as giving an overview of the scope of the project. The physical effects that SimCADO models are described in Sect. 3. A description of how we validated SimCADO by comparing simulated VLT/HAWK-I read-out frames to real images from the ESO archive can be found in Sect. 4 and predictions for the sensitivity of the ELT/MICADO system are presented in Sect. 5. A discussion of the results, assumptions and issues with the simulated images is presented in Sect. 6.

2. SimCADO – the Python package for simulating MICADO observations

2.1. Motivation and Scope

The scientific return of instruments like the ELT and MICADO is the primary reason for building such complex pieces of machinery. Knowing in advance what the capabilities of an instrument will be, and preferably knowing just how well the instrument will perform for different configurations is invaluable during the design phase. Furthermore, MICADO and the other ELT instruments (e.g. HARMONI, Thatte et al. 2010; METIS, Brandl et al. 2008; etc.) are being built by trans-national consortia, with many members from different institutes in different countries. As such the nodes in the consortia enjoy a certain level of geographic displacement. Each node in the consortia therefore often defaults to generating their own simulated data for the task to which they have been assigned. Additionally, the end users of the instrument also want to know how the instrument will behave and how useful it will be for their personal scientific projects well in advance so that they may prepare for when the instrument becomes available. All of these points can be considered true for almost all large instrument projects in modern day science – hence why there has been a very concerted effort by the scientific community, and very notably by the astronomical community to develop full scope instrument data simulators for major projects (see e.g. HSIM for ELT/HARMONI, Zieleniewski et al. 2015; the ELT/METIS simulator, Schmalzl et al. 2012; PhoSim for the LSST, Peterson et al. 2015; TOAD for 4MOST, Winkler et al. 2014; WebbPSF for JWST, Perrin et al. 2015; IRIS Data Simulator for TMT, Wright et al. 2016; etc.).

2.2. The SimCADO target users

We have developed SimCADO for use primarily within the MICADO consortium, but also for interested external parties. SimCADO's main strength is that it gives all members of the consortium a common tool to generate simulated data for their assigned tasks. We see the following use cases for SimCADO:

The science team: During the current design phase the science team members are running feasibility studies to determine which science cases are the biggest drivers for the design of the instrument. By using a common tool to generate simulated images, the science team, and those using the findings of the science team to make design decisions, can be confident that the results are all consistent.

The astronomy community at large: Although first-light for the ELT is slated for 2024, preparation work needs to begin well in advance so that the astronomical community can “hit the ground running” once the ELT and MICADO are online. Many of the ideas that will be tested post-2024 will need to be developed over the coming years. It is therefore important that the astronomical community have a tool that enables new ideas to be thoroughly tested, and where necessary, preparation observations to be conducted, before applying for time with MICADO. SimCADO can help test the feasibility of observations for new ideas.

MICADO and ESO data flow teams: In order to create a reliable set of reduced data products which are available from the beginning of operations, the data reduction pipeline must be developed before the first data are collected. Development of the pipelines can happen concurrently to the development of the instruments, however without a telescope there is little that can be done to validate these pipelines before the commissioning of the telescope and instruments. SimCADO takes into account all processes that affect the incoming light as it travels from the source to the detector. As such SimCADO can substitute for the ELT and MICADO by producing so-called “dirty” raw detector frames for the reduction pipeline, thus allowing the pipelines to be validated well in advance of the commissioning phase.

Observation preparation software: Given the capabilities and expense of the ELT/MICADO system, observation time will be costly and in high demand. Therefore it is prudent to optimise observations to maximise the scientific output from any time on-sky. Currently, exposure time calculators are provided to assist in observation preparation. However, given the myriad celestial environments encountered during observations, single numbers based on look-up tables are often not enough to accurately predict exposure times. For the ELT/MICADO system, using SimCADO together with the preparation software will allow the user to not only determine the required exposure time, but also to visualise and assess the effect of surrounding objects on the detectability of the target object. This should help to reduce the number of non-detections during actual observations and increase the scientific output of the MICADO and the ELT.

The data archive: The ability to produce simulated data also allows the development of a data archive to proceed prior to the availability of real data. SimCADO images will be used to help define the data products offered by MICADO and the method of storage and retrieval well before the instrument generates any images of its own accord.

Instrument design team: SimCADO relies heavily on input from the different consortium work packages in order to produce images representative of the whole instrument. This in turn means that, by providing multiple sets of input data for a specific component in the optical train, a work package can use SimCADO to test the effect of different component designs on the final image quality. By using a standard set of use cases and weighting the importance of each aspect of the various science cases, trade-off analyses can be conducted. It should however be noted that due to its scope and design, SimCADO is not meant to replace ray tracing programs such as ZEMAX (see Sect. 2.3). For such cases the SimCADO output should only be used to

guide more realistic physics-based simulations, e.g. with ZEMAX, before making any final decisions.

The MAORY consortium: MICADO will be the first and main beneficiary of the MAORY AO module (Diolaiti 2010). Consequently the development of the MAORY module is inextricably linked to MICADO. Design choices made in the MAORY consortium will have a direct impact on the quality of the science that MICADO will be able to produce. By using SimCADO, members of the MAORY consortium will also be able to see directly how these design choices will affect MICADO observations.

2.3. SimCADO as an Instrument Data Simulator

First and foremost SimCADO was conceived as an instrument data simulator (IDS), not an end-to-end (E2E) simulator. An IDS differs from an E2E simulator in the following way: an E2E simulator models the interactions between each object and each element in the optical train with the incoming photons in a physically realistic manner, i.e. taking into account the physical interactions between photons and computer representations of physical objects along the optical train (see photon-tracing in PhoSim for the LSST: Peterson et al. 2015). An IDS, on the other hand, turns the effects of each element in the optical train into mathematical operators, which are then applied to an input “image” (a 2D/3D representation of the sky). IDSs require much less computation power and are therefore much better suited for quick, personalised simulations and prototyping. However, this comes at the cost of flexibility. E2E simulations can create images for any physical configuration of the optical train, as long as a physical model of all components exist in memory. IDSs only generate output for a certain configuration if data (often originally created by an E2E simulation) already exists and can be converted into a series of mathematical operators. A good example is the case of the PSF. Given a point source with a certain brightness, the PSF will appear on the focal plane of an E2E simulation by only supplying a model of the physical objects along the light’s path (spiders, mirrors, pupil stops, etc.). An E2E simulator needs only the values pertaining to the physical positions and dimensions of these objects. An IDS on the other hand is able to project a PSF onto the focal plane because a mathematical description (either a 2D image array or a 2D function) of that PSF has been supplied. The IDS then convolves this description with one or many point sources. Regardless of how the optical train changes, unless this mathematical description has been updated from another source (i.e. output from a separate E2E simulator) the IDS images will continue to display the same PSF.

The main advantage of developing and using an instrument data simulator lies in its speed and ease of use. Because IDSs rely on the results of other simulations, IDS simulations are many orders of magnitude faster than those conducted with E2E simulators. Our main goal with SimCADO was to provide a tool that gives the casual user the ability to simulate images for MICADO in a matter of minutes on their own laptop. Such an approach is advantageous to both the user and the developer when compared to the alternative model: the user must submit a simulation request to a dedicated “simulations” team. With SimCADO running on the user’s laptop, both the time the user must wait for results and the work load of the simulations team are drastically reduced. This in turn allows the simulations team to direct their efforts towards improving the software and keeping the instrument configuration up to date.

Further justification for concentrating our efforts on an IDS rather than an E2E package comes from the fact that for the majority of cases (excluding those from the design team), the optical train stays exactly the same. Therefore there is no need to re-simulate from scratch each and every photon interaction (as an E2E simulator would do) every time a simulation is run.

3. The physical effects modelled by SimCADO

SimCADO takes into account effects for all optics elements between the light source and the detector. This includes the atmosphere, the telescope, the instrument, and the detector array. We have designed SimCADO in such a way as to allow any optical train to be modelled, providing all the relevant data is available¹. The default configuration is for the ELT/MICADO optical train. For testing purposes we have configured SimCADO to reproduce the effects of the VLT/HAWK-I optical train (see Sect. 4). In this section we describe the effects of the optical elements that the current version (0.4) of SimCADO takes into account.

For a full description and discussion of the internal workings of the SimCADO package, the reader is directed to the paper by Leschinski et al. (2016) and to the online SimCADO documentation.²

3.1. Atmosphere

Transmission and Emission: The SkyCalc tool³ (Noll et al. 2012; Jones et al. 2013) provides accurate spectral models of the atmospheric transmission and emission (see Fig. 1 for the transmission and emission curves). For SimCADO we have taken the default model, which uses atmospheric conditions averaged over the whole year and a unity airmass. In a future release we hope to include the functionality to query the SkyCalc server directly from within SimCADO. However until such time, if the user is interested in investigating the effects of different atmospheric conditions on the resulting detector output, SimCADO accepts ASCII text files generated by the online SkyCalc tool as input for simulation runs.

As an alternative to using the default spectral energy distribution provided by SkyCalc, the user may instruct SimCADO to use a certain sky background emission for a given broadband magnitude in mag/arcsec².

Atmospheric diffraction: For effects that act along all three relevant simulation dimensions (x, y, λ) SimCADO uses an adaptive layered approach. Briefly this means that SimCADO determines how separated in spectral space two individual images can be before a noticeable spatial shift between two adjoining layers occurs. This parameter can be set in the SimCADO configuration file. By default a new spectral bin is created once the shift due to the atmospheric dispersion is greater than one pixel (i.e. 4 mas and 1.5 mas in the wide-field and zoom modes, respectively). The spatial shifts induced by the atmosphere are calculated according to the formulae from Stone (1996) and from the review by Pedraz⁴. In order to avoid unnecessarily increasing the computational workload, any shifts induced by the atmospheric

¹ We have also created configuration packages for the HST+WFC3 system and the VLT/HAWK-I systems.

² <http://www.univie.ac.at/simcado>

³ <https://www.eso.org/observing/etc/bin/gen/form?INS.MODE=swspectr+INS.NAME=SKYCALC>

⁴ <http://www.caha.es/newsletter/news03b/pedraz/newslet.html>

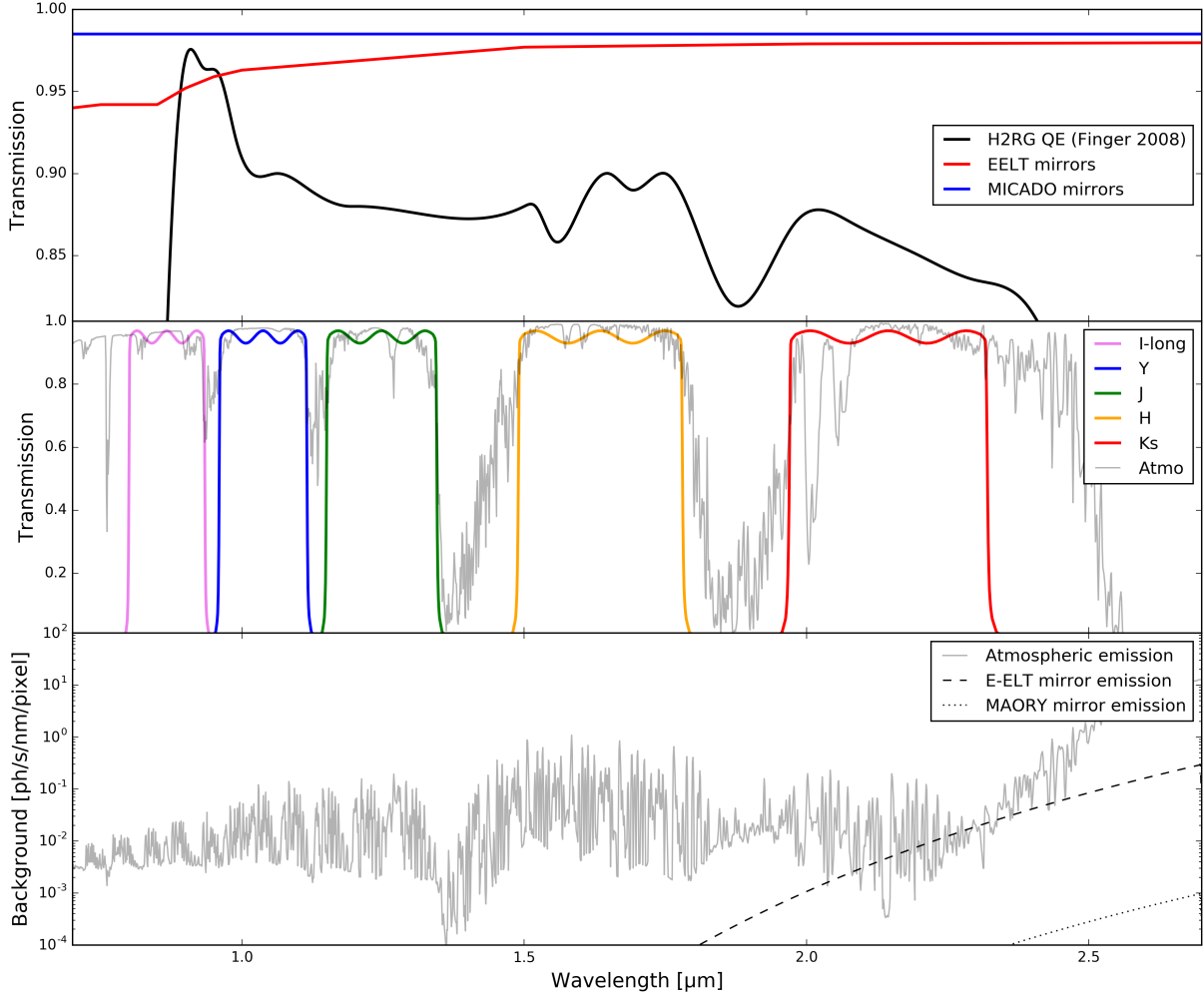


Fig. 1. Default transmission and emission curves used by SimCADO. Top: The mirror transmission curves for both the ELT and MICADO plotted together with the quantum efficiency (QE) curve for the HAWAII 2RG detectors. The ELT will use a AgAl mirror coating with a MgF₂ protective layer (Bocca et al. 2006) while the 14 MICADO mirrors will be gold coated (Davies et al. 2016). SimCADO uses the QE curve for the H2RG detectors because this information for the H4RG detector is not currently available to the public. As soon as the QE curve for the 4k detectors becomes available, the SimCADO defaults will be updated. Middle: A selection of broadband filters for MICADO (IYJHKs) based on theoretical filter properties. SimCADO ships with a collection of curves for the filters currently foreseen for use in MICADO. The atmospheric transmission curve used by SimCADO was generated by the skycalc tool (Noll et al. 2012; Jones et al. 2013) and can be adjusted for zenith distance. Bottom: the photon background flux per MICADO wide-field mode pixel (i.e. 4 mas) coming from the atmosphere and from the ELT and MAORY mirror grey-body emission. The units are photons per second per nanometer calculated for the full area of the ELT's mirrors. The sky background emission spectrum was generated using the skycalc tool with the default parameters. The ELT mirror emission is for an ambient dome temperature of 0 degrees Celsius and combines the emission from all five of the ELT's mirrors. The MAORY mirror emission is assuming warm optics at the dome temperature and the optical train as detailed by Diolaiti (2010) and Diolaiti et al. (2016). The total area of the MAORY mirrors is taken to be 3.4 m².

dispersion are inversely scaled according to the performance parameter for the atmospheric dispersion corrector (ADC). By default this is set to 100 % – i.e. no atmospheric dispersion is included.

PSF variability : SimCADO does not compute the atmospheric point spread function itself based in atmospheric parameters. Instead it requires a PSF to be provided, either by the other teams working in conjunction with the MICADO consortium (i.e. the SCAO and MCAO simulation teams) or by the user.

PSFs will be discussed in greater detail in Sect. 3.2; however, it is worth mentioning here that SimCADO provides a series of functions for generating “ELT”-like PSFs based on the POPPY PSF simulation package (Perrin et al. 2015). The function `simcado.psf.poppy_ao_psf()` allows the user to specify the level to which the seeing halo is added to an ideal diffraction limited PSF, thus allowing the user to create PSFs for different seeing conditions.

Currently SimCADO does not automatically include time variability in the PSF or in the atmospheric parameters. How-

ever, SimCADO's implementation in Python allows the user to script many different simulation configurations, thus providing the functionality to implement temporally varying atmospheric conditions. An automated method for doing this is foreseen for later releases of SimCADO.

3.2. The ELT

Point Spread Function: Being an IDS, SimCADO does not need to know how the PSF is generated or what happened to it before the instrument focal plane. All SimCADO needs is the total (wavelength dependent) effect of the whole optical train on the spatial distribution of light on the focal plane. How the atmosphere deforms the PSF and how the AO modules correct for this are outside the scope of SimCADO. Only the net effect of the two counteracting operations are important for simulations.

Currently the two adaptive optics (AO) modes that will be offered with MICADO are:

- single conjugate (SCAO, Clénet et al. 2016), which will provide diffraction-limited imaging with Strehl ratios of > 60 % in Ks-band in the centre of the field of view.
- multi-conjugate (MCAO) in conjunction with the MAORY module, which will provide diffraction-limited imaging of the full MICADO field of view with Strehl ratios between 30 % and 50 % in Ks band (Diolaiti et al. 2016)

Currently, SimCADO only provides a SCAO PSF from the AO simulation efforts of Clénet et al. (2015, obtained via private communication). MCAO PSFs will be included as soon as the MAORY consortium releases them for public use. Additionally SimCADO also provides functionality to generate lower fidelity PSFs using an analytical model. This model is not as accurate as the E2E simulations but it does allow the user to conduct comparative studies. For example, the user can investigate how different Strehl ratios will affect the results for a certain science case. The analytical PSF is generated by summing two weighted PSFs, a diffraction-limited PSF and a seeing-limited PSF, according to the equation:

$$\text{PSF}_{\text{Analytical}} = \text{SR} \times \text{PSF}_{\text{Diffraction}} + (1 - \text{SR}) \times \text{PSF}_{\text{Seeing}}, \quad (1)$$

where SR is the desired Strehl ratio, $\text{PSF}_{\text{Diffraction}}$ is the diffraction-limited PSF generated by the POPPY package (Perrin et al. 2015) for a 39 m diameter segmented mirror with six support beams for the secondary mirror (see Fig. 2), and $\text{PSF}_{\text{Seeing}}$ is a PSF following a Moffat profile with a full width half maximum (FWHM) corresponding to the seeing limit of the observations. For the seeing-limited PSF, SimCADO uses a FWHM of 0.8'' by default. The default Strehl ratio for the analytical PSF is set to the Strehl ratio that MAORY is required to provide, i.e. 30 % in K band and 12 % in J band (Diolaiti et al. 2016). Currently, SimCADO does not vary the shape of the PSF over the field, as would be consistent with AO observations. We are however developing this functionality for a future release

Transmission and emission: SimCADO uses the reflectivity curve provided by the ESO Data Reference Mission (DRM) for the ELT⁵ for an aluminium-silver mirror coating with a magnesium fluoride protective layer (AgAl-MgF_2). This is currently the preferred mirror coating for all five of the ELT mirrors. For comparison SimCADO also provides the transmission curve for

a pure aluminium coating (as used at the VLT). The reflectivity in the near infrared regime is almost constant at ~ 98 %.

The grey-body emission for the ELT is calculated by looping through each of the mirrors designated in the optical design. The emitted flux is calculated by considering the area, emissivity and temperature of each mirror. Transmission losses for each mirrors grey-body flux due to the subsequent mirrors in the optical path are also taken into account in the loop.

Wavelength independent spatial effects: Effects related to unwanted movements of the telescope are also built into SimCADO. Wind jitter and vibrations due to the cooling equipment introduce a further blurring term into the image. This can be modelled by convolving the final focal plane image with a 2D Gaussian distribution. The FWHM of the Gaussian is a function of the frequency spectra and the strengths of both the vibrations and the wind. At this stage we have assumed that the ELT's vibration damping mechanisms will remove the vast majority of vibrations. As such default vibrations in SimCADO are modelled with a 2D Gaussian with a FWHM of 0.001'', thus removing this effect from the default simulations.

SimCADO provides the functionality to simulate the smear introduced by sub-optimal mechanical performance of the ELT's tracking system. However a quick back-of-the-envelope calculation shows that the update frequency of the ELT's stepper motors needs to be on the order of 10 – 100 kHz if the sky is to move less than a MICADO pixel length between updates. This is well within the scope of modern day stepper motor technology and so by default SimCADO assumes that the ELT's tracking system will not cause noticeable image smearing.

3.3. MICADO

We have developed SimCADO during the preliminary design phase of MICADO. The default configuration for SimCADO is continually updated to reflect the most recent design of the instrument. Values presented in this subsection are correct at the time of publication, but need not be identical to those in the most recent version of the SimCADO package. See Davies et al. (2016) for the MICADO design at the time of writing.

Transmission: SimCADO takes into account all optical surfaces along the instrument optical train including: the cryostat entrance window (4 surfaces), the internal fold mirrors, the atmospheric dispersion corrector (4 prisms, 8 surfaces), the zoom optics, the filters (2 surfaces) and the pupil placeholders. Additional surfaces needed for the spectroscopy mode include the entrance slit and the grisms. These will be described in a companion paper on the SimCADO spectroscopy mode.

Currently by default all the mirrors are assumed to be coated with gold with a reflectivity of 98.5 % across the whole spectral range. The filter curves shown in Fig. 1 are theoretical predictions for the MICADO filters (R. Davies, private communications). The real filters will not have such a clean oscillatory transmission structure. Additionally SimCADO ships with all generic visual and NIR broadband filters (UBVRI $ZYJHK$ Ks) and a series of common narrow band filters for NIR observations, taken from the Spanish virtual observatory database⁶. The user is also able to direct SimCADO to use any filter curve for which they have an ASCII file containing wavelength and trans-

⁵ <https://www.eso.org/sci/facilities/eelt/science/drm/>

⁶ <http://svo2.cab.inta-csic.es/theory/fps3/index.php?mode=browse>

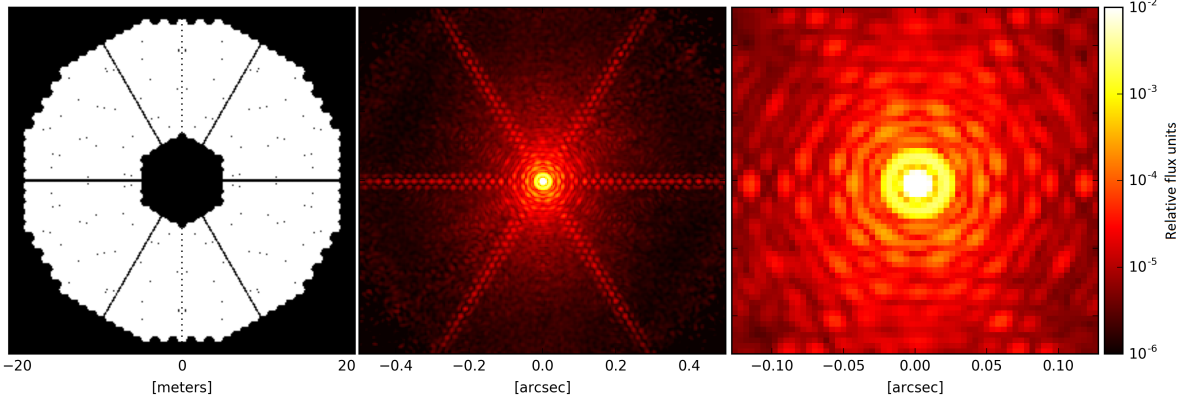


Fig. 2. Left: the ELT pupil with the full mirror configuration, not taking into account any circular obscuration in subsequent pupil planes. Middle: the current SCAO PSF used by SimCADO as developed by Clenet et al. (2013). The PSF has a Strehl Ratio of 68 % in the Ks band over a 4'' FoV. The effects of a segmented mirror on the diffraction spikes are clearly visible. Right: a cutout of the central 0.25'' of the PSFs. The effect of the segmented mirror is also present in the structure of the Airy rings around the core of the PSF.

Table 1. The root-mean-square wavefront error expected for each surface in the MICADO optical train. The total wavefront error is expected to be on the order of 76 nm, which translates to a decrease in PSF peak strength of $\sim 5\%$ at $2.2\text{ }\mu\text{m} \sim 14\%$ at $1.25\text{ }\mu\text{m}$ (R. Davies, private communication)

Wavefront error rms [nm]	Surfaces	Material	Optical element
20	11	gold	Mirror
10	4	glass	Entrance window
10	2	glass	Filter
10	8	glass	ADC

mission values by using the `TransmissionCurve` object. See the SimCADO documentation for more information.

Non Common Path Aberrations (NCPAs): The default PSFs do not take into account the NCPAs due to the difference in optical path to the wave-front sensors and to the detector array. Characterising the MICADO NCPAs is still an active topic. We will include both the spatial and spectral effects of the NCPAs in a later release of SimCADO once a model exists to describe the spatial effect. In the meantime we are able to use wave-front error budgets to determine an approximate wavelength-dependent effective transmission loss, Δf_{peak} , based on the exponential form of the Strehl ratio (Mahajan 1991):

$$\Delta f_{\text{peak}} = e^{-(2\pi WFE_{\text{total}}/\lambda)^2}, \quad (2)$$

where WFE_{total} is the combined r.m.s. wavefront error expected for all surfaces along the MICADO optical path and λ is the wavelength at which the observations are conducted. Table 1 details the individual wavefront errors that SimCADO uses to calculate WFE_{total} . The total wave front error is expected to be on the order of 76 nm which translates to a decrease in PSF peak strength of $\sim 5\%$ at $2.2\text{ }\mu\text{m}$, and $\sim 14\%$ at $1.25\text{ }\mu\text{m}$ (R. Davies, private communication).

Atmospheric Dispersion Corrector (ADC): Like the PSF, the effect of atmospheric dispersion is visible in all three instrumen-

tal dimensions (x, y, λ). In order to simulate this effect SimCADO creates an image for each one of a series of spectral bins within the filter wavelength range (see Leschinski et al. 2016 for a detailed description of how SimCADO does this). The bin width is chosen in such a way that the elongation induced by the atmospheric dispersion is never greater than one pixel (i.e. 4 mas in wide field mode, or 1.5 mas in zoom mode). If the ADC is working perfectly then the atmospheric dispersion is completely removed and the spectral bin width is equal to the full width of the filter. If the ADC is turned off, the relative shift of an image over the full J-band is around 0.19'', or almost 50 wide-field pixels, at a zenith distance of 60 degrees. To maintain a relative offset between images of less than a single pixel, SimCADO must generate images for each of the almost 50 wavelength bins. Each image is offset relative to the image of the reddest bin. By stacking all the images (including offsets) on the detector plane the dispersion caused by the atmosphere can be reproduced in the final output image. By default SimCADO assumes that the ADC achieves its design specification of no more than a 1 mas dispersion residual and so does not need to introduce any extra image slices. The functionality is nevertheless included in SimCADO.

Derotator: A perfectly functioning derotator is essential for maintaining the astrometric accuracy of sources near the edges of the detector plane. Similar to the ADC we have implemented the effect of a less-than-perfect derotation by combining a series of image slices for which the shift at the edge of the detector array is less than one pixel. However as the sky rotation is a purely spatial effect, the image slices are generated for temporal bins (i.e. a series of short “exposures”), as opposed to the spectral bins for the ADC (again, see Leschinski et al. 2016 for further details). By default, SimCADO assumes perfect derotation, but as always the defaults will be updated as soon as more information becomes available.

Instrumental Distortion: Another effect that is important for accurate astrometric measurements is the instrumental distortion. Although not included in the publicly available version of SimCADO at the time of writing (version 0.4) this functionality is currently being developed and will be included in future releases

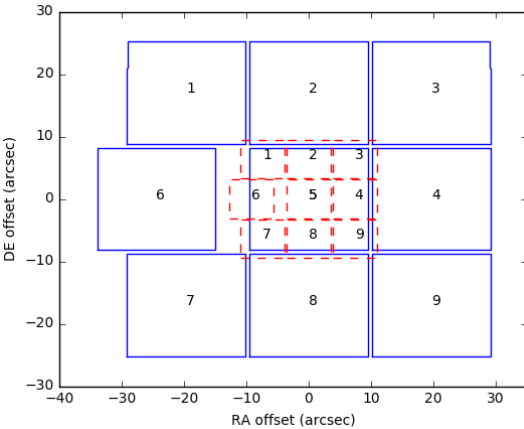


Fig. 3. The footprints of the two imaging modes for MICADO. The wide-field mode (solid lines) has an on-sky footprint of $\sim 55'' \times 50''$, while the zoom mode (dashed lines) has an on-sky footprint of $\sim 21'' \times 19''$. The H4RG will only be 3-side buttable due to the placement of the read-out electronics, the result of which is the extended gap between chips 5 and 6 in the middle row.

of the package. The implementation of the instrumental distortion will be discussed in a companion paper detailing the spectroscopic capabilities of SimCADO.

3.4. MICADO Detector Array

The current design for MICADO includes a 3×3 array of HAWAII-4RG chips (Davies et al. 2016). SimCADO takes into account the positions of the chips in the focal plane as well as the gaps between the nine chips, the electronic noise characteristics of the HAWAII chips as well as their linearity characteristics. Detailed information is not publicly available and so we have based the detector characteristics primarily on the H2RG chips, the predecessors to the H4RGs.

Electronic noise: Rauscher (2015) created the python package NGHxRG⁷ to simulate read noise frames for the HAWAII-2RG detectors used in the JWST NIRSpec instrument (Posselt et al. 2004). SimCADO uses this package to create noise frames for the HAWAII-4RG detector series. Included in the noise frames are: white (read) noise, residual bias drifts, pink $1/f$ noise and alternating column noise. Picture frame noise can also be included. However, as there are not yet any estimates for the MICADO detector array, SimCADO bases its picture frame noise on the default file provided by the NGHxRG package. The default parameters used when generating the noise frames are given in default configuration file in Appendix B.1.

Detector gaps: In its base configuration, the MICADO detector plane will consist of 9 H4RG detectors, each covering slightly more than $16'' \times 16''$ on sky. Because of the read-out electronics, each chip will only be 3-side buttable, meaning that one of the eight outer chips must be placed further from the central chip than its counterparts. This can be seen in the on-sky footprints of the zoom and wide-field modes in Fig. 3. SimCADO contains

configuration files detailing the positions of the detector chips for each of these base modes.

Linearity, Saturation, Persistence and Cross-Talk: Because detailed data on the H4RG chips are not yet publicly available, we have assumed that they will have a similar performance to the H2RG chips which are found in many current NIR instruments (e.g. VLT/HAWK-I, JWST/NIRSpec). The data for the linearity curve and saturation limits have therefore been taken from the HAWK-I detector array. As persistence and pixel cross-talk are more complex to model, SimCADO does not currently simulate these two effects. We plan to implement them in a later version of SimCADO.

Read-out schemes: SimCADO currently has two functions for reading out the chips on the detector array: “non-destructive” and “super-fast”. The non-destructive mode mimics the functionality of the HAWAII-4RG chips, which allows the user to measure the pixel values without actually destroying the content of the pixels. This mode allows any non-destructive read-out scheme to be implemented, including the commonly used Fowler, double-correlated or up-the-ramp schemes. However, this mode is not the default and the scheme must be defined by the user.

For exposure times longer than the shortest exposure time for MICADO (2.6 s), observations will be background limited. Thus it is superfluous to calculate the read noise of each frame. Instead, by default, SimCADO uses a so-called “super-fast” read-out function. The “super-fast” function does not read out a series of single exposures every 2.6 s, rather it creates a single read-out with an exposure time equal to the duration of the full observations (i.e. `EXPTIME = NOBS*DIT`). Shot noise in the image scales as the square root of the total observation time. It is no surprise that the super-fast mode is NOBS times faster than the non-destructive read-out mode. For observations using the super-fast function which are greater than ~ 10 minutes, we recommend “turning off” SimCADO’s detector linearity functionality so that the signal increases linearly with exposure time over the full duration of the observation. In future releases this will occur automatically based on the chosen mode.

4. Validating SimCADO by modelling the VLT/HAWK-I optical system

Aside from testing during the coding phase, we tested the accuracy of SimCADO by comparing simulated raw detector readout images to raw observations from HAWK-I on UT4 at the VLT. HAWK-I, the High Acuity Wide-field K-band Imager (Kissler-Patig et al. 2008), is a present-day analogue to MICADO’s imaging modes and thus a good test-bed for these comparisons. We created a configuration file that reflects the UT4/HAWK-I optical train from the publicly available instrument data on the ESO website⁸ and from HAWK-I calibration data from the ESO archive to create a version of SimCADO that simulates raw observations for the VLT/HAWK-I optical train. The first test was to see whether the HAWK-I version of SimCADO could reproduce the sensitivity limits of the VLT/HAWK-I system as given in Kissler-Patig et al. (2008). The second test involved simulating images of two globular clusters and comparing them against the real images from the ESO archive. The raw images used for

⁷ <http://jwst.nasa.gov/resources/nghxrg.tar.gz>

⁸ <http://www.eso.org/sci/facilities/paranal/instruments/HAWK-I.html>

the comparison were several J and Ks images of the globular clusters M 4 and NGC 4147, downloaded from the ESO archive. In the following sections we describe the validation process.

4.1. Modelling HAWK-I with SimCADO

To create a model of the HAWK-I optical train, SimCADO required the following data:

- an estimate of the Point Spread Function (PSF) for the whole VLT/HAWK-I system,
- transmission/reflectivity curves for each of the surfaces along the optical path,
- and details of the HAWAII-2RG detector characteristics

Additionally, a description of the globular clusters to be observed was needed. Creating the source description is described in more detail in Sect. 4.3.

The PSF: The seeing-limited nature of the UT4/HAWK-I optical train greatly simplified simulations. The combined system PSF can be described by a diffraction limited Moffat profile for the round monolithic mirrors of the UT4 telescope (Dierickx et al. 1990) combined with a Gaussian profile for the atmospheric contribution. To include the effect of the “spiders” that are part of the support structure for the secondary mirror, we used the POPPY package to generate a diffraction limited PSF for an 8.2 m circular aperture with a 1.1 m secondary obscuration and four support beams with a width of 0.1 m. We then convolved this diffraction-limited PSF with a 0.5'' 2D Gaussian profile to mimic the seeing-limited nature of HAWK-I observations. This artificial PSF can be seen in the bright stars in Fig. 7.

Transmission curves for the optical train: The combined optical train of HAWK-I and the VLT’s UT4 contains 7 aluminium-coated mirrors, an entrance window, a series of standard NIR filters and a detector plane with 4 HAWAII-2RG chips. The transmission, reflectivity and quantum efficiency curves for each of these elements were combined in SimCADO. The resulting transmission curve has an average transmission value of 0.52, which is very similar to the average value of 0.5 assumed by the online exposure time calculator provided by ESO.⁹

The detector array: Four HAWAII-2RG chips (Loose et al. 2007) are used in HAWK-I. The detector noise was generated internally by SimCADO using the NGHxRG package (Rauscher 2015). The quantum efficiency curve was taken from Finger et al. (2008). The detector linearity curve was extracted from the Ks-band archive image HAWK-I_2015-06-10T05_12_28.683. It was determined by fitting Gaussian profiles to the wings of a series of saturated stars in the raw observations and comparing the theoretical height of the best-fit Gaussian profile to the actual pixel values in saturated regions. The plate scale used by SimCADO was 0.106''.

The flat field effect of the whole system was neglected for these tests. The archive images were not flat field corrected, and no flat field was applied to the simulated images. This decision was made because the vast majority of the stars in the globular clusters were located in the central region of the image where the flat field effect only plays a minor role with regards to the photometric accuracy.

⁹ <https://www.eso.org/observing/etc/bin/simu/HAWK-I>

Table 2. Limiting magnitudes calculated for HAWK-I from images generated by SimCADO, the ESO ETC and taken from Kissler-Patig et al. (2008). The SimCADO limiting magnitudes were calculated based on a 5σ detection in a grid of 100 stars with magnitudes spread linearly between 14^m and 27^m in the respective filters. The FWHM for the SimCADO PSF was chosen to match the “Image Quality” parameter given by the ETC. For a seeing value of 0.8'' in V band and an airmass of 1.2, the resulting FWHM for J, H and Ks (Br γ) band respectively was 0.62'', 0.58'', 0.53''.

Filter	Exposure	SimCADO	ETC	KP+2008
J	1 hr	23.8 ^m	24.2 ^m	23.9 ^m
	1 min	21.5 ^m	22.0 ^m	
	2 sec	19.7 ^m	20.1 ^m	
H	1 hr	22.7 ^m	23.3 ^m	22.5 ^m
	1 min	20.5 ^m	21.0 ^m	
	2 sec	18.8 ^m	19.2 ^m	
Ks	1 hr	21.9 ^m	22.2 ^m	22.3 ^m
	1 min	19.7 ^m	19.9 ^m	
	2 sec	17.8 ^m	18.1 ^m	
Br γ	1 hr	21.6 ^m	20.9 ^m	
	1 min	19.5 ^m	18.7 ^m	
	2 sec	17.5 ^m	16.8 ^m	

4.2. HAWK-I Sensitivity with SimCADO

As a first test we compared the limiting magnitudes of images generated with SimCADO to both the limiting magnitudes given by Kissler-Patig et al. (2008), and those given by the exposure time calculator (ETC) on the ESO website. For the SimCADO model of HAWK-I we determined the limiting magnitudes by simulating images of a grid of 100 stars with magnitudes ranging from 15^m to 27^m in each of the HAWK-I filters. The grid was “observed” for a series of exposure times ranging from 2 seconds to 1 hour. As the positions of the stars were known, we used aperture photometry to calculate the signal to noise ratio (SNR) for each of the stars in each of the exposure and filters. The limiting magnitude for image was set by the star with a SNR closest to, but not lower than 5σ . The results for various exposure times are shown in Table 2 and for the J-band in Fig. 4.

It can be seen from Table 2 that the limiting magnitudes for SimCADO in the J and H filters are within 0.2^m of the values given by Kissler-Patig et al. (2008), although there is a $\sim 0.5^m$ discrepancy between SimCADO and the ETC. In the Ks filter the discrepancy is only $\sim 0.3^m$. The Br γ filter shows the biggest deviation of $\sim 0.7^m$. The observation parameters used in SimCADO were set to be identical to those described by Kissler-Patig et al. (2008), namely: seeing of 0.8'' in V-band and an airmass of 1.2. Fig. 4 shows the evolution of several relevant detection limits (e.g. 5σ for photometry, $\sim 250\sigma$ for astrometry) for HAWK-I as determined by SimCADO.

4.3. Comparison of SimCADO images with real observations

To test how well SimCADO reproduces the spatial aspects of an observation, we downloaded four raw FITS files of the globular clusters M 4 and NGC 4147 from three different observing runs conducted between 2007 and 2015 from the ESO archive. Table 3 lists the main parameters of these observations. Globular clusters by virtue of their age contain very little gas or dust and hence essentially no star formation activity. This makes them easy objects to model for SimCADO. We chose this series of raw images to test the performance of SimCADO over multiple observing configurations.

Table 3. The raw un-reduced HAWK-I data from the ESO archive used in this study. The three observations of M 4 were used to test the photometric accuracy of SimCADO under the assumption that the background level remains similar. The observation of NGC 4147 was used to test the background flux under different exposure lengths.

ESO archive filename	Filter	Exposure [s]	V-band seeing [arcsec]	Airmass	Object
HAWK-I.2015-06-10T05_12_28.683.fits	Ks	10	0.9	1.05	M 4
HAWK-I.2007-08-05T01_34_45.908.fits	Ks	10	NA	1.05	M 4
HAWK-I.2007-08-05T23_14_33.748.fits	J	10	1.1	1.02	M 4
HAWK-I.2014-01-19T07_49_48.826.fits	J	2	0.74	1.44	NGC 4147

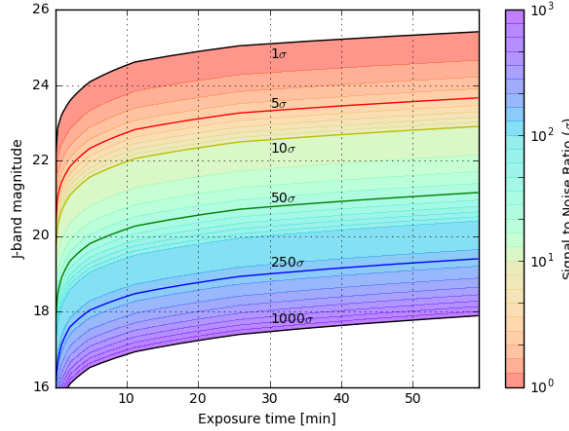


Fig. 4. A grid of hundred stars were observed for different durations between 1 and 60 minutes using SimCADO configured to model the UT4/HAWK-I optical system. The 5σ contour in this graph is $\sim 0.5^m$ lower than the theoretical 5σ detection limits as returned by the ESO HAWK-I ETC. However the one hour 5σ magnitude limit ($J = 23.7^m$) is within 0.2^m of the limit published by Kissler-Patig et al. (2008).

In order to simulate the raw images we generated SimCADO-readable Source objects for the globular clusters M 4 and NGC 4147 using the 2MASS sky coordinates and apparent magnitudes of all sources in the respective HAWK-I fields of view. These Source-objects were fed into the SimCADO model of HAWK-I and the Detector module was read out. The resulting images were analogues of the raw images generated by the HAWK-I detector chips. They contained raw pixel counts in ADUs. We used three-radius fixed aperture photometry to determine the total flux of each star and then compared flux values to the theoretical fluxes calculated from the 2MASS magnitudes. The SimCADO fluxes are in excellent agreement with the 2MASS fluxes. This was to be expected as the 2MASS catalogue provided the input for the SimCADO source model. Fig. 5 was included this figure to show the reliability of SimCADO when propagating flux through the model of the optical train. The deviation from the one-to-one line in Fig. 5 is due to SimCADO recreating the non-linearity of the HAWAII-2RG detectors for pixel counts higher than $\sim 100,000$. While it would have been possible to re-run the analysis without a perfectly linear detector response, it was not deemed necessary to illustrate SimCADO’s ability to accurately propagate flux through the optical train.

The same fixed aperture photometry method was also applied to the raw HAWK-I images from the archive. Fig. 6 shows a comparison between the total aperture flux for stars in a real K-band image of M 4 and its simulated counterpart. There is a good correlation between the fluxes extracted from the two im-

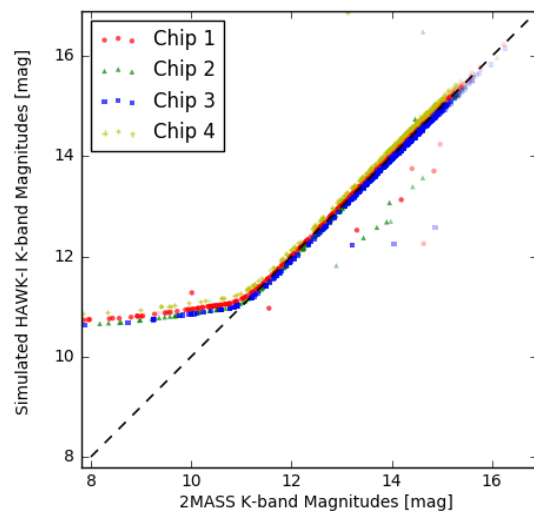


Fig. 5. Instrumental K-band magnitudes from an observations of M 4 simulated with SimCADO (SimCADO output) versus K-band magnitudes from the 2MASS catalogue (SimCADO input). The one-to-one correlation was to be expected because the brightness levels of the stars in the simulated images were based on the 2MASS catalogue. The cloud of points below the line shows where two stars were close enough together that the pipeline chose the wrong star. It was set up to choose the brightest star within a $1''$ radius around each coordinate in the 2MASS catalogue. The deviation from the one-to-one line around $K_s = 11^m$ is due to SimCADO reproducing the the HAWK-I detector saturation limit. The effect of the different gain values for the HAWK-I detector chips is also visible as the slight offset between the different coloured dots. The instrumental zero-point used was 27.2^m .

ages. For chips 1 and 2 more than 75 % of stars with A-grade 2MASS photometry fall within these $\pm 0.3^m$ of the one-to-one line. For chips 3 and 4 it is more than 85 %. Approximately 55 % of the sources with C-grade or less photometry flags fell outside the $\pm 0.3^m$ zones. When investigating these sources we found a large fraction to be single entries in the 2MASS catalogue which were resolved into two stars in the HAWK-I images. In these cases our photometric pipeline selected the brightest of the resolved stars in the HAWK-I images and measured its flux. The flux of the star in SimCADO was based on the 2MASS catalogue, which includes the flux from all the unresolved stars, and was thus brighter in the simulated images. This is the primary cause of the scatter seen above the one-to-one line in Fig. 6. As the artificial globular cluster for SimCADO is based on the 2MASS catalogue for M 4, there are no sources fainter than the 2MASS detection limit. The presence of the fainter background sources, and thus a non-uniform increase in the background flux in the real images further reduced the accuracy of the photomet-

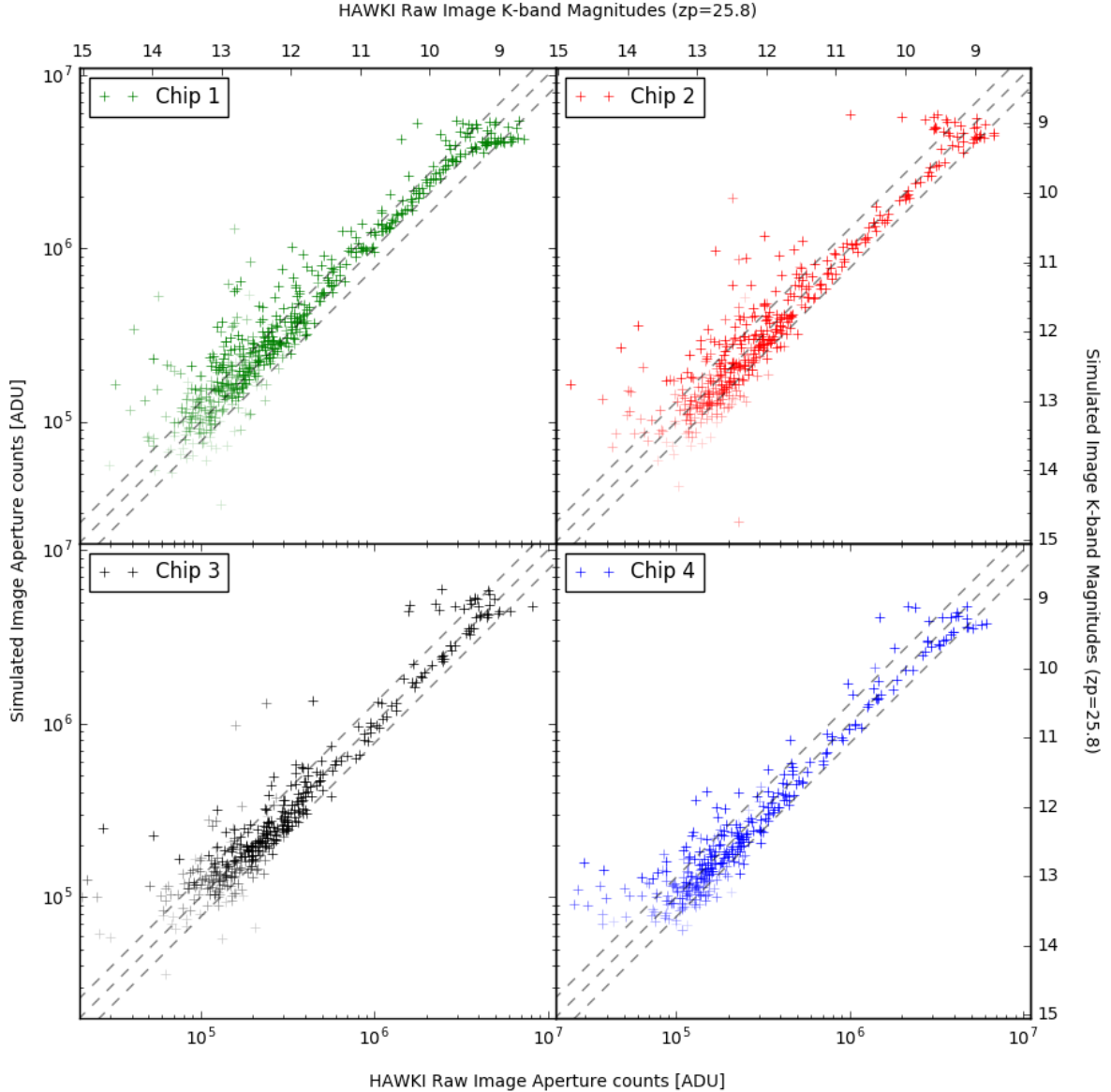


Fig. 6. Flux counts from aperture photometry of the stars in the simulated and real Ks-band images of M 4. Each detector chip is plotted separately here as they cover different regions of M 4 and have different gain factors. The strength of the symbols is determined by the photometric quality flag in the 2MASS catalogue. The dashed lines are the $\pm 0.3^m$, or 30 % flux difference intervals. For chips 1 and 2 more than 75 % of stars with A-grade 2MASS photometry fall within these bands. For chips 3 and 4 this is $> 85\%$. Approximately 55 % of the sources with C-grade or worse 2MASS photometry flags fell outside the $\pm 30\%$ bands. When investigating these sources we found a large fraction to be single entries in the 2MASS catalogue, but were resolved out into two (or more) stars in the HAWK-I images. Photon statistics only play a role for aperture fluxes on the order of 10^4 counts.

ric measurements for sources with magnitudes $K_s > 12^m$. In this faint regime “hot” or “dead” pixels also affect the accuracy of the photometry. As we did not provide SimCADO with a pixel map for HAWK-I, malfunctioning pixels included in the simulated images were not the same as those on the HAWK-I detectors. These pixels are the primary cause of the scatter below the one-to-one line in Fig. 6. Finally, the small but uniform $< 0.1^m$ shift

in the photometry between detector chips was caused by the difference in the detector gain factors (Kissler-Patig et al. 2008).

Aside from reproducing the expected stellar fluxes on the detector plane, and more important for making predictions for MICADO and the ELT, is SimCADO’s ability to accurately reproduce the background flux distribution. For the strength of the sky background for the raw archive images, we assumed standard sky background magnitudes as given by Cuby et al. (2000).

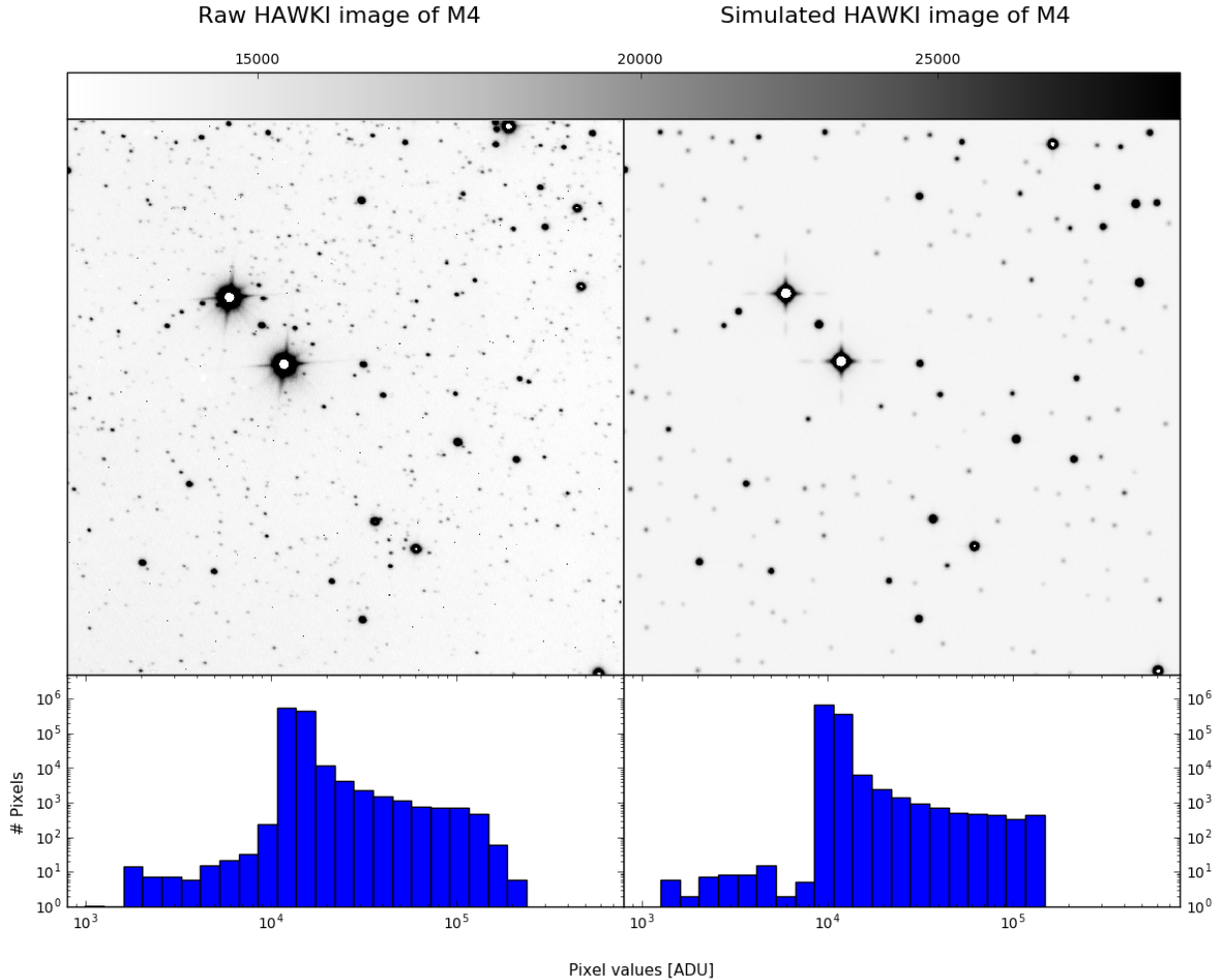


Fig. 7. Top: A comparison of a raw HAWK-I image (left) with a simulated image (right) from SimCADO for the same field near M 4. Features created by the optical train (e.g. diffraction spikes) and by the detector (e.g. saturation) can be seen in both the real and simulated images. The apparent size of the PSF for the brightest stars in the simulated images is smaller than in the real images because SimCADO does not currently model leakage from saturated pixels into neighbouring pixels. The simulated images were based on the 2MASS catalogue. As such no sources fainter than the 2MASS detection limit were simulated. Bottom: The distribution of pixel counts for the real (left) and simulated (right) images is given here to illustrate that SimCADO is capable of recreating observations with no “real world” input. The discrepancy in the shape of the histogram for pixel counts less than 10 000 is due to the low resolution custom made linearity curve used by SimCADO. Because of this the saturated pixels in the brightest stars are not modelled correctly in SimCADO. However, as such pixels are often flagged as unusable by reduction pipelines, refining the accuracy of the linearity curve for SimCADO was deemed less than critical.

This assumption was adequate for SimCADO to reproduce the shape of the flux histogram as shown in Fig. 7. It should be noted that the sky background varied between the three sets of archival data. This resulted in background fluxes from SimCADO being $\sim 0.1^m$ lower than the backgrounds in the raw J and Ks images from the 2007 observations of M 4. For the 2015 Ks-band observation the simulated image had a background flux on the order of about 0.4^m fainter than in the raw HAWK-I image. Given that Moreels et al. (2008) report that NIR sky backgrounds can vary up to 0.75^m per night, we conclude that this difference is due to the observational conditions¹⁰. Further work is currently being done to implement an extended background model so that Sim-

CADO is able to also reliably reproduce the sky background for various combinations of observing conditions such as airmass, seeing and precipitable water vapour.

5. Predictions for MICADO’s point source sensitivity

MICADO will offer diffraction-limited imaging with a PSF width of about 7 and 12 milli-arcseconds in the J and Ks filters respectively. This will allow stars in densely populated regions such as the centres of globular clusters to be easily resolved (an example is shown in Fig. 10). Indeed the majority of the primary science cases for MICADO revolve around accurately resolving point sources. Thus it is important to know the sensitivity limits of the imaging mode well in advance of MICADO going on-sky. Here we present the results of a series of SimCADO simulations

¹⁰ <https://www.eso.org/sci/observing/phase2/ObsConditions.html>

aimed at determining the observational limits for MICADO. The model of the optical train used for these simulations was the default MICADO wide-field imaging mode, as described in Sect. 2. The method for measuring the signal-to-noise ratio was identical to the method used for the HAWK-I verification run described in Sect. 4, except the minimum integration time was extended to 2.6 seconds. This reflects the read-out time of the HAWAII-4RG detectors. Also the grid of stars used for the test observations included only stars with magnitudes between 16 and 32 as the extended diffraction spikes from stars brighter than 16th magnitude extended into the background annuli used for photometry of the neighbouring stars.

The PSFs for these simulations were produced by the SCAO working group for the MICADO consortium (F. Vidal, private communication) specifically for inclusion in the SimCADO package. They were generated using the current state-of-the-art adaptive optics simulations and describe the residual PSF after the AO loop has been closed. The simulations were run for a 14.7^m guide star that is 5'' off-axis. The targets were observed at the zenith. The Strehl ratio of the PSFs were 0.29, 0.51 and 0.68 for the J, H and Ks band respectively.

5.1. Point source sensitivity vs. exposure time

For studies of stellar populations, the detection limit is often set to 5σ , where σ is the level of total background noise inside an aperture set around a star. However, in order to achieve a high level of astrometric precision (e.g. down to levels of $\sim 1/30$ th of a pixel, or $\sim 10 \mu\text{as}$), a much higher signal-to-noise ratio is required, e.g. $\sim 250\sigma$ (D. Massari, private communication). Table 4 lists MICADO's limiting magnitudes for the photometric and astrometric cases. For an exposure time of 5 hours, we find the limiting magnitudes (Vega) for a 5σ detection to be 28.7^m, 27.9^m and 27.3^m in the J, H and Ks broadband filters respectively. For the narrow-band filter Br γ we find a limiting magnitude of 26.0^m. The J and H limiting magnitudes match those from the ELT exposure time calculator¹¹ to within 0.1^m. The Ks estimate is 0.2^m weaker than that from the ETC.

For astrometric purposes, we find the limiting magnitudes to be 24.2^m, 23.5^m, 22.9^m in J, H and Ks filters and 21.7^m in the Br γ filter. All magnitudes are given in the Vega system¹². Fig. 8 is an expanded graphical representation of Table 4 that shows the full range of limiting magnitudes for observations from the shortest integration time to a full 10 hour observing program and for signal-to-noise ratios of 1σ to 1000 σ .

5.2. Point source saturation limits

Given the ELT's collecting area of 978,m², it is also important when determining observational strategies to know the saturation limits of the detectors. Basic aperture photometry is only reliable when the maximum pixel values inside the aperture are below the saturation threshold. Advanced techniques such as PSF fitting will naturally allow this threshold to be extended. However, given the unorthodox shape, the many sharp artefacts, and the dynamic nature of an AO corrected PSF, the use of advanced photometric methods will prove challenging. Therefore in order to set conservative limits on the accuracy of photometry for bright sources with MICADO we decided to define photometric reliability as stars with only unsaturated pixels.

¹¹ https://www.eso.org/observing/etc/bin/simu/elt_ima

¹² To convert to the AB system ~ 0.9 , ~ 1.4 and ~ 1.85 should be added to the J, H and Ks magnitudes respectively.

The minimum read-out time for a full H4RG detector will be ca. 2.6 seconds. MICADO will also offer a fast readout mode for windowed regions of the detector capable of reading out e.g. a 100×100 pixel area at a rate of 200 Hz (DIT ~ 5 ms). To calculate the bright star limits we took the brightest star from the simulated images that had no values over the correctable non-linear regime. As there is little data publicly available for the performance of HAWAII-4RG detectors, we assumed their characteristics will be similar to the HAWAII-2RG chips. According to Loose et al. (2007), all detectors in the HAWAII-RG family have a correctable linearity regime (within 5%) of $\sim 10^5 \text{ e}^-/\text{pixel}$ with a full well depth of $< 1.5 \cdot 10^5 \text{ e}^- \text{ pixel}^{-1}$. Table 5 shows the brightest magnitudes that can be observed in the J, H, Ks and Br γ filters without any pixels saturating.

As a sanity check, we compared the limits in Table 5 to the saturation limits given by the ELT exposure time calculator provided by ESO. The ETC uses a slightly different configuration for the imaging mode, the most notable differences being a collecting area of 1100 m² and a plate scale of 5 mas. After normalising the results from the ETC, we find that SimCADO matches the ETC's calculations to within 0.1^m. This is pleasantly surprising given the large number of assumptions built into the ETC.

It is worth noting that in the standard wide-field imaging mode with an integration time of 2.6 s, MICADO will saturate around the detection limit of the 2MASS survey, i.e. $J = 15.8^m$, $H = 15.1^m$ and $K_s = 14.3^m$ (Skrutskie et al. 2006). On the one hand, this is a testament to the extreme increase in observing capabilities that the ELT and MICADO will provide. On the other hand, this will prove problematic for observers as all telescope pointings within $\sim 25''$ of a 2MASS source will need to account for the effects of overly bright sources in the field of view. Given that the diffraction spikes of the ELT's PSF are long and prominent, there is a good chance that they will cause issues with the reduction and analysis of fainter, more interesting regions.

5.3. Spectral type with distance

Four of the major science drivers for MICADO rely on determining the properties of stellar populations. Hence we found it prudent to use the sensitivity estimates from SimCADO to calculate limiting distances for a 5σ detection for different spectral types. Fig. 9 shows the apparent magnitude of a selection of main-sequence stars with increasing distance as well as the sensitivity limits for MICADO for a range of exposure times. We used the main sequence absolute magnitudes given in Table 5 of Pecaut & Mamajek (2013)¹³. As the brightest stars in the main sequence cover almost the same magnitude range as all giant and most supergiant stars, those readers interested in the limiting distances for stars that have left the main sequence are requested to use the distances for a main sequence star with an equivalent absolute magnitude.

Using SimCADO we have determined that MICADO should be able to detect all A-type stars in Centaurus A at a distance of 4 Mpc with a 5 hour observation. A 1 hour observation should be sufficient to detect all stars down to the Hydrogen burning limit ($M < 0.08M_\odot$) in the Magellanic Clouds (~ 50 kpc). However at this distance all stars brighter than B1V will saturate within the shortest exposure time (DIT = 2.6 s). For more case specific distance limits based on the SimCADO limiting magnitudes, we

¹³ Additional information for the L and T dwarves (not reported by Pecaut & Mamajek 2013) were taken from the associated website http://www.pas.rochester.edu/~emamajek/EEM_dwarf_UBVIJHK_colors_Teff.txt

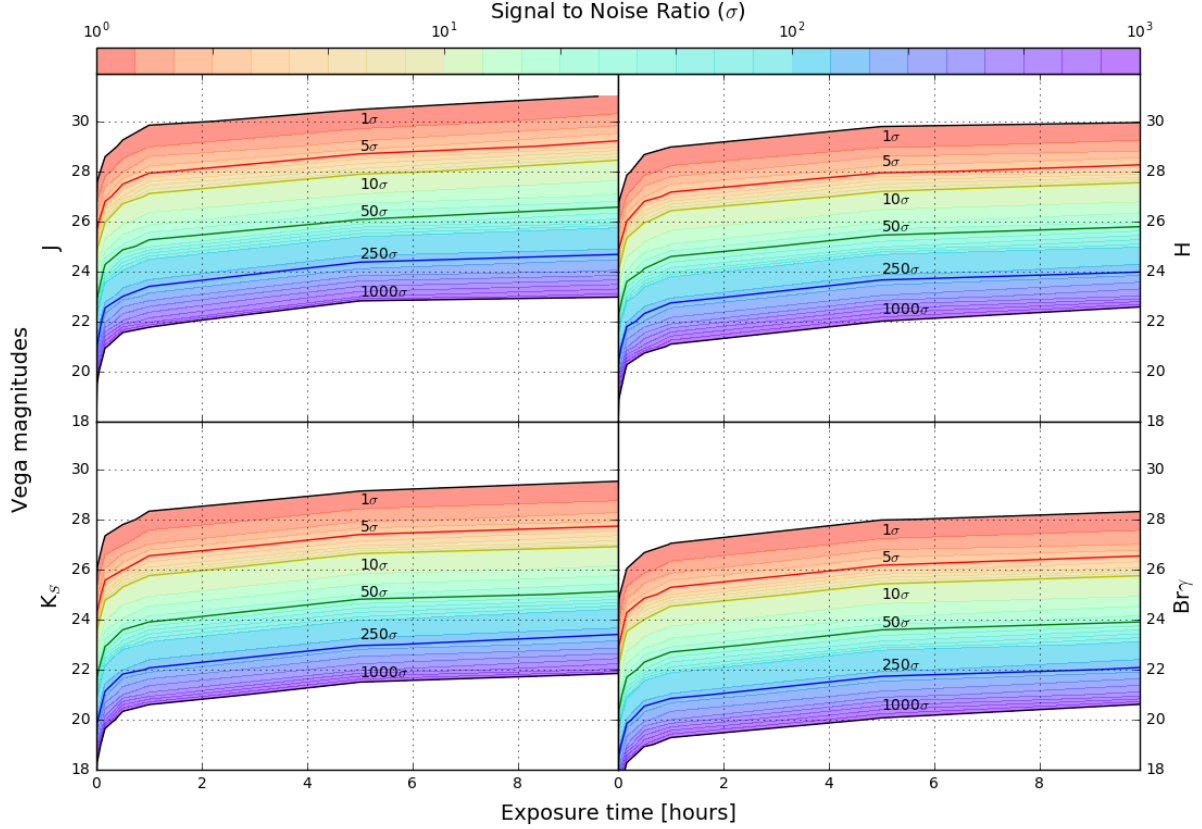


Fig. 8. Limiting magnitude plots for the wide field (4 mas/pixel) imaging mode of MICADO at the ELT in Vega magnitudes. Signal-to-noise ratios above 5σ are sufficient for photometry. High precision astrometry requires stronger detections $\sim 250\sigma$. It should be noted that these magnitudes apply to the current design of MICADO and the ELT. At the time of publication MICADO is still in its preliminary design phase. As such we expect small changes in these values as the MICADO design matures.

Table 4. Specific point-source sensitivities for the NIR broadband filters J, H and Ks and the narrow band filter Br γ . 5σ and 10σ are generally accepted detection limits for photometric measurements, while for accurate astrometry signal-to-noise ratios above 250σ are required. The errors on these magnitudes are $\pm 0.1^m$. It should be noted that these magnitudes apply to the current design of MICADO and the ELT. At the time of publication MICADO is still in its preliminary design phase. As such we expect small changes in these values as the MICADO design matures.

Filter	SNR	2.6 sec	10 sec	1 min	10 min	1 hr	5 hrs	10 hrs
J	5σ	23.4 ^m	24.4 ^m	25.6 ^m	26.7 ^m	27.8 ^m	28.7 ^m	29.0 ^m
	10σ	22.6 ^m	23.6 ^m	24.8 ^m	26.0 ^m	27.0 ^m	27.9 ^m	28.2 ^m
	250σ	18.7 ^m	19.9 ^m	21.1 ^m	22.4 ^m	23.4 ^m	24.2 ^m	24.6 ^m
H	5σ	23.0 ^m	23.8 ^m	24.8 ^m	26.0 ^m	27.0 ^m	27.9 ^m	28.3 ^m
	10σ	22.2 ^m	23.0 ^m	24.0 ^m	25.3 ^m	26.2 ^m	27.1 ^m	27.5 ^m
	250σ	18.6 ^m	19.4 ^m	20.4 ^m	21.7 ^m	22.7 ^m	23.5 ^m	23.9 ^m
Ks	5σ	22.4 ^m	23.1 ^m	24.1 ^m	25.6 ^m	26.4 ^m	27.3 ^m	27.7 ^m
	10σ	21.6 ^m	22.4 ^m	23.4 ^m	24.8 ^m	25.6 ^m	26.5 ^m	26.9 ^m
	250σ	18.0 ^m	18.9 ^m	19.8 ^m	21.0 ^m	22.1 ^m	22.9 ^m	23.3 ^m
Br γ	5σ	20.6 ^m	21.8 ^m	22.9 ^m	24.1 ^m	25.2 ^m	26.0 ^m	26.3 ^m
	10σ	19.8 ^m	21.0 ^m	22.1 ^m	23.4 ^m	24.4 ^m	25.2 ^m	25.6 ^m
	250σ	16.0 ^m	17.1 ^m	18.4 ^m	19.8 ^m	20.8 ^m	21.7 ^m	22.1 ^m

direct the reader to Fig. 9. The equivalent plot for the Ks filter is included in the Appendix. These distance estimates are based on an ideal case scenario of an isolated star and the current design of the MICADO optical train. Therefore Fig. 9 should be understood as illustrating upper limits for the distance estimates. For

example, we have also assumed no extinction along the line of sight. Nor have we taken into account the increased background levels in crowded field. Both effects will undoubtedly reduce the distance estimated by varying amounts. To what degree the level

of crowding affects these distance estimates will be the focus of a companion paper.

6. Discussion, open issues and assumptions

6.1. Discussion on the differences between the simulated and the real HAWK-I images

Overall the simulated images of M 4 and NGC 4147 compared favourably with the raw observations from the ESO archive. The distribution of pixel flux, background level and noise, total star fluxes and positions, detector noise and saturation, were well reproduced in the simulated images. Magnitudes derived from aperture photometry on the simulated images matched almost perfectly with the 2MASS catalogue for all stars with $J, K_s > 11^m$. When comparing photometry between the simulated and archive images, around two thirds of all the stars measured had flux differences between the images within $\pm 0.3^m$. The scatter seen in Fig. 6 is a combination of unresolved sources in the 2MASS catalogue being resolved by HAWK-I, and SimCADO not including the hot pixels on the HAWK-I detectors. Hence this scatter shows that there is a need for a better description of the globular clusters. An extrapolation of the source catalogue down to the detection limit of HAWK-I would be desirable. However, as the coordinates of the fainter sources are unknown, this would likely cause the scatter to increase rather than decrease. With the ELT's ability to detect sources down to $J \approx 29^m$, the prevalence of background sources in this regime will indeed need to be addressed and simulated accurately.

The level of background flux generated by SimCADO for the J and K_s filters is in line with the flux levels returned by the ESO exposure time calculator for HAWK-I. However, only archive J and K_s images from 2007 had background levels as low as the ETC and SimCADO. The other two J and K_s images had levels 10 % and 30 % higher. While there is an abundance of information on the weather conditions during the observations, we were unable to find estimates for the measured sky background. We therefore used the standard Paranal background magnitudes for the simulations. As NIR sky background levels can vary by up to 0.75^m over the course of a night (Moreels et al. 2008), we do not see the difference between the simulated and real background fluxes in these images as a major failure of the software. Moreover, sky dynamic background variation is yet another effect that should be added to a future release of SimCADO.

A final caveat for the software verification is that the model of the optical train for UT4/HAWK-I is based on the information available on the ESO website and from the HAWK-I user manual. Despite our due diligence it is possible that some of the data used by SimCADO is inaccurate or not up to date. In order to further test how SimCADO reacts to different sets of observing conditions (airmass, seeing, etc), we submitted a ESO proposal in Period 100 for technical time on HAWK-I. We are waiting on the completion of the observing run before embarking on a new validation campaign. This should allow us to further increase the accuracy of the simulated images by allowing us to implement each aspect of the atmospheric background separately.

6.2. Accuracy of the SimCADO sensitivity predictions

SimCADO was verified by comparing simulated images with real HAWK-I observations. Furthermore, estimates from SimCADO images of the detection and saturation limits for observations with MICADO fall within 0.1^m of the values given by the ELT exposure time calculator (after normalising the two optical

train configurations). These two results give us confidence that MICADO's sensitivity can be accurately predicted from simulations with SimCADO. These simulations have however been conducted using several simplifications. For example, the atmospheric conditions were assumed to mirror those of the average night at Paranal. Given that the NIR sky background can vary up to $\sim 0.2^m$ within 15 minutes (Moreels et al. 2008) and that it is also dependent on the level of water in the air as well as the airmass of the pointing, it is clear that the true detection limits of MICADO will vary from this first round of predictions with SimCADO. Furthermore, the PSF used for the current round of SimCADO predictions was uniform across the field of view. This will definitely not be the case. Reductions in the Strehl ratio of $> 50\%$ over the MICADO field of view are expected for SCAO observations (Clénet et al. 2015). Such variations will have a marked impact on sensitivity in the outer regions of the MICADO focal plane.

Another challenge for estimating the performance of the telescope and instrument will be the ELT's PSF. Accurate photometry of bright sources, extracting faint sources that are covered by the wings of the brighter sources, and accurate astrometry all rely on accurate knowledge of the shape of the PSF. As can be seen in Fig. 10, the segmented nature of the diffraction spikes of the SCAO PSF could easily confuse a star finding algorithm. Additionally, the PSF will rotate with respect to the field over the course of an observing run due to the ELT's alt-azimuth mount. This would greatly complicate the standard stack and subtract technique for data reduction. Arguably though, this may prove advantageous as it will provide a natural rotational dithering, which may smooth out the sharp features of the PSF. An alternative approach would be to deconvolve the images with a spatially varying model of the PSF. This would however require multiple descriptions of the PSF for each detector frame, which could slowly become a challenging data management task. Whether this task belongs in the automated data pipeline or is left to the user is still undecided. A different approach would be to use a blind deconvolution algorithm (Vorontsov & Jeffries 2017). Recent results are encouraging, although it remains to be seen how well this approach works for spatially varying PSFs. In any case, the complex PSF of the ELT will present a challenge to standard data analysis techniques. How the PSF artefacts of bright stars affect the surrounding environment is a question that should be considered in the earliest stages of planning observations with the ELT and MICADO.

6.3. Future functionality for SimCADO

The results of the first verification run show that SimCADO is capable of recreating observations with only descriptions of the optical elements as input. There are, however, still several aspects that require attention by the development team. In short they are:

Atmospheric variations: SimCADO uses a standardised spectrum from SkyCalc, scaled to the required background level, to provide the sky background flux for any chosen filter. Currently this atmospheric spectrum is independent of the observational setup, i.e. it does not change as airmass or PWV conditions change. For the verification run described here, these points were not relevant: the archival data for M 4 were taken close to zenith and the image of NGC 4147 (airmass ~ 1.44) was primarily used as a control for its different exposure length. Functionality to accurately model the effects of different observational conditions

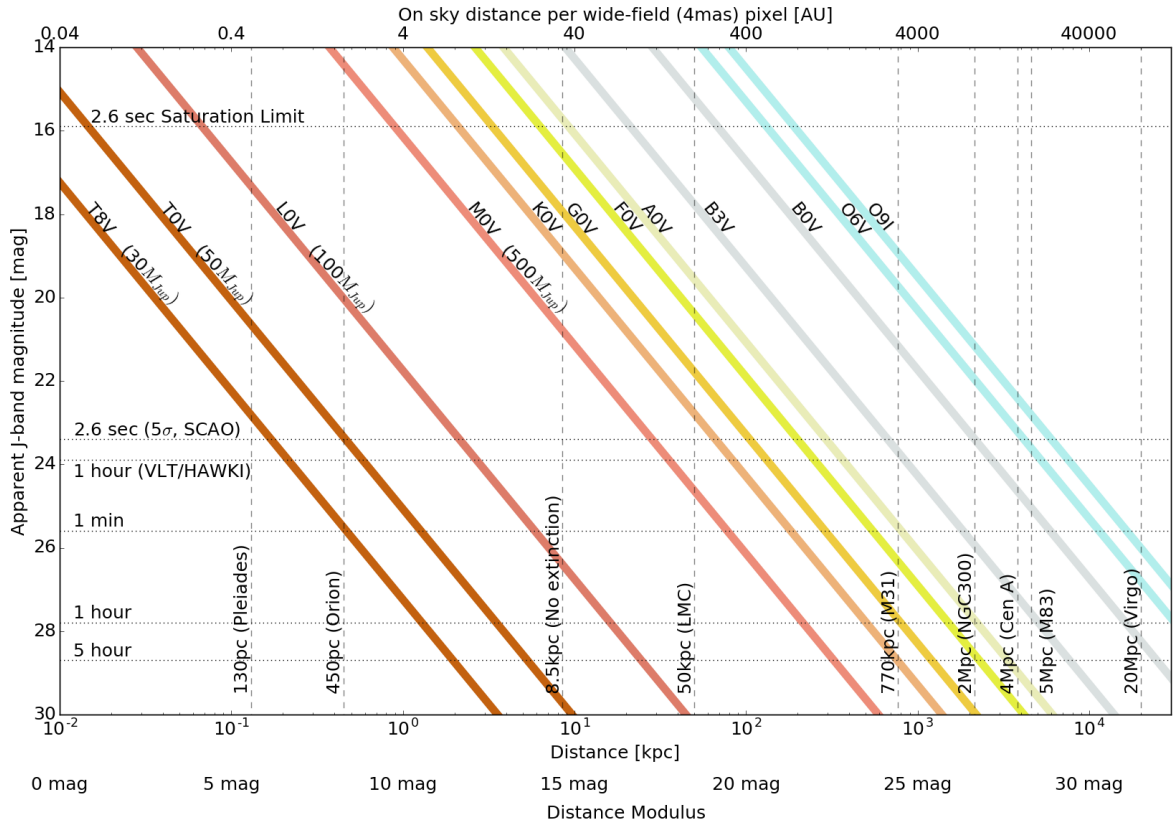


Fig. 9. The coloured lines represent the apparent magnitude of the major spectral types with increasing distance. The dashed horizontal lines, unless otherwise stated, represent the 5σ detection limits for various exposure times with MICADO. When a coloured line crosses below a horizontal line, it means that this type of main-sequence star will no longer be detectable by MICADO at the distance where the cross occurs. As a reference, the dashed vertical lines show distances to well known astronomical objects. It is worth noting that what HAWK-I can do in 1 hour, MICADO can do in 2.6 seconds. While this comparison may seem ludicrous, the ELT has a primary mirror $\sim 20\times$ larger than of UT4 at the VLT and the smaller plate scale of MICADO means a factor of $\sim 35\times$ less background flux per pixel.

are in development and will be included in a future release of the software.

PSF variability: While not as important for a seeing-limited instrument, the variations in the shape of the PSF over the field of view for observations conducted with adaptive optics is not a trivial effect. The development team is currently in the process of implementing functionality to include the off-axis PSFs provided by the SCAO and MCAO simulation teams. Furthermore the PSF is based on the post-AO PSF delivered by the AO simulation teams. The exposure times are assumed to be long enough that the PSF should not vary noticeably between exposures. Whether or not this assumption holds for all time scales remains to be investigated.

Distortion effects: For photometric studies optical distortions are a nuisance. For astrometric studies they are critical. SimCADO includes the functionality to shift point sources on the sub-pixel level. As such we are currently investigating the best way to implement the use of distortion maps in the model of the optical train.

Spectroscopy: MICADO will also include the optics to function as a long slit spectrograph. Development is ongoing with the implementation of this mode into SimCADO.

Although there is still much work to do, SimCADO is already capable of simulating raw detector read-outs for each of the MICADO imaging modes. This alone covers the majority of the primary science drivers for MICADO. It should also be noted that MICADO is still in the preliminary design phase and so the composition of the optical train, and therefore the default data installed alongside SimCADO, are likely to change in the future. However, we foresee no radical changes to the design, and thus no radical changes to the sensitivity estimates we have presented in this paper.

7. Summary

As part of the design activities for the MICADO instrument we have developed an instrument data simulator in Python: SimCADO. The software is capable of generating detector frames for any given optical train configuration and source object description. A summary of our activities and results is as follows:

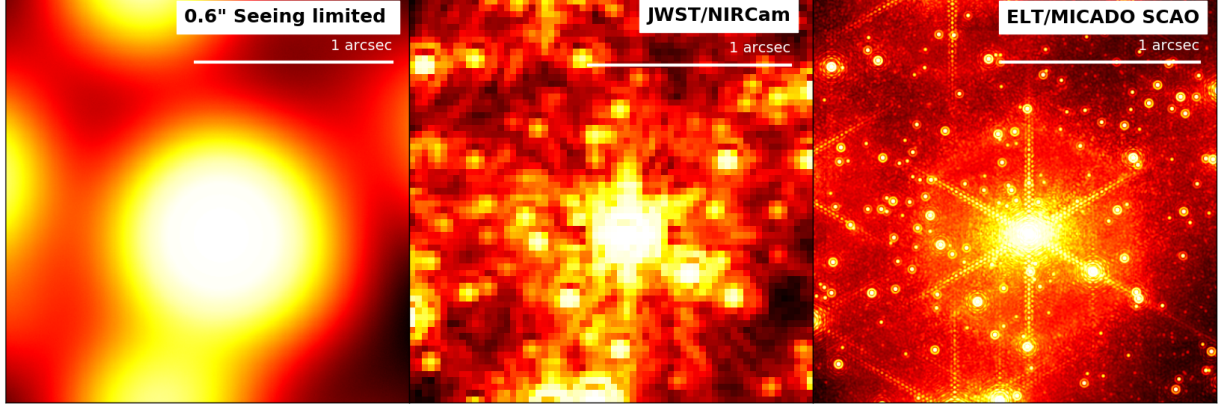


Fig. 10. An illustration of the improvement in resolution that MICADO will provide for observations of densely populated regions. Left: A dense stellar field observed with 0.6 arcsecond seeing. Middle: The same field as will be observed by NIRCam on JWST. Right: A prediction of how the dense stellar field will look when observed by MICADO in wide-field mode (4 mas/pixel).

Table 5. Saturation limits for MICADO assuming an effective detector well depth of $10^5 \text{ e}^-/\text{pixel}$. The shortest integration time for a full detector will be $\sim 2.6 \text{ s}$, while a faster readout mode will be available for smaller windowed regions (Davies et al. 2010). Given the current detector specifications a 100×100 pixel window might achieve a readout frequency of 200 Hz, or 5 ms per exposure. The limits are split between the two default imaging modes of MICADO: Wide-field mode (4 mas/pixel, $\sim 50''$ FoV), and the zoom mode (1.5 mas/pixel, $\sim 20''$ FoV).

Filter	DIT	Wide field	Zoom
J	2.6 s	15.9 ^m	13.6 ^m
	0.005 s	9.1 ^m	6.8 ^m
H	2.6 s	15.6 ^m	13.4 ^m
	0.005 s	8.8 ^m	6.6 ^m
K _s	2.6 s	14.8 ^m	12.5 ^m
	0.005 s	8.0 ^m	5.7 ^m
Br γ	2.6 s	12.0 ^m	9.9 ^m
	0.005 s	5.2 ^m	3.1 ^m

- In conjunction with the MICADO instrument team we have developed a modular python package that allows us to model each element in the optical train separately. The software allows the user to fully control the configuration of the optical train as well as the description of the astronomical object to be observed. Images produced by the package are in the standard FITS format and can be treated as coming directly from a telescope.
- We configured SimCADO to mimic the UT4/HAWK-I optical train and “observed” two globular clusters with this setup. A comparison to archive data for the same globular clusters showed that SimCADO is capable of reproducing all the major and most of the minor effects that are seen in raw detector frames from HAWK-I. A photometric comparison shows a one-to-one correlation between the flux observed in the archive and simulated images. Although there is scatter around this line, the primary source of uncertainty lies with the photometric analysis of the archive data and not with the simulated images. Additionally SimCADO is able to reproduce the detection limits given by the ESO exposure time calculator for a 1-hour observation with HAWK-I.
- Using the configuration for the ELT/MICADO optical train we simulated a grid of stars to find the detection limits for

different exposure times. We have shown that the 5 hour detection limits in Vega magnitudes are: $J = 28.7^m$, $H = 27.9^m$ and $K_s = 27.3^m$, while the saturation limit for the shortest exposure time (MINDIT = 2.6 s) in the wide-field (4 mas/pixel) mode are similar to the 2MASS detection limits: $J = 15.9^m$, $H = 15.6^m$ and $K_s = 14.8^m$. The use of the zoom mode (1.5 mas/pixel) in conjunction with a narrow band filter, such as the Br γ filter, would reduce increase this limit to $\sim 9.9^m$.

- With these detection limits we have shown that MICADO will be capable of detecting individual A0 V stars at a distance of 4 Mpc (Centaurus A), while any star brighter than B1 V at a distance of 50 kpc (LMC) will saturate during the a single minimum length exposure.
- We will be adding the following functionality to SimCADO in the near future: a long slit spectrographic mode, field variable PSFs, variations in atmospheric conditions, as well as further support for the high time resolution and astrometric imaging modes.

We encourage anyone who may want to use the ELT and MICADO for future observations to use SimCADO to simulate their science case in advance. Not only will this help the community to get a feel for what MICADO will be capable of and where possible problems with an observing strategy will be, feedback from users will help us to develop the software in such a way as to meet the needs of the astronomical community.

Acknowledgements. SimCADO incorporates Bernhard Rauscher’s HxRG Noise Generator package for python (Rauscher 2015). This research made use of POPPY, an open-source optical propagation Python package originally developed for the James Webb Space Telescope project (Perrin et al. 2015). This research made use of Astropy, a community-developed core Python package for astronomy (Astropy Collaboration et al. 2013; The Astropy Collaboration et al. 2018). This research made use of Photutils (Bradley et al. 2017). This research has made use of “Aladin sky atlas” developed at CDS, Strasbourg Observatory, France (Bonnarel et al. 2000; Boch & Fernique 2014). SimCADO makes use of atmospheric transmission and emission curves generated by ESO’s SkyCalc service, which was developed at the University of Innsbruck as part of an Austrian in-kind contribution to ESO. Based on data obtained from the ESO Science Archive Facility under request number Leschinski, #331857. This publication makes use of data products from the Two Micron All Sky Survey, which is a joint project of the University of Massachusetts and the Infrared Processing and Analysis Center/California Institute of Technology, funded by the National Aeronautics and Space Administration and the National Science Foundation (Skrutskie et al. 2006). This research is partially funded by the project IS538003 of the Hochschulraumstrukturmittel (HRSM) provided by the Austrian Government

and administered by the University of Vienna. The authors would also like to thank all the members of the consortium for their effort in the MICADO project, and their contributions to the development of this tool.

References

- Astropy Collaboration, Robitaille, T. P., Tollerud, E. J., et al. 2013, A&A, 558, A33
- Bocca, M., Vucina, T., Araya, C., Vera, E., & Ahhee, C. 2006, Thin Solid Films, 502, 275
- Boch, T. & Fernique, P. 2014, in Astronomical Society of the Pacific Conference Series, Vol. 485, Astronomical Data Analysis Software and Systems XXIII, ed. N. Manset & P. Forshay, 277
- Bonnaire, F., Fernique, P., Bienaymé, O., et al. 2000, A&AS, 143, 33
- Bradley, L., Sipocz, B., Robitaille, T., et al. 2017, astropy/photutils: v0.4
- Brandl, B. R., Lenzen, R., Pantin, E., et al. 2008, in Proc. SPIE, Vol. 7014, Ground-based and Airborne Instrumentation for Astronomy II, 70141N
- Clénet, Y., Buey, T., Rousset, G., et al. 2016, in Proc. SPIE, Vol. 9909, Society of Photo-Optical Instrumentation Engineers (SPIE) Conference Series, 99090A
- Clénet, Y., Gendron, E., Gratadour, D., Rousset, G., & Vidal, F. 2015, A&A, 583, A102
- Clénet, Y., Gratadour, D., Gendron, E., Rousset, G., & Sevin, A. 2013, in Proceedings of the Third AO4ELT Conference, ed. S. Esposito & L. Fini, 29
- Cuby, J. G., Lidman, C., & Moutou, C. 2000, The Messenger, 101, 2
- Davies, R., Ageorges, N., Barl, L., et al. 2010, in Proc. SPIE, Vol. 7735, Ground-based and Airborne Instrumentation for Astronomy III, 77352A
- Davies, R., Schubert, J., Hartl, M., et al. 2016, in Proc. SPIE, Vol. 9908, Society of Photo-Optical Instrumentation Engineers (SPIE) Conference Series, 99081Z
- Dierickx, P., Enard, D., Merkle, F., Noethe, L., & Wilson, R. N. 1990, in Proc. SPIE, Vol. 1236, Advanced Technology Optical Telescopes IV, ed. L. D. Barr, 138–151
- Diolaiti, E. 2010, The Messenger, 140, 28
- Diolaiti, E., Ciliegi, P., Abicca, R., et al. 2016, in Proc. SPIE, Vol. 9909, Society of Photo-Optical Instrumentation Engineers (SPIE) Conference Series, 99092D
- Finger, G., Dorn, R. J., Eschbaumer, S., et al. 2008, in Proc. SPIE, Vol. 7021, High Energy, Optical, and Infrared Detectors for Astronomy III, 70210P
- Gilmozzi, R. & Spyromilio, J. 2007, The Messenger, 127
- Jones, A., Noll, S., Kausch, W., Szyszka, C., & Kimeswenger, S. 2013, A&A, 560, A91
- Kissler-Patig, M., Pirard, J.-F., Casali, M., et al. 2008, A&A, 491, 941
- Leschinski, K., Czoske, O., Köhler, R., et al. 2016, in Proc. SPIE, Vol. 9911, Society of Photo-Optical Instrumentation Engineers (SPIE) Conference Series, 991124
- Loose, M., Beletic, J., Garnett, J., & Xu, M. 2007, in Proc. SPIE, Vol. 6690, Focal Plane Arrays for Space Telescopes III, 66900C
- Mahajan, V. N. 1991, Aberration theory made simple
- Moreels, G., Clairemidi, J., Faivre, M., et al. 2008, Experimental Astronomy, 22, 87
- Noll, S., Kausch, W., Barden, M., et al. 2012, A&A, 543, A92
- Pecaut, M. J. & Mamajek, E. E. 2013, ApJS, 208, 9
- Perrin, M. D., Long, J., Sivaramakrishnan, A., et al. 2015, WebbPSF: James Webb Space Telescope PSF Simulation Tool, Astrophysics Source Code Library
- Peterson, J. R., Jernigan, J. G., Kahn, S. M., et al. 2015, ApJS, 218, 14
- Posselt, W., Holota, W., Kulinyak, E., et al. 2004, in Proc. SPIE, Vol. 5487, Optical, Infrared, and Millimeter Space Telescopes, ed. J. C. Mather, 688–697
- Rauscher, B. J. 2015, PASP, 127, 1144
- Schmalzl, E., Meisner, J., Venema, L., et al. 2012, in Proc. SPIE, Vol. 8449, Modeling, Systems Engineering, and Project Management for Astronomy V, 84491P
- Skrutskie, M. F., Cutri, R. M., Stiening, R., et al. 2006, AJ, 131, 1163
- Stone, R. C. 1996, PASP, 108, 1051
- Thatte, N., Tecza, M., Clarke, F., et al. 2010, in Proc. SPIE, Vol. 7735, Ground-based and Airborne Instrumentation for Astronomy III, 77352I
- The Astropy Collaboration, Price-Whelan, A. M., Sipőcz, B. M., et al. 2018, ArXiv e-prints [arXiv:1801.02634]
- Vorontsov, S. V. & Jefferies, S. M. 2017, Inverse Problems, 33, 055004
- Winkler, R., Haynes, D. M., Bellido-Tirado, O., Xu, W., & Haynes, R. 2014, in Proc. SPIE, Vol. 9150, Modeling, Systems Engineering, and Project Management for Astronomy VI, 91500T
- Wright, S. A., Walth, G., Do, T., et al. 2016, in Proc. SPIE, Vol. 9909, Society of Photo-Optical Instrumentation Engineers (SPIE) Conference Series, 990905
- Zieleniewski, S., Thatte, N., Kendrew, S., et al. 2015, MNRAS, 453, 3754

Appendix A: Distance estimates for main sequence stars in Ks filter

Fig. A.1 shows the Ks-band equivalent of Fig. 9. As described in Fig. 9 the coloured lines represent the apparent magnitude of the major spectral types with increasing distance. The dashed horizontal lines, unless otherwise stated, represent the 5σ detection limits for various exposure times with MICADO. When a coloured line crosses below a horizontal line, it means that this type of main sequence star will no longer be detectable by MICADO at the distance when the cross occurs. As a reference the dashed vertical lines show distances to well known astronomical objects.

Appendix B: Comparison of the HAWK-I and MICADO configuration files

Although the SimCADO package is in the public domain, it currently does not have a software licence. Nevertheless we encourage anyone interested in simulating future ELT/MICADO observations to use SimCADO and to report any bugs to the authors. In the interests of transparency and reproducibility, we have included the configuration files that we used to generate SimCADO models of both the HAWK-I and MICADO optical trains. We are also willing to share any of the data files that subsequent users may need in order to reproduce our results. Please contact the authors directly. The software can be found at www.univie.ac.at/simcado

Appendix B.1: The MICADO configuration file

The standard configuration file used for the MICADO wide-field (4 mas plate scale) imaging mode.

```
#####
# Observation Parameters
#####

OBS_DATE          0
OBS_TIME          0
OBS_RA            90.
OBS_DEC           -30.
OBS_ALT           0
OBS_AZ             0
OBS_ZENITH_DIST   0
OBS_PARALLACTIC_ANGLE 0
OBS_SEEING         0.6
OBS_FIELD_ROTATION 0

OBS_EXPTIME       60
OBS_NDIT           1
OBS_NONDESTRUCT_TRO 2.6
OBS_REMOVE_CONST_BG no
OBS_READ_MODE      single
OBS_SAVE_ALL_FRAMES no

OBS_INPUT_SOURCE_PATH none
OBS_FITS_EXT        0
OBS_OUTPUT_DIR       "./output.fits"

#####
# Simulation Parameters
#####

SIM_DETECTOR_PIX_SCALE 0.004
SIM_OVERSAMPLING        1
SIM_PIXEL_THRESHOLD      1

SIM_LAM_TC_BIN_WIDTH    0.001
SIM_SPEC_MIN_STEP        1E-4

SIM_FILTER_THRESHOLD     1E-9
SIM_USE_FILTER_LAM      yes
# if "no"
SIM_LAM_MIN              1.9
SIM_LAM_MAX              2.41
SIM_LAM_PSF_BIN_WIDTH    0.1
SIM_ADC_SHIFT_THRESHOLD  1

SIM_PSF_SIZE            1024
SIM_PSF_OVERSAMPLE      no
SIM_VERBOSE              no
SIM_SIM_MESSAGE_LEVEL    3

SIM_OPT_TRAIN_IN_PATH   none
SIM_OPT_TRAIN_OUT_PATH  none
SIM_DETECTOR_IN_PATH    none
SIM_DETECTOR_OUT_PATH   none

#####
# Atmospheric Parameters
#####

ATMO_USE_ATMO_BG        yes
ATMO_TC                  TC_sky_25.tbl
ATMO_EC                  EC_sky_25.tbl
ATMO_BG_MAGNITUDE        13.6

ATMO_TEMPERATURE          0
ATMO_PRESSURE             750
ATMO_REL_HUMIDITY         60
ATMO_PWV                  2.5

#####
# Telescope Parameters
#####

SCOPE_ALTITUDE           3060
SCOPE_LATITUDE            -24.589167
SCOPE_LONGITUDE           -70.192222

SCOPE_PSF_FILE            scao
SCOPE_STREHL_RATIO        1
SCOPE_AO_EFFECTIVENESS    100
SCOPE_JITTER_FWHM         0.001
SCOPE_DRIFT_DISTANCE      0
SCOPE_DRIFT_PROFILE        linear

SCOPE_USE_MIRROR_BG       yes
SCOPE_NUM_MIRRORS          5
SCOPE_TEMP                 0
SCOPE_M1_TC                TC_mirror_EELT.dat
SCOPE_MIRROR_LIST          EC_mirrors_EELT_SCAO.tbl
```

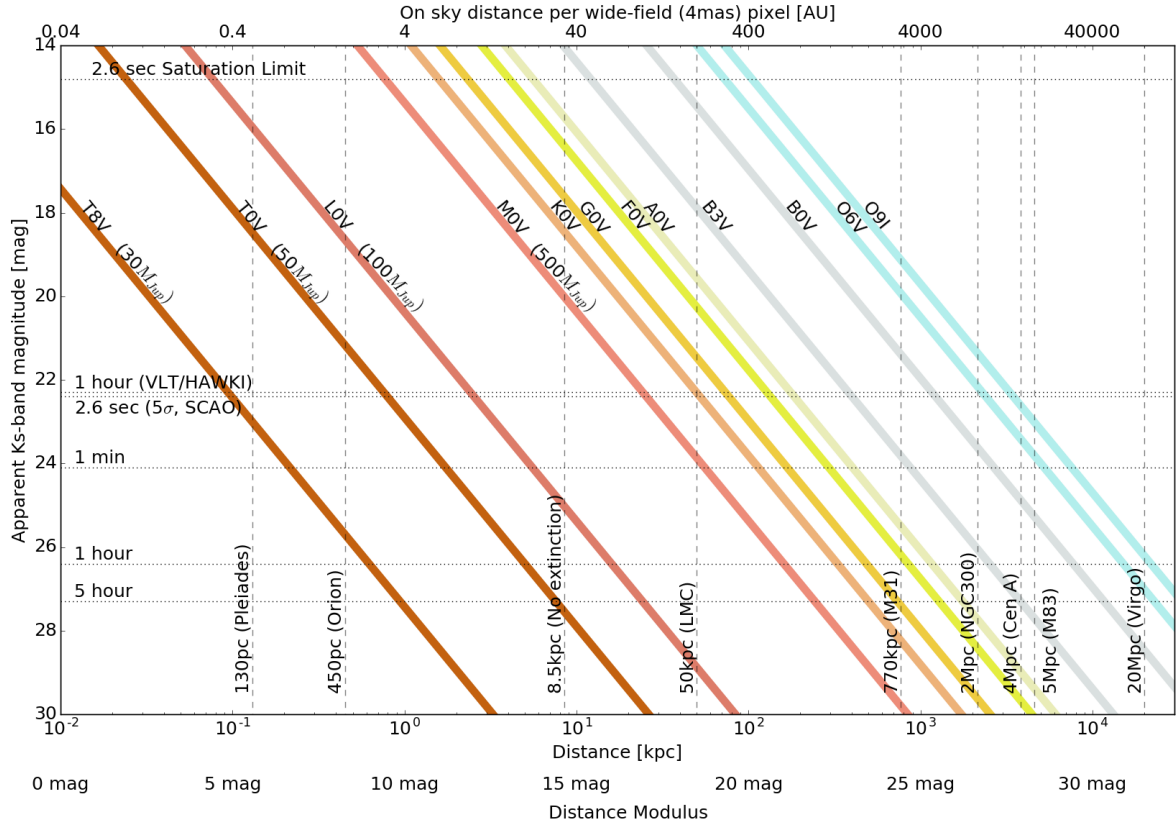


Fig. A.1. The Ks-band equivalent of Fig. 9.

```
#####
# Instrument Parameters
INST_ADC_NUM_SURFACES      8
INST_ADC_TC                  TC_ADC.dat
INST_TEMPERATURE              -190
INST_DEROT_PERFORMANCE        100
INST_DEROT_PROFILE            linear
INST_ENTR_NUM_SURFACES       4
INST_ENTR_WINDOW_TC          TC_window.dat
INST_DISTORTION_MAP          none
INST_WFE                      data/INST_wfe.tbl
INST_FLAT_FIELD               none
INST_DICHROIC_NUM_SURFACES   2
INST_DICHROIC_TC              TC_dichroic.dat
#####
# Spectroscopy parameters
SPEC_ORDER_SORT               HK
SPEC_SLIT_WIDTH                narrow
INST_PUPIL_NUM_SURFACES       2
INST_PUPIL_TC                  TC_pupil.dat
#####
# MICADO, collimator 5x, wide-field 2x (zoom 4x)
INST_NUM_MIRRORS              11
INST_MIRROR_TC                 TC_mirror_gold.dat
#####
# Detector parameters
INST_USE_AO_MIRROR_BG         yes
INST_AO_TEMPERATURE             0
INST_NUM_AO_MIRRORS            7
INST_MIRROR_AO_TC              TC_mirror_gold.dat
INST_MIRROR_AO_LIST             EC_mirrors_ao.tbl
FPA_USE_NOISE                  yes
FPA_READOUT_MEDIAN             4
FPA_READOUT_STDEV               1
FPA_DARK_MEDIAN                0.01
FPA_DARK_STDEV                  0.01
INST_ADC_PERFORMANCE           100
FPA_QE                         TC_detector_H2RG.dat
```

```

FPA_NOISE_PATH      FPA_noise.fits          SCOPE_NUM_MIRRORS      3
FPA_GAIN            1                      SCOPE_M1_TC           TC_mirror_aluminium.dat
FPA_LINEARITY_CURVE FPA_linearity.dat     SCOPE_MIRROR_LIST     EC_hawki_vlt_mirrors.tbl
FPA_FULL_WELL_DEPTH 1E5

FPA_PIXEL_MAP       none                  ##### Parameters regarding the instrument
# if FPA_PIXEL_MAP == none
FPA_DEAD_PIXELS    1
FPA_DEAD_LINES     1
INST_TEMPERATURE   -130
INST_ENTR_NUM_SURFACES 4
INST_FILTER_TC     TC_filter_Ks_HAWKI.dat
INST_PUPIL_NUM_SURFACES 2
INST_NUM_MIRRORS   4
INST_MIRROR_TC     TC_hawki_mirror.dat
INST_USE_AO_MIRROR_BG no
INST_AO_TEMPERATURE 0
INST_NUM_AO_MIRRORS 0
INST_ADC_PERFORMANCE 0
INST_ADC_NUM_SURFACES 0
INST_ADC_TC         none
INST_WFE            INST_hawki_wfe.tbl
HXRG_NUM_OUTPUTS   64
HXRG_NUM_ROW_OH    8
HXRG_PCA0_FILENAME FPA_nirspec_pca0.fits
HXRG_OUTPUT_PATH   none
INST_WFE            INST_hawki_wfe.tbl
HXRG_PEDESTAL     4
HXRG_CORR_PINK    3
HXRG_UNCORR_PINK  1
HXRG_ALT_COL_NOISE 0.5
INST_WFE            INST_hawki_wfe.tbl
HXRG_NAXIS1        4096
HXRG_NAXIS2        4096
HXRG_NUM_NDRO      1
INST_WFE            INST_hawki_wfe.tbl
##### General detector parameters
# General detector parameters
FPA_READOUT_MEDIAN 12
FPA_QE              TC_hawki_H2RG.dat
FPA_LINEARITY_CURVE FPA_hawki_linearity.dat
FPA_CHIP_LAYOUT     FPA_hawki_layout_cen.dat
##### NXRG Noise Generator package parameters
# NXRG Noise Generator package parameters
# See Rauscher (2015) for details
# http://arxiv.org/pdf/1509.06264.pdf
HXRG_NUM_OUTPUTS   32
HXRG_NUM_ROW_OH    8

```

Appendix B.2: The HAWKI configuration file

Rather than listing the full configuration for SimCADO as in Sect. B.1, we simply list the parameters that were changed in order to create an optical train for UT4/HAWKI at the VLT.

```
#####
# Parameters regarding the "observation"
```

```
OBS_RA             245.885625
OBS_DEC            -26.53835
OBS_SEEING         0.6
```

```
OBS_EXPTIME       10
OBS_NDIT           1
```

```
#####
# Parameters relating to the simulation
```

```
SIM_DETECTOR_PIX_SCALE 0.106
```

```
#####
# Parameters regarding the telescope
```

```
SCOPE_ALTITUDE     2635
SCOPE_LATITUDE     -24.589167
SCOPE_LONGITUDE    -70.192222
SCOPE_PSF_FILE     PSF_HAWKI_poppy.fits
```

Science use case: Studying the initial mass function with MICADO

4.1 Overview

The natural continuation from the observability predictions in the previous chapter is an investigation of the composition of various stellar populations at different distances from the Earth. Arguably one of the most interesting mysteries of the universe revolves around the remarkably constant stellar mass spectrum of different stellar populations. The so-called initial mass function is an empirically derived function which describes the amount of stars within a given mass range expected to form from the fragmentation of a collapsing interstellar gas cloud.

The IMF is the product of this fragmentation process (Offner et al. 2014). When the inward acting gravitational force is not sufficiently counteracted by the gas pressure, a cloud begins to collapse in on itself. While the physics behind the collapse mechanism were first explored in the early 1900s (Jeans 1902), a single theory of star formation has not yet appeared which satisfactorily explains the observed distribution of stellar masses. That being said, by combining all the known physics in recent numerical simulations (e.g. Bonnell et al. 2006; Haugbølle et al. 2018), it has been shown that various formation models can indeed reproduce the shape of the observed IMF.

There are two popular functional forms for the IMF: a (broken) power law description, known as the Salpeter (1955) or Kroupa (2001) IMF, or a log-normal description, known as a Chabrier (2003) IMF. Figure 4.1 (a reproduction of figure 1 from Goodwin et al. 2008) shows a comparison of the two popular IMF descriptions. For the range with the most numerous stellar masses, i.e. $0.1 M_{\odot} < M < 10 M_{\odot}$, the two descriptions are, to within current observational and statistical limits, almost indistinguishable. The observed heavy tail at the high mass end points towards the canonical Salpeter power law shape, however both the uncertainties

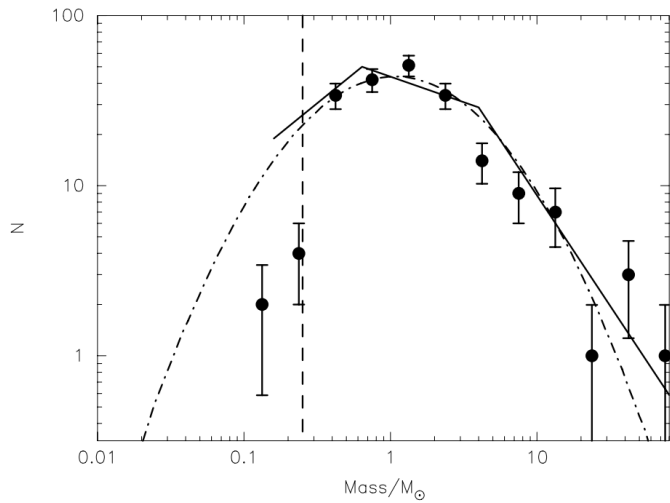


Figure 4.1. Reproduced from Goodwin (2008). The figure shows the shape of the two most popular descriptions of the initial mass function. The solid line shows the broken power law description of the IMF and the dashed line shows the log-normal description of the IMF. The figure is actually describing the core mass function, however this is irrelevant for the purpose of illustrating the shapes of the two most popular functional forms of the IMF. The vertical dashed line shows the sensitivity limits to observations of dense molecular cores (dots).

due to small number statistics for high mass stars, and the improbability of a physical process occurring in discrete power-law steps makes many authors (e.g. Hennebelle and Chabrier 2008; Maschberger 2013) sceptical that this is the true form of the IMF. Hennebelle and Chabrier (2008) successfully derived an analytical theory which reproduces both the log-normal turnover and the power-law tails of the two competing IMF descriptions, however they agree that the theory still falls short of a complete description of cloud fragmentation.

The equation of the Salpeter/Kroupa IMF is given by:

$$\Phi(m) = \frac{dN}{dm} \propto m^{-\alpha} \quad (4.1)$$

where $\Phi(m)$ is the fraction of stars contained in a certain mass range $m + dm$. For stars heavier than $0.5 M_{\odot}$, $\alpha = 2.3$. In the broken power law approach suggested by Kroupa (2001), there are breaks at $0.5 M_{\odot}$ and $0.08 M_{\odot}$, with the corresponding

exponents being $\alpha = 1.3$ and $\alpha = 0.3$ respectively for masses less than the break-mass. The equivalent equation for the Chabrier IMF is given by:

$$\Psi(\log m) \sim e^{\frac{-(\log m - \log m_c)^2}{2\sigma^2}} \quad (4.2)$$

where $\Psi(\log m)$ is the number of stars in a certain logarithmic mass range of $\log m + d\log m$, $\log m_c$ and σ are the mean mass and the variance in $\log m$ respectively. The mean mass appears to differ between regions and environments. Figure 3 in the review by [Bastian et al. \(2010\)](#) shows fitted IMF curves for 15 open and globular clusters. The mean masses vary between $\sim 0.1 M_{\odot}$ and $\sim 0.8 M_{\odot}$. [De Marchi et al. \(2010\)](#) show that for the same clusters the mean mass appears to increase with age.

Many studies have however reported that the shape of the IMF for different regions is, within the errors of the observations, consistent with a single functional description of the IMF. This would imply that the process behind the shape of the IMF is universal. Indeed according to [Ascenso et al. \(2009\)](#) any variations that have been observed can be explained by observational completeness effects, such as crowding and detection limitations.

As observational determinations of the initial mass function are based on counting the number of stars in set mass bins, any IMF determination is intrinsically linked to the quality of the observations. The current generation of telescopes allow us stars well into the brown-dwarf regime in the nearest star forming regions like Orion and even Trumpler 14 ([Ascenso et al. 2007](#)). However there is a physical limit defined by the diffraction limit of a telescope as to how many stars can be extracted from any given observation. The more distant the region of interest, the smaller the fraction of stars which can contribute to determining the region's IMF. The ELT and MICADO will offer a diffraction limit $\sim 5\times$ smaller than any of the current generation of 8 m-class telescopes, which will allow up to $\sim 25\times$ more stars to be extracted from densely populated regions. Additionally the $\sim 978 \text{ m}^2$ collecting area of the ELT will allow MICADO to reach detection limits 1 to 2 magnitudes fainter than the Hubble space telescope. These two facts combined will give MICADO an unparalleled ability to detect the essentially all the stars in any of the

young star forming clusters in the Milky Way, and in the Large and Small Magellanic Clouds.

Given that the universality of the IMF is such an important topic (addressed in section 4.3), I conducted a study to see just how many stars in certain mass ranges could be observed by MICADO for different environments. The goal was to determine the limits for the lowest reliably observable mass for a range of different distances and stellar densities. Given that observing time on MICADO will be in high demand from all areas of astronomy, I believe it is important to know exactly what MICADO will be able to deliver in terms of IMF studies. This will help us to keep our expectations in check, but also enable us to determine which will be the most efficient observing strategies for the limited time available.

In this chapter I present the first draft of a manuscript to be submitted to *Astronomy and Astrophysics*. In the paper I discuss finding the lowest reliably observable mass for dense stellar regions. To do this I used SimCADO to create 42 mock young stellar clusters with densities ranging from 10^2 stars arcsec $^{-2}$ to 10^5 stars arcsec $^{-2}$ and placed them at distances from 8 kpc to 5 Mpc. I observed them with SimCADO and extracted as many stars as possible using a custom detection and subtraction algorithm. The limiting observable mass for each cluster was determined based on the statistics of the extracted masses compared to the initial masses. The major result of the paper is that MICADO will easily be able to determine the shape of the IMF in the sub-solar regime in the Large Magellanic Cloud, however the Brown Dwarf regime is still out of reach for extragalactic clusters.

4.2 Publication Details

The paper concentrates mainly on the possibilities of determining the extragalactic IMF, however after discussing the manuscript with several others we decided that it should also contain a section on the advances MICADO will bring to determining the IMF inside Milky Way clusters. Thus I have not yet submitted the paper. Furthermore, the analysis to determining the lowest observable mass could be improved by (first learning, then) using the DAOPHOT photometry package for doing PSF photometry and subtraction. I plan on re-running the analysis with DAOPHOT before submitting the paper.

Title: SimCADO II: Simulating limits to future studies of the IMF with the ELT and MICADO

Authors: Kieran Leschinski and João Alves

Status: Under internal review. To be submitted in May 2018.

Own contributions: Everything related to this study.

SimCADO II: Simulating limits to future studies of the IMF with the ELT and MICADO

K. Leschinski¹ and J. Alves¹

Department of Astrophysics, University of Vienna, Vienna, Austria
e-mail: kieran.leschinski@univie.ac.at

Received TBD; accepted TBD

ABSTRACT

Context. The MICADO near infrared imager on the Extremely Large Telescope will offer diffraction limited imaging over almost an arcminute field of view. With a sensitivity equivalent to the Hubble Space Telescope, MICADO will open up the densest regions of young stellar clusters which are currently limited by confusion. This will allow us to study aspects such as a cluster's IMF in great detail in the Galaxy's densest environments as well as outside the Milky Way.

Aims. The goal of this study was to determine the extent of the parameter space which MICADO will open up for the field of resolved young stellar populations and for studies on the initial mass function. The main question to which we sought an answer was: What is the lowest mass star that MICADO will be able to observe for a given stellar density and distance?

Methods. We used SimCADO, the instrument simulator package for MICADO, to generate observations of 42 dense stellar regions with densities similar to the cores of young stellar clusters. The densities of these stellar fields ranged from 10^2 to 10^5 stars arcsec^{-2} and the fields were placed at distances from 8 kpc to 5 Mpc from the Earth. The lowest reliably observable mass for each stellar field was determined via a PSF photometry and subtraction algorithm.

Results. Our results show that stellar densities of $>10^3$ stars arcsec^{-2} will be easily resolvable by MICADO. At a distance of 2 Mpc stars with $M > 2 M_\odot$ will still be resolved in fields of $>10^4$ stars arcsec^{-2} , allowing the high-mass end of the IMF to be studied in e.g. NGC 300. The lowest reliably observable mass in the LMC will be around $0.1 M_\odot$ for clusters with densities $<10^3$ stars arcsec^{-2} . MICADO will open up the stellar content of the cores of all dense young stellar clusters in the Magellanic clouds, allowing the sub-solar mass turnover of the IMF to be studied in detail.

Conclusions. We have shown that MICADO will have access to star clusters 10x denser than what JWST will be able to access, and over 100x denser than those imaged by Hubble. This will allow access to all the members of the densest star clusters in the Milky Way and all $M > 0.1 M_\odot$ members in the Magellanic clouds. While the sensitivity of MICADO will not allow us to study the brown dwarf regime outside the Milky Way, it will provide extraordinary coverage of the turnover of the IMF in the M-dwarf mass regime in the LMC and SMC.

1. Introduction

The Initial Mass Function (IMF) and its consequences are found in almost all fields of astronomy and astrophysics. It is the empirically derived mass distribution of stars produced during a star formation event. In galactic astronomy the IMF is important because it determines not only the fate of the environment surrounding a star formation region, but in the longer term also the composition of older stellar populations as well as the galaxy as a whole. The relative numbers of low to high mass stars also has a huge impact on the mass cycle of a galaxy. The more mass is locked up in low mass stars, the smaller the reservoir of gas for the next generation of stars is. For archeoastronomy, the IMF is a critical parameter for determining the star formation history of a galaxy. On the more theoretical side, hydrodynamic simulations of galaxies and cosmological simulations of galaxy clusters use the IMF to determine the strength of feedback mechanisms governing the movement of energy and material. In short the IMF is an extremely important parameter in astronomy. Some may find it humorous that for all its importance, the shape of the IMF is still determined empirically and its origins are hotly debated.

In his original work, Salpeter (1955) used a single power law distribution with a slope of 2.35 to describe the IMF for masses greater than $\sim 1 M_\odot$. This was later modified as a series of broken power laws to include the stars below below the hydrogen burning limit by Kroupa (2001). In contrast Chabrier (2003) pro-

posed a log-normal distribution with a power law modification for the high and low mass regions. As the two descriptions are very similar in the most populated region between $0.1 M_\odot$ and $10 M_\odot$, it has proved very difficult to decide which model more aptly describes the IMF.

Furthermore regardless of where observers look, it appears that the shape of the IMF is a constant. Each star forming region produces on average the same relative amount of stars per mass bin as any other star forming region. Conclusive deviations from the accepted IMF are elusive, yet there is one major aspect stopping general acceptance of a universally constant IMF: the fact that we lack enough statistics of regions that are substantially different from the solar vicinity. Table 1 shows, even in the closest star forming galaxies like the large and small Magellanic clouds, only the Hubble space telescope (HST) has the sensitivity to reach the sub-solar mass stars (See references in Table 1). Long exposures with HST can reach just below the first break in the Kroupa power law at $0.5 M_\odot$ (Da Rio et al. 2009; Kalirai et al. 2013; Geha et al. 2013), but not far enough into the lower mass regions to put constraints on the shape of the IMF in extragalactic environments. Adding to observers' woes is the lack of spatial resolution. At the distance of the LMC, star forming regions can contain anywhere from 10^2 to 10^5 stars arcsec^{-2} . A perfect example of why current studies struggle to reliably determine the IMF for dense stellar populations outside the Milky Way is given in Figure 1 of Sirianni et al. (2000). The picture

Table 1. A compilation of mass limits for a selection of studies of the IMF outside the Milky Way with the Hubble space telescope. It should be noted that for the study by Gallart et al. (1999) the estimated global star formation history was consistent with a Salpeter slope, rather than a Salpeter slope being extracted from the photometric data.

Galaxy	Target	Distance kpc	Mass range M_{\odot}	IMF Slope(s)	Break Mass M_{\odot}	Reference
LMC	R136	50	2.8-15	2.22		Hunter 1995
LMC	NGC 1818	50	0.85-9	2.23		Hunter 1997
LMC	R136	50	1.35-6.5	2.28, 1.27	2.1	Sirianni 2000
LMC	LH 95	50	0.43-20	2.05, 1.05	1.1	Da Rio 2009
SMC	NGC 330	62	1-7	2.3		Sirianni 2002
SMC	NGC 602	62	1-45	2.2		Schmalzl 2008
SMC		62	0.37-0.93	1.9		Kalirai 2013
Hercules		135	0.52-0.78	1.2		Geha 2013
Leo IV		156	0.54-0.77	1.3		Geha 2013
Leo I*		250	0.6-30	2.3		Gallart 1999

shows a cluster core being completely dominated by the flux of the brightest stars. Thus studies of the IMF are limited to the outer regions of these clusters where stellar densities are low enough for individual low mass stars to be resolved. The age of a cluster and the resulting level of mass segregation can also skew the results when considering the IMF in massive clusters (Lim et al. 2013), however without being able to study the core of such clusters inside and outside the Milky Way, it is difficult to determine to what extent this plays a role. Thus in order to systematically study the lower mass, and arguably most interesting, part of the IMF we will need telescopes with higher spatial resolution and better sensitivity than the current generation of ground and space based telescope.

In the middle of the next decade, the generation of the extremely large telescopes will begin. ESO’s Extremely Large Telescope (ELT) (Gilmozzi & Spyromilio 2007) with the help of advanced adaptive optics (Diolaiti 2010) will offer the power to resolve spatial scales at the diffraction limit of a 40m-class mirror. This will provide an improvement of a factor of $\sim 15\times$ over HST and a factor of $\sim 6\times$ over the future JWST telescope. With a collecting area of 978 m^2 the ELT will have at least the same sensitivity as the HST in sparse field and will be able to observe much deeper than HST in crowded fields. The MICADO instrument (Davies et al. 2010, 2016) will be the ELT’s first-light near-infrared (NIR) wide-field imager and long slit spectrograph. With a plate scale of 4 mas and an AO corrected field of view of almost a square arcminute, MICADO aims to address exactly this niche.

Determining to what extent MICADO will improve our ability to study the IMF and other properties of dense stellar populations is the main focus of this paper. In this paper we have attempted to addressed the following two questions: What is the lowest mass star that MICADO will be able to observe for a given density and distance? What instrumental effects will play a critical role when undertaking such studies with MICADO and the ELT? In our quest for answers we used SimCADO, the instrument data simulator for MICADO (Leschinski et al. 2016), to simulate a wide range of densely populated stellar fields at various distances, which can act as cluster proxies. The current version of SimCADO takes into account all the major and most of the minor spatial and spectral effects along the line of sight between the source and the detector. We used the software to generate realistic images of our model stellar fields and then conducted several iterations of PSF photometry and star subtraction to extract as many stars as possible from the simulated observations. The extracted stars were compared with the input cata-

logue to determine the completeness of the extraction and to define a “limiting reliably observable mass” for the different stellar field densities and distances.

This paper is organised in the following way: Section 2 describes the stellar fields used in our simulations and how the simulations were run. In this section we also describe the algorithm for detecting and subtracting stars in the simulated images. In Section 3 we describe the results of the simulations and discuss their validity in the context of possible future observations of real young stellar clusters. Section 4 summarises our results.

2. Data sets

The best way to determine the IMF is to look at a population of stars which is still young enough that all the original members are still around, yet old enough that the main phase of star formation activity is over. If a population is too young, it will not have finished forming all its stars. Too old and the most massive members will already have gone supernova. Dynamical effects will also have led to evaporation of stars from the cluster. Ideally the population should also be old enough for any remaining gas and dust to have been expelled or dispersed. Unfortunately such ideal conditions do not exist. Star formation happens on time scales of 10^6 years. The most massive stars chew through their hydrogen reserves within the first several ten million years and move off the main sequence. Given that the dispersion time for stellar clusters is on the order of hundreds of millions of years, at any point in time relatively few of the observable new clusters will be so youthful. The majority of IMF studies focus on the clusters which come closest to meeting these conditions - namely open clusters (OC) and young massive clusters (YMC). It should be mentioned that OB associations also provide a laboratory for studying the IMF. However as these are older and in many cases more spread out, the chances of contamination from background sources and missing ejected stars is higher. Furthermore, the high mass end of the IMF cannot be observed as the highest mass stars have already left the main sequence, and some have ended as supernova.

2.1. Parameter Space

The HST has a diffraction limit of $\sim 0.1''$ at $1.2 \mu\text{m}$ and can reach magnitudes of up to $J=28.6^m$ (Rajan & et al. 2011) in a 10 hour observation. Using AO assisted ground based instruments like NACO at the VLT, diffraction limited observations can be achieved over small ($\sim 1'$) fields of view. The diffraction limit of

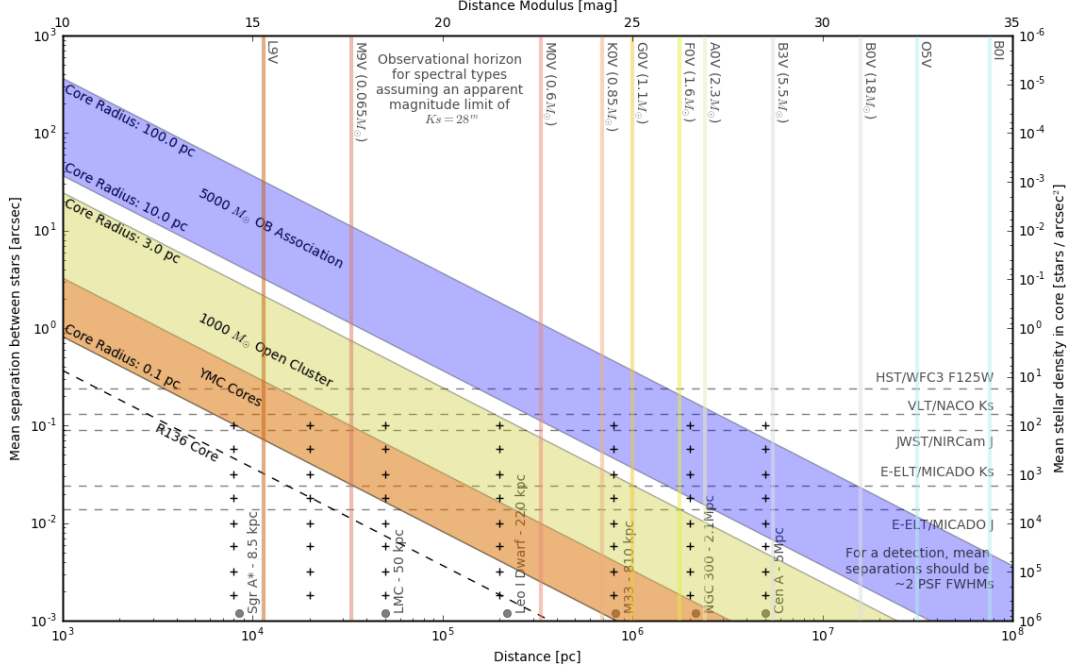


Fig. 1. The crosses represent the parameter space covered by the simulated stellar fields in this study relative to the estimated core stellar densities for the three major categories of young stellar populations: open clusters (green), young massive clusters (orange), and OB associations (blue). The vertical lines represent the furthest distance at which a certain type of main sequence star will still be above the detection limit of MICADO, i.e. $K_s = 28^m$. The dashed horizontal lines show the theoretical confusion limit for MICADO, JST, HST and NACO/VLT. The confusion limit assumes an average minimum distance of $2 \times$ the PSF FWHM between stars. Obviously for NACO confusion would not play as much of a role as the instruments sensitivity limit is $K_s \sim 24^m$.

the VLT telescopes is $\sim 0.03''$ at $1.2\mu m$, $3 \times$ smaller than HST, however NACO only has a sensitivity limit of around $J=24^m$. As boundary conditions for our suite of stellar fields we took the resolution limit of HST, as cluster cores with densities lower than this are already accessible to the HST. Assuming an average of one star per FWHM, our lower density limit was set to 100 stars arcsec^{-2} . To find the upper density limit we first took the theoretical diffraction limit of the ELT: 7 mas at $1.2\mu m$, or 2×10^4 stars arcsec^{-2} . However as faint stars drop below the telescope's detection limit the effective density of detectable stars decreases with increasing distance. As we wanted crowding limited observations at large distances ($> 1 \text{ Mpc}$), we increased the true stellar density by a factor of $15 \times$ so that the $M > 1 M_\odot$ stars alone would meet the crowding criterion. Thus we set the upper limit for the true stellar density to 3×10^5 stars arcsec^{-2} .

Current telescopes are capable of detecting almost all main sequence stars above the hydrogen burning limit ($\sim 0.08 M_\odot$) within a few kiloparsecs of the Sun. Detecting all main sequence stars in clusters which are further a field, e.g. in the galactic centre and beyond, is where MICADO's increased sensitivity and resolution will bring the greatest breakthroughs. Indeed the question of whether the IMF is truly universal dictates that we study the IMF outside the Milky Way. Therefore we placed our model proxy-clusters at distances corresponding to some of the more well known celestial landmarks: The Galactic Centre ($\sim 8 \text{ kpc}$), the LMC ($\sim 50 \text{ kpc}$), Leo I dwarf galaxy

($\sim 200 \text{ kpc}$), M33 ($\sim 800 \text{ kpc}$)¹, NGC 300 ($\sim 2 \text{ Mpc}$), and Cen A ($\sim 5 \text{ Mpc}$). Figure 1 shows the parameter space covered by average ($\sim 1000 M_\odot$) open clusters with radii between 0.1 pc and 3 pc and average OB Associations ($\sim 5000 M_\odot$) with radii between 10 pc and 100 pc as distance from Earth increases. The lower bounds of the open cluster parameter space also covers the cores of YMCs. Average cluster properties were derived for the OB Associations from Mel'Nik & Efremov (1995), for the open clusters from Piskunov et al. (2007), and for the YMCs from Portegies Zwart et al. (2010).

2.2. Artificial stellar fields

In this study we generated densely populated stellar fields, that could function as proxies for the dense regions at the cores of young stellar clusters. The parameter space covered by these cluster proxies are shown with the crosses in Figure 1. The stellar fields were populated by continually drawing stars from an IMF until the required stellar density was reached. The mass of each star was drawn at random from an IMF distribution with minimum and maximum masses of $0.01 M_\odot$ and $300 M_\odot$. The IMF

¹ The author recognises that the location of the ELT in the southern hemisphere means that M33 will effectively be unobservable. We provide this data point because M33 will, with luck, be visible to the Thirty Meter Telescope.

followed a standard Kroupa (2001) broken power law distribution with breaks at $0.08 M_{\odot}$ and $0.5 M_{\odot}$ and standard slope exponents². The absolute J and K_S magnitudes for each star were calculated by interpolating Table 5 in Pecaut & Mamajek (2013)³ for the given mass. The requisite distance modulus for the stellar fields was added to give each star an apparent magnitude. It should be noted that we did not include extinction in the distance modulus as this varies with the line of sight. The stars were assigned random coordinates within the 2 arcsec bounding box. Although true clusters follow some sort of luminosity profile, and hence density profile, for this study we were primarily interested in the densest regions, i.e. the worst case scenario. Hence distribution of stars in our stellar fields followed a uniform random distribution. In real observations the decline in density with radial distance will therefore be advantageous and offer an improvement over our pessimistic approach.

2.3. Observations

To “observe” our stellar fields we used the standard imaging mode of SimCADO (Leschinski et al. 2016) which mimicked observations with the wide-field mode of MICADO at the ELT. The core regions of open clusters and YMC have radii on the order of ~ 1 pc (Portegies Zwart et al. 2010). At a distance of 200 kpc (\sim Leo 1 Dwarf), this translates to an angular diameter of $\sim 2''$. Thus we thought it safe to assume that the stellar density within the inner $2'' \times 2''$ region should remain relatively constant. For the sake of computational effort we decided to restrict to observations to this $2'' \times 2''$ window in the centre of the detector.

At the very least multi-band photometry is required to determine the mass of a star. Therefore detections in at least the J and K_S filters is necessary. We deemed a detection in the K_S filter to be critical for any study of the IMF and therefore restricted our observations to this filter. The reason for this is as follows: The sky background in the K_S filter is the highest of all NIR filters and the stellar flux is for all main sequence stars (and many brown dwarfs) weakest in the K_S filter. If a source is undetectable in the K_S filter it will not be possible to determine its mass accurately. Given the AO-nature of the observations and the expected low Strehl ratio at $1.2\mu\text{m}$ (Clénet et al. 2016), it could be argued that defections in the J filter will be more difficult. In the end the fluxes of the stars and the sky are set by nature, whereas the Strehl ratio is a question of engineering and optical design. The stars cannot be made brighter, whereas optical quality can be improved. Hence we deemed a detection in the K_S filter to be the critical point for determining the mass of cluster members.

Exposure times were kept to 1 hour for no other reason than observing time at the ELT will be in very high demand once it comes on line and observations in two or more filters are needed to accurately determine the mass of stars.

2.4. Source extraction and matching

Figures A.1 and A.2 in the Appendix show a graphical representation of the process described in this section. They show two examples of “observed” stellar fields placed at a distance of 50 kpc

² By “standard” we mean: $\alpha = 0.3$ for $M < 0.08M_{\odot}$, $\alpha = 1.3$ for $0.08M_{\odot} < M < 0.5M_{\odot}$, and $\alpha = 2.3$ for $M > 0.5M_{\odot}$ as defined in Kroupa (2001)

³ Masses are actually not given in Table 5, but rather in the online supplement at http://www.pas.rochester.edu/~emamajek/EEM_dwarf_UBVIJHK_colors_Teff.txt

and containing 10^3 and 10^4 stars arcsec $^{-2}$ respectively. The stark features of the SCAO PSF⁴ are clearly visible in the images. The diffraction core of the PSF is however still well modelled by a Gaussian distribution. To find and measure the stars in the images we used the following method:

1. Find the brightest star in the image with DAOStarFinder from photutils (Bradley et al. 2017)
2. Find the centre of the star in a 5×5 pixel window around the coordinates given by DAOStarFinder
3. Fit a 2D Gaussian profile to the core of the star
4. Scale an image of a reference star to match the amplitude, baseline and offset of the found star
5. Subtract the scaled reference star from the image
6. Repeat until DAOStarFinder no longer finds any sources above 5σ

In practice we found that we could subtract ~ 100 stars at once and thus greatly increase the speed of the process. The amplitudes and baselines were converted to magnitudes based on the reference star. Our reference star was a solitary “field” star with a magnitude of K_S=15, observed for the minimum MICADO exposure time of 2.6 s. We calculated masses for each star based on the observed fluxes in the K_S filter. This step is only permissible because of the simplified context of this study. We are free to equate the luminosity function with an equivalent mass function because all our stellar fields have the intrinsic property that they only contain main sequence stars and the luminosity and mass functions enjoy a one-to-one relationship for this conversion in the K_S filter, mathematically speaking. Furthermore, our primary goal is to determine what the lowest reliably observable mass is, based on how well MICADO will perform in crowded field - not to directly measure the mass of the original stars. We feel that this step does not detract from achieving the goal of this study.

Finally we cross-matched the coordinates of the extracted sources with the original table of coordinates to determine what fraction of stars were correctly detected with our algorithm. Due to noise and confusion from very close stars the centroid coordinates of the extracted star was not always exactly equal to the original coordinates. The cross-matching algorithm was instructed to search for the closest star within a 25 mas radius. If a fainter or brighter star happened to be closer, then the algorithm chose that star from the catalogue as the match. We determined whether the extracted masses for stars in a certain mass bin were “reliable” by binning the extracted stars according to mass. We then took the mean and standard deviation of all stars within a mass bin. As long as the mean extracted mass to true mass ratio was in the range 1.0 ± 0.1 and the standard deviation was less than 0.1, the mass bin was classed as reliable. By this definition the lowest reliably detectable mass for a stellar field was given by the lower edge of the lowest mass bin which satisfied these criteria.

3. Results and Discussion

3.1. The lowest reliably observable masses for given stellar densities and distances.

The first of the questions we asked with this study – “What is the lowest mass star that MICADO will be able to observe reliably

⁴ The PSF user here was from a simulation of the SCAO mode from MAORY. It was only released internally within the MAORY consortium. By default the SimCADO package comes with a SCAO PSF generated by the MICADO consortium, which is in the public domain.

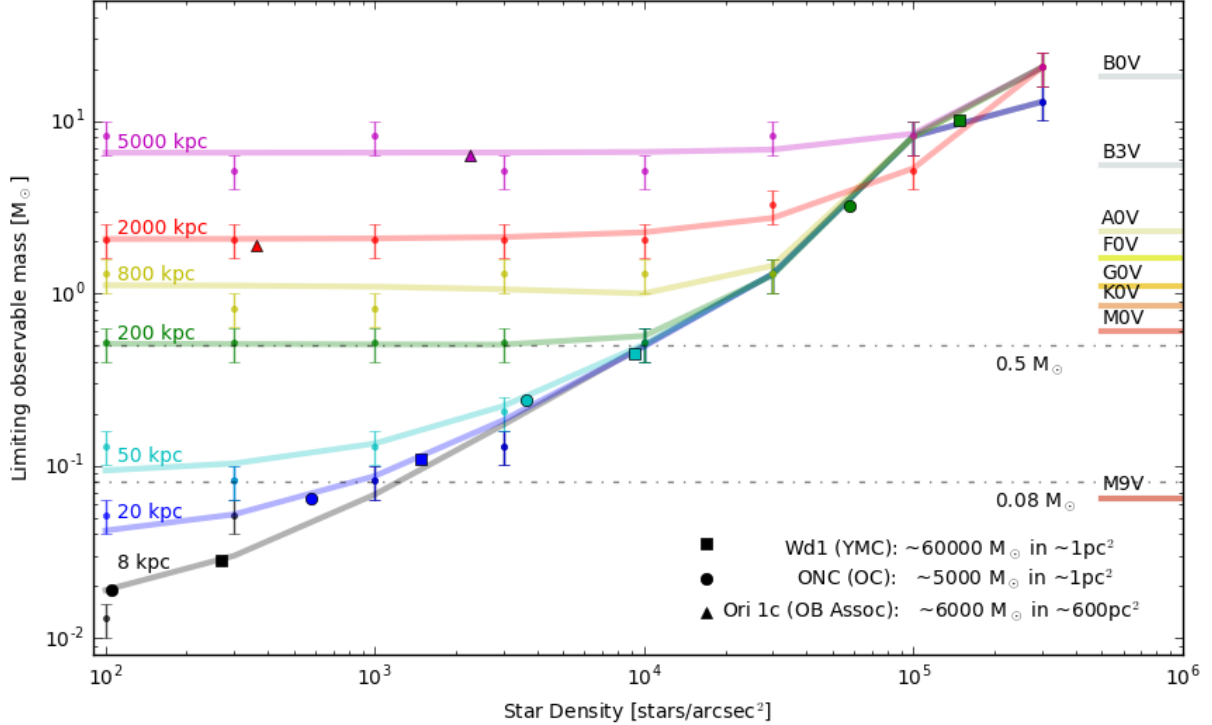


Fig. 2. This graph is the answer to the first question we posed: what is the lowest observable mass for given stellar densities and distances? The errors in the observable mass are 0.2 dex and correspond to the size of the mass bins used. Two trends are visible in the best fit lines for each distance: the flat regime shows that the limiting mass is based on the sensitivity limit of MICADO, while the exponential regime shows where crowding becomes the limiting factor. The cavity to the lower right shows the mass-stellar density parameter space in which stars will not be observable. Here the stellar density includes all the stars in a given area down to $0.01 M_{\odot}$, not just the stars above the sensitivity limit. Hence for the cases where observations are sensitivity limited, the effective observable star density is, in the cases with greater distance, much lower. In these cases the stars below the sensitivity limit only contribute to a higher background flux.

for a given density and distance?" – can be answered by Figure 2. For each of the distances and densities we have plotted the lowest reliable mass bin. The scatter in the plot reflects the random nature of the simulations. The positions of the stars in each of the stellar field were randomised, the sampling of the mass function was random and shot noise was applied to the image as part of SimCADO's read-out process. Thus no two stellar fields were the same. Each stellar field configuration was only run once. We therefore only have one data point for each density and distance. The bin size used for the reliability statistics was set to 0.2 dex, and is therefore the uncertainty in the limiting observable mass.

From Figure 2 we can immediately see the two limiting regimes of sensitivity and crowding. The flat parts of the curves in Figure 2 show the densities for which MICADO will be sensitivity limited at each distance and the diagonal regions show when crowding becomes the limiting factor. For example observations of a cluster at a distance of 8 kpc observations will always be crowding limited for densities above $100 \text{ stars arcsec}^{-2}$. At a distance of 200 kpc observations will be limited by sensitivity up to a density of $10^4 \text{ stars arcsec}^{-2}$, thereafter crowding will be the dominant factor. At 5 Mpc all observations will be sensitivity limited. As a reference we have also included in Figure 2 the approximate stellar densities for three well known young clusters *if they were located at the distance of the cluster proxies*. For example, if the YMC Westerlund 1 were to be located

in the LMC, it would fall in to the crowding-limited regime for MICADO. The lowest reliably observable mass in the densest region of the core would only be $\sim 0.5 M_{\odot}$. This is equivalent to what HST is capable of observing in the outer rim territories of LMC cluster. For clusters in the LMC with stellar densities less than 10^3 we see that MICADO will be limited by sensitivity to masses above $0.1 M_{\odot}$. While this mass is only $0.3 M_{\odot}$ lower than what current observations with Hubble can achieve, it should be emphasised that this increase of "only" $0.3 M_{\odot}$ will reveal the majority of M-type stars, which account for almost three quarters of all main sequence stars (Ledrew 2001). Given that the limit of current studies is around the $0.5 M_{\odot}$ knee from Kroupa (2001), opening up this range will allow future studies to pin down exactly what the shape of the IMF looks like in the LMC clusters.

As previously noted the exposure time for the simulated images was one hour. By observing for longer times, the lowest observable mass will decrease, however the change is disproportionate to the exposure time. Leschinski et al. (2016) show that increasing the exposure time to 10 hours per cluster only increases the sensitivity limit by around 1.5^m and 1^m in the J and K_S filters respectively. For the case of the LMC, this would drop the lowest observable mass to around $0.06 M_{\odot}$, i.e. just below the hydrogen burning limit.

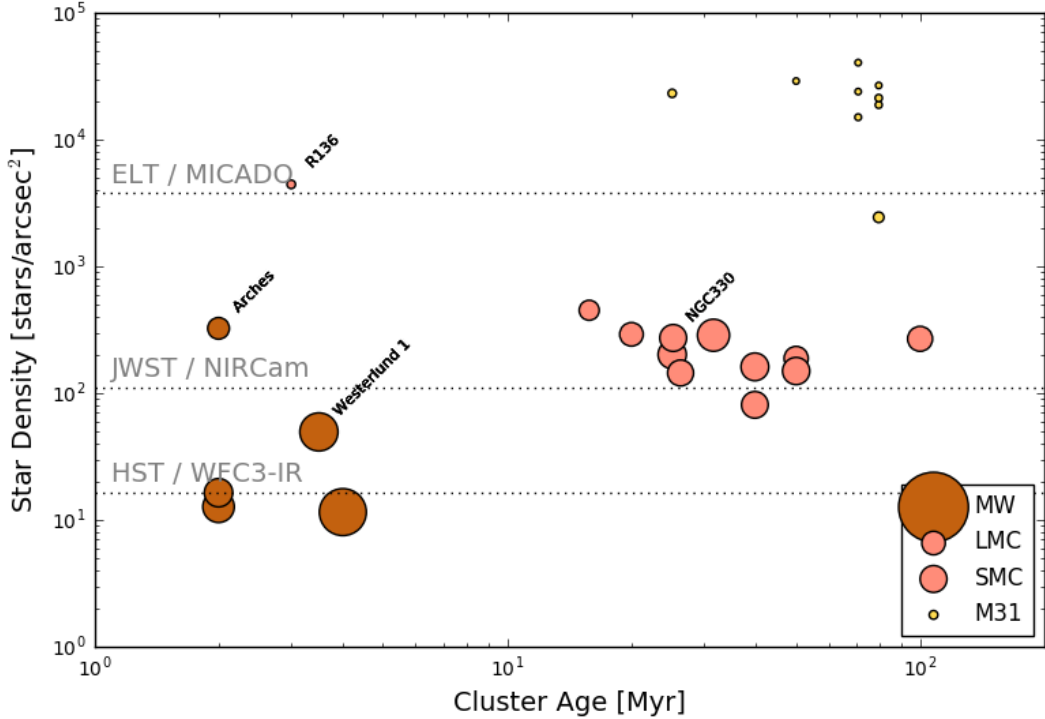


Fig. 3. The stellar densities in the cores of the clusters listed in Table A.1 assuming a sensitivity limit of $K_S=28^m$. The size of the circles is proportional (including an offset) to the relative on-sky size of the cluster cores. The colours reflect the lowest possible reliably observable mass, as shown in Figure 2 and listed in Table A.1. Brown: $M>0.01M_\odot$; Pink: $M>0.1M_\odot$; Yellow: $M>0.9M_\odot$. The densities shown here take into account the sensitivity limit and therefore are only for the potentially observable stars, i.e. any low luminosity stars with $K_S>28^m$ are omitted from the density calculation. This is equivalent to all stars in the Milky Way, M-class stars and brighter in the LMC, and G-class stars and brighter in M31. Only clusters from Portegies Zwart et al. (2010) which had a defined core radius, r_c , are shown. The dashed lines in this figure represent the limit to the resolving capability of the HST, JWST and ELT. We define the limiting density as the mean distance between stars being equal to $2.5 \times$ the PSF FWHM. Given the predicted PSF shapes for the latter two telescopes, these lines may prove to be somewhat optimistic. Nevertheless the graphic illustrates the point that cores of the majority of young clusters are far too dense for either HST or JWST observations. Thus it will require the ELT (or similar) to study the most heavily populated regions of these clusters.

It should also be noted the majority of young clusters have core which are less dense than that of Westerlund 1, and therefore the limiting observable mass will also be lower than the $0.5 M_\odot$ mass quoted for a Westerlund 1-like YMC in the LMC. Given MICADO's resolving power it will therefore also be possible to determine to what extent apparent mass segregation has played a role in previous studies of the IMF in the LMC. More to the point MICADO will enable us to understand the apparent deviations from the Salpeter IMF as reported by Da Rio et al. (2009), Geha et al. (2013) and Kalirai et al. (2013).

At distances of 100 kpc to 200 kpc and with careful photometry and longer observations MICADO should be able to detect stars down to the sensitivity limit of $0.5 M_\odot$. This will only be possible though for clusters with stellar densities less than 10^4 stars arcsec^{-2} . As a reference an ONC-like cluster at a distance of 200 kpc will have a stellar density on the order of 10^5 stars arcsec^{-2} . Such observations will be useful for determining the composition of OB associations and sparser (older) open clusters, if there were any present in the non-Magellanic satellites of the Milky Way. Nevertheless MICADO will still allow us ob-

serve the fabled $0.5 M_\odot$ knee in the field population of the nearest low metallicity dwarf spheroidal galaxies.

Closer to home MICADO should be able detect $10 M_{Jup}$ objects in an ONC-like clusters at a distance of 8 kpc. The Arches cluster is an obvious candidate for such studies, and given its proximity to the galactic centre makes it an ideal case to study the IMF under extreme conditions. The main hindrance to such observations is not the almost 2 mag of variable K_S -band extinction along the line of site (Espinoza et al. 2009), but rather the brightest stars in the cluster. The effectiveness of MICADO observations will also be limited by the brightest stars in the field. Leschinski (2018, in prep) state that point sources with magnitudes $K_S>14.8^m$ will saturate the MICADO detectors within the 2.6 s minimum exposure time. There are very few regions in the cores of Milky Way open clusters which do not contain stars brighter than $K_S\sim 15^m$, making deep MICADO observations of these regions difficult.

3.2. The cores densities of young star clusters

The second of the questions we asked with this study was “What instrumental effects will play a critical role when undertaking such studies with MICADO and the ELT?”. The instrumental effect which would play the largest role regarding the accuracy of the estimates given here is our knowledge of the PSF. For this study we used a single SCAO PSF. We assumed that the PSF orientation stayed the same for the length of the observation. Consequently we had a very good model of our reference star for the PSF subtraction. This will obviously not be the case for real observations as the pupil of the telescope will rotate with respect to the sky, causing an axial broadening of the PSF over the course of an observing run. On the one hand this broadening should improve the results from our subtraction method as it will smooth out many of the sharp features of the instantaneous PSF. On the other hand we will lose information on both the structure of the PSF and the extent of the wings. Thus the PSF subtraction algorithm will less accurately be able to estimate the background level when fitting the reference PSF to a star. As a consequence faint stars caught in the PSF wings of the brighter stars may not be detected as often as they would be if the PSF remained rotationally aligned with the sky. A hybrid approach to the faint star subtraction problem may be the following: Subtract the brightest stars from each individual exposure using an instantaneous PSF derived from the brightest stars in that exposure, then stack the residual images and extract the faintest stars using a rotationally broadened PSF. Further investigation is required to determine whether this approach would indeed increase the detection rate for faint stars.

Although it may seem obvious, one final point is worth mentioning. From our simulations it is clear that resolving stellar densities of 10^3 stars arcsec^{-2} is well within the capabilities of MICADO. With an optimised PSF fitting and subtraction algorithm, extracting upwards of 5×10^3 stars arcsec^{-2} should also be in the realms of possibility. 5×10^3 stars arcsec^{-2} is equivalent to approximately one star in the equivalent area of ~ 2.5 ELT H-band PSF FWHMs. This is similar to being able to resolve every star in the core of an ONC-like cluster in the LMC. For JWST and HST the equivalent stellar densities are only 160 stars arcsec^{-2} and 20 stars arcsec^{-2} respectively. Although MICADO may not have the sensitivity of a space-based telescope, the resolving power will give us full access to the core populations of dense stellar clusters in the major satellites of the Milky Way.

3.3. The cores densities of young star clusters

These simulations are a nice theoretical exercise, however without an application to observations they are not all that useful. Figure 3 shows the estimated stellar densities in the cores of the open clusters and YMCs compiled by Portegies Zwart et al. (2010). The density values, $\log_{10}(\rho)$, only take into account the stars with apparent magnitudes above the sensitivity limit of MICADO and thus reflect the “real” observable density for the clusters (Also listed in Table A.1). The limits set for HST, JWST and MICADO are the critical stellar density above which our extraction algorithm struggles to detect and remove more than 90% of the stars in a field. We find that for the Galactic clusters, the resolution of JWST will be sufficient to resolve all stars in the cluster’s core down to the sensitivity limit of the instrument. For clusters in the galactic plane though JWST observations will struggle to disentangle the cluster stars from the field stars. To robustly determine cluster membership observations of the proper motion of the cluster relative to the field will be required. Stolte

et al. (2008) show that the proper motion of the Arches cluster near the Galactic centre is $\sim 5 \text{ mas yr}^{-1}$, around a sixth the size of a pixel in the JWST NIRCam instrument. MICADO, in contrast, will have a plate scale of 1.5 mas in the zoom mode, meaning the cluster’s members could be determined by observations spaced only several months apart.

Resolving the cores of the young clusters in the Magellanic clouds will not be possible with JWST. Based on the compiled ages listed in Portegies Zwart et al. (2010) MICADO should give us access to the cores of young clusters in the LMC which cover a wide range of ages. This will allow a much deeper understanding of the dynamical processes (e.g. evaporation, core collapse, etc.) involved in the evolution of these clusters. Additionally observations of a series of LMC clusters with varying ages will give a much better picture of how the initial mass function evolves into the present day mass function, and how the dynamical evolution of the cluster influences the observations and calculations of a cluster’s IMF.

4. Conclusion

MICADO and the ELT will offer us the chance to finally resolve the core populations of the densest star clusters in the Milky Way and in neighbouring galaxies out to distances of a several hundred kiloparsecs. By turning MICADO towards young stellar clusters we hope to finally answer the question as to whether the IMF is indeed universal, or whether the shape of the distribution changes when we leave the Galaxy. Currently the answers are locked up inside young stellar clusters, which by nature have very high stellar densities. Observations of these clusters are primarily limited by confusion. Exactly how much of the stellar populations will be visible to MICADO is what we wanted to address with this study.

This study aimed to answer two questions: What is the lowest mass star that MICADO will be able to observe reliably for a given stellar density and distance? And what instrumental effects will play a critical role when undertaking such studies with MICADO and the ELT? In order to answer these we used the instrument simulator for MICADO (SimCADO) to generate “observations” of 42 dense stellar regions. These regions had stellar densities similar to what would be observed if one were to place an open cluster or a young massive cluster at various distances from Earth. Here we present a brief summary of the results:

- We have shown that MICADO will easily be able to resolve stellar populations with stellar densities of 10^3 stars arcsec^{-2} . With proper knowledge of the PSF and an optimised detection and subtraction algorithm densities of 5×10^3 stars arcsec^{-2} should also be achievable.
- Given that MICADO observations will be bound by the instrument’s sensitivity to both the brightest and faintest sources in the field of view, MICADO is best suited to investigate the shape of the IMF in clusters in the outer edges of the Milky Way as well as the nearest galaxies. For real world science cases this means that the cores of dense young star clusters such as R136 in the LMC and NGC330 in the SMC will be resolvable with MICADO.
- Observations focusing on the initial mass function of clusters in the LMC will be limited by sensitivity, not crowding, to $0.1 M_\odot$. This means that investigations of the brown dwarf knee ($\sim 0.08 M_\odot$) will not be possible outside the Milky Way, however MICADO’s resolution will allow the low mass turn over region of the IMF ($0.1 M_\odot < M < 0.5 M_\odot$) to be extensively investigated in the Magellanic clouds, and the high mass function out to distances of 5 Mpc.

- The brown dwarf population will be accessible in the cores of the densest Milky Way clusters, e.g. in the Arches and Westerlund clusters. Objects with masses on the order of $10 M_{Jup}$ will be accessible by MICADO for clusters within 8 kpc of Earth. The only caveat is that an appropriate observation strategy must be found to mask the many bright ($m_{K_s} < 15''$) stars in these clusters.
- Finally accurate knowledge of the ELT's PSF will be absolutely essential for good photometry and PSF subtraction algorithms. The sharp structures created by the segmented mirror design lead to many fake low luminosity star detections if either the PSF is not well known or the extraction algorithm is not capable of differentiating between a star and an artefact of the PSF.

Acknowledgements. KL would also like to express his gratitude to Gijs Verdoes Kleijn, Eline Tolstoy, and Ric Davies for the insightful and helpful comments and discussions regarding future possible observations with the ELT. SimCADO incorporates Bernhard Rauscher's HxRC Noise Generator package for python (Rauscher 2015). This research made use of POPPY, an open-source optical propagation Python package originally developed for the James Webb Space Telescope project (Perrin et al. 2015). This research made use of Astropy, a community-developed core Python package for astronomy (Astropy Collaboration et al. 2013; The Astropy Collaboration et al. 2018). This research made use of Photutils (Bradley et al. 2017). This research has made use of "Aladin sky atlas" developed at CDS, Strasbourg Observatory, France (Bonnarel et al. 2000; Boch & Fernique 2014). SimCADO makes use of atmospheric transmission and emission curves generated by ESO's SkyCalc service, which was developed at the University of Innsbruck as part of an Austrian in-kind contribution to ESO. This research is partially funded by the project IS538003 of the Hochschulraumstrukturmittel (HRSM) provided by the Austrian Government and administered by the University of Vienna.

References

- Astropy Collaboration, Robitaille, T. P., Tollerud, E. J., et al. 2013, A&A, 558, A33
Boch, T. & Fernique, P. 2014, in Astronomical Society of the Pacific Conference Series, Vol. 485, Astronomical Data Analysis Software and Systems XXIII, ed. N. Manset & P. Forshay, 277
Bonnarel, F., Fernique, P., Bienaymé, O., et al. 2000, A&AS, 143, 33
Bradley, L., Sipocz, B., Robitaille, T., et al. 2017, astropy/photutils: v0.4
Chabrier, G. 2003, PASP, 115, 763
Clénet, Y., Buey, T., Rousset, G., et al. 2016, in Proc. SPIE, Vol. 9909, Society of Photo-Optical Instrumentation Engineers (SPIE) Conference Series, 99090A
Da Rio, N., Gouliermis, D. A., & Henning, T. 2009, ApJ, 696, 528
Davies, R., Ageorges, N., Barl, L., et al. 2010, in Proc. SPIE, Vol. 7735, Ground-based and Airborne Instrumentation for Astronomy III, 77352A
Davies, R., Schubert, J., Hartl, M., et al. 2016, in Proc. SPIE, Vol. 9908, Society of Photo-Optical Instrumentation Engineers (SPIE) Conference Series, 99081Z
Diolaiti, E. 2010, The Messenger, 140, 28
Espinoza, P., Selman, F. J., & Melnick, J. 2009, A&A, 501, 563
Gallart, C., Freedman, W. L., Aparicio, A., Bertelli, G., & Chiosi, C. 1999, AJ, 118, 2245
Geha, M., Brown, T. M., Tumlinson, J., et al. 2013, ApJ, 771, 29
Gilmozzi, R. & Spyromilio, J. 2007, The Messenger, 127
Kalirai, J. S., Anderson, J., Dotter, A., et al. 2013, ApJ, 763, 110
Kroupa, P. 2001, MNRAS, 322, 231
Ledrew, G. 2001, JRASC, 95, 32
Leschinski, K., Czoske, O., Köhler, R., et al. 2016, in Proc. SPIE, Vol. 9911, Society of Photo-Optical Instrumentation Engineers (SPIE) Conference Series, 991124
Lim, B., Chun, M.-Y., Sung, H., et al. 2013, AJ, 145, 46
Mel'Nik, A. M. & Efremov, Y. N. 1995, Astronomy Letters, 21, 10
Pecaut, M. J. & Mamajek, E. E. 2013, ApJS, 208, 9
Perrin, M. D., Long, J., Sivaramakrishnan, A., et al. 2015, WebbPSF: James Webb Space Telescope PSF Simulation Tool, Astrophysics Source Code Library
Piskunov, A. E., Schilbach, E., Kharchenko, N. V., Röser, S., & Scholz, R.-D. 2007, A&A, 468, 151
Portegies Zwart, S. F., McMillan, S. L. W., & Gieles, M. 2010, ARA&A, 48, 431
Rajan, A., & et al. 2011, WFC3 Data Handbook v. 2.1 (STScI)
Rauscher, B. J. 2015, PASP, 127, 1144
Salpeter, E. E. 1955, ApJ, 121, 161
Sirianni, M., Nota, A., Leitherer, C., De Marchi, G., & Clampin, M. 2000, ApJ, 533, 203
Stolte, A., Ghez, A. M., Morris, M., et al. 2008, ApJ, 675, 1278
The Astropy Collaboration, Price-Whelan, A. M., Sipócz, B. M., et al. 2018, ArXiv e-prints [arXiv:1801.02634]

Table 1. The age and observable stellar densities for a selection of young massive clusters found both in and outside the Milky Way, as listed in Portegies Zwart et al. (2010). The densities have been calculated to only include stars which are brighter than $K_s=28^m$, as fainter stars will not be detectable by MICADO. The table lists the parameters for the clusters shown in Fig. 3.

Galaxy	Cluster	Distance kpc	Age Myr	log(Mass) M_\odot	Core radius arcsec	$\log_{10}(\rho)$ stars arcsec $^{-2}$	Limiting mass M_\odot
Cores resolvable by HST							
MW	ONC	0.4	1	3.7	100	-1.6	0.01
Cores resolvable by JWST							
MW	Trumpler-14	2.7	2	4	10.7	1.1	0.01
MW	Quintuplet	8.5	4	4.0	24	1.1	0.04
MW	NGC3603	3.6	2	4.1	8.6	1.2	0.01
MW	Westerlund-1	5.2	3.5	4.5	15.9	1.7	0.01
LMC	NGC2214	50	39.8	4.0	7.5	1.9	0.1
Cores resolvable by MICADO							
LMC	NGC1847	50	26.3	4.4	7.1	2.2	0.1
LMC	NGC2157	50	39.8	4.3	8.2	2.2	0.1
LMC	NGC1711	50	50.1	4.2	7.9	2.2	0.1
LMC	NGC1818	50	25.1	4.4	8.5	2.3	0.1
LMC	NGC2164	50	50.1	4.2	6.1	2.3	0.1
SMC	NGC330	63	25.1	4.6	7.7	2.4	0.15
LMC	NGC2136	50	100	4.3	6.6	2.4	0.1
MW	Arches	8.5	2	4.3	4.9	2.5	0.04
LMC	NGC1850	50	31.6	4.9	11	2.5	0.1
LMC	NGC2004	50	20	4.4	5.8	2.5	0.1
LMC	NGC2100	50	15.8	4.4	4.1	2.7	0.1
M31	B257D	780	79.4	4.5	0.8	3.4	0.9
Only outer regions resolvable by MICADO							
LMC	R136	50	3	4.8	0.41	3.7	0.1
M31	B066	780	70.8	4.3	0.10	4.2	0.9
M31	B040	780	79.4	4.5	0.15	4.3	0.9
M31	B043	780	79.4	4.4	0.19	4.3	0.9
M31	B318	780	70.8	4.4	0.05	4.4	0.9
M31	B448	780	79.4	4.4	0.05	4.4	0.9
M31	Vdb0	780	25.1	4.9	0.37	4.4	0.9
M31	B327	780	50.1	4.4	0.05	4.5	0.9
M31	B015D	780	70.8	4.8	0.06	4.6	0.9

star_density 1000.0 dist 50000.0 mass 1000.0

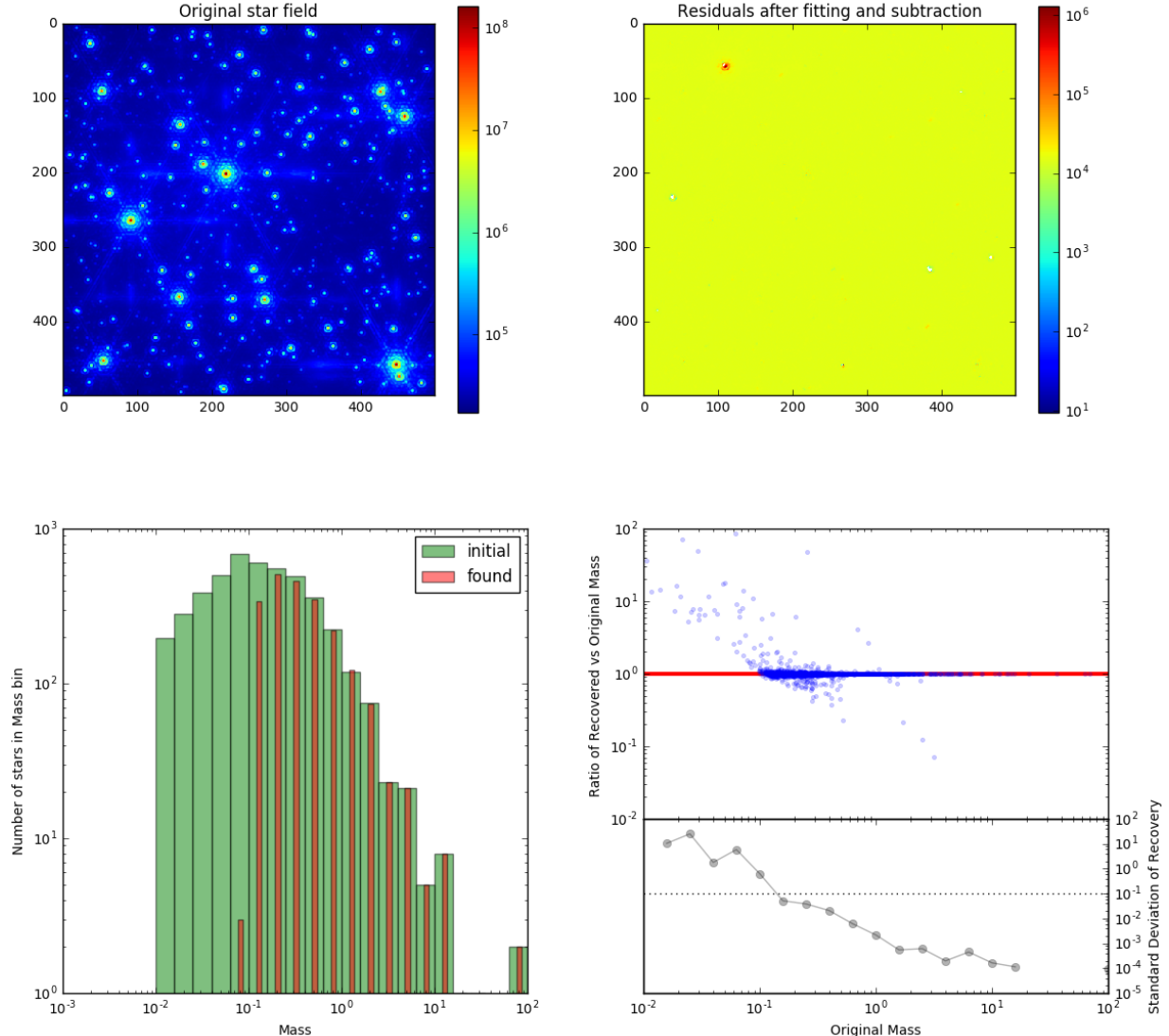


Fig. 1. Results of extracting stars from a 1000 stars arcsec^{-2} cluster at a distance of 50 kpc. Top left: The original 2'' \times 2'' stellar field with a density of 10^3 stars arcsec^{-2} . The stars in the field have masses between $0.01 M_\odot$ and $300 M_\odot$. The PSF used in this study was an instantaneous SCAO PSF, similar to what would be seen on a single MICADO detector 2.6 s exposure. Top right: The same field after our detection and subtraction algorithm has iteratively removed all the stars. 10^3 stars arcsec^{-2} are extracted reasonably easily by our algorithm. Bottom left: The fraction of extracted stars in each mass bin which matched up with the original list of stars. The majority of stars more massive than $0.1 M_\odot$ were detected. Bottom right: The upper panel shows the ratio of extracted mass to original mass. The vast majority of the almost 4000 stars in the image fell almost perfectly on the red one-to-one line. The minor scatter around the line is due to a combination of our detection algorithm not being able to discern between very close stars, and contamination for the PSF artefacts, e.g. the segmented diffraction spikes. The lower panel shows the standard deviation of masses around the one-to-one line in a certain mass bin. A mass bin was deemed reliable if the average recovered to original mass ratio was in the range 1 ± 0.1 and the standard deviation was less than 10%.

star_density 10000.0 dist 50000.0 mass 10000.0

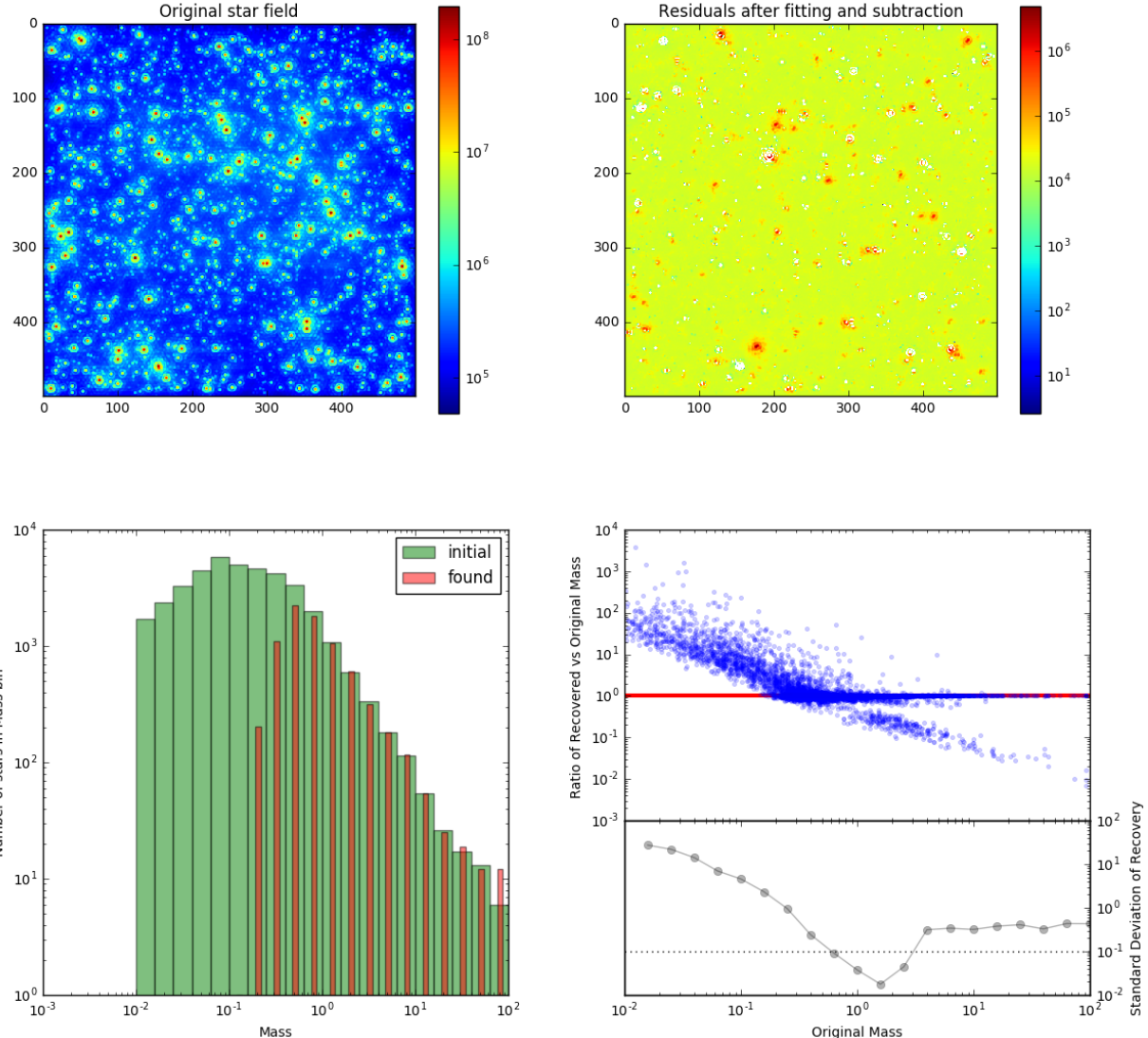


Fig. 2. Same as Fig. A.1 but for a stellar density of 10^4 stars arcsec^{-2} . At these densities the number of “double” stars has increased to the point where our detection algorithm was unable to accurately fit and subtract the a number of the bright stars. Although a large number of incorrect mass determinations are visible in the big blue cloud, still around 60% of the ~40 000 sources in this image fall on the red one-to-one line. The segmented PSF meant that the the algorithm detected many fake sources which skewed the detection statistics in both the high and low mass regimes. We are still looking into ways of preventing this from happening in future studies.

Optimal filter design for MICADO with SimCADO

5.1 Overview

This chapter continues with the theme on the previous chapter: applying SimCADO to real world situations. Here I present a pilot study conducted with SimCADO to find the optimal flux blocking level for the MICADO broad and narrow band filters, which will allow MICADO to provide a photometric precision of less than 1%. No filter is able to block 100% of the flux outside of the designated filter bandpass. Depending on the properties of the filter coating a certain percentage of flux in the so-called wings of the filter, i.e. blue- and red-wards of the edges of the filter's bandpass, will always leak though. Filter coatings can be manufactured to block almost any level of flux. However as the blocking requirement increases, so too does the cost. Hence, for the sake of the budget, it is important to know just how much of the flux outside of the bandpass needs to be blocked. The blocking requirement is set by the instrument top-level requirements for photometric accuracy. For MICADO, this top-level requirement dictates that MICADO shall provide photometric accuracy at the level of 0.01 mag. This translates to a requirement that the fraction of flux leaked through the filter wings compared to the flux transmitted through the filter's bandpass be no more than 1%.

The levels of leaked flux in each of the red and blue wings naturally depends on which object is observed: stars will generally always dominate the leaked flux in the blue wing, while the thermal component of the atmosphere will dominate the flux in the red wing. The blocking coefficient for each of the wings can be manufactured individually, and so in this study I optimised the blocking coefficients for each wing based on the dominant source of leaked photons.

The exact method I used and the results from the study are presented in this chapter in the form of a technical note submitted to the MICADO optics design team.

5.2 Publication Details

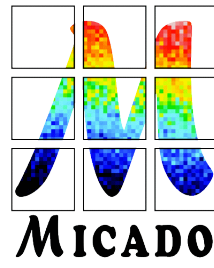
Title: Phase B Technical Note: Filter Wing Transmission Levels

MICADO Doc. No.: ELT-TRE-MCD-56306-0056

Authors: Kieran Leschinski

Status: Accepted by the MICADO Consortium

Own contributions: Everything related to the study described in this technical note.



ELT - MICADO

Phase B

Technical Note: Filter Wing Transmission Levels

Doc. No.: ELT-TRE-MCD-56306-0056

Issue: 1.0

Date: 08.03.2018

Author(s): K. Leschinski

Name

Date

Signature

WP Manager: G. Verdoes Kleijn.....

Name

Date

Signature

Proj. Responsible R. Davies.....

Name

Date

Signature

MICADO Consortium

Contents

1 Executive Summary	4
2 Applicable documents and references	4
3 Definitions	5
4 Context	5
5 Data	6
5.1 Spectra	6
5.2 Filter Set	6
6 Method	7
6.1 Total wing flux leakage	9
6.2 Wing transmission coefficients to maintain a <1% flux increase	10
6.3 Splitting the red wing into near-red and thermal-red windows	10
7 Results	13
7.1 Transmission coefficients excluding a thermal-red blocking filter	13
7.2 Transmission coefficients including a thermal-red blocking filter	15
8 Summary	16
9 Ideas for future experiments	18

1 Executive Summary

This technical note describes the level of flux suppression that filters should provide outside their designated wavelength range in order to ensure flux leaks from outside the wavelength range remain under 1% of the total filter throughput. This document is not meant to set the requirements for fabrication of the filter set, but rather serve as a guide to aid in the decision making process. After reading the document, it should be clear that:

- the transmission coefficient of the blue wing of the filter profiles is dictated by the key astronomical cases
- the transmission coefficient of the red wing of the filter profiles is dictated by the level of atmospheric background flux
- in general broad band filters require a blocking coefficient of at least 10^{-3} , while narrow band filters will require a blocking coefficient on the order of 10^{-4} . The notable exceptions are the J and Pa β filters, which will require a further factor of 10 suppression on the red wing.
- a thermal-red ($\lambda > 2.35 \mu\text{m}$) blocking filter with a transmission coefficient on the order of 10^{-2} will relax the suppression requirements for the red wing of all filters by at least a factor of 2.5.

Table 5 in Section 8 succinctly summarises the results of this technical note.

2 Applicable documents and references

Reference	Title	Remarks
ELT-TRE-MCD-56300-0014	MICADO Masks, Stops, and Filters Description	Version 17.11.2016
Leschinski et al. (2016)	SimCADO: an instrument data simulator package for MICADO at the E-ELT	Proc. SPIE, Vol 9911, id. 991124, doi: 10.1117/12.2232483
Noll et al. (2012)	An atmospheric radiation model for Cerro Paranal. I. The optical spectral range	A&A, Vol 543, id.A92, doi: 10.1051/0004-6361/201219040
Jones et al. (2013)	An advanced scattered moonlight model for Cerro Paranal	A&A, Vol 560, id.A91, doi: 10.1051/0004-6361/201322433

3 Definitions

Term	Definition
Blocking Coefficient	A filter's ability to block the light in the so-called wings of the filter, i.e. at wavelengths outside the designated transmissive region of spectral space.
Suppression level	See Blocking Coefficient. These terms are used interchangeably
Wing (Red, Blue)	Wavelength region outside the filter cut-off wavelength λ_{cutoff} . For example, the red wing refers to all wavelengths red-wards of λ_{red}
Cut-off wavelength	The wavelength for which the transmission is 50% of the average peak transmission.
Near-red, thermal-red	Two regions of the red wing for filters. The thermal-red refers to only wavelengths red-wards of $\lambda = 2.35 \mu\text{m}$. Near-red is the wavelength region between the filter's red cut-off and $\lambda = 2.35 \mu\text{m}$.
Bandpass	The wavelength region between the red and blue cut-offs
SimCADO	The MICADO instrument data simulator software. Described in Leschinski et al. (2016)
Wide-field mode	MICADO's default imaging mode with a full chip read-out time of 2.6s and a plate scale of 4 mas.
SkyCalc	The ESO tool for generating synthetic sky spectra. See Noll et al. (2012) and Jones et al. (2013).
docstrings	Function/Class documentation accessible from within a python environment

4 Context

Procuring a set of large filters for MICADO is an expensive endeavour. In an ideal world the flux suppression of a filter outside its specified bandpass would be 100%. Unfortunately the real world is not ideal and the cost of producing a filter increases as a filter's suppression level requirement increases. In order to achieve MICADO's goal of providing photometric accuracy at or below 0.01^m, the light seeping through the filter wings must be less than 1% of the integrated light coming through the filter's designated wavelength range, or bandpass. In this technical note the blocking coefficients required for a sub set of common filters across the near infrared wavelength range have been determined using the the current default set-up of SimCADO. The filters studied in this technical note were: J, H, Ks, Pa β , H-cont, and Br γ

The code used for this technical note can be found on the SimCADO website under <http://www.univie.ac.at/simcado/examples/Notebooks.html>. The SimCADO functionality is included in the SimCADO submodule `simcado.sandbox.filter_wings`. See the relevant function docstrings for documentation. When running the code SimCADO was told not to take into account photon shot noise in order to calculate accurate values on the incoming flux. For the stars, all other sources of light (atmosphere, mirror blackbody emission) were turned off. When using the sky emission spectrum from SkyCalc, SimCADO also added the greybody emission from the telescope mirrors.

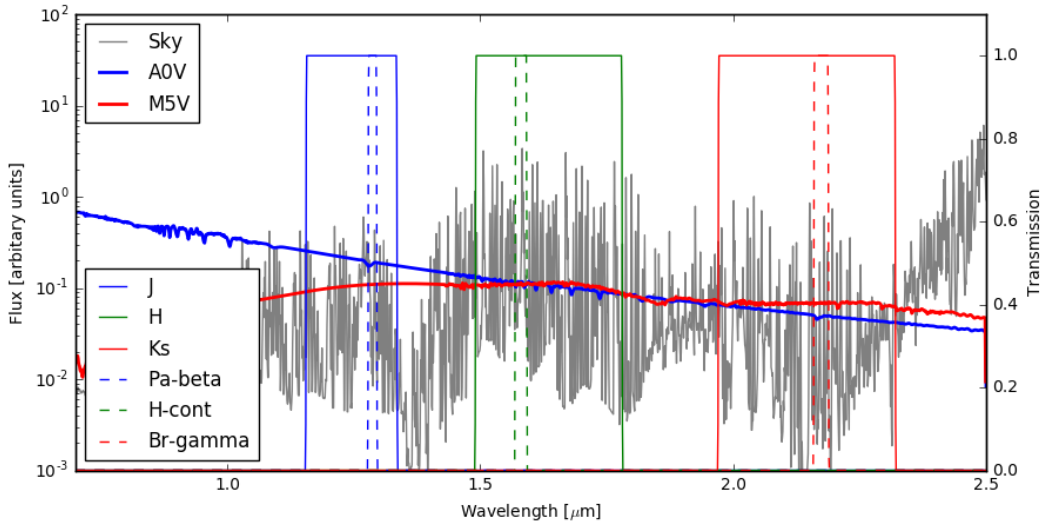


Figure 1: The wavelength range covered by MICADO with the spectra for two stars (A0V and M5V) and a general atmospheric emission spectrum generated by SkyCalc. The broad band (solid) and narrow band (dashed) filters used in this technical note are include for reference. For this study we used top-hat profiles with perfect transmission in the filter bandpass and varied the wing transmission.

5 Data

5.1 Spectra

As there is a veritable zoo of different celestial objects, each with a unique spectrum, one cannot just assume a flat light source. For the purposes of this experiment we used spectra for the following common astronomical sources: an A0V star, an M5V star and the sky emission according to the ESO SkyCalc tool¹. Figure 1 is solely for illustration purposes - the units vary for each spectrum. As we are looking for the relative flux difference per filter, the units are of little importance. The crux of the experiment lies in the fact that we cover the cases of flux decreasing (A0V), and increasing (M0V) from shorter to longer wavelength, as well as the sky background.

5.2 Filter Set

For the purpose of explaining the method we will use the H-band filter. The same method was applied to the six filters listed in Table 1.

For the sake of this experiment, all filter curves are assumed to be top-hats with a transmission coefficient of 1 between the red, λ_{Red} , and blue, λ_{Blue} , cut-off wavelengths. The wing transmission coefficients were adjusted in the range 10^{-2} and 10^{-5} as necessary to achieve the goal of <1% flux leakage in the wings. The edges to the wavelength range of these simulations were $0.5 \mu m$ and $3.0 \mu m$. The MICADO detectors should not be sensitive to photons outside the range $0.6 \mu m < \lambda < 2.5 \mu m$ and therefore act as a natural filter outside this range.

¹<https://www.eso.org/observing/etc/bin/gen/form?INS.MODE=swspectr+INS.NAME=SKYCALC>

Table 1: Details of the filter profiles used for this study. Filter transmission was modelled as a top-hat between the λ_{Blue} and λ_{Red} cut-off wavelengths.

Name	λ_{Blue} [μm]	λ_{Red} [μm]	$\Delta\lambda$ [μm]
J	1.155	1.335	0.180
H	1.490	1.780	0.290
Ks	1.970	2.320	0.350
Pa β	1.278	1.295	0.017
H-cont	1.569	1.592	0.023
Br γ	2.159	2.188	0.029

All transmission curves along the MICADO optical train, including the atmospheric and telescopic transmissions, were taken into account when calculating flux. All transmission curves except the filter curve remain the same throughout this experiment. All SimCADO parameters were kept at their default values for the MICADO wide-field mode. As the H4RG QE curve is not yet publicly available, we assumed that it will be similar to the H2RG curve and used this curve for the detectors.

6 Method

We began by finding the flux of each source through three spectral windows defined by the red and blue cut-offs for each filter. We also investigated the effect of splitting the red wing into two sections: the near red wing ($\lambda < 2.35 \mu\text{m}$) and the thermal red wing ($\lambda > 2.35 \mu\text{m}$). For the purpose of describing the method, we will concentrate on the H filter.

The original three spectral windows for the H-band filter were defined as $\Delta\lambda_{Blue}: 0.3 \mu\text{m} < \lambda < 1.49 \mu\text{m}$; $\Delta\lambda_{Filter}: 1.49 \mu\text{m} < \lambda < 1.78 \mu\text{m}$; $\Delta\lambda_{Red}: 1.78 \mu\text{m} < \lambda < 3.0 \mu\text{m}$. For each window a top hat filter curve was created and combined with the transmission curve of the ELT/MICADO optical train. These combined transmission curves were then applied to the stellar and sky spectra and the resulting spectrum was integrated over the wavelength range of the window. This gave a measure of the total flux through each of these windows with no filter in place. The fluxes for the wings were scaled by assuming a uniform transmission coefficient for the wings (e.g. 10^{-2}), and the resulting flux was compared to that coming through the actual filter bandpass. By varying the transmission coefficients for the wings we were able to find the optimal blocking coefficients for each wing to ensure that the leaked flux remained under 1% of the total filter throughput.

The upper panel of Figure 2 shows the fractional increase in flux versus transmission coefficients for the wings of the H filter for the three different spectra. As expected for an A0V star the blue wing contributes 5× more to the total leaked flux compared to the red wing. For an M5V star, the red and blue wings contribute almost equally to the leaked flux. For the sky background though, the contribution from the red wing is $\sim 25\times$ greater than from the blue wing. The majority of this leaked flux is due to the increase in atmospheric emission red-wards of $2.35 \mu\text{m}$ (See Figure 1). This becomes more apparent if we split the red wing into two windows, red-wards and blue-wards of $2.35 \mu\text{m}$, as is shown in the lower panel of Figure 2. Here we see that the atmospheric emission red-wards of $2.35 \mu\text{m}$ is a factor of two greater than that in the near-red window. For the stars, the blue wing is still the greater source of leaked light. The thermal red window will be discussed in Section 6.3. To illustrate the method behind the experiment, only the full red wing and the blue wing will be discussed in the following sections.

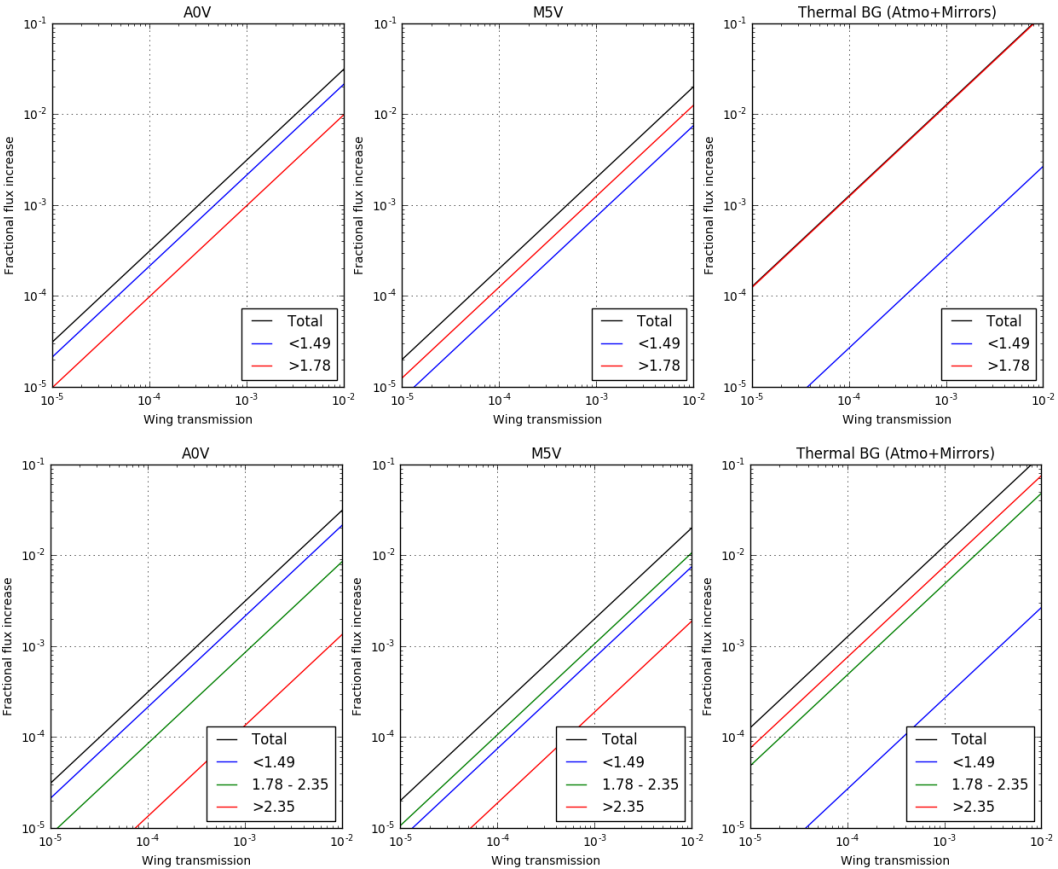


Figure 2: Top: The relationship between fractional increase in flux and transmission coefficients of the wings for the H filter, for three different spectra. The black line shows the total increase in flux due to leakage through both red and blue wings, the red line is the increase due to leakage through the red wing. Bottom: The same as the upper panels except the red wing has been split into near-red ($\lambda < 2.35 \mu\text{m}$) and thermal red ($\lambda > 2.35 \mu\text{m}$) wavelength regions.

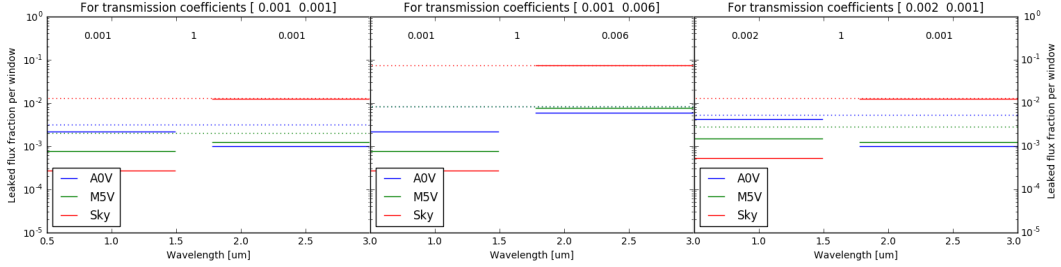


Figure 3: Fractional leaked flux values for various wing transmission coefficients. The solid lines show the integrated flux per wing relative to the total flux coming through the filter, i.e. the fraction of leaked flux per wing. Note that the lines are not wavelength dependent, rather they show the level of integrated flux over the window - hence the flat curve. The extent of the flat line is to show the extent of the window used for the integration. The dotted lines show the level of combined flux leakage by both wings for each of the AOV, M5V and sky spectra. Left: The leaked fractions for a blanket wing transmission coefficient of 10^{-3} for blue and red wings. Centre: The leaked flux fractions optimised for a stellar (AOV or M5V) spectrum. Note that the leaked sky flux is almost at the 10% level. Right: Transmission coefficients optimised for all spectra and with the lowest acceptable flux suppression level for the wings.

Table 2: For the case of a blanket wing transmission coefficient of 10^{-3} . The fraction of flux leaked through the red and blue wings of the H filter compared to the flux through the actual H filter bandpass. The column “Total” is the combined flux of both wing windows (blue, red) compared to the flux through the filter bandpass.

Spectrum	$\lambda < 1.49 \mu\text{m}$	$\lambda > 1.78 \mu\text{m}$	Total
AOV	0.0021	0.0010	0.0031
M5V	0.0007	0.0012	0.0020
Sky	0.0002	0.0123	0.0125

6.1 Total wing flux leakage

MICADO aims to restrict the total amount of flux leakage to no greater than 1% of the total filter transmission. This could be achieved for a broadband H filter by requiring a blanket wing transmission coefficient of 10^{-3} . However blindly specifying this level of flux suppression for the wings is inefficient and may needlessly incur higher production costs. To better estimate the level of suppression actually required for each filter we looked at the contribution to the flux leakage from each window (red wing, blue wing, filter bandpass).

Figure 3 shows the fraction of flux leaked through the red and blue wings for each of the three spectra (the exact values are given in Table 2). The left panel shows the level of flux leakage for a blanket transmission coefficient of 10^{-3} to both wings. The goal of a $<1\%$ flux increase is achieved for all sources (stars and sky background), even though that level of suppression is not required for the blue wing. The flux leakage is the blue wing is dominated by the stars and so the transmission coefficient for the blue wing must be chosen to reflect this. It can be relaxed slightly from the value of 10^{-3} .

Leakage in the red wing is most problematic for the sky background. A transmission coefficient

Table 3: Left: Required transmission levels for the wings based on different input spectra. These levels are based on the assumption that 50% of the leaked flux is contributed by each wing. Right: Residual leaked flux from the optimised wing transmission coefficients. The optimal transmission coefficients were found by iterating over the percentages that each wing contributes to the total leaked flux.

			0.002	0.001	Selected Transmission
Required Transmission			Leaked Flux Fraction		
λ	<1.49 μm	>1.78 μm	<1.49 μm	>1.78 μm	Total
A0V	0.0023	0.0051	0.0042	0.0001	0.0052
M5V	0.0067	0.0040	0.0014	0.0012	0.0027
Sky	0.0188	0.0004	0.0005	0.0123	0.0128

of 10^{-3} is just enough to hold the increase in flux to the $\sim 1\%$ level. If we were to ignore the sky background and only concentrate on the increase in flux from stars (middle panel of Figure 3), then the transmission coefficient could be relaxed to almost 10^{-2} . This would imply that the level of leaked background level would increase up to $\sim 10\%$ of the total transmitted flux. **However as the increase in background would be uniform over the field of view, this would simply lead to a higher background noise. The photometric accuracy for the object of interest would remain unaffected.** It remains to be shown whether this statement is true.

6.2 Wing transmission coefficients to maintain a <1% flux increase

The most lenient wing transmission coefficients that allow us to maintain a 1% flux increase for the three sources of light can be found by diving the desired fractional flux increase by the relative flux through a wing window. See Figure 5 for a graphical example of this. Determining the optimal combination of suppression levels is an iterative approach which starts by assuming that each wing contributes 50% of the leaked flux to the allowable 1% flux budget. There is a bit of wiggle room here regarding this assumption, as is demonstrated in Section 7.

The values in Table 3 shows the transmission coefficients needed to maintain an increase in flux of less than 1% due to wing leakage for our three sources in the H filter. In the blue wing, accurate photometry of blue stars requires that the transmission be no greater than 10^{-3} . On the red wing, it is the sky background which dominates the leaked flux. To restrict this to $<1\%$ the red wing transmission would need to be 4×10^{-4} .

By using the transmission coefficients given in Table 3 for an A0V star ($\sim 10^{-3}$ for the blue wing and $\sim 5 \times 10^{-3}$ for the red wing) the increase in flux is keep to $<1\%$, however the sky background increases to 6.2%. Thus we need to choose the transmission coefficients for each wing based on the source that has the largest influence on the flux leakage.

As mentioned above, we can apportion the leaked flux differently and still maintain a $<1\%$ increase. If we relax and strengthen the wing transmission coefficients to 2×10^{-3} and 1×10^{-3} for the blue and red wings respectively, we maintain a flux leakage of $\sim 1.1\%$ regardless of the source.

6.3 Splitting the red wing into near-red and thermal-red windows

As can be seen from Figure 3, the amount of stellar flux leaked by the red wing is a factor of two less than the flux from the atmospheric background. The vast majority of this flux comes from the

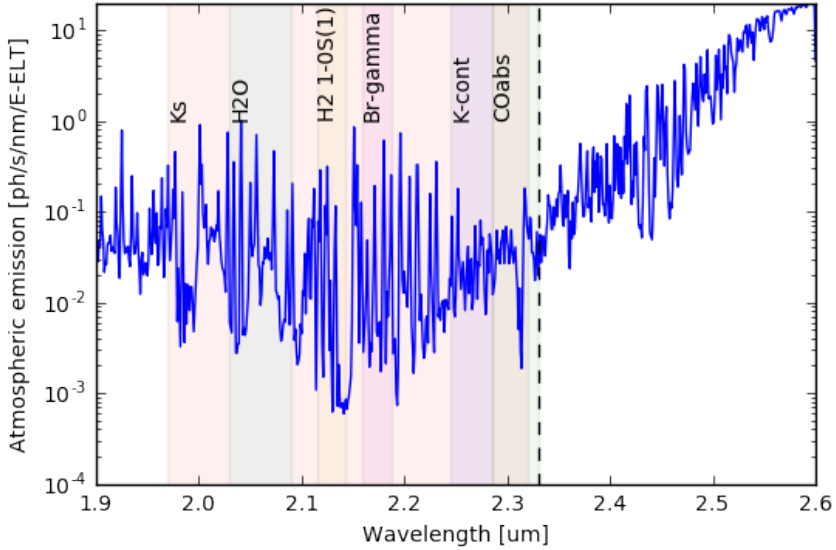


Figure 4: The bandpasses for the proposed broad, medium and narrow band filters in the $1.9 \mu\text{m} < \lambda < 2.3 \mu\text{m}$ atmospheric window. The dashed line is the approximate red cut-off for the CO-absorption line narrow band filter, which extends slightly red-wards of the Ks filter cut-off. The wiggly blue line is the general atmospheric emission spectrum from SkyCalc. Here the increase in the background flux due to the thermal component of the atmosphere is evident.

thermal background of the atmosphere, red-wards of $\lambda = 2.35 \mu\text{m}$ (see Figure 1). Questions remain about whether or not we actually need to filter out this increase in background flux due to its quasi homogeneous distribution over the focal plane. However if we do wish to filter it out, we have two options:

1. manufacture all filters in such a way as to block the full red wing down to a level of 10^{-3} , or
2. take advantage of MICADO's second filter wheel and manufacture a separate thermal red filter with the sole purpose of blocking light red-wards of $\lambda = \sim 2.35 \mu\text{m}$.

This would allow us to relax the requirements on the red wing of all other filters. Considering that MICADO has ~ 30 filter slots and that manufacturing filters is not cheap, it is worth investigating this second option.

Based on the wavelength coverage of the filters in the Ks-band, it makes sense to set the thermal-red wing border to $\lambda = 2.35 \mu\text{m}$ (the Ks filter will have a red cut-off at $\lambda \sim 2.32 \mu\text{m}$ and the CO-absorption narrow band filter at $\lambda \sim 2.33 \mu\text{m}$). This way the thermal-red filter can be used in conjunction with the selection of filters currently slated for use in one of MICADO's filter wheels. Alternatively it may be worth giving one of the other optical components a special coating that blocks all light red-wards of $\lambda = 2.35 \mu\text{m}$ so that both filter wheels can be used with the thermal-red blocking capability.

As transmission coefficients are multiplicative, the thermal-red filter may not need to have an extremely low transmission red-wards of $\lambda = 2.35 \mu\text{m}$. A factor of 0.01 would probably suffice as the

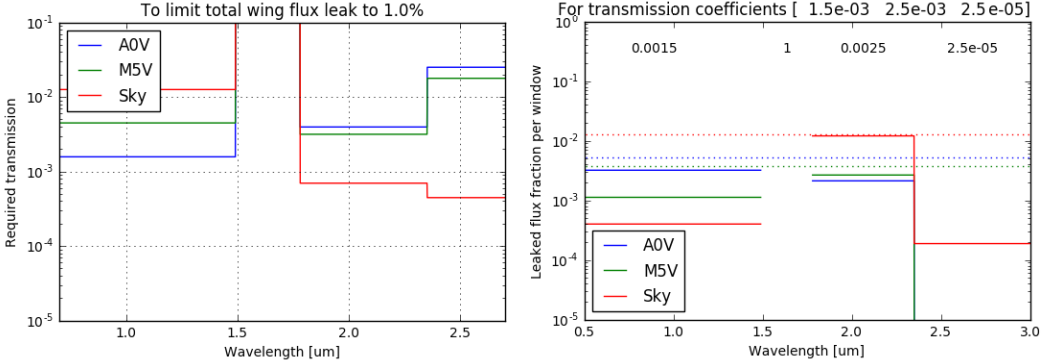


Figure 5: Left: The required transmission to maintain a total leaked flux fraction under 1% in the H filter. The initial contributions from each of the 3 wing windows was 33%. Right: Optimised transmission coefficients for the H filter including a thermal-red filter with a blocking capability of 10^{-2} . Similar to Figure 3, the solid lines show the integrated flux per wing relative to the total flux coming through the filter. The dotted lines show the level of the combined flux leaked through all wing windows for each of the A0V, M5V and sky spectra.

Table 4: The same as Table 3 however the red wing was split into near-red and thermal-red windows. Left: Required transmission level for the wings based on different input spectra. Right: Residual leaked flux from the optimised wing transmission coefficients. The optimal transmission coefficients were found iterating over the percentages that each wing contributes to the total leaked flux. The original assumption was 33% per wing window (blue, near-red, thermal-red).

				0.0015	0.0025	2.5E-6	Chosen Trans.
Required Transmission				Leaked Flux Fraction			
Spectra	<1.49 μm	1.78-2.35 μm	>2.35 μm	<1.49 μm	1.78-2.35 μm	>2.35 μm	Total
A0V	0.0015	0.0039	0.0249	0.0032	0.0021	3.3E-6	0.0053
M5V	0.0044	0.0031	0.0177	0.0011	0.0026	4.6E-6	0.0037
Sky	0.0125	0.0006	0.0004	0.0004	0.0120	0.0002	0.0126

scientific filters already have a factor of $\sim 10^{-3}$ built into them. When combined this would give each filter an approximate total suppression level of $\sim 10^{-5}$ for $\lambda < 2.35\mu\text{m}$.

We ran the calculations for the required transmission coefficients again for the H filter, but this time with three wing windows. We split the red wing into near-red and thermal-red, with the border at $\lambda = 2.35\mu\text{m}$. This time we started with the assumption that the required transmission coefficients were based on equi-portioned flux leakage ($\sim 33\%$) in each window. Hence the transmission coefficients for each source (stars, sky) should be taken with a pinch of salt.

Figure 5 and Table 4 show the refined required transmission coefficients when an extra thermal-red filter is included. Again we see that the transmission coefficient for the blue wing needs to be strictest in order to block the blue excess in early type stars and strictest in the red wing to block the atmosphere. By using a thermal-red filter with a transmission coefficient of 10^{-2} , the requirement on the near-red wing can be relaxed to 2.5×10^{-3} - an improvement by a factor of 6. The blue-wing coefficient must stay at 1.5×10^{-3} in order to maintain photometric accuracy of the early type stars.

7 Results

We calculated transmission coefficients for 6 common board and narrow band filters: J, H, K_s, Pa β , H-cont, and Br γ . The required blocking coefficients for the case without a thermal-red filter and assuming equal amounts of flux leakage in each wing are shown in Figure 6. The optimised transmission coefficients and the residual flux leakage from these coefficients are shown in Figure 7. Figures 8 and 9 show the same but for the case where a thermal-red blocking filter (for $\lambda > 2.35 \mu\text{m}$) is included. The figures are summarised in Table 5.

7.1 Transmission coefficients excluding a thermal-red blocking filter

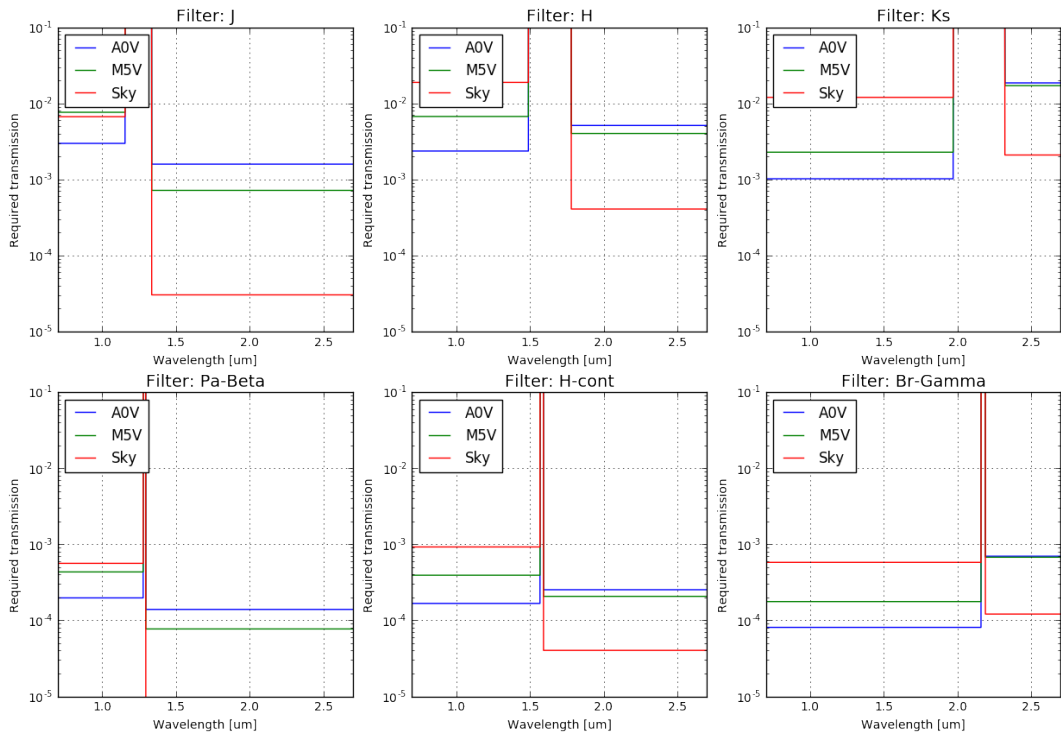


Figure 6: The same as the left panel of Figure 5. The horizontal lines show the required transmission for the wings to maintain the leaked flux at the 1% level for each of the 6 filters in this study. These transmission coefficients were determined under the assumption that each wing contributes 50% to the total leaked flux. These coefficients were used as the initial guess for the optimising routine.

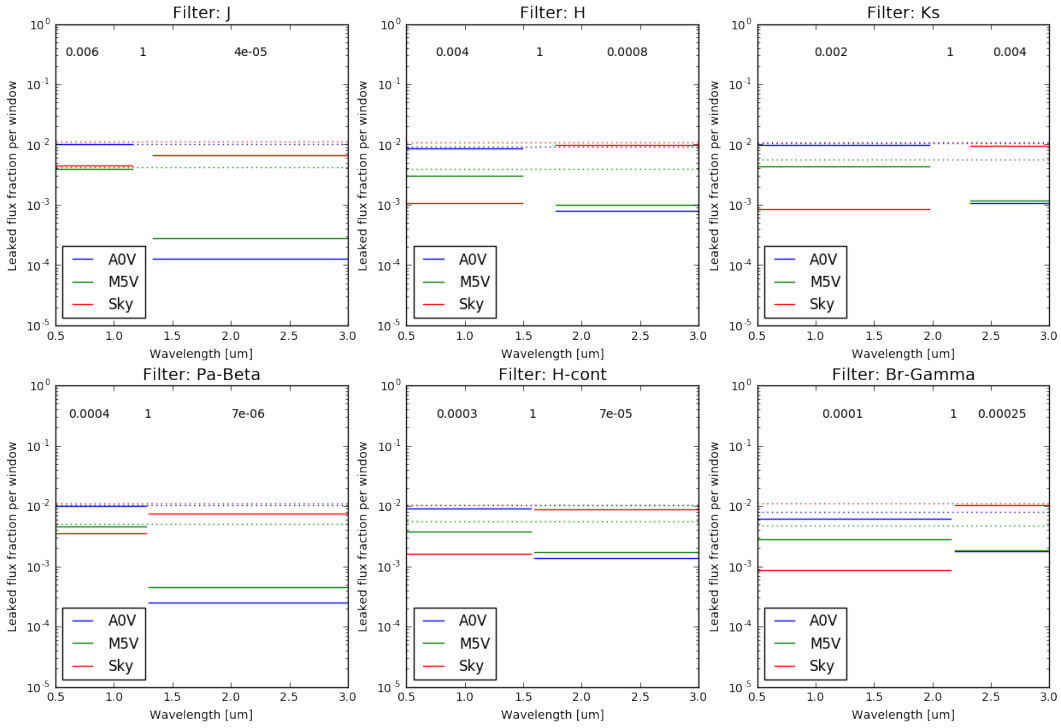


Figure 7: The solid lines show the fraction of flux due to leakage for each window. The solid lines are not continuous functions of wavelength, but rather show the integrated flux through the wavelength region defined by the straight line as a fraction of the flux through the actual filter's wavelength range. The dotted lines show the level of the total flux leaked through the wings. This is not wavelength dependent, but merely the total level of flux transmitted through the wing windows as a fraction of the total flux through the filter. The numbers above each region are the optimised transmission coefficients for the wings of the filter.

7.2 Transmission coefficients including a thermal-red blocking filter

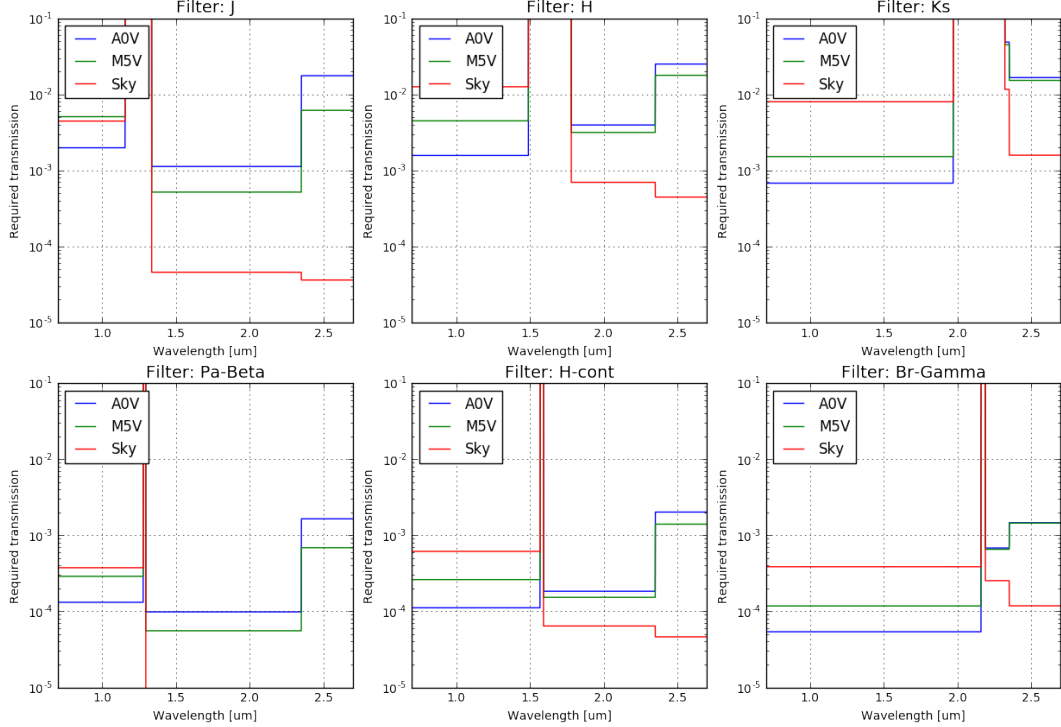


Figure 8: The same as Figure 6 but with the red wing being split between near and thermal-red windows at $\lambda = 2.35 \mu\text{m}$. The initial assumption was that each window contributes 33% to the total leaked flux.

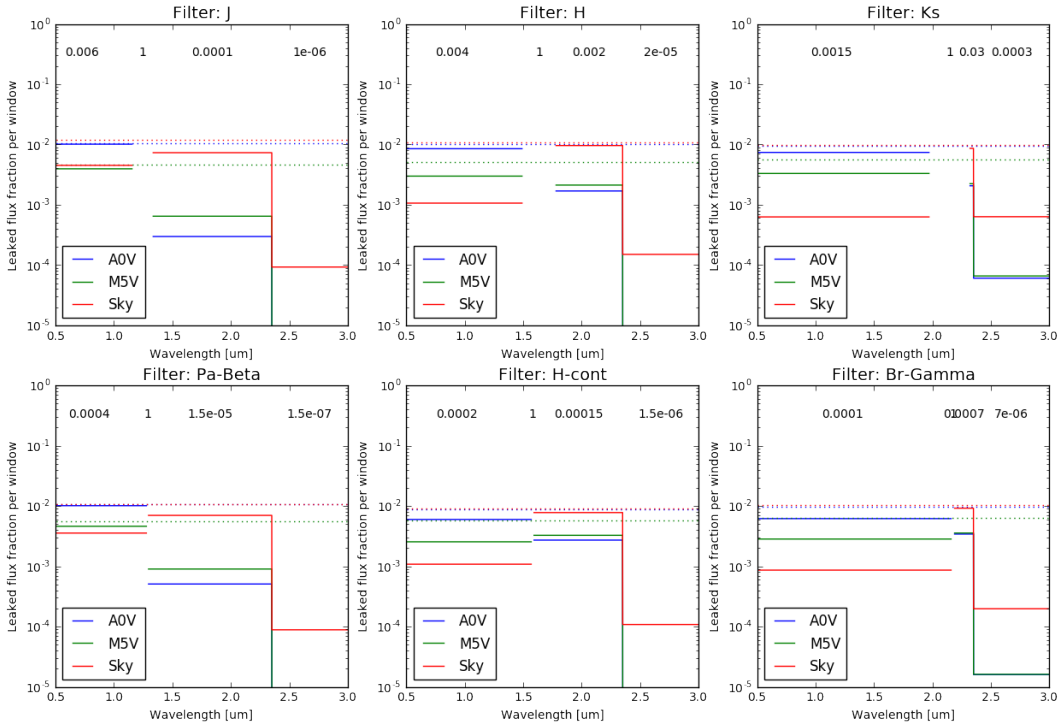


Figure 9: Same as Figure 7 except including a thermal-red filter with a blocking coefficient of 10^{-2} less than the near-red wing. Blocking in the wavelength range $\lambda > 2.35 \mu\text{m}$ is therefore a combination of the thermal-red filter and the red-wing of the actual filter.

8 Summary

This technical note can be summarised by the following points:

- The transmission coefficient of the blue wing is dominated by the need to have accurate photometry of blue objects (i.e young stellar populations). We found that a transmission coefficient of between 1.5×10^{-3} (Ks) and 6×10^{-3} (J) will be needed for broadband filters and between 1×10^{-4} ($\text{Br}\gamma$) and 4×10^{-4} ($\text{Pa}\beta$) for narrow band filters.
- The transmission coefficient for the red wing is dominated by the need to remove the sky background. The inclusion of a thermal-red filter with a transmission coefficient of 10^{-2} for $\lambda > 2.35 \mu\text{m}$ would lead to a relaxation of the blocking coefficient of the red-wing by a factor of 2.5 on average. If the thermal-red filter is included, red wing transmission coefficients of between 1×10^{-4} (J) and 3×10^{-2} (Ks) are needed for the broad band filters and between 1.5×10^{-5} ($\text{Pa}\beta$) and 7×10^{-4} ($\text{Br}\gamma$) for the narrow band filters.
- The thermal-red filter could be included on a different optical element, i.e. the entrance window, so that all slots in both filter wheels remain available.

In general broad band filters require a blocking coefficient of at least 10^{-3} , while narrow band filters will require a blocking coefficient on the order of 10^{-4} . The notable exceptions are the J and

Table 5: Summary table for Figures 6, 7, 8 and 9. The optimised transmission coefficients for the red and blue wings for each filter are given in the upper half of each table. The total residual leaked flux fraction due to a combination of the blue and red wings (excluding and including a 10^{-2} thermal-red filter) for the two stellar spectra (A0V and M5V) and the sky background emission spectrum are given in the lower half of each table. The final row is the factor by which the red wing transmission coefficient of each filter can be reduced if a thermal-red filter is included.

No Thermal Red filter						
Filter	J	H	Ks	Pa β	H-cont	Br γ
Optimized wing transmission coefficients						
Blue Wing	0.0060	0.0040	0.0020	0.0004	0.0003	0.0001
Red Wing	4.0E-5	0.0008	0.0040	7.0E-6	7.0E-5	0.0003
Residual flux leak						
A0V	0.0102	0.0093	0.0109	0.0104	0.0104	0.0080
M5V	0.0042	0.0040	0.0056	0.0051	0.0055	0.0047
Sky	0.0111	0.0109	0.0104	0.0109	0.0103	0.0112
With Thermal Red filter						
Filter	J	H	Ks	Pa β	H-cont	Br γ
Optimized wing transmission coefficients						
Blue Wing	0.0060	0.0040	0.0015	0.0004	0.0002	0.0001
Red Wing	0.0001	0.0020	0.0300	1.5e-5	0.0002	0.0007
Residual flux leak						
A0V	0.0104	0.0102	0.0095	0.0106	0.0087	0.0096
M5V	0.0046	0.0051	0.0056	0.0055	0.0058	0.0064
Sky	0.0119	0.0108	0.0099	0.0106	0.0090	0.0103
Average red wing relaxation factor with thermal red filter						
Improvement	2.5x	2.5x	7.5x	2.14x	2.14x	2.8x

Pa β filters, which will require a further factor of 10 suppression on the red wing. **A possible solution to this would be to split the IJ and HK spectroscopic order sorting filters between the two filter wheels and use these for extra wing blocking.** The IJ order sorting filter could sit on the opposite filter wheel to the shorter wavelength filters (I, J, Pa β , etc). This would provide an extra level of 10^3 red-wing suppression, thereby relaxing the requirements for the wings of these other filters. A similar case could be made for the HK order sorting filter and the set of longer wavelength filters. The results of calculations relating to the use of the order sorting filters will be included in an update to this technical note.

One last point to note is that the quantum efficiency of the HAWAII-4RG detector chips has been taken into account in this study. The natural thermal-red blocking capabilities of the chips are therefore already included in the calculations.

9 Ideas for future experiments

This technical note is to be seen as a short investigation into how to most efficiently and cost effectively manufacture and position the filters in the two MICADO filter wheels, such that the flux leakage requirements are met. The two main ideas which warrant future consideration include: 1. studying the impact of **using the IJ and HK spectroscopy order sorting filters as additional blocking filters**, and 2. studying the **extent to which leaked thermal-red flux affects the accuracy of photometry, given that the additional flux is primarily from the sky spectrum and will be uniformly distributed** over the field of view.

End of technical note

6

Future Work

In this chapter I present the main areas in which I intend to work during the coming years. These include extending the functionality of SimCADO, running a more rigorous validation campaign with newly acquired HAWK-I data, and applying SimCADO to various science cases.

During the last three years I have worked relatively autonomously on SimCADO. Github statistics show that I contributed 80% of the SimCADO code base and 100% of the documentation. The three papers presented here and the HAWK-I proposal were written solely by me, with occasional suggestions by the co-authors. The verification of SimCADO and predictions for MICADO were also 100% my own work. I would therefore like to pre-emptively warn the reader of my frequently use of the first-person singular pronoun in this chapter. Far from being a show of arrogance, it reflects the level of solitude that I expect will continue during the further development of SimCADO.

6.1 SimCADO Road Map

This thesis shows that the development of SimCADO has reached the first level of maturity. The software is capable of modelling the major effects of an optical train accurately. That said there are still many optical effects and two observing modes which have not been included in SimCADO, as well as functionality to make SimCADO more user friendly. The following sections briefly list the aspects which we plan to implement of the coming year. An additional goal of mine is to adapt SimCADO to model the other two first light instruments for the ELT. These topics are addressed in the following subsections. Table 6.1 lists the functionality which I would like to include in the package, as well as the priority of each effect. The highest priorities are currently the implementation of the spectroscopic mode and reviewing the mirror thermal emission and detector read-out noise models. Re-implementing the easy detector window functionality is also a high priority, given the need for user friendliness.

Table 6.1. Road map for the further development of SimCADO. PDR in this table refers to the MICADO preliminary design review, scheduled for October/November 2018.

Functionality	Priority	Timeline
SimCADO core code structure		
Code Interface document	!!!	July 2018
Documented code structure	!!	July 2018
Code structure reorganisation	!!	Oct 2018
Unification of the variable names	!	Post PDR
Astropy units	!	Post PDR
Saving and loading of optical trains	!!!	July 2018
Pre-packages instrument files	!!!	July 2018
Graphical user interface (GUI)	!	Post PDR
Command line interface (CLI)	!!	Post PDR
Additional observing modes		
Spectroscopy	!!!!	June 2018
Astrometry	!	Post PDR
High time resolution	!	Post PDR
Source objects		
2D descriptions of extended source objects	!!	Oct 2018
Overhaul of memory usage for images $>1024^2$ pixels	!!	Oct 2018
Extension of spectra to MIR range	!!!	SimMETIS
Upgrade of the spectral module to pysynphot	!!	Post PDR
Pre-telescope effects		
Cosmics	!	Post PDR
Airmass, Seeing, PWV	!!!	July 2018
Zodiacal light	!	Post PDR
Background objects with Astroquery	!	Post PDR
Instrument and telescope optical train		
Variable PSFs over the field of view	!!!!	June 2018
Review mirror thermal emission	!!!!	April 2018
Flat-fielding	!!!	July 2018
Detector model		
Better model of NDRO modes	!!!!	June 2018
Easy definition of detector windows	!!!!	April 2018
Use of more than one noise frame	!!!!	April 2018
Distortion	!!	Post PDR
Persistence	!	Post PDR
Review sub pixel treatment	!!!!	April 2018
More accurate hot/dead pixel model	!	Post PDR

6.1.1 Future functionality for SimCADO

Design and Implementation

SimCADO was developed relatively rapidly in order to allow the MICADO science team ample time to begin simulations before the preliminary design review. And as the saying goes: “Good coding practice involves 50% Design, 50% Coding, 50% Testing, 50% Documentation”. In the coming year we would like to rectify this practice. To do this I would like to redefine and extend the software interface document as well as attach stricter constraints on the data which each class accepts, holds and returns.

As far as improvements to the code base go, I would like to unify the use of the `astropy.units` package to manage the flux through the system. This was partially omitted from the current design because we decided to make SimCADO as general as possible. For the `OpticalTrain` class I want to implement the functionality to save current `OpticalTrain` objects to disk and load these saved objects back in to SimCADO. This functionality will save a lot of time as the slowest aspect of SimCADO is currently the function which combines all effects from the individual optical elements into a single array of global effects. Doing this will also open the door to providing “instrument packages”. I envisage a package to contain a saved version of a single `OpticalTrain` that represents a single observing mode for a certain telescope plus instrument configuration. An example of such a package would be one which hold all the data relating to the ELT/MICADO/Wide-field imaging mode. This will allow SimCADO to easily exchange packages that simulate other systems, e.g. VLT/HAWKI or JWST/NIRCam, and thus provide the user the opportunity to quickly generate direct comparisons of the same astronomical sources with multiple instruments.

SimCADO is currently available as a Python package, however the astronomical community has not (yet) completely converted to using Python. Hence to allow non (and anti) Pythonistas to use SimCADO I intend to create a command line interface (CLI) for SimCADO. Ideally this could be extended to creating a graphical user interface (GUI) however this has lower priority.

Source objects

The current version of SimCADO breaks each Source object into numerous point sources for each MICADO pixel. As the majority of the sky is essentially empty, the description allows SimCADO to save memory and processing power by neglecting all pixels that would contain no astronomical source. This can speed up simulations by factors of well over $100\times$ for clusters of point sources. However this technique offers little in the way of simulation speed increases for (extended) sources which are created from images. In the coming months I want to implement a 2D Source class that is able to better manage the arrays associated with extended sources. How exactly this will be done is still up for debate.

With a view towards implementing imagers for other wavelength ranges in SimCADO (see the next section) it will be necessary to extend the spectral range of the included spectral library red-wards of the $2.5\text{ }\mu\text{m}$ limit in the [Pickles \(1998\)](#) catalogue. Here I see a synergy with another one of my plans: to upgrade the spectral module to make use of the Python package `pysynphot` ([STScI Development Team 2013](#)). This package handles the description of emission and transmission curves, and stellar spectra in a more in-depth manner. It would also allow us to integrate the various spectral libraries, for both stars and galaxies, which `pysynphot` can support.

Atmosphere model

Only the emission and transmission curves are currently addressed by SimCADO. Given that my HAWK-I observations to quantify the extent to which airmass and seeing should be included in SimCADO were executed over Christmas 2017 (see Section [6.2](#)), we should implement the functionality to simulate these effects. Above the atmosphere there are also the interstellar effects that may be useful to have: zodiacal light, interstellar extinction, background sources. The background stars can be loaded using the Python package `astroquery` ([Ginsburg et al. 2017](#)). However these interstellar effects are currently not a high priority.

Instrument optical design

A major aspect which still needs to be included, which is essential for modelling any AO assisted instrument, is the variability in the PSF over the field of view. SCAO PSFs should be elongated along the radial axis, and the elongation should increase with distance from the position of the guide star. MCAO PSFs should remain axially stable, but the Strehl ratio of the PSF should reduce with distance from the guide stars. Thankfully both the MICADO SCAO and MAORY MCAO simulation teams have produced FITS cubes with images of the PSF for various positions in the field of view. How these cubes should be used by SimCADO will require a bit more thinking. One way of implementing the variable PSF would be to define a radius of influence for each PSF. Using a `masked_array` from `numpy` only the pixels inside the radius of influence would be convolved with the regional PSF. Depending on the grid spacing of the off-axis PSFs delivered by the two AO teams, it may be noticeable from the change in PSF shape where one region of influence ends and the next begins. This will be the best compromise between computation time and accuracy of the field varying PSF, however I will need to look more closely into just how much of a hit the computation time will take when this functionality is included.

Detector model

The detector is one of the most crucial parts of the optical train to model accurately. Read noise does not scale in the same way as shot noise and so it is imperative to have an accurate representation of the read noise in each image. Furthermore, because of the 4 mas plate scale, the sky background pixel flux in a minimum length exposure (2.6 s) will be on the same order of magnitude as the read noise ($\sim 10 \text{ ph s}^{-1} \text{ pixel}^{-1}$). By default SimCADO uses the “super-fast” read-out mode, which extrapolates the total read noise from a single simulated read noise frame ([Rauscher 2015](#)). While this gives an accurate average value for the total read-out noise, I would like to do a more in-depth investigation as to how similar the noise properties are compared with a true multi-DIT observation. In the coming year I would also like to implement a series of non destructive detective sampling techniques, like up-the-ramp and fowler sampling, to mimic the actions of the

HAWAII-4RG read-out electronics. With the HxRG noise generator software from [Rauscher \(2015\)](#), this should be straight forward.

An additional feature which I would like to implement is detector persistence. This will be important given the saturation limit of $K_s \sim 15^m$. MICADO will most definitely be pointed towards bright targets as there is lots of science to be done in the nearby universe. Although saturating sources will not permanently damage the detectors, the brighter an object is, the longer a ghost image will persist on the detector. How this effect should be built into the SimCADO will require a bit of thought. It is not critical functionality for science case studies however it will be important for building the data reduction pipeline.

6.1.2 Additional observing modes

In the MICADO baseline there are two additional observing modes – the spectroscopic and the astrometric modes. The spectroscopic mode is currently under development. The plan is to add the functionality which maps the spectral order traces to the detector array to the `OpticalTrain` class. It should be the spectroscopic analogue to the `image_in_range()` function. This needs to be implemented within the coming months for the science team to be able to make use of it before the MICADO preliminary design review. It therefore has the highest priority on the whole wish-list of new functionality.

Whether or not the astrometric mode is implemented in SimCADO is still up for debate. The MICADO astrometric working group (AWG) must first decide on a list of critical instrumental effects before these can be added to SimCADO. That said, the majority of the sources of jitter involved in the astrometric error budget are on scales smaller than 1 mas. Although SimCADO was not built with such small movements in mind, it would still be possible to implement a astrometric add-on to SimCADO. The easiest place to apply such small variations would be in the `Source` object before it is “observed”. Although this is not 100% realistic, it is the net effect of the variations in the position of a point source in the detector images which needs to be extractable. Whether or not the order in which the positional variations is important, and where in the `OpticalTrain` they are applied, is a topic which needs to be investigated in conjunction with the AWG. We will continue to discuss

this, however there is currently no time frame for the implementation of this special astrometric mode.

6.1.3 General ELT first-light simulation package

There has been interest from both the METIS consortium and certain people at ESO to use SimCADO for purposes outside the scope of the MICADO consortia. We have been contacted by the METIS team about possibly implementing a version of METIS in SimCADO. I have also been invited to ESO to run a SimCADO workshop with the ESO fellows. Ideally I would like to continue developing SimCADO with a view towards creating a full ELT first-light simulator, with observing modes available for each of the first light instruments. I am of the opinion that the next generation of exposure time calculators should indeed be visual ones, where the user can see what an observation might look like, and more to the point, just how the PSF might affect the observation, before they apply for telescope time. SimCADO would be the perfect tool for this. Slowly but surely SimCADO is making a name for itself inside the ELT community and I'm very excited to see where this goes in the future!

6.2 Detailed verification of various atmospheric components with HAWKI

As stated in Chapter 3 we verified the accuracy of SimCADO by using archive data from HAWK-I on UT4 at the VLT. During the verification run the static components of SimCADO worked as they should and the flux throughput matched the numbers given in [Kissler-Patig et al. \(2008\)](#) and in the HAWK-I user manual. However the final stellar flux in the images simulated by SimCADO was on average about 30% higher than the flux in the real HAWK-I images. While this is somewhat concerning, it was not seen as a show stopper, given that [Moreels et al. \(2008\)](#) states that the sky background can vary by up to 70% over the course of a night. The increase in background is in part due to a high water content in the atmosphere, which in turn can lead to a higher atmospheric extinction. Additional aspects such as the change in Strehl ratio due to variable Seeing were also not taken into account when generating the atmosphere for the observations in SimCADO. As the telescope and

instrument were behaving as expected, we added a minor atmospheric extinction term to the star fluxes in the SimCADO images.

In order to test SimCADO against a uniform and self-consistent set of test data covering various airmasses and seeing conditions, I applied for observing time with HAWK-I during the ESO observing period 100. The proposal was ranked as an A level proposal and the full 5 hours of observing time were granted. The proposal is included in Appendix A. The aim of the proposal was to determine the extent of how the major atmospheric effects (Seeing, Airmass, PWV) contribute to the level of atmospheric emission and transmission. The idea was to observe two globular clusters, M30 and NGC 1851, at a variety of different Seeing conditions ($<0.8''$, $1.0''$, $1.2''$, $1.5''$, and $\sim 2''$) and Airmasses (<1.05 , 1.2 , 1.5 and >2.0). As stated in the proposal: “The need for complete coverage of the airmass-seeing-(exposure time) space is three fold. Firstly, various seeing conditions need to be sampled to decouple the atmospheric extinction/emission due to airmass from the decrease in PSF peak flux due to the seeing. Secondly, various airmasses need to be sampled in order to decouple the telescope emission from the atmospheric emission, and lastly, various exposure times are required to decouple the detector noise components from the background”. Three of the five observing blocks were completed during the last observing semester (Oct 2017 - Feb 2018). Over the coming months I plan to undertake the comparison of these images with simulated images from SimCADO.

I see the steps involved in this next verification run being similar to the initial verification run, only on a larger scale. This project may progress in the following manner:

1. Extract the stars in each image above the 5σ threshold. Compile a catalogue and compare the raw photometry to the stars in the [Cohen et al. \(2015\)](#) catalogue.
2. Map the photometric slopes for the stars in each image against the values of Airmass, Seeing, and PWV. Determine the best fit for each exposure time and each filter.
3. Create a similar catalogue with the HAWK-I ETC (which is based on SkyCalc) for each of the corresponding Airmass, Seeing, and PWV values.

4. Repeat the same set of observations with SimCADO for the corresponding sky conditions.
5. Compare the three sets of photometric catalogues (HAWK-I, ETC, SimCADO) for each unique sky condition.

Obviously the ideal case would be that all three catalogues match from the beginning. This inevitably will not be the case. However given the large parameter space that our observations have covered, I expect the troubleshooting to be minimal.

In order for this second verification run to be successful SimCADO will require additional functionality. This will include adding code to the SimCADO atmospheric model to take into account the changes to the PSF due to the Seeing, as well as adding code to alter the atmospheric emission and transmission curves based on Airmass and PWV. Additionally it require the use of a more accurate photometry package, like Photutils ([Bradley et al. 2017](#)). Aspects of the optical train which may still be missing, e.g. the flat field corrections, will also need to be added to SimCADO.

6.3 Science feasibility studies with SimCADO

Now that the code base for the first version of SimCADO is mostly complete, it can be used to investigate the feasibility of different science cases. In chapter 4 I showed the work that I have started regarding determining the limits for future studies of the IMF using MICADO. In this section I outline three other science cases related to star formation. Given that SimCADO can be used to simulate many different scenarios for a science case, the following topics revolve around determining the limits of what will be observable by MICADO.

6.3.1 The shape of the IMF

In chapter 4 I discussed the limiting stellar mass that MICADO will be able to observe for various distances and densities. These limits are useful for studies of

the sub-solar mass region of the IMF. Determining the true shape of the IMF as well as whether the shape remains constant regardless of environment is key for many fields of astrophysics. SimCADO will not be able to probe the physics behind the shape of the IMF, but it will allow us to determine which observations will be necessary to finally answer the questions: Kroupa or Chabrier? I.e. does the IMF follow a broken power law distribution or a log-normal distribution? By answering this question theoreticians will be able to concentrate their work on describing the physical processes that lead to the true distribution.

The key to determining which distribution the IMF actually follows lies in observations of the M-dwarf mass regime, i.e. $\sim 0.1 < M < 0.5 M_{\odot}$. Both the power law and log-normal distributions look very similar in this regime, making it very difficult to determine which functional form is the “true” IMF. Observations of high density massive young clusters, similar to what was shown in chapter 4, may hold the key to this measurement. Only by observing very large numbers of M-dwarfs (on the order of 1000s per mass bin) will it be possible to beat down the statistical errors enough to reveal the underlying shape of the mass function. Young massive clusters like Trumpler 14 and Westerlund 1 offer environments where this may be possible. YMCs in general have masses in excess of $10^4 M_{\odot}$. By assuming that 75% of the mass is tied up in M-dwarfs and the average M-dwarf mass is $\sim 0.2 M_{\odot}$, there should be on the order of 30×10^3 M-dwarfs in these clusters. If we could extract 90% of the M-dwarfs from images of these YMCs, then we may have large enough statistics to finally show either a broken power law or a log-normal mass function.

As a follow up to the study presented in chapter 4 I intend to do exactly this: create two (or more) clusters, each with the stars’ masses sampled from the competing mass functions, and then extract as many stars as possible. The goal will be to state whether a sufficient number of stars can be extracted in each mass-bin to reliably determine which mass function was used for which cluster.

6.3.2 Variation in the IMF of the Galactic centre (and elsewhere)

Continuing with the theme of star formation and the initial mass function, stars with ages below 10 Myr have been found within the Milky Way’s central parsec (Lu

et al. 2009). Given the extreme conditions, e.g. high stellar density, high interstellar radiation field, and a strong gravitational potential, it is uncertain how these stars came to be in this region. Did they form in the centre or have they migrated very quickly inwards? The presence of the Arches and Quintuplet clusters of young stars shows that at Galactic radii of ~ 50 pc star formation is possible. Resolving the stellar population of the inner parsec down to the M-dwarf regime will not only help us answer the question of where these young inner-parsec stars came from, but also give us a glimpse of how, if at all, star formation can occur in such extreme environments. By resolving a large fraction of the sub-solar mass population we will be able to construct the initial mass function for this region, which in turn will help to confirm or reject the notion of IMF universality.

Current observations are heavily limited by both confusion and extinction. With MICADO's detection limits of around $K=28^m$, it will be possible to resolve the stars down to the hydrogen burning limit anywhere in the Milky Way, depending on the level of extinction. Objects with several tens of Jupiter masses will be detectable with in a few kiloparsecs of the Sun. This level of sensitivity will allow us to investigate the universality of the IMF. Using SimCADO I intend to generate images of several different young stellar populations at the distance of the Galactic centre, each with a different characteristic mass and spread in its initial mass function. By using a PSF extraction and subtraction technique, e.g. the one from chapter 4, I plan to reconstruct the IMF for each of the populations. Such a study should allow us to determine by how much the IMF in the Galactic centre must differ from the Salpeter value for variations to be incontrovertibly observable. This will also help to produce a list of criteria that real observations need to fulfil to prove that the shape of the IMF is, or is not, universally constant.

6.3.3 The spatial structure of star formation in the early universe

It is estimated that the first galaxies at redshifts higher than $z > 5$ had sizes around 1 kpc (Bouwens et al. 2004). At these redshifts this corresponds to an angular size of around $\sim 0.2''$. With HST these galaxies are no more than blobs of a few pixels. MICADO should be able to resolve these galaxies down to the ~ 50 pc level. High resolution cosmological simulations show various modes of star formation (Oser et al. 2010; Genel et al. 2012), from Jeans fragmentation of massive primordial

clouds to waves of star formation due to galactic winds. With MICADO it should be possible to observe the structure of the massive star formation regions in these first galaxies. We will therefore be able to determine when, where, and which star formation mechanism is the dominant mechanism.

Large cosmological simulations like EAGLE ([Schaye et al. 2015](#)), NutFB ([Powell et al. 2011](#)) and Illustris ([Vogelsberger et al. 2014](#)) have produced catalogues of how these galaxies may look. I have started exploring a collaboration with the NutFB team, whereby they will supply the 3D mass distributions and calculated star formation rates for a sub-sample of these first galaxies with redshifts from 3 to 10. I would then project these galaxies onto the sky and supply suitably redshifted spectra for the star forming and non star forming regions. SimCADO will allow me to “observe” these galaxies in a manner similar to what MICADO and the ELT will be able to do. By comparing the modes of star formation between the various cosmological simulations, I will be able to make a catalogue of possible observations. From this catalogue it should be reasonably straight forward to determine which star formation modes have unique observational structures, and which ones show redundant characteristics. Once MICADO comes on-line it will then be a simple matter of comparing the non-redundant characteristics in real observations against those in the catalogue. The most interesting result will be if none of the simulated galaxies in the catalogue match what is in the observations.

Summary and Conclusion

7.1 Summary

The main goal of this thesis is to present SimCADO, the instrument data simulator for MICADO and the ELT, starting with its conception, progressing through the development and verification process, and ending with a scientific and an instrumental use case. These major points have been presented in the form of four documents: one proceedings paper for SPIE, two scientific manuscripts which will be submitted to A&A, and one MICADO consortium internal technical note. In this section I recap the main aspects of each of these papers and list their major results.

7.1.1 The design of SimCADO

The first SPIE proceedings paper in chapter 2 presents the concept for SimCADO and describes the structure of the software. The main points of the paper are given in the following paragraphs.

The initial reason for developing SimCADO was to enable the development of the data reduction pipeline to proceed in parallel with the development of the instrument, however many other use cases for the software have been found. Currently SimCADO's main goal is to provide a common platform, with which ideas relating to the development of MICADO can be tested and exchanged between different groups inside and outside the MICADO consortium. SimCADO's intended audience within the MICADO consortium includes: the science team, the data reduction pipeline team, the preparation software team, the data archive software team, and various work packages inside the instrument design team. Externally, SimCADO may be useful to both the MAORY and METIS consortia. I also hope that the astronomy community finds SimCADO useful both for determining the feasibility of ideas and projects, as well as for preparing the observations.

The data model for SimCADO includes 4 major classes (shown in figure 2.1):

Source contains both spatial and spectral descriptions of one or more sources.

OpticalTrain contains numerical descriptions of the effects that each optical element has on the incoming wavefront, including: spectral effects like variable transmission and emission from the atmosphere, the mirrors of the telescope, relay optics, and MICADO; residual spatial distortions from e.g. the AO PSFs, the ADC, and the telescope rotation.

Detector (and the sub-class Chip) describe the conversion from photons to electrons, and produce the final FITS files with the raw images from each of the chips in the detector array. Electronic effects are also modelled by this class, e.g. read noise, hot/dead pixels, read-out mode.

UserCommands contain a list of all the valid keyword-value variable pairs which control how the OpticalTrain and Detector should be modelled, as well as how a simulated observation should be conducted. See figure 2.3

SimCADO simulates images by passing an OpticalTrain and a Detector to a Source object and calling the function `.apply_optical_train()`. This causes the spatial and spectral effects included in the OpticalTrain to be applied to the description of the Source. The resulting spectral cube is collapsed and a normalised image is passed to the Detector object. The Detector creates FITS files of the simulated observations by calling the function `.read_out()`. SimCADO also offers a one-step simulations function `.run()` which combines all these tasks and takes, as its only mandatory argument, a Source object.

7.1.2 Verifying SimCADO and predicting MICADO sensitivity levels

The second paper, included in chapter 3, presents the development and verification of SimCADO. It also includes the first predictions of the point source sensitivity of MICADO. The main points of the chapter are summarised in following paragraphs.

The effects modelled by the current version of SimCADO when simulating MICADO images include: from the Atmosphere: transmission, background emission, dispersion; from the ELT: residual AO PSF, main mirror and relay optics transmission and grey-body emission, wind jitter, pupil rotation; for MICADO: mirror and cryostat window transmissions, non-common path aberrations, derotator residuals, ADC residuals, wide-field and zoom observing modes; and from the Detector array: read noise, hot/dead pixels, destructive and non-destructive read out modes, non-linearity, saturation, detector windowing

The accuracy of the simulated images was verified by comparing these images against real images from the ESO archive of the globular clusters M 4 and NGC 4147, observed with the HAWK-I instrument. The flux of point sources in the simulated images was compared to the flux of the corresponding sources in the archive images. Over 75% of the flux measurements for A-grade (2MASS) point sources in both images differed by less than 0.3^m . See figure 3.6. The 1-hour limiting sensitivity limits given by SimCADO were 0.2^m brighter in the J and H filters, and 0.4^m brighter in the Ks filter than those given by Kissler-Patig et al. (2008). See table 3.2

Using the current design I used SimCADO to predict the point source sensitivity limits for MICADO. These are listed in table 3.4 and also presented graphically in figure 3.8. The 5 hour detection limits in Vega magnitudes are $J=28.7^m$, $H=27.9^m$, and $Ks=27.3^m$. For $Br\gamma$ the limit is $Br\gamma = 26.0^m$.

In a similar fashion I used SimCADO to estimate the limiting magnitudes for saturation of a point source within the minimum possible exposure time of 2.6 s. For the 4 mas wide-field imaging mode these are $J=15.9^m$, $H=15.6^m$ and $Ks=14.8^m$. By using the $Br\gamma$ narrow band filter and the 1.5 mas zoom mode, the saturation limit can be reduced to $Br\gamma = 9.9^m$ - see table 3.5. Applying the detection limits to main sequence stars, figure 3.9 and figure 3.11 show that MICADO will be able to detect almost all M-dwarf stars in the Magellanic clouds, and all stars more massive than A0V at a distance of 4 Mpc, i.e. in Centaurus A. Stars with absolute magnitude brighter than $M_J \leq -3$ (B0V) will be visible in the Virgo galaxy cluster at a distance of ~ 20 Mpc.

7.1.3 Observational limits of future IMF studies with SimCADO

Chapters 4 and 5 show two use cases for the SimCADO software. Chapter 4 includes the manuscript for a short paper detailing the lowest reliably observable mass in young star clusters at various distances for a one hour MICADO observation. These limits have implications for future observations of the initial mass function inside and outside the Milky Way. The main points presented in the manuscript are summarized here.

I used SimCADO to simulate images of 42 dense stellar regions with densities between 10^2 and $\sim 10^5$ stars arcsec $^{-2}$ and for distances between 8 kpc and 5 Mpc. This parameter space covers the range where MICADO offers the greatest advantage over current and future telescopes (e.g. VLT, JWST) and is shown graphically in figure 4.2.

After extracting stars from the crowded images I showed that clusters with stellar densities of $\sim 10^3$ stars arcsec $^{-2}$ will be easily resolved with MICADO. With good knowledge of the PSF and a subtraction algorithm optimised for a segmented mirror PSF, extracting $\sim 5 \cdot 10^3$ stars arcsec $^{-2}$ may be possible. The equivalent crowding limits for JWST and HST are around 160 and 20 stars arcsec $^{-2}$ respectively. MICADO's resilience to crowding will allow us to study the true IMF of cluster cores down to $0.1 M_{\odot}$ in the LMC, $\sim 0.5 M_{\odot}$ in the Milky Way's nearby satellite dwarf galaxies, and $\sim 1 M_{\odot}$ at a distance equivalent to M31 (~ 800 kpc).

The brown dwarf population ($M < 0.1 M_{\odot}$) will be accessible in the cores of the densest Milky Way clusters (e.g. Westerlund 1, Trumpler 14, etc), as long as a solution is found to remove the many very bright ($K_S > 15^m$) stars in these clusters. The diffraction spikes from the segmented mirror contain many discrete artefacts and can extend well over an arcsecond depending on a stars brightness. This in turn is responsible for many false detections of faint stars. Thus a key caveat of any such observations with the ELT is that accurate knowledge of the PSF is essential for robust science.

7.1.4 Determining the optimal filter coating design for MICADO

Chapter 4 shows a use case for SimCADO as part of the MICADO filter wheel design efforts, in the form of a technical note to the MICADO consortium. Manufacturing large science grade filters with the appropriate coatings is expensive and MICADO will contain upwards of 30 filters. Therefore it is necessary to find the optimal design for each filter which achieves the scientific accuracy requirements, but also does not cost an arm and a leg. The main points addressed in this study are summarised thusly.

I used SimCADO to simulate the flux leakage through the filter wings (i.e. regions outside a filters bandpass) for 3 broad and 3 narrow band filters: J, H, Ks, Pa β , H-cont, and Br γ . The baseline requirement on MICADO is $\pm 0.01^m$ photometric accuracy, meaning that the flux leaking through the wings must remain under 1% of the total transmitted flux. The requirement for red wing blocking for each filter is dominated by the sky background. The blue wing requirement is dominated by blue astronomical objects, e.g. massive stars.

In general terms, the broad- and narrow-band filters need wing blocking coefficients on the order of 10^{-3} and 10^{-4} respectively, with the notable exceptions of the J band and Pa β red-wings needing blocking coefficients of 4×10^{-5} and 7×10^{-6} respectively. Table 5.7 lists the exact coefficients. On average all red-wing blocking coefficients can be relaxed by a factor of 2.5 if another optical element (pupil wheel) is given a coating which provides an additional blocking coefficient of 10^{-2} for the thermal-red ($\lambda > 2.35\mu m$) wavelength range.

Another possibility to reduce flux leakage through either the red or blue wings would be to place the IJ and HK spectroscopic order sorting filters in the pupil wheel. Although I have not yet done the caluculations, by removing all thermal emission red-wards of $1.45\mu m$, I believe that the red wing blocking coefficients of the J and Pa β filters can be brought back in line with the average necessary blocking coefficients, i.e. $O(10^{-3})$.

7.1.5 Future work with SimCADO

The work towards building MICADO will continue over the next 7 years. In that time both the instrument and the software will undergo changes. In chapter 6 I discussed the work I wish to complete over the the coming year or two. This includes adding functionality to SimCADO, verifying a new atmospheric model against newly acquired HAWK-I data, and applying SimCADO to several science cases related to star formation. The scope of the future work regarding SimCADO is summarised in this section.

The short term SimCADO roadmap includes: adding a spectroscopy mode, functionality for using the field varying PSF cubes provided by the SCAO and MCAO teams, self-contained exchangeable instrument packages, verifying the accuracy of the sub-pixel points source movement, more user friendly access to detector windows, extended atmospheric effects like seeing and zenith distance.

The medium to long term roadmap for SimCADO includes: Implementing a simulator for METIS, adding in the effects of detector persistence and optical distortion, allowing the user to add natural background sources (galaxies, stars etc) by connecting SimCADO to Simbad, better modelling of cosmic rays and hot/dead pixels, tools for a GUI and CLI, and an overhaul of the spectral module to include functionality from the astropy.units and pysynphot packages. Use the data from my successful HAWK-I technical time proposal to verify the accuracy of the new atmosphere model.

The science cases that I wish to investigate with SimCADO primarily revolve around the topic of star formation inside and outside the milky way, with an emphasis on the initial mass function. My interest lies mainly in two of the widely debated aspects of the IMF, namely: 1) which functional form is the true shape of the IMF, i.e. a log-normal or a broken power law distribution?, and what types of observations will we need to prove either Kroupa or Chabrier right (or wrong)?; 2) is the notion of universality indeed valid, i.e. is the IMF the same in all environments and at cosmic times? and, will the ELT be able to provide the observations needed to definitively confirm or deny IMF universality? Breaking from the topic of the IMF, I would also like to generate imagery for some of the galaxies from the NutFB suite of cosmological simulations in order to study the structure of the star forming regions in high-z galaxies.

7.2 Concluding remarks

It is my hope that the chapters of this thesis show that the SimCADO project has been, and will continue to be a worthwhile endeavour. Over the next seven years until MICADO goes on sky, SimCADO will be able to provide both the MICADO consortium and the astronomy community with the means to simulate future observations of the infrared universe. Such simulations have the potential to benefit the astronomy community in numerous ways. Firstly they will enable the feasibility of different science topics to be investigated before observation time on the ELT is granted. This will hopefully reduce the pressure on the facility. Additionally such simulations will allow the community to develop new tools specifically designed to work with data from the ELT and its unique PSF well before the telescope becomes operational.

My work in this thesis will hopefully serve as a jumping off point for future work, both by myself and by others. The conception, implementation, and verification of SimCADO are presented here, along with several examples of how the software can be used to simulate, and make predictions from, hypothetical observations. The software is ready to be used to investigate the many science cases for which the ELT and MICADO will be perfectly suited. I have no doubt though that the universe which SimCADO will simulate and the unknown universe which MICADO will eventually observe will (through no fault of SimCADO) be as different as day is to night. I, for one, very much look forward to seeing just how different the real near infrared universe turns out to be.

References

- J. Ascenso, J. Alves, S. Vicente, and M. T. V. T. Lago. NTT and VLT diffraction limited imaging of Trumpler 14: revealing a massive core-halo cluster. *Astronomy and Astrophysics*, 476:199–215, December 2007. doi: 10.1051/0004-6361:20077210.
- J. Ascenso, J. Alves, and M. T. V. T. Lago. No evidence of mass segregation in massive young clusters. *Astronomy and Astrophysics*, 495:147–155, February 2009. doi: 10.1051/0004-6361/200809886.
- N. Bastian, K. R. Covey, and M. R. Meyer. A Universal Stellar Initial Mass Function? A Critical Look at Variations. *Annual Review of Astron and Astrophys*, 48:339–389, September 2010. doi: 10.1146/annurev-astro-082708-101642.
- I. A. Bonnell, C. J. Clarke, and M. R. Bate. The Jeans mass and the origin of the knee in the IMF. *Monthly Notices of the RAS*, 368:1296–1300, May 2006. doi: 10.1111/j.1365-2966.2006.10214.x.
- R. J. Bouwens, G. D. Illingworth, J. P. Blakeslee, T. J. Broadhurst, and M. Franx. Galaxy Size Evolution at High Redshift and Surface Brightness Selection Effects: Constraints from the Hubble Ultra Deep Field. *Astrophysical Journal, Letters*, 611:L1–L4, August 2004. doi: 10.1086/423786.
- Larry Bradley, Brigitta Sipocz, Thomas Robitaille, Zé Vinícius, Erik Tollerud, Christoph Deil, Kyle Barbary, Hans Moritz Günther, Mihai Cara, Ivo Busko, Michael Droettboom, Azalee Bostroem, Erik Bray, Lars Andersen Bratholm, T. E. Pickering, Matt Craig, Geert Barentsen, Sergio Pascual, Simon Conseil, adonath, Johnny Greco, Wolfgang Kerzendorf, Miguel de Val-Borro, StuartLittlefair, Sara Ogaz, P. L. Lim, Leonardo Ferreira, Francesco D’Eugenio,

and Benjamin Alan Weaver. astropy/photutils: v0.4, October 2017. URL <https://doi.org/10.5281/zenodo.1039309>.

- B. R. Brandl, T. Agócs, G. Aitink-Kroes, T. Bertram, F. Bettonvil, R. van Boekel, O. Boulade, M. Feldt, A. Glasse, A. Glauser, M. Güdel, N. Hurtado, R. Jager, M. A. Kenworthy, M. Mach, J. Meisner, M. Meyer, E. Pantin, S. Quanz, H. M. Schmid, R. Stuik, A. Veninga, and C. Waelkens. Status of the mid-infrared E-ELT imager and spectrograph METIS. In *Ground-based and Airborne Instrumentation for Astronomy VI*, volume 9908 of *Proceedings of the SPIE*, page 990820, August 2016. doi: 10.1117/12.2233974.
- G. Chabrier. Galactic Stellar and Substellar Initial Mass Function. *Publications of the ASP*, 115:763–795, July 2003. doi: 10.1086/376392.
- R. E. Cohen, M. Hempel, F. Mauro, D. Geisler, J. Alonso-Garcia, and K. Kinemuchi. Wide Field Near-infrared Photometry of 12 Galactic Globular Clusters: Observations Versus Models on the Red Giant Branch. *Astronomical Journal*, 150:176, December 2015. doi: 10.1088/0004-6256/150/6/176.
- R. Davies, N. Ageorges, L. Barl, L. R. Bedin, R. Bender, P. Bernardi, F. Chapron, Y. Clenet, A. Deep, E. Deul, M. Drost, F. Eisenhauer, R. Falomo, G. Fiorentino, N. M. Förster Schreiber, E. Gendron, R. Genzel, D. Gratadour, L. Greggio, F. Grupp, E. Held, T. Herbst, H.-J. Hess, Z. Hubert, K. Jahnke, K. Kuijken, D. Lutz, D. Magrin, B. Muschielok, R. Navarro, E. Noyola, T. Paumard, G. Piotto, R. Ragazzoni, A. Renzini, G. Rousset, H.-W. Rix, R. Saglia, L. Tacconi, M. Thiel, E. Tolstoy, S. Trippe, N. Tromp, E. A. Valentijn, G. Verdoes Kleijn, and M. Wegner. MICADO: the E-ELT adaptive optics imaging camera. In *Ground-based and Airborne Instrumentation for Astronomy III*, volume 7735 of *Proceedings of the SPIE*, page 77352A, July 2010. doi: 10.1117/12.856379.
- G. De Marchi, F. Paresce, and S. Portegies Zwart. On the Temporal Evolution of the Stellar Mass Function in Galactic Clusters. *Astrophysical Journal*, 718:105–111, July 2010. doi: 10.1088/0004-637X/718/1/105.
- E. Diolaiti. MAORY: A Multi-conjugate Adaptive Optics RelaY for the E-ELT. *The Messenger*, 140:28–29, June 2010.
- E. Diolaiti, P. Ciliegi, R. Abicca, G. Agapito, C. Arcidiacono, A. Baruffolo, M. Bellazzini, V. Biliotti, M. Bonaglia, G. Bregoli, R. Briguglio, O. Brissaud, L. Busoni, L. Carbonaro, A. Carlotti, E. Cascone, J.-J. Correia, F. Cortecchia, G. Cosentino,

- V. De Caprio, M. de Pascale, A. De Rosa, C. Del Vecchio, A. Delboulb  , G. Di Rico, S. Esposito, D. Fantinel, P. Feautrier, C. Felini, D. Ferruzzi, L. Fini, G. Fiorentino, I. Foppiani, M. Ghigo, C. Giordano, E. Giro, L. Gluck, F. H  nault, L. Jocou, F. Kerber, P. La Penna, S. Lafrasse, M. Lauria, E. le Coarer, M. Le Louarn, M. Lombini, Y. Magnard, E. Maiorano, F. Mannucci, M. Mapelli, E. Marchetti, D. Maurel, L. Michaud, G. Morgante, T. Moulin, S. Oberti, G. Pareschi, M. Patti, A. Puglisi, P. Rabou, R. Ragazzoni, S. Ramsay, A. Riccardi, S. Ricciardi, M. Riva, S. Rochat, F. Roussel, A. Roux, B. Salasnich, P. Saracco, L. Schreiber, M. Spavone, E. Stadler, M.-H. Sztefek, N. Ventura, C. V  rinaud, M. Xompero, A. Fontana, and F. M. Zerbi. MAORY: adaptive optics module for the E-ELT. In *Society of Photo-Optical Instrumentation Engineers (SPIE) Conference Series*, volume 9909 of *Proceedings of the SPIE*, page 99092D, July 2016. doi: 10.1117/12.2234585.
- J. S. Dunlop. Observing the First Galaxies. In T. Wiklind, B. Mobasher, and V. Bromm, editors, *The First Galaxies*, volume 396 of *Astrophysics and Space Science Library*, page 223, 2013. doi: 10.1007/978-3-642-32362-1_5.
- A. Eckart and R. Genzel. Observations of stellar proper motions near the Galactic Centre. *Nature*, 383:415–417, October 1996. doi: 10.1038/383415a0.
- S. Genel, T. Naab, R. Genzel, N. M. F  rster Schreiber, A. Sternberg, L. Oser, P. H. Johansson, R. Dav  , B. D. Oppenheimer, and A. Burkert. Short-lived Star-forming Giant Clumps in Cosmological Simulations of $z=2$ Disks. *Astrophysical Journal*, 745:11, January 2012. doi: 10.1088/0004-637X/745/1/11.
- A. M. Ghez, M. Morris, E. E. Becklin, A. Tanner, and T. Kremenek. The accelerations of stars orbiting the Milky Way's central black hole. *Nature*, 407:349–351, September 2000. doi: 10.1038/35030032.
- R. Gilmozzi and J. Spyromilio. The European Extremely Large Telescope (E-ELT). *The Messenger*, 127, March 2007.
- A. Ginsburg, M. Parikh, J. Woillez, A. Groener, S. Liedtke, B. Sipocz, T. Robitaille, C. Deil, B. Svoboda, E. Tollerud, M. V. Persson, L. S  guin-Charbonneau, C. Armstrong, J. Mirocha, M. Droettboom, J. Allen, F. Moolekamp, R. Egeland, L. Singer, K. Barbary, F. Grollier, D. Shiga, H. Moritz G  nther, J. Parejko, J. Booker, E. Rol, Edward, A. Miller, and K. Willett. Astroquery: Access to online data resources. *Astrophysics Source Code Library*, August 2017.
- S. P. Goodwin, D. Nutter, P. Kroupa, D. Ward-Thompson, and A. P. Whitworth. The relationship between the prestellar core mass function and the stellar initial

- mass function. *Astronomy and Astrophysics*, 477:823–827, January 2008. doi: 10.1051/0004-6361:20078452.
- D. N. B. Hall. The Development And Use Of The HAWAII 2RG Array And SIDECAR ASIC For 1 - 5 Micron IR Observations With A Preview Of The Coming HAWAII 4RG-15. In *American Astronomical Society Meeting Abstracts #217*, volume 43 of *Bulletin of the American Astronomical Society*, page 425.07, January 2011.
- T. Haugbølle, P. Padoan, and Å. Nordlund. The Stellar IMF from Isothermal MHD Turbulence. *Astrophysical Journal*, 854:35, February 2018. doi: 10.3847/1538-4357/aaa432.
- P. Hennebelle and G. Chabrier. Analytical Theory for the Initial Mass Function: CO Clumps and Prestellar Cores. *Astrophysical Journal*, 684:395-410, September 2008. doi: 10.1086/589916.
- W. Herschel. Experiments on the Solar, and on the Terrestrial Rays that Occasion Heat; With a Comparative View of the Laws to Which Light and Heat, or Rather the Rays Which Occasion Them, are Subject, in Order to Determine Whether They are the Same, or Different. Part I. By William Herschel, LL. D. F. R. S. *Philosophical Transactions of the Royal Society of London Series I*, 90:293–326, 1800.
- J. H. Jeans. The Stability of a Spherical Nebula. *Philosophical Transactions of the Royal Society of London Series A*, 199:1–53, 1902. doi: 10.1098/rsta.1902.0012.
- M. Kissler-Patig, J.-F. Pirard, M. Casali, A. Moorwood, N. Ageorges, C. Alves de Oliveira, P. Baksai, L. R. Bedin, E. Bendek, P. Biereichel, B. Delabre, R. Dorn, R. Esteves, G. Finger, D. Gojak, G. Huster, Y. Jung, M. Kiekebush, B. Klein, F. Koch, J.-L. Lizon, L. Mehrgan, M. Petr-Gotzens, J. Pritchard, F. Selman, and J. Stegmeier. HAWK-I: the high-acuity wide-field K-band imager for the ESO Very Large Telescope. *Astronomy and Astrophysics*, 491:941–950, December 2008. doi: 10.1051/0004-6361:200809910.
- P. Kroupa. On the variation of the initial mass function. *Monthly Notices of the RAS*, 322:231–246, April 2001. doi: 10.1046/j.1365-8711.2001.04022.x.
- J. R. Lu, A. M. Ghez, S. D. Hornstein, M. R. Morris, E. E. Becklin, and K. Matthews. A Disk of Young Stars at the Galactic Center as Determined by Individual Stellar Orbits. *Astrophysical Journal*, 690:1463–1487, January 2009. doi: 10.1088/0004-637X/690/2/1463.

- T. Maschberger. On the function describing the stellar initial mass function. *Monthly Notices of the RAS*, 429:1725–1733, February 2013. doi: 10.1093/mnras/sts479.
- C. E. Max. Introduction to Adaptive Optics. In *American Astronomical Society Meeting Abstracts #214*, volume 214 of *American Astronomical Society Meeting Abstracts*, page 711, May 2009.
- P. J. McCarthy, J. Fanson, R. Bernstein, D. Ashby, B. Bigelow, N. Boyadjian, A. Bouchez, E. Chauvin, E. Donoso, J. Filgueira, R. Goodrich, F. Groark, G. Jacoby, and E. Pearce. Overview and status of the Giant Magellan Telescope Project. In *Ground-based and Airborne Telescopes VI*, volume 9906 of *Proceedings of the SPIE*, page 990612, August 2016. doi: 10.1117/12.2234505.
- S. Meingast, J. Alves, D. Mardones, P. S. Teixeira, M. Lombardi, J. Großschedl, J. Ascenso, H. Bouy, J. Forbrich, A. Goodman, A. Hacar, B. Hasenberger, J. Kainulainen, K. Kubiak, C. Lada, E. Lada, A. Moitinho, M. Petr-Gotzens, L. Rodrigues, and C. G. Román-Zúñiga. VISION - Vienna survey in Orion. I. VISTA Orion A Survey. *Astronomy and Astrophysics*, 587:A153, March 2016. doi: 10.1051/0004-6361/201527160.
- G. Moreels, J. Clairemidi, M. Faivre, D. Pautet, F. Rubio da Costa, P. Rousselot, J. W. Meriwether, G. A. Lehmann, E. Vidal, J. L. Chau, and G. Monnet. Near-infrared sky background fluctuations at mid- and low latitudes. *Experimental Astronomy*, 22:87–107, October 2008. doi: 10.1007/s10686-008-9089-6.
- S. S. R. Offner, P. C. Clark, P. Hennebelle, N. Bastian, M. R. Bate, P. F. Hopkins, E. Moraux, and A. P. Whitworth. The Origin and Universality of the Stellar Initial Mass Function. *Protostars and Planets VI*, pages 53–75, 2014. doi: 10.2458/azu_uapress_9780816531240-ch003.
- L. Oser, J. P. Ostriker, T. Naab, P. H. Johansson, and A. Burkert. The Two Phases of Galaxy Formation. *Astrophysical Journal*, 725:2312–2323, December 2010. doi: 10.1088/0004-637X/725/2/2312.
- A. J. Pickles. A Stellar Spectral Flux Library: 1150-25000 Å. *Publications of the ASP*, 110:863–878, July 1998. doi: 10.1086/316197.
- L. C. Powell, A. Slyz, and J. Devriendt. The impact of supernova-driven winds on stream-fed protgalaxies. *Monthly Notices of the RAS*, 414:3671–3689, July 2011. doi: 10.1111/j.1365-2966.2011.18668.x.

- B. J. Rauscher. Teledyne H1RG, H2RG, and H4RG Noise Generator. *Publications of the ASP*, 127:1144–1151, November 2015. doi: 10.1086/684082.
- G. H. Rieke and M. J. Lebofsky. The interstellar extinction law from 1 to 13 microns. *Astrophysical Journal*, 288:618–621, January 1985. doi: 10.1086/162827.
- F. Rigaut, B. Neichel, M. Bocca, C. d’Orgeville, G. Arriagada, V. Fesquet, S. J. Diggs, C. Marchant, G. Gausach, W. N. Rambold, J. Luhrs, S. Walker, E. R. Carrasco-Damele, M. L. Edwards, P. Peshev, R. L. Galvez, T. B. Vucina, C. Araya, A. Gutierrez, A. W. Ebbers, A. Serio, C. Moreno, C. Urrutia, R. Rogers, R. Rojas, C. Trujillo, B. Miller, D. A. Simons, A. Lopez, V. Montes, H. Diaz, F. Daruich, F. Colazo, M. Bec, G. Trancho, M. Sheehan, P. McGregor, P. J. Young, M. C. Doolan, J. van Harmelen, B. L. Ellerbroek, D. Gratadour, and A. Garcia-Rissmann. GeMS: first on-sky results. In *Adaptive Optics Systems III*, volume 8447 of *Proceedings of the SPIE*, page 84470I, July 2012. doi: 10.1117/12.927061.
- G. Rousset, F. Lacombe, P. Puget, N. N. Hubin, E. Gendron, T. Fusco, R. Arsenault, J. Charton, P. Feautrier, P. Gigan, P. Y. Kern, A.-M. Lagrange, P.-Y. Madec, D. Mouillet, D. Rabaud, P. Rabou, E. Stadler, and G. Zins. NAOS, the first AO system of the VLT: on-sky performance. In P. L. Wizinowich and D. Bonaccini, editors, *Adaptive Optical System Technologies II*, volume 4839 of *Proceedings of the SPIE*, pages 140–149, February 2003. doi: 10.1117/12.459332.
- E. E. Salpeter. The Luminosity Function and Stellar Evolution. *Astrophysical Journal*, 121:161, January 1955. doi: 10.1086/145971.
- J. Schaye, R. A. Crain, R. G. Bower, M. Furlong, M. Schaller, T. Theuns, C. Dalla Vecchia, C. S. Frenk, I. G. McCarthy, J. C. Helly, A. Jenkins, Y. M. Rosas-Guevara, S. D. M. White, M. Baes, C. M. Booth, P. Camps, J. F. Navarro, Y. Qu, A. Rahmati, T. Sawala, P. A. Thomas, and J. Trayford. The EAGLE project: simulating the evolution and assembly of galaxies and their environments. *Monthly Notices of the RAS*, 446:521–554, January 2015. doi: 10.1093/mnras/stu2058.
- STScI Development Team. pysynphot: Synthetic photometry software package. Astrophysics Source Code Library, March 2013.
- N. Thatte, M. Tecza, F. Clarke, R. L. Davies, A. Remillieux, R. Bacon, D. Lunney, S. Arribas, E. Mediavilla, F. Gago, N. Bezawada, P. Ferruit, A. Fragoso, D. Freeman, J. Fuentes, T. Fusco, A. Gallie, A. Garcia, T. Goodsall, F. Gracia, A. Jarno, J. Kosmalski, J. Lynn, S. McLay, D. Montgomery, A. Pecontal, H. Schnetler,

H. Smith, D. Sosa, G. Battaglia, N. Bowles, L. Colina, E. Emsellem, A. Garcia-Perez, S. Gladysz, I. Hook, P. Irwin, M. Jarvis, R. Kennicutt, A. Levan, A. Longmore, J. Magorrian, M. McCaughrean, L. Origlia, R. Rebolo, D. Rigopoulou, S. Ryan, M. Swinbank, N. Tanvir, E. Tolstoy, and A. Verma. HARMONI: a single-field wide-band integral-field spectrograph for the European ELT. In *Ground-based and Airborne Instrumentation for Astronomy III*, volume 7735 of *Proceedings of the SPIE*, page 77352I, July 2010. doi: 10.1117/12.857445.

M. Vogelsberger, S. Genel, V. Springel, P. Torrey, D. Sijacki, D. Xu, G. Snyder, D. Nelson, and L. Hernquist. Introducing the Illustris Project: simulating the coevolution of dark and visible matter in the Universe. *Monthly Notices of the RAS*, 444:1518–1547, October 2014. doi: 10.1093/mnras/stu1536.

P. Wizinowich, D. S. Acton, C. Shelton, P. Stomski, J. Gathright, K. Ho, W. Lupton, K. Tsubota, O. Lai, C. Max, J. Brase, J. An, K. Avicola, S. Olivier, D. Gavel, B. Macintosh, A. Ghez, and J. Larkin. First Light Adaptive Optics Images from the Keck II Telescope: A New Era of High Angular Resolution Imagery. *Publications of the ASP*, 112:315–319, March 2000. doi: 10.1086/316543.

HAWK-I observing proposal to verify SimCADO

A

A.1 Overview

The observing time proposal is for an extension of the work described in chapter 3. The plan for a second and more detailed verification run is described in chapter 6.

In order to verify the accuracy of SimCADO with varying atmospheric conditions we applied for 5 hours of observing time with HAWK-I. The data in the ESO archive only covers the best seeing and airmass conditions. As one would expect, no observer would willingly observe at high airmass and with bad seeing conditions if better conditions were available. However such observations are exactly what we need to test the various components of the atmospheric model in the SimCADO OpticalTrain module. The rationale for this is given in the scientific context section of the proposal.

A.2 Submission Details

Title: Phase B Technical Note: Filter Wing Transmission Levels

Principal Investigator: Kieran Leschinski

Time requested: 5 hours

Instrument: VLT/HAWK-I

Status: Accepted by the ESO time allocation committee. Rank: A

Own contributions: Everything related to this proposal.



APPLICATION FOR OBSERVING TIME

PERIOD: 100A

Important Notice:

By submitting this proposal, the PI takes full responsibility for the content of the proposal, in particular with regard to the names of CoIs and the agreement to act according to the ESO policy and regulations, should observing time be granted.

1. Title										Category: L-0
Verification of the MICADO @ E-ELT image simulator: SimCADO										
2. Abstract / Total Time Requested										
Total Amount of Time: 0 nights VM, 5 hours SM										
SimCADO is the instrument data simulation package for MICADO @ E-ELT. In order to verify the critical algorithms which model the atmosphere and the telescope/instrument optical train, we propose to observe two globular clusters over a range of seeing (0.8"-2"), airmass (1.0-2.0) and Exposure time (2.5s-40s) values with a version of SimCADO adapted to model HAWKI @ UT4. 5 hours of observation time will ensure that SimCADO can accurately simulate telescope/instrument imagery from existing systems, allowing us to confidently make predictions about the future capabilities of the MICADO @ E-ELT system. A preliminary version of the software is already publically available (www.univie.ac.at/simcado) for anyone wishing to test the future observability with MICADO of complex targets beyond the scope of an ETC. SimCADO also plays a critical developmental role within the MICADO consortium.										
3. Run	Period	Instrument	Time	Month	Moon	Seeing	Sky	Mode	Type	
A	100	HAWKI	1h	any	n	0.8	CLR	s		
B	100	HAWKI	1h	any	n	1.0	CLR	s		
C	100	HAWKI	1h	any	n	1.2	CLR	s		
D	100	HAWKI	1h	any	n	1.4	CLR	s		
E	100	HAWKI	1h	any	n	n	CLR	s		
4. Number of nights/hours				Telescope(s)				Amount of time		
a) already awarded to this project:										
b) still required to complete this project:										
5. Special remarks:										
6. Principal Investigator: Kieran Leschinski, kdleschinski@gmail.com, AT, Universitaet Wien, Institut fuer Astrophysik										
6a. Co-investigators:										
R.	Davies	Max Planck Institut fuer extraterrestrische Physik,D								
J.	Alves	Universitaet Wien,Institut fuer Astrophysik,AT								
W.	Zeilinger	Universitaet Wien,Institut fuer Astrophysik,AT								
G.	Verdoes-Kleijn	Kapteyn Institute,University of Groningen,NL								
Following CoIs moved to the end of the document ...										

7. Description of the proposed programme

A – Scientific Rationale:

SimCADO is the instrument data simulation tool for the future MICADO @ E-ELT system (Leschinski et al., 2016), and a preliminary version is already available to the astronomical community (www.univie.ac.at/simcado). This user-friendly software package is designed to simulate both raw detector read outs and “perfectly” reduced science images from MICADO. It not only plays an integral part in the design and development of the MICADO NIR imaging instrument (Davies et al., 2016), but will also be **an essential tool for the astronomical community to develop and refine the science cases that will be observed by the E-ELT and MICADO**. Furthermore, SimCADO will allow observers in the future to avoid non-detections (which will be a waste of precious E-ELT observing time) by helping astronomers to **visualise via simulations the often complex on-sky environments surrounding their targets** (e.g. gravitationally lensed galaxies, sub-structures in high-z galaxies, resolved stellar populations in star formation regions) and hence to determine whether or not their observations will indeed be successful – a much needed improvement over the limits of the standard ETCs that are currently used to plan observing strategies. Fig 1a shows an example observation of M30.

First light for the E-ELT and MICADO is slated for 2024, and as such there is no way of directly testing the accuracy of simulated observations. In order to address this issue, and following ESO’s recommendation, we have **created a version of SimCADO which instead models the HAWKI @ VLT optical path as well as the atmospheric contributions to image quality at Paranal**. If SimCADO can accurately simulate images from HAWKI + UT4, then we can be confident that it will manage the jump to a 39m E-ELT.

Our first blind tests with single J and Ks archival HAWKI images of M4 were (mostly) successful. **Statistical deviations between the simulated and real images were on the order of <0.2 mag (see Figure 1b) with a small systematic offset**. The sky background model caused a large spread in the photometry at faint magnitudes. Normally the software uses the output from the ESO SkyCalc tool, which generates both transmission and emission spectra for the sky for a given set of parameters – with the airmass and PWV playing the most significant roles. However, we found the sky emission curve in the Ks-band under-estimated the background flux by almost 2 magnitudes. We (currently) correct for this by pinning the background emission spectrum to the standard ESO Paranal sky background magnitudes. However **this doesn’t allow SimCADO to properly simulate the effect of airmass on the background flux** – a significant effect when calculating the flux reaching the detector. Additionally the FWHM of the seeing-dependent PSF also affects the final detectable flux, resulting in the background flux being a convolution of the effects of airmass, seeing and exposure time acting on a combination of airmass-dependent sky-background, airmass-independent telescope background and exposure-time-independent detector effects.

As the E-ELT / MICADO optical train will be very sensitive to small variations in both parameters, any simulation software which aims to generate accurate observational data must also take the airmass and seeing conditions into account. SimCADO includes algorithms to model the 2D-effects of these two parameters, however without a way to verify them, any predictions based on simulated data must also include the uncertainties introduced by these un-verified algorithms. We have **looked extensively through the ESO archive for suitable data, but have found only a very limited number** of observations that would allow us to systematically test partial regions of this parameter space while keeping all other parameters fixed (see Fig 1c). For the vast majority of **observations in the archive, conditions were “unfortunately too good”**. This proposal requests observations of 2 clusters at a range of seeing, airmass, and exposure times, in order to provide a consistent and complete data set against which we can test individual SimCADO parameters to resolve out discrepancies in both the stellar and background fluxes between simulated and observed images.

B – Immediate Objective:

In order to test SimCADO’s implementations of the above-mentioned atmospheric effects, we compiled an extensive list of observations from the ESO archive for a range of globular clusters. Many observations in the archive enable us to check singular combinations (i.e. 2 data points) of any two atmospheric effects, however there was **no systematic coverage of the airmass-seeing-exposure time parameter space**. Figure 1c shows the space covered by the best candidate for using archival data: NGC288, which suffers from severely low stellar densities. In hindsight this lack of parameter space coverage was obvious: **why would an astronomer elect to observe at large zenith distances, or with bad seeing, if conditions permitted otherwise**. In order to validate the predictive power of SimCADO we therefore require a set of observations of the same object that fully, and more importantly, uniformly covers the airmass-seeing plane (see Fig 1c). In other words, a set of data which allows us to vary only one parameter in the simulations (e.g. airmass or exposure time) while keeping all others constant and still allows for a comparison with real images (See Box 8). The grey circles in Figure 1c show the ideal level of airmass-seeing plane coverage that we wish to achieve. **The need for complete coverage of the airmass-seeing-(exposure time) space is three fold**. Firstly, various seeing conditions need to be sampled to **decouple the atmospheric extinction/emission** due to airmass from the decrease in PSF peak flux due to the seeing. Secondly, various airmasses need to be sampled in order to **decouple the telescope emission** from the atmospheric emission, and lastly, various exposure times are required to **decouple the detector noise components** from the background.

7. Description of the proposed programme and attachments

Description of the proposed programme (continued)

We propose to **observe two globular clusters, M30 (NGC 7099) and NGC1851**, for which independent photometric catalogues of the cluster members are available (Cohen et al, 2015, AJ). For each of the observations we will create matching simulated images with SimCADO taking into account the varying atmospheric parameters. We will then compare various aspects of the images (photometry, detector linearity, PSFs, total transmission, background level and variation, etc) in order to verify and improve SimCADO's algorithms. With a relatively small investment of observing time (<5 hours), we will be able to optimise a simulation tool, that will benefit the astronomical community up to, and indeed past, first-light for MICADO and the E-ELT.

For references, please refer to Box 10

Attachments (Figures)

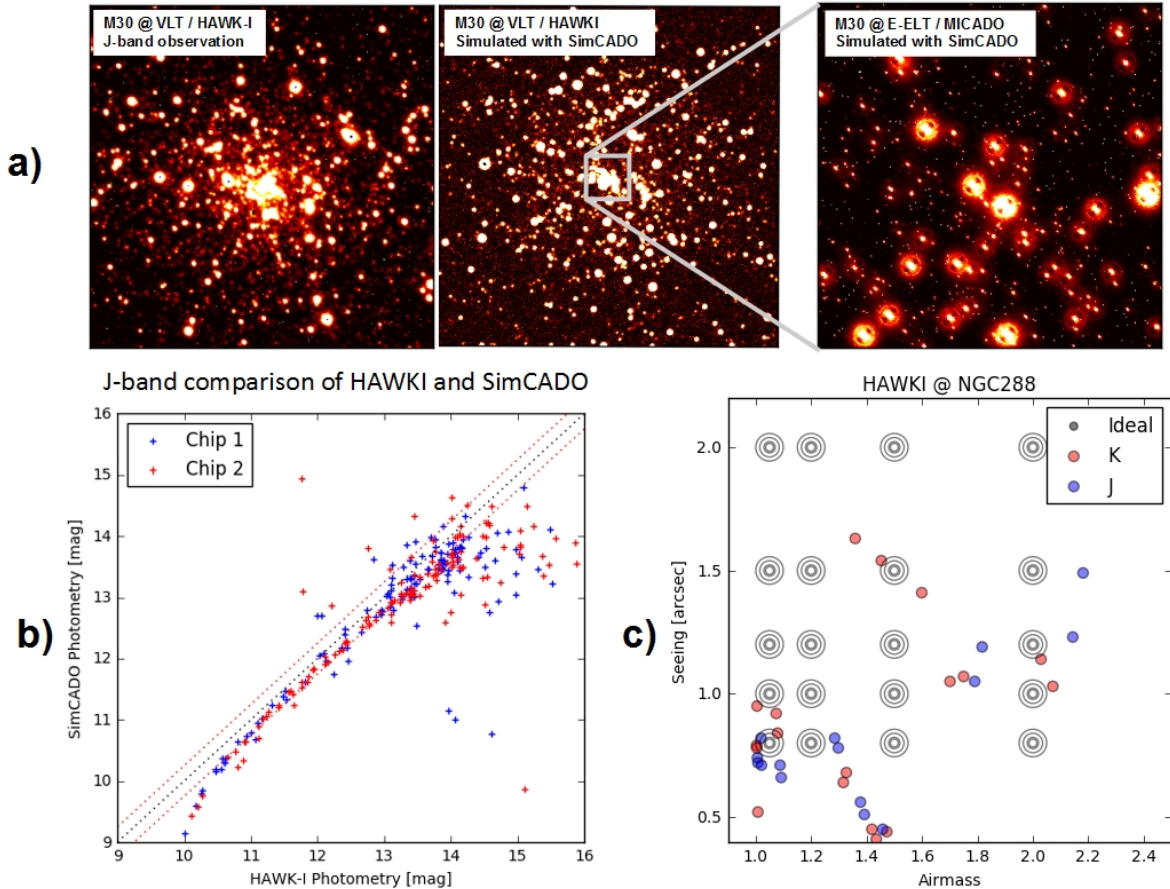


Fig. 1: a): A demonstration of the capabilities of SimCADO. Left: a cutout of a real observation from HAWKI of the core of M30. Middle: the same field generated with version of SimCADO adapted to reflect the HAWKI/VLT setup with the Cohen et al. (2015) catalogue. Right: the zoomed section of the core as would be seen by MICADO/E-ELT, generated by SimCADO. The low mass stars were added by extrapolating the J-band luminosity function. b): Results from our blind test with photometry of stars in M4 in a raw HAWKI image from the ESO archive. The SimCADO images were generated using an independent photometric estimate - the 2MASS catalogue. The plot shows the correlation between the J-band magnitudes derived from the SimCADO and HAWKI images. The major deviations are due to the incorrect scaling of the atmospheric background and the fact that we needed to derive our own linearity curve for the HAWK detectors. c): The coverage of the airmass-seeing parameter space for archival data for NGC288. The red circles are the Ks-band observations, the blue circles for J-band. The size of the circles represent the exposure time. The grey concentric circles show the coverage we will need in order to comprehensively validate SimCADO's algorithms.

8. Justification of requested observing time and observing conditions

Lunar Phase Justification: Lunar phase is irrelevant in the NIR

Time Justification: (including seeing overhead) In order to systematically sample the parameter space of airmass, seeing and Exposure time (which is not covered in the archive), we need to observe the same targets when the atmospheric conditions happen to be as we need them. It is unlikely that the full range of seeing conditions will be present in one night while the targets are at their required ranges of airmass. Thus, as we require 5 different seeing conditions, we request 5 runs to be executed on nights when the atmospheric conditions are around the (below) specified ranges.

To test SimCADO thoroughly we require a matrix of observations for both NGC1851 and M30 which cover the following range of parameters and values:

- 5 seeing values: $<0.8''$, $1.0''$, $1.2''$, $1.5''$ and $\sim 2''$

Deviations of up to 1 pixel width in the seeing FWHM are acceptable, i.e. $\pm 0.1''$. The $0.8''$ constraint allows us resolve the faintest background source which will be “washed out” in images with worse seeing. This allows us to get a handle on how many point sources are contributing to the background level in images with seeing $> 0.8''$.

- 4 airmass values: <1.05 , 1.2, 1.5 and >2.0

Deviations of up to ± 0.05 airmasses are acceptable.

- 5 Exposures in J and Ks filters: 2.5, 5, 10, 20, 40s

The increasing exposure time will allow us to decouple the detector contributions from the stellar fluxes while allowing us to simultaneously map the appearance of the faintest sources with exposure time and test our implementation of detector linearity as the background in Ks-band approaches the saturation limit.

We are applying to observe >3 data points along each “dimension” in case any images is unusable.

Total per Object per airmass: 7.5 min (inc. overheads)

Total per Night : 60 min (inc. overheads)

Grand total: 5 hours (inc. overheads)

8a. Telescope Justification:

HAWKI @ VLT is the current day analogue of the future MICADO @ E-ELT instrument.

8b. Observing Mode Justification (visitor or service):

Service - the flexibility of service mode is required to cover the wide range of observing conditions.

8c. Calibration Request:

Standard Calibration

9. Report on the use of ESO facilities during the last 2 years

9a. ESO Archive - Are the data requested by this proposal in the ESO Archive (<http://archive.eso.org>)? If so, explain the need for new data.

Observations available in the archive do not fulfil our criteria in terms of coverage of airmass, seeing, and exposure time (as shown in Fig 1c). Science observations are (usually) conducted under best possible conditions, and not to test the atmospheric effects on the science object: why observe at an airmass of 2.0 when the target transits the Zenith?

9b. GTO/Public Survey Duplications:

No GTO or Public Survey regions cover out targets

10. Applicant's publications related to the subject of this application during the last 2 years

Leschinski (... Davies) et al., 2016, SPIE, 518, 567: SimCADO - an instrument data simulator package for MICADO at the E-ELT

Davies (... Leschinski) et al., 2016 Proc SPIE, 9908, 99081Z, MICADO: first light imager for the E-ELT
Deep (... Davies) et al., 2011, A&A, 531, A151, An E-ELT case study: colour-magnitude diagrams of an old galaxy in the Virgo cluster

Noll (... Kausch) et al., 2012, A&A, 543, A92, An atmospheric radiation model for Cerro Paranal. I. The optical spectral range

Jones (... Kausch) et al., 2013, A&A, 560, A91, An advanced scattered moonlight model for Cerro Paranal

11. List of targets proposed in this programme

Run	Target/Field	α (J2000)	δ (J2000)	ToT	Mag.	Diam.	Additional info	Reference star
ABCDE NGC 1851		05 14 06.76	-40 02 47.6	2.5	7.1	4 min	To be observed at various airmasses and seeing values	
ABCDE NGC 7099		21 40 22.12	-23 10 47.5	2.5	6.8	5 min	Messier 30 - To be observed at various airmasses and seeing values	

Target Notes: NCG7099 sets as NGC1851 rises, so the target with the lowest airmass constraint that still needs to be observed should be observed first.

12. Scheduling requirements

13. Instrument configuration

Period	Instrument	Run ID	Parameter	Value or list
100	HAWKI	A	IMG	J, Ks
100	HAWKI	B	IMG	J, Ks
100	HAWKI	C	IMG	J, Ks
100	HAWKI	D	IMG	J, Ks
100	HAWKI	E	IMG	J, Ks

6b. Co-investigators:

...continued from Box 6a.

W.	Kausch	Universitaet Wien, Institut fuer Astrophysik, AT
O.	Czoske	Institut fuer Astro- und Teilchenphysik, Universitaet Innsbruck, AT
R.	Köhler	Institut fuer Astro- und Teilchenphysik, Universitaet Innsbruck, AT
M.	Mach	Universitaet Wien, Institut fuer Astrophysik, AT

ADASS Conference Proceedings

B

Aside from the SPIE conference proceeding presented in chapter 2, I have also authored two conference proceedings papers and been a co-author of three more. Both of my first author proceedings papers appear in the publications of the astronomical society of the pacific ADASS conference proceedings series.

“The Astronomical Data Analysis Software and Systems (ADASS) conference is held each year at a different hosting astronomical institution. The conference provides a forum for scientists and programmers concerned with algorithms, software and software systems employed in the acquisition, reduction, analysis, and dissemination of astronomical data. An important element of the program is to foster communication between developers and users with a range of expertise in the production and use of software and systems. The program consists of invited talks, contributed oral and display papers, tutorials, user group meetings and special interest group meetings (called BOFs).” Source: <http://www.adass.org/index.html>

B.1 Astronomical Data Analysis Software and Systems 2015

The ADASS 2015 conference in Sydney, Australia was the first major conference of my PhD, and also the first time the concept for SimCADO was presented. In these proceedings I describe the rationale for building SimCADO as well as a possible solution for dealing with the seemingly huge array sizes that would be encountered if the full MICADO field of view should be described in spatial and spectral dimensions.

SimCADO - An end-to-end instrument data simulator for MICADO on the E-ELT

Kieran Leschinski¹, Oliver Czoske¹, Rainer Köhler^{2,1}, Werner Zeilinger¹, Wolfgang Kausch^{1,2}, Norbert Przybilla², João Alves¹, Michael Mach¹, Gijs Verdoes Kleijn³, Richard Davies⁴, Ronny Ramlau^{5,6}, Roland Wagner⁶, Thorsten Ratzka⁷, Robert Greimel⁷, Martin Leitzinger⁷, Veronika Schaffenroth², Manuel Güdel¹, Bodo Ziegler¹

¹*Department of Astrophysics, University of Vienna, Austria;
kieran.leschinski@univie.ac.at*

²*Institute for Astro- and Particle Physics, University of Innsbruck, Austria*

³*Kapteyn Astronomical Institute, University of Groningen, Netherlands*

⁴*Max Planck Institute for Extraterrestrial Physics, Garching, Germany*

⁵*Industrial Mathematics Institute, Johannes Kepler University, Linz, Austria*

⁶*Radon Institute for Computational and Applied Mathematics, Austrian Academy of Sciences, Linz, Austria*

⁷*Institute for Physics/IGAM NAWI, Graz, University of Graz, Austria*

Abstract. MICADO will be the first-light wide-field imager for the European Extremely Large Telescope (E-ELT) and will provide diffraction limited imaging (7 mas at $1.2\ \mu\text{m}$) over a $\sim 53''$ field of view. As part of the development of this instrument we are building an end-to-end instrument data simulator. SimCADO generates a full model of the optical train from source to detector readout. SimCADO is thus a tool to provide simulated detector array images to both the science and instrument development teams. Here we present an overview of the inner workings of SimCADO and outline our plan for its further development.

1. Motivation for developing SimCADO

Building a new instrument is an iterative process between the science team and the design team. The design team requires a list of science drivers in order to tailor the instrument design and fulfil the science requirements. The science team on the other hand requires information on the instrument design and its expected performance in order to generate a list of realistic science drivers. This mutual dependency therefore requires a high degree of communication between both teams if an efficient and timely design of the instrument is to happen. A quick and easy-to-use instrument data simulator is one way of providing a platform to facilitate the transfer of information between both teams. The goals of SimCADO are thus fourfold:

1. collect and use the most recent results of detailed subpackage simulations to facilitate continual science case analysis,
2. estimate the performance of MICADO to aid design decisions,
3. generate realistic mock detector frames for developing and testing the pipelines and
4. provide a tool to the astronomical community to assist in the evaluation and planning of observation strategies.

2. What is SimCADO?

SimCADO is a python package that will enable the construction of a virtual model of the optical path through the atmosphere, the E-ELT (Gilmozzi & Spyromilio 2007) and MICADO (Davies et al. 2010) and then visualise how astronomical objects will appear on the detector array. For the development of SimCADO, we have chosen to use an array-based approach instead of a photon-following approach. Photon-following approaches like the LSST PhoSim tool (Peterson et al. 2015), offer a high degree of accuracy, however they require access to massive computing facilities. Array-based approaches, like those used in the METIS (Schmalzl et al. 2012) and HARMONI (Ziele-niewski et al. 2014) simulators, are fast and are designed to run on personal computers. The accuracy of these array-based approaches are expected to be sufficient for scientific feasibility studies and the current trade-off analyses.

Although SimCADO has been constructed with MICADO in mind, in practice any telescope can be modelled as long as the user has the relevant technical data for the desired telescope configuration. The SimCADO python package consists of a series of class objects which represent different aspects of the optical elements. In general these class objects can be split into three major categories:

- objects which affect the spatial distribution of incoming photons,
- objects which introduce wavelength-dependent changes to the incoming photons,
- objects which represent photon sources (e.g. science target, sky background, detector noise, etc)

The user is free to choose the combination of these class objects which best describes the elements in the optical system. For example, the point spread function (PSF) of the E-ELT's system of five mirrors may be represented by one 3-dimensional (x,y,λ) wavelength-dependent image cube combined with a 1-dimensional (λ) spectral curve for the mirror reflectivity.

As MICADO has just entered the preliminary design phase, the initial versions of SimCADO will be shipped with the technical data generated during the Phase A study. Hence SimCADO will, at first, only be able to simulate images based on this information. As more and more details about the individual subsystem components become available, these will be incorporated into SimCADO updates, allowing SimCADO to more faithfully represent the real detector array output.

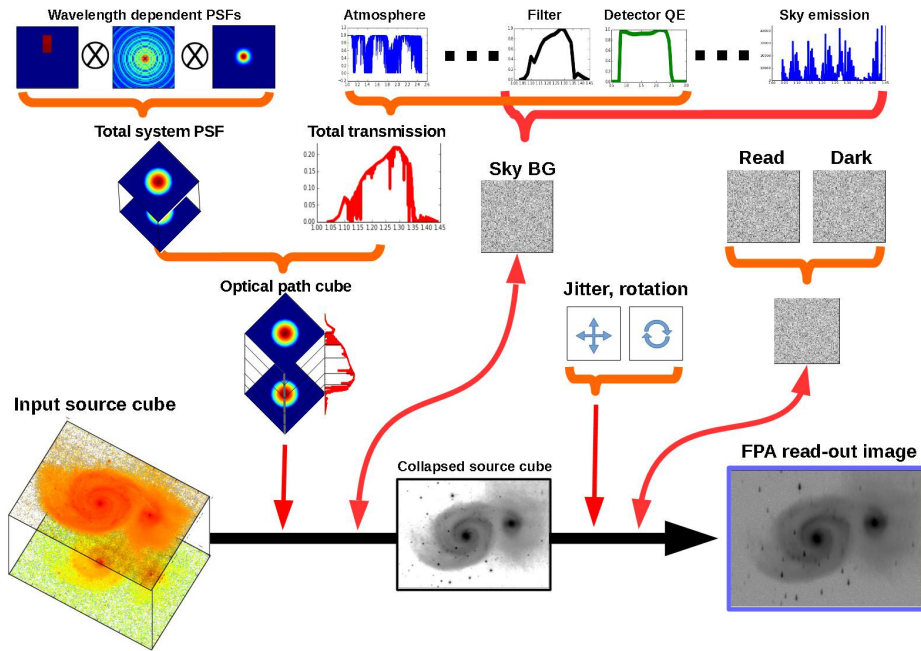


Figure 1. SimCADO builds a model of the optical path out of a combination of basic building blocks. The PSF cube objects represent 2D spatial effects caused by the optical elements (either wavelength independent or dependent). The spectral curve objects contain wavelength dependent information, e.g. transmission curves.

3. How to generate an optical train

Due to the modular way in which we have designed SimCADO, generating a simple optical path model is a matter of $\sim 20 - 30$ lines of python code. Figure 1 shows the steps needed to generate a rudimentary telescope model. In this section we give a brief run down of the python commands needed to achieve this.

This (non-exhaustive) list of classes and functions is purely to illustrate the main steps involved in generating an optical path model. SimCADO provides pre-configured high-level functions for simulating the MICADO optical train, however the user is free to use the basic building blocks to test other optical configurations.

PsfCube() and SystemPsf(): PSF cubes are used to represent a series of wavelength dependent PSFs in order to model the major spatial effects - e.g. atmospheric dispersion, telescope diffraction, atmospheric seeing - not removed by the adaptive optics (AO) system, etc. The class `PsfCube()` can currently generate PSFs with a Gaussian, Airy, Moffat, or shifted point kernel for a list of wavelengths at a specific pixel scale. Alternatively the user may import a FITS cube with PSFs. The `SystemPsf()` object takes a list of `PsfCube` instances and produces a single PSF cube which describes the whole optical train. It is this combined PSF cube that the object will “see” when the optical train is applied to the input source cube.

SpectralCurve() and **SystemCurve()**: Reflectivity curves, transmission curves and emission curves all use this class. Once read, the curve is resampled to the specified resolution. Multiple `SpectralCurve` instances can be combined in a single `SpectralCurve()` object where all spectral curves are resampled to the coarsest resolution before being combined along a new common wavelength range. The `SystemCurve` can then be linked straight to the `SystemPsf`.

InputCube() and **OutputCube()**: The “science” data cube contains spatial and wavelength information about the target to be “observed” with MICADO. Information in the The data are imported along with information in the FITS header as an instance of the `InputCube`. The `OutputCube` represents the science data cube after it has passed through the optical path model. It is as if all the photons had (figuratively) stopped still just in front of the focal plane array (FPA). Spectral and spatial information is still preserved up until this point. The `OutputCube` is also converted to photon counts per second so that the conversion to electrons in the focal plane array is straight forward.

Fpa(): The final Focal Plane Array (FPA) readout is generated by creating an `Fpa` instance. It produces realistic photon noise estimates by simulating the full detector sampling scheme as appropriate for IR detectors. The `FPA` class also simulates various sources of detector noise for the HAWAII 4RG, following the `HxRG Noise Generator` package developed for the JWST (Rauscher 2015).

Although most of the core features have been implemented, SimCADO is still in an early phase of development. We plan to release an alpha version of the code with the core features to the MICADO science team in January 2016 for testing purposes, with the dual goals of evaluating how the code performs as well as the user experience.

Acknowledgments. This publication is supported by the Austrian Ministry of Science, Research and Economy (bmwfw) through project IS538003 (Hochschulraumstrukturmittel). GVK acknowledges support by the Netherlands Research School for Astronomy (NOVA) and Target. Target is supported by Samenwerkingsverband Noord Nederland, European fund for regional development, Dutch Ministry of economic affairs, Pieken in de Delta, Provinces of Groningen and Drenthe.

References

- Davies, R., et al. 2010, in SPIE Conf. Series, vol. 7735 of SPIE Conf. Series, 2. [1005.5009](#)
- Gilmozzi, R., & Spyromilio, J. 2007, The Messenger, 127, 11
- Peterson, J. R., et al. 2015, ApJS, 218, 14. [1504.06570](#)
- Rauscher, B. J. 2015, PASP, 127, 1144. [1509.06264](#)
- Schmalzl, E., et al. 2012, in SPIE Conf. Series, vol. 8449 of SPIE Conf. Series, 1
- Zieleniewski, S., Thatte, N., Kendrew, S., Houghton, R., Tecza, M., Clarke, F., Fusco, T., & Swinbank, M. 2014, in SPIE Conf. Series, vol. 9147 of SPIE Conf. Series, 93

B.2 Astronomical Data Analysis Software and Systems 2016

The following year the ADASS conference was held in Trieste, Italy. By this stage the structure of SimCADO had been defined and the I was almost finished writing the code for the Imaging modes. This proceedings paper is similar to the SPIE paper from chapter 2 in many respects.

SimCADO - a python package for simulating detector output for MICADO at the E-ELT

Kieran Leschinski¹, Oliver Czoske^{2,1}, Rainer Köhler^{2,1}, Michael Mach¹, Werner Zeilinger¹, Gijs Verdoes Kleijn³, Wolfgang Kausch^{1,2}, Norbert Przybilla², João Alves¹, Richard Davies⁴

¹*Department of Astrophysics, University of Vienna, Austria;
kieran.leschinski@univie.ac.at*

²*Institute for Astro- and Particle Physics, University of Innsbruck, Austria*

³*Kapteyn Astronomical Institute, University of Groningen, Netherlands*

⁴*Max Planck Institute for Extraterrestrial Physics, Garching, Germany*

Abstract.

SimCADO is the instrument data simulation software for the E-ELT's near-infrared wide-field imaging camera - MICADO. Written in Python, SimCADO allows the user to simulate possible future observations of astronomical objects with the 39m European Extremely Large Telescope (E-ELT). In these proceedings we present a brief introduction into how to use SimCADO.

1. Introduction

Within the next 10 years a new generation of extremely large telescopes will become available to the astronomical community. These telescopes and the instruments attached to them will allow observations of the faintest and most distant phenomena in the Universe. The first-generation near-infrared wide-field imaging camera for the European Extremely Large Telescope (Gilmozzi & Spyromilio 2007) will be MICADO (Davies et al. 2016). As part of its development we have created a Python package – SimCADO – which simulates the output of the MICADO detector array (Leschinski et al. 2016).

With the help of the SCAO and MCAO observing modes, MICADO will have the ability to observe at the diffraction limit in the $0.7\text{--}2.5\mu\text{m}$ wavelength range. It will offer a wide field (4mas/pixel) and a zoom (1.5mas/pixel) imaging mode, as well as a long-slit spectrographic mode. For each of these modes the SimCADO package combines the effects that elements along the optical path have on photons traveling from their point of origin, through the E-ELT+MICADO system and onto the detector chips. The output of a SimCADO simulation run is therefore akin to the raw output expected from the MICADO detector array.

SimCADO is, and will be, used by various teams within the MICADO consortium. Consortium-internal uses of SimCADO include: providing a single platform for the science team to solidify the science drivers for MICADO; acting as a stand-in for the MICADO instrument to aid in creating the specifications for the data flow infrastructure; as a preliminary tool for design trade-off studies; generating updated

data tables for the ESO exposure time calculator; etc. SimCADO will be a useful tool for simulating a broad variety of astrophysical objects and processes in order to efficiently prepare observing programs for MICADO at the E-ELT. In these proceedings we provide an overview of the internal working of the SimCADO package and describe an example of a use-case simulation.

2. The inner workings of SimCADO

The SimCADO package contains four main classes, each of which represents an independent part of the simulation process. A detailed description of these classes and the methods contained within can be found in Leschinski et al. (2016).

Source	holds all the spatial and spectral information pertaining to the celestial object of interest.
OpticalTrain	holds information on the spatial, spectral, and (in the future) temporal effects that each element in the optical train has on the incoming light.
Detector	contains information on the individual chips in the focal plane array and how they convert incoming “photons” into pixel counts in the final FITS image. This conversion uses the code developed by Rauscher (2015) to model detector noise.
UserCommands	contain a keyword-value-pair style dictionary with all the parameters required to successfully run a simulation.

If the casual user is only interested in simulating future MICADO imagery, they may use the convenience function `simcado.run()` which uses the default parameters based on the current design of both the E-ELT and MICADO. Thus the casual user will only need to be familiar with the first of the four classes, i.e. “Source”.

The Source object contains spectral (SEDs, weights) and spatial (x,y) information about the object of interest. In order to save memory, and thus computing time, this information is split and stored separately. Two arrays (`<Source>.x`, `<Source>.y`) hold the coordinates of each “pixel” containing photon emission above a certain threshold (default is > 0 ph/s). The array `<Source>.spectra` contains all the unique spectral energy distributions (SEDs) in the field of view (FoV). `<Source>.ref` links each set of coordinates with the corresponding spectrum. As many coordinates may reference the same unique spectrum (e.g. all G2V stars in the FoV), each coordinate also contains a spectrum scaling factor (`<Source>.weight`)

3. Working with ‘Source’ objects in SimCADO

Source objects can be created in many ways, although in all cases the user must provide some sort of spectrum and the spatial coordinates of the emission regions (where the distance units are in arcseconds from the centre of the FoV). For convenience, SimCADO provides stellar spectra from the Pickles (1998) library. The following lines of code create a Source object for a single K=20 G2V star in the centre of the FoV:

```
>>> import simcado.source as src
```

```
>>> lam, spec = src.SED("G2V", "K", 20.)
>>> my_star = src.Source(lam=lam, spec=spec, x=[0], y=[0], ref=[0])
```

In case the object is an extended source, SimCADO can also create a Source object from a 2D numpy array (e.g. read in from the data extension of a FITS file). In this case the user must also specify, at the very least, the plate scale (pix_res) of the image. SimCADO represents the continuous emission regions as a series of point sources on an over sampled grid. In order to maintain the illusion of continuity, the spacing between these point sources is well under the Nyquist sampling size of the MICADO detector chips. Additionally, the energy units of the image and a zero-flux threshold value are optional but highly recommended.

```
>>> ## br_gamma is the emission spectrum for the nebula at 2.16um
>>> m42 = astropy.io.fits.getdata("orion.fits")
>>> my_nebula = src.source_from_image(m42, lam, br_gamma, pix_res=0.004)
```

Science fields very rarely contain only single objects. Thus SimCADO allows the user to combine Source objects using the "+"-operator, in order to build up a more realistic picture of the simulated observations. For example, the G2V star from earlier may be added to the centre of the Orion nebula by simply adding the two Source objects. In this way many individual objects may be combined to create Source objects which contain all the components of a real observational field.

```
>>> obs_field = my_star + my_nebula
```

4. Running a SimCADO simulation

SimCADO offers several levels of control over how a simulation is run. At the highest level, SimCADO assumes default parameters for everything and only requires a Source object to create mock observations. This level of control is suitable for testing the feasibility of science cases. By creating and modifying a UserCommands dictionary, the user has access to approximately 100 parameters which dictate how SimCADO applies the effects of the optical train to the incoming light. By modifying one or more parameters the user can simulate different optical path configurations and therefore investigate the effects that these changes will have on the quality of the MICADO observations. At the lowest level, the user can over-ride the inbuilt data for the optical train, e.g. provide different adaptive optics PSF images, change the detector layout, use different mirror reflectivity curves, etc. This level of control allows the user to study the effects of different materials and/or designs for the optical train. It must be stated though, that SimCADO is not designed to replace detailed trade-off studies and that any results with SimCADO should solely be used to "test the water".

A simple simulation using all the default values can be achieved using the command:

```
>>> simcado.simulation.run(source [, filename, cmd])
```

If a filename is specified, the SimCADO output is written to disk in the form of a FITS file, otherwise SimCADO returns to the user (e.g. console, ipython notebook, etc) an `astropy.io.fits.HDUList` object with the readout images from the detector chips.

Alternatively, the user can control each step of the simulation and extract intermediate data (i.e. noiseless images, detector noise frames, etc.). An example of a step-wise simulation could be:

```
>>> my_source = simcado.source.source_1E4_Msun_cluster()
>>> my_commands = simcado.UserCommands()
>>>
>>> my_optics = simcado.OpticalTrain(my_commands)
>>> my_detector = simcado.Detector(my_commands)
>>>
>>> my_source.apply_optical_train(my_optics, my_detector)
>>> my_detector.readout(filename='my_obs.fits')
```

For more detailed information, please see the online documentation at:
<http://www.univie.ac.at/simcado/>

5. Conclusion and future development plans

The core structure of SimCADO, as well as a first implementation of the imaging modi for MICADO have been implemented. It is now possible to simulate mock output imagery for the MICADO focal plane array using the current instrument and telescope design parameters. The current version of the package is available upon request. Over the coming months we plan to implement MICADO’s spectroscopic mode, as far as the current design will allow. We also plan to create a version of SimCADO for the currently operating HAWK-I instrument at the VLT, so that we can rigorously test the photometric accuracy of SimCADO.

Acknowledgments. This publication is supported by the Austrian Ministry of Science, Research and Economy (bmwfw) through project IS538003 (Hochschulraumstrukturmittel). GVK acknowledges support by the Netherlands Research School for Astronomy (NOVA) and Target. Target is supported by Samenwerkingsverband Noord Nederland, European fund for regional development, Dutch Ministry of economic affairs, Pieken in de Delta, Provinces of Groningen and Drenthe.

References

- Davies, R., et al. 2016, Micado: first light imager for the e-elt. URL <http://dx.doi.org/10.1117/12.2233047>
- Gilmozzi, R., & Spyromilio, J. 2007, The Messenger, 127, 11
- Leschinski, K., et al. 2016, Simcado: an instrument data simulator package for micado at the e-elt. URL <http://dx.doi.org/10.1117/12.2232483>
- Pickles, A. J. 1998, PASP, 110, 863
- Rauscher, B. J. 2015, PASP, 127, 1144. 1509.06264

B.3 Quotes which did not reach the title page

“The research astronomer has moved from the position of the single-handed captain of a small boat, struggling with the wheel and the sails, to the captain of the Starship Enterprise, commanding the fundamentals but letting others to carry out the appropriate actions in the best way.”

Catherine Cesarsky: ESO Director General 1999-2007, IAU President 2006-2009

“Do. Or do not. There is no try”

Yoda

“I may not have gone where I intended to go, but I think I have ended up where I needed to be.”

Douglas Adams: The Long Dark Tea-Time of the Soul

“I love deadlines. I love the whooshing noise they make as they go by.”

Douglas Adams: The Salmon of Doubt

“Karl Jansky”

Google Michi

*“Kaylee: Wash, tell me I’m pretty...
Wash: Were I unwed, I would take you in a manly fashion.”*

Firefly